An Engineering Study of the Recovery of Shear Sensitive Biological Materials by High Speed Disk Stack Centrifugation

by

Nicholas James Murrell B.Eng (Hons)

Thesis submitted for the degree of
Doctor of Philosophy

in

Biochemical Engineering

The Advanced Centre for Biochemical Engineering
Department of Biochemical Engineering
University College London
Torrington Place
London
WC1E 7JE

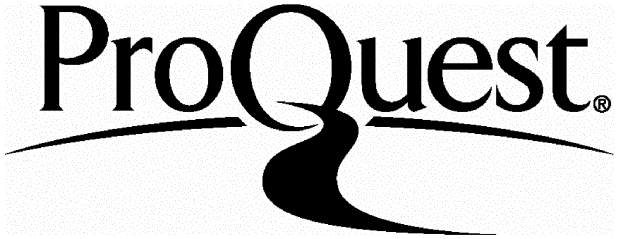

For Casey the Irish Setter

(for being reassuringly dumber than I am)

ACKNOWLEDGEMENTS

Before I start it's a sad fact that the acknowledgements page of a thesis gets read a lot more than the rest of it. For those of you that intend to go further a handy guide: if you're interested in centrifugation go straight to Chapter 6 where a summary is provided. If it's fermentation or spheroplasts you're after I'm afraid you'll have to read rather more!

Firstly I have to thank my mother and father, both for making this possible and for their own unique contributions. You're the best!

Next my supervisor and friend Nigel Titchener-Hooker. Thanks Nigel for using large type and short words on the signposts along the way, without which I'd probably still be stuck in Milton Keynes, and for keeping the money rolling in!

Also thanks to Parvis Ayazi-Shamlou, who made the numbers dance. Thanks Parvis.

I'd like to thank everyone in the UCL_{ACBE} 2nd floor research labs, both old and new, but particularly Martin Smith and Alistair Hughes. Without their unique form of madness I'd surely have gone insane. Also Martin's technical advice and assistance was invaluable.

Which brings us to the UCL technical staff. I'd like to thank all the team but particularly Billy "Mr. Fixit" Doyle, Chris "hit it better" Seaton and Clive "we can do that" Orsborn for all their advice and expertise, without which most of this would literally not have been possible. Thanks guys.

The α-amylase team at UCL for all their help and advice, particularly Claire Turner, Rob Brown and Emma Fischer; and John Maybury, the particle sizing king.

And last but not least, Dr. (formerly Miss) Paula Agutter. Thanks for your help and advice, for pouring beer down my throat and listening when things didn't go well, and for celebrating when they did. Cheers!

ABSTRACT

Advances in genetic engineering have led to the ability to express a product protein to specific locations within an organism. Of particular interest is expression to the periplasmic space, the area between the outer membrane and the inner (cytoplasmic) membrane. The target protein is then correctly folded to it's active form. This avoids an inefficient re-folding stage in the processing chain and enables the use of selective disruption techniques such as lysozyme treatment to release only the contents of the periplasmic space, thereby simplifying later purification. Such genetic manipulation however results in a much weakened cell which is liable to disruption by conventional cell harvest techniques such as disk stack centrifugation. It is the processing of such materials that forms the focus of this thesis.

The initial phase of the work focuses on establishing a periplasmic system with high levels of expression. The effect of yeast extract addition to a defined fermentation media in decreasing segregational plasmid instability and thus increasing product titres is investigated. The yeast extract is found to be preferentially metabolised and thus induce diauxic growth with the associated lag phase allowing an increase in plasmid copy number and hence a higher product titre (from 15 I.U. min^{-1} ml^{-1} on a defined media to 100 I.U. $min^{-1}ml^{-1}$ using yeast extract).

High speed disk stack centrifugation is the unit operation of choice for cell harvest because of its' continuous nature of operation. Such machines though are known to expose material to significant shear fields in the feed (acceleration) zone at the entrance to the bowl which results in disruption and, in the case of periplasmic systems, product loss. The theoretical flow regime within the feed zones of both a standard semi-hermetic and an experimental hydro-hermetic (soft shear) feed disk stack centrifuge are considered and the areas within the feeds causing disruption identified. Estimates are made of the shear rates developed in both machines. The degree of disruption to a periplasmic expressing organism is characterised for both designs. The standard bowl was found to disrupt 15% of cells with release of up to 30% of product at optimal flow rate for good recovery. Operation with a soft-shear design gave figures of 2% and 7% respectively. The effect of varying flow rate and rotational speed upon cell disruption is investigated, with an increase in disruption being observed with rotational speed and an increase with flow rate followed by a decrease as flooding occurred in the standard design.

The results of this work were used to design lab scale mimics based on both a spinning disk and a power dissipation disruption mechanism occurring within the centrifuge feed zones. These were then tested with whole cells to examine their utility in predicting product loss during a cell harvest process and shown to reproduce the disruption seen within the centrifuge feed zones. To examine the generality of the scale down approach this study was then extended to shear-sensitive polyethylene glycol protein precipitates produced from yeast homogenate.

The results of this study will enable the prediction of the levels of disruption occurring to a biological material during passage through a disk stack centrifuge. A greater understanding of the mechanisms causing such disruption has been achieved which can be utilised to optimise operating conditions to minimise damage and hence maximise recovery.

CONTENTS

TABLE OF FIGURES

TABLES

1.0 INTRODUCTION

1.1 Aim of Thesis

The interaction occurring between structurally weak biological solids and the processing environment is widely recognised as a major source of product degradation and yield loss throughout a bioprocess. Chief amongst the interactions causing such processing losses is hydrodynamic shear. A common unit operation which has been observed to be damaging to such solids (both genetically modified whole cells which are weaker than their wild-type counterparts, and precipitates/flocs) is that of centrifugation, with high speed disk stack centrifuges being particularly disruptive. These machines are frequently employed in both cell harvest and floc/precipitate removal. Although some information exists as to the location and possible magnitude of such disruptive regions within these machines no thorough investigation has previously been conducted into the shear forces generated and the mechanisms causing the observed damage. Because of this there exists no method of predicting the processing loss such a unit operation will induce without conducting a substantial programme of pilot scale experimentation. The aim of this thesis is therefore to examine the disruption caused to two different biological systems (whole cell genetically modified *E.coli* and yeast homogenate protein precipitates) by passage through two designs of disk stack centrifuge, the standard semi-hermetic design and the new "low shear" hydro-hermetic version, under a range of processing conditions. In this way conclusions will be drawn about the mechanical aspects of the centrifuge most likely to be the cause of such damage to the test systems. A theoretical appraisal of the forces developed within such regions will be made and appropriate laboratory scale mimics devised and tested. These mimics are aimed at reproducing the disruption observed during centrifugal recovery. This would allow a rapid assessment to be made of potential yield loss/ drop in centrifuge performance when processing a new product whilst still operating at a laboratory scale, thus offering the opportunity to speed up process development. Conclusions will also be drawn about the best mode of operation of a disk stack centrifuge to minimise such disruption.

1.2 *E.coli* as a host organism for foreign protein production.

The production of a foreign protein using as a host a genetically modified micro-organism (GMO) involves two distinct stages of host system selection. The micro-organism itself must be chosen, and then the plasmid containing the product expression system must be produced and cloned into the host. The Gram-negative bacteria *Escherichia coli* is frequently selected as the organism of choice. This is because it has been extensively researched (second only to yeast) and is considered well characterised. This offers two important advantages. Fermentation conditions for the efficient growth of the organism are for the most part well established and understood, fine tuning only for plasmid retention and product expression is necessary. More importantly, persistent use of many different strains of *E.coli* have shown it to be in the majority of circumstances both safe and resistant to genetic mutation. This very much simplifies the safety issues raised when using a GMO for large scale production, and means that the final system developed for protein production is stable: it will not mutate over the many generations involved in each fermentation and thus each cell harvested from a fermentation will be identical within the bounds of population distribution. This simplifies the many problems associated with product concentration and purification during downstream processing. It also means that it is very unlikely that any unforeseen biological safety hazards will occur as a result of mutation.

1.2.1 The structure of *E.coli*

E.coli is a Gram-negative bacteria (this describes it's reaction to Christian Gram' s common staining procedure (Gram,1884) and indicates the structure of it's cell wall as will be explained later) commonly found in the intestines of warm-blooded animals. Morphologically it exists in the shape of a rod, typically 2 microns long by 1 micron wide.

E.coli structurally contains several distinct regions. The majority of the cell is termed the cytoplasm. This is located within the cytoplasmic membrane, the inner membrane of the cell wall. It contains the bulk of the cells' proteins, it's genetic information and is also the area where most of the operations necessary for it's existence occur. Within this is a large ill-defined region called the nuclear zone, the dominant control centre for cell operation, and ribosomal areas, where the majority of the cell's protein synthesis occurs. Also contained within the cytoplasm are bubble-like structures called storage granules. All these features are suspended in the cytoplasmic fluid.

Because bacteria live in an environment over which they have no control, the cell wall serves two purposes. Firstly to control entry of the various chemicals necessary for the cells survival into the cell, and to prevent entry of anything toxic or not required. Therefore the cytoplasm typically has a high internal osmotic pressure. Thus the second function of the cell wall is to provide mechanical rigidity, unlike that of mammalian cells which themselves exist in a carefully controlled environment. Since this project is primarily concerned with the disruption of bacteria by mechanical forces, which equates to the destruction of the cell wall, the structure of the wall will now be considered in some detail.

1.2.1.1 The Cell Wall

The Gram-negative cell wall, such as is present in *E.coli*, differs from the Gram-positive in one crucial respect. The Gram-positive cell wall consists of a single membrane, the cytoplasmic membrane, which forms a permeability barrier and thus controls entry of chemicals into the cell. It is typically about 8 nm thick. It is surrounded by what is commonly known as the wall itself, a layer of the bacterial protein peptidoglycan. This is typically 15-80 nm thick and is what provides the mechanical strength of the cell.

The Gram-negative bacterial cell wall is more complex. This consists of an outer membrane, typically of 8 nm thickness. Attached to the inside of this is the peptidoglycan layer, with a thickness of between 6 and 11 nm. Between this and the

inner, cytoplasmic membrane, is a region known as the periplasmic space. This forms about 10 percent of the total cell volume, and contains a number of enzymes, sugars and amino acid binding proteins (approximately 3-5% of the total cellular protein). It is between 7 and 15 nm deep.

1.2.1.2 The Outer Membrane (OM)

The OM of the *E.coli* cell wall forms a semi-permeable barrier to the cell. Although it maintains an osmotic pressure of up to 5 atmospheres in the periplasmic space, it is somewhat leaky, particularly when expressing a foreign protein in large quantities to the periplasmic space: such a protein can leak in appreciable quantities to the surrounding environment (i.e. fermentation media).

The major constituent of the OM is Lipopolysaccharide (LPS). This forms between 3 and 8% of the cells dry weight (Rietschel *et al*, 1984). LPS itself is an ampiathic molecule made up of three distinct regions. The hydrophilic portion is represented by the O-antigenic polysaccharide and core oligosaccharide units, in turn linked to the hydrophobic glycolipidic Lipid A residue. The first of these units has been found to be highly variable in structure, the other two are very highly conserved. The molecular weight of individual molecules varies from 8000 to 50000 according to the number of repeating saccharide units that make up the O-antigenic polysaccharide.

LPS is anchored in to the OM partly by the fatty acyl chains of the Lipid A portion (Morrison, 1985) (this is its' contribution to the formation of the OM bilayer), partly by interactions with divalent cations such as Mg^{2+} and Ca^{2+} (Rottem & Leive, 1977, and Coughlin *et al*, 1985) and partly by interactions with proteins (LPS has been found to interact with all major OM proteins) (Nikaido & Vaara, 1985).

LPS forms the outer section of the OM bilayer. The inner section is formed by phospholipid. At normal temperatures, i.e. 37°C, the OM is essentially fluid, as it must be to allow transport across the membrane. LPS becomes fluid at around 22°C

(Emmerling, Henning and Gulik-Krzywicki, 1977) and at temperatures below this little or no growth is seen in *E.coli*.

1.2.1.2.1 Outer Membrane Proteins

The OM of Gram-negative bacteria is perforated with a series of hydrophilic channels, formed by proteins called porins. The cell produces up to 10^5 copies of each type of channel (Nikaido & Vaara, 1985) with some being constitutively expressed, whilst others are inducible under specific growth conditions. They can be divided into two classes: the general diffusion porins which are chemically non-specific, and the specific porins that contain substrate-specific binding sites (Nikaido & Vaara, 1985). Together they are responsible for the transport of large molecules across the OM.

In addition to porins there are a number of other proteins associated with the OM. Chief amongst these are the lipoproteins which can be subdivided into two groups. The Braun lipoprotein (Braun, 1975) is a small protein existing in high copy numbers in the OM of *E.coli*, and the peptidoglycan-associated lipoproteins (PAL's) (Mizuno, 1979).

The Braun lipoprotein is covalently linked to the peptidoglycan layer along a third of its structure. One suggested role for this protein is as a periplasmic space-keeper, linking the OM to the peptidoglycan layer at a fixed distance of approximately 5 nm (Braun, 1975).

PAL's are non-covalently associated with the peptidoglycan layer (Mizuno, 1979). These include porins, and other proteins such as 21K and OmpA. It is suggested that these associated proteins play an important role in the maintenance of cell shape and osmotic stability.

Overall the OM can be looked at as a molecular sieve. The holes of the sieve are provided by the porins, and these define the size of hydrophilic molecule that can pass through the membrane into the periplasm. Although this is a gross oversimplification (in fact several classes of molecules can pass directly across the membrane without

using the porins (including specific proteins, DNA under some circumstances, and some antibiotics)) it does provide a good overview of the OM's structure and purpose.

1.2.1.3 The Peptidoglycan Layer

Peptidoglycan, or murein, forms the essential cell wall polymer of bacteria. It is thought of as having properties approximately analogous to viscoelastic polymers (Thwaites & Mendelson, 1985). It is the peptidoglycan layer that gives the bacterial wall its shape and rigidity.

Peptidoglycan is a heteropolymer made up of glycan strands crosslinked by peptides. The essential building units of the polymer are a β-1,4 linked disaccharide of N-acetylmuramic acid (NAM), N-acetylglucosamine (NAG), a tetrapeptide which varies in structure from species to species and is attached to the NAM, and a bridging pentapeptide comprised entirely of glycyl residues which joins the glycan strands together. By using four chemical linkages per disaccharide unit, a giant network structure which comprises the cell sacculus, a large single macromolecule which surrounds the entire cell, is formed (see Figure 1.1).

Although in theory each glycan chain could be almost infinitely long, in practice 70% of *E.coli* glycan chains have an average length of 9 disaccharide units, whilst the other 30% have an average length of 45 units (Harz *et al*, 1990).

Molecular modelling (Burge *et al*, 1977) studies verified with such techniques as NMR and X-ray diffraction (Burge *et al*, 1977; Burge, Adams *et al*, 1977; Labischinski, 1979; Naumann *et al*, 1982; and Barnickel *et al*, 1980) show that the glycan strands adopt a regular helical conformation, whilst the bridging pentapeptides can exist in several arrangements. The relaxed stress free conformation gives rise to a ring-shaped arrangement in close proximity to the sugar strand (Barnickel, Naumann *et al*, 1983), but under stress each peptide can extend by up to 400% of its' length (Barnickel, Naumann *et al*, 1983b) . It is this enormous elasticity which enables the cell to respond to changes in osmolarity by corresponding volume adaptation.

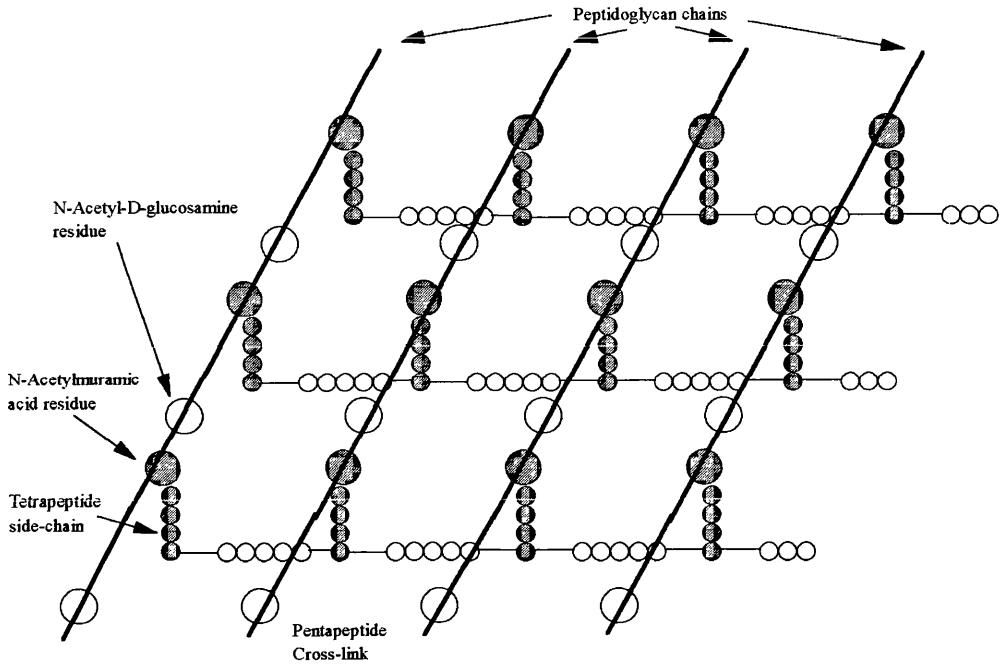

Figure 1.1: The Structure of Peptidoglycan Chains

There is some discussion as to whether the peptidoglycan exists as a distinct layer within the periplasm, or whether it is in fact multilayered. It is presently thought likely that neither of these extreme models accurately describe the situation, and that the real state is somewhere between the two (there is not enough peptidoglycan in a *E.coli* cell to form even two complete layers (Wientjes *et al*, 1991). However, the cell maintains it's shape even during division with a drastically reduced peptidoglycan content, a finding which is not consistent with the single layer theory (Park, 1993). The layer is known to thicken drastically in cells at the end of the growth cycle, from 6-8 nm in exponentially growing cells to around 11 nm in cells in the stationary phase (Labischinski & Johannsen, 1986).

As has already been stated, the peptidoglycan layer is enormously flexible, with the extension of the crosslinked peptides by up to 400% allowing volume increase under

osmotic pressure changes. However, spheroplasts formed from gram-negative bacteria by the removal of the peptidoglycan layer tend to form spheres. This implies that the peptidoglycan sacculus is also responsible for the cells rigidity and maintenance of it's shape. This can be attributed to the inflexibility of the sugar chains: only a low degree of rotation around the β-1,4 linkage is permitted and therefore bending of the chains is not possible. As a result, parallel sugar chain arrays within a two dimensional peptidoglycan plane will not increase in length under stress. Thus rigidity and elasticity are attained simultaneously (Labischinski & Maidhof, 1994).

Again, this is a simplification of the real situation. Murein chemistry is extremely complex: there are more than 80 different muropeptides found in *E.coli* (Holtje & Glauner, 1990). There is also an unusual crosslinking method found in addition to the common one described above. It has also been proposed that peptidoglycan has a chemically different structure in the cylindrical section of the cell to that in the spherical polar regions: it has so far proved impossible to verify this. However, the above description is sufficient to explain how the layer provides the cell with mechanical strength, which is required for an understanding of how bacterial cells are disrupted.

1.2.1.4 The Periplasmic space

The periplasm comprises the molecules and ions that are located within the space between the inner membrane (IM) and the outer membrane (OM). It can therefore be viewed as a region for transhipment of molecules between the cytoplasm and the exterior of the cell. It has been estimated to be between 7-15 nm deep and to occupy up to 10 % of the cells total volume. However, this can increase drastically when the cell is expressing a foreign protein (to between 20 and 40%). It can be viewed as a very viscous gel layer between the OM and IM.

As has already been discussed, molecules may enter the periplasm through the OM in one of three ways: through non-specific porins, through specific porins, or by direct transport across the OM (Kadner, 1990). However, transport from the cytoplasm to the periplasmic space is more complex. It may require the insertion of specific leader sequences on the C or N termini of proteins (Lee *et al*, 1992). Proteins transported to the periplasmic space may end up with part of the protein exposed at the outer surface of the IM, they may be completely excreted into the periplasm or they may be targeted to the OM itself, or for release through the OM (Lory, 1992). For passage through the OM two basic mechanisms are employed: special leader sequences may be included on the protein which are recognised by the export machinery, alternatively a temporary local connection between the IM and the OM may be formed which allows the protein to be exported directly from the cytoplasm to the environment (Bayer, 1968). These sites are believed to also serve in macromolecule import. It should be noted that formation of such bridges disrupts the peptidoglycan layer, and if a large number are present can cause substantial weakening of the cell. Enzymes and toxins are also exported from the cytoplasm to the outside by a variety of different mechanisms.

The periplasm itself contains a large number of proteins necessary for the life of the cell. These can be divided into three major groups (Oliver & Beckwith, 1981):-

- Binding proteins (used to transport amino acids, carbohydrates and vitamins across the inner membrane)

- Enzymes for detoxification

- Other proteins

In addition to these resident proteins there will of course be a variety of different proteins in transit from the cytoplasm to the outside of the cell.

The periplasm also contains two classes of polymer: the peptidoglycan sacculus, and membrane-derived oligosaccharides (MDO's). The synthesis of MDO's is controlled by

the osmolarity of the cell; low osmotic pressure in the growth media increases their synthesis dramatically. They have an overall negative charge, contributing to the maintenance of the periplasm at the same osmotic condition as the cytoplasm, and are believed to affect the function of the OM pores (Kennedy, 1982).

As has already been stated the periplasmic space is known to be osmotically leaky under certain conditions. It is generally maintained at the same osmotic pressure as the cytoplasm. However, the overall osmotic pressure of the cell varies with the cell's environment (Csonka, 1989). In a growth media with a high osmolarity the cell takes in more ions to compensate for the increased external pressure. *E.coli* will tolerate brief exposure to relatively high osmotic pressure (suspension in up to 30% w/v sucrose solution), with no appreciable loss of viability (Bayer, 1991). However, a sudden increase in external osmotic pressure will cause plasmolysis: an outflow of water from the cytoplasm, a retraction of the IM from the OM and a corresponding widening of the periplasmic space (Bayer, 1968). This is however, a relatively short lived and reversible condition as the cell reacts by taking up more ions.

More serious is a sudden reduction in external osmotic pressure after cells have adjusted to an environment of high osmotic pressure. This leads to a sudden swelling of the cytoplasm, which in turn increases pressure on the periplasmic space. Under these conditions the periplasmic contents may be ejected into the medium. Pre-treatments such as with EDTA/Lysozyme lysis mixture increase this effect and form the basis of periplasmically expressed product recovery techniques (Neu & Heppel, 1965).

1.2.2 Vector Design

The term vector is given to foreign DNA fragments introduced into growing cells which encode for the production of a recombinant product. A successful vector should therefore have these properties (Bailey & Ollis, 1986):

- Will replicate in and be retained by the cell

- Will accommodate product encoding foreign DNA fragments of various sizes
- Can be inserted easily into the host cell
- Has a selection marker for rapid selection of cells containing the marker
- Contains only one target site for one or more restriction endonucleases.

In practice two different classes of vector are utilised for *E.coli* rDNA product production: bacteriophage vectors and plasmid vectors.

Bacteriophages can be viewed as a form of virus which infect bacteria. In most cases they are designed to infect a cell with their genetic information, replicate within the cell and then, by inducing cell lysis, many daughter phages are produced for subsequent rounds of infection. However, certain types of phage under the correct conditions will introduce their DNA into a cell where it then becomes recombined into the host's genetic material. It is then copied every time the cell replicates. By introducing product encoding DNA into the bacteriophage, this system can be used as a vector.

The more common system of introducing foreign DNA to a host cell is by using a plasmid. A plasmid is a DNA circle that is maintained within the cell as separate from the bacterial chromosome and duplicates separately from it. They are non-essential for cell survival, although they may confer useful properties upon the cell, such as antibiotic resistance.

The plasmid must obviously be maintained within a growing cell population at relatively high copy numbers in order for efficient product expression to take place. This is achieved via the use of selection markers. Industrially two systems are popular.

The first is antibiotic resistance. By using a plasmid that confers resistance to a given antibiotic upon the cell, and by adding that antibiotic to the fermentation media, it is possible to ensure that only cells which retain the plasmid survive. Although this is a relatively straightforward method, it has several disadvantages. Firstly, the handling of large quantities of antibiotics industrially during media preparation poses a significant

safety hazard to the staff performing such an operation. Secondly, from the biosafety viewpoint, the possible release of a recombinant bacteria with antibiotic resistance to the environment is not acceptable. A third problem is that the antibiotic must be later removed from the product stream, further complicating purification.

The second, and more elegant, method of ensuring plasmid stability is to use a cell that is incapable of manufacturing an essential element, such as an amino acid, and adding the genetic information necessary for it's production to the plasmid. Thus any cell which does not have an intact copy of the plasmid will not survive. This has the added benefit of not involving any extra additions to the media, and thus not complicating downstream processing.

1.2.2.1 Product expression strategies

Once a vector has been selected a product expression strategy must be considered before the product encoding DNA itself is added to it. There are two major elements to be considered here. The first is to consider what 'trigger' to use to begin product expression. The second is to consider what compartment of the cell the product is to be secreted to.

Obviously the simplest 'trigger' is to have product expressed continuously during the fermentation. However, there is a major disadvantage associated with this strategy. Because this involves the utilisation of the cells limited resources to make a protein which is, as far as the cell is concerned, completely useless, it can seriously reduce cell growth/viability. As product yield is both a function of total biomass per fermentation and product per cell, this is obviously a serious handicap. The most efficient strategy is therefore to grow the cell population to a given concentration, and then, after cell growth has ceased, to switch on product expression. The design of the trigger to induce the expression of product is very variable. However, industrial systems tend to work in one of two ways. Either the product DNA is organised on the plasmid in the form of an operon, such that an inducer is needed before product expression can begin, or the heat shock reaction is used.

A popular inducer is IPTG, a gratuitous inducer of the *lac* operon. Therefore by adding the control system of the *lac* operon onto the plasmid, it is possible to switch on product expression by adding IPTG to the fermentation media at the appropriate time. This, of course, has the disadvantage that the chemical will have to be removed during downstream purification.

An alternative system is to utilise the heat shock reaction of the host cells. Micro-organisms cope with elevated temperatures by expressing a number of enzymes which are only expressed when the cell encounters a temperature higher than that to which it is adjusted (in *E.coli* raising the temperature from 37°C to 42°C is enough to induce production of heat shock enzymes). By using a promoter sequence from such an enzyme on the plasmid, simply raising the temperature of the media will switch on product expression.

An equally important question is where the product is to be expressed to. As has been explained, there are basically three compartments available for product expression in the Gram-negative cell: the cytoplasm, the periplasm and complete secretion to the outside of the cell.

1.2.2.1.1 Expression to the Cytoplasm

There are several problems associated with product expression to the cytoplasm. Chief amongst these is solubility. If the product is expressed in large quantities to the cytoplasm of the cell it tends to reside in insoluble inclusion bodies. Furthermore, the protein within these inclusion bodies is generally not in a biologically active state (Sharma, 1986). Although work is in progress to overcome these problems, currently a cytoplasmic expression strategy implies that downstream processing will involve the solubilisation of the inclusion bodies, and a renaturation step to achieve biological activity. This is difficult to achieve, as the kinetics of protein folding are poorly understood, and often leads to a large reduction in the yield of the process (Bailey & Ollis, 1986).

1.2.2.1.2 Secretion to the Extracellular Medium

This concept is well established in organisms such as *Streptomyces* as it greatly simplifies product recovery and purification, allowing the cells to be removed from the fermentation broth and disposed of immediately. Thus the product does not have to be separated from the host cells' proteins. As disulphide bond formation generally occurs in the periplasmic space of *E.coli* it might be expected that the secreted product would be biologically active. However, laboratory strains of *E.coli* do not naturally secrete any protein extracellularly. Despite this there are several systems under development which use leader sequences of proteins from other host cells to target the product for extracellular secretion, such as the signal sequence from murine spleen RNase used to target bovine RNaseA (Schein *et al*, 1992). These systems tend to produce only low levels of product. More promising is the use of the *E.coli* native pathway which translocates the 107kDA α-haemolysis protein directly from the cytoplasm of uropathogenic strains to the extracellular medium. This system transplanted into laboratory strains is proving a reliable mechanism for secreting recombinant proteins to the extracellular environment (Blight *et al*, 1992).

1.2.2.1.3 Expression to the Periplasmic Space

Translocation of proteins to the periplasmic space requires the products of the *E.coli sec* genes and an N-terminal targeting sequence (Blight *et al*, 1992) which is removed during transport. A large number of proteins have been successfully secreted to the periplasm of *E.coli* using a variety of leader sequences, although there seem to be no hard and fast rules as to which leader sequence will work best for a given protein. Therefore, a large amount of experimentation is necessary when considering vector design. This system also works at product concentrations of up to 20% of the cell's total protein. The formation of inclusion bodies in the periplasm is very uncommon, the overexpressed protein is generally in a soluble state. Furthermore, although products

expressed to the periplasm are not always correctly folded, many are and therefore exist in a biologically active form (Little *et al*, 1989).

Periplasmic expression offers one further advantage. During downstream processing it is possible to disrupt selectively only the OM of the cell, thus releasing the periplasmic contents. This very much simplifies the problems of purification, as the product will need to be separated from only the other proteins resident in the periplasm, not the complete cellular contents.

There are several disadvantages associated with this system however. The first of these is that the periplasmic space can be leaky, as previously explained, particularly when it contains a large amount of protein. As the first stage of any processing will almost certainly be to separate the cells from the media, which will be thrown away, any leakage before this separation is complete (including shear induced leakage) will lead to a potentially large yield loss before purification has really begun. Another problem is that accumulation of signal sequences in the periplasm can induce the heat-shock stress response, and this can cause increased proteolysis (Wild *et al*, 1993). Furthermore it is not always possible to identify a leader sequence to target a protein to the periplasmic space, and inclusion bodies can still be formed under certain circumstances.

Despite these problems this expression strategy is becoming increasingly important industrially.

1.2.3 Microbial Test System

The majority of work in this thesis was performed using *E.coli* JM107 pQR126. This is a recombinant K12 strain. The α-amylase product was derived from *Streptomyces thermoviolaceus* CUB 74, which has been cloned successfully into a variety of hosts. The plasmid contains a leader sequence to allow secretion into the periplasmic space (Bahri & Ward, 1990, and French, 1993) and a gene encoding for kanamycin resistance. The expression system is *LacZ*: this does not require induction due to the

reduced amount of repressor molecules present. The α-amylase product is a 50 kD protein.

1.3 Cell Disruption

As has already been stated during the discussion of *Escherichia coli,* the advantages of periplasmic expression are two fold. The genetic aspects, namely the ability of the cell to fold correctly a product into its' native state, thus removing any need for a time consuming, difficult and yield reducing renaturation step, and the purification aspects, namely the need to disrupt only the outer membrane of the cell, thus greatly simplifying the subsequent processing problems. The periplasmic space contains only approximately 5% of the total free protein of the cell allowing a purification strategy to be greatly simplified because of the reduced number of contaminants. The difficulty in utilising this second, and significant advantage, is in finding a disruption technique of sufficient force to release 100% of a cell suspension's periplasmic contents, whilst at the same time selective enough to leave the much weaker inner membrane intact. Added to this is the need to remove subsequently the product rich liquid stream from remaining cell debris without any further damage to the cytoplasmic membrane. These constraints are likely to lead to a multi-stage primary processing requirement, and one that is considerably more complex than a simple high-pressure homogenisation followed by selective separation. However, the subsequent advantages to be gained, both in yield increase and the reduction of expense obtained through the simplification of the secondary processing and purification, may for some products, far outweigh this disadvantage.

Because a large part of the work contained within this thesis focuses on the disruption of whole cells during passage through a disk stack centrifuge, and the importance of selective release techniques in maximising the benefits of periplasmic expression, it is useful to review the basis of cell disruption unit operations in current use.

1.3.1 Methods of Disruption

There are a large range of different disruption techniques available to the process designer, and the most applicable one will depend on precisely where in the cell body the product is located, and most importantly cell wall strength. This last parameter is not easy to characterise, since little is known about the cell membranes absolute strength. However, it is certain that cell strength varies depending on growth conditions and the point at which the cells are harvested. However, broadly speaking disruption methods may be split into five categories:

- **Non-mechanical Disruption**
    - Physical Disruption
    - Chemical Disruption
    - Biological Disruption

- **Mechanical Disruption**
    - Liquid Shear
    - Solid Shear

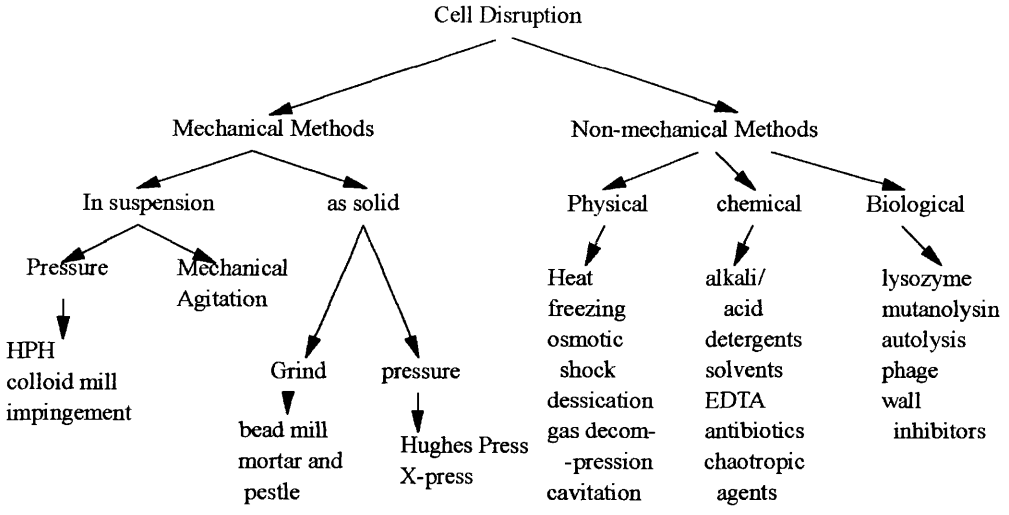

Figure 1.2: Methods of Microbial Disruption

1.3.1.1 Non-mechanical Cell Disruption

1.3.1.1.1 Physical Disruption

Cavitation

It is possible to force vapour cavities to form within a liquid stream. This may be achieved in several ways: by a local increase in liquid velocity, as described by Bernoulli, by rapid vibration of a boundary to flow which in turn causes rapid vibrations within the liquid, by setting up ultrasonic vibrations within the liquid or through the overall reduction of a liquids static pressure. The cavities that are formed in this manner will subsequently collapse and rebound until, at the end of the process, an overall increase in pressure causes their destruction. This process is known as cavitation, and is associated with local variations in pressure of the order of 1000MPa. Because of the large pressure variation, when the cavities finally collapse, large amounts of mechanical energy are released into the main body of the liquid and these subsequently set up a series of elastic waves which disintegrate into eddies. Cavitation is already well known for achieving a fine dispersion of fragmented solid particles or gas bubbles in a liquid, and for the damage it can cause to both pumps and to pipework. Therefore two distinct methods have been considered for applying this powerful disruption technique to cells: ultrasonic cavitation and hydrodynamic cavitation (Bailey & Ollis, 1986).

A cavitation-based mechanism of disintegration was proposed for yeast's by Doulah (Doulah, 1977) based on drop breakup in hydrodynamic fields. In this model, drop breakage occurs when the dynamic pressure difference across a drop exceeds it's surface energy. It has been suggested (Harrison, 1990) that the important parameter when assessing the effects of fluid induced stresses on cells in turbulent fluid flow is

the ratio of the cell size to that of the smallest eddies. The size of such eddies can be calculated using the Kolmogoroff scale of microturbulence:

$$\lambda_k = \left(\frac{\nu^3}{\varepsilon}\right)^{1/4} \qquad \textbf{(1.1)}$$

where ε = energy dissipation rate (J s^{-1})

ν = fluids kinematic viscosity (m^2 s^{-1})

λ_κ = size of the smallest eddy (m)

Eddies of a scale larger than the cell will simply impart a motion to that cell which will move it from place to place. Eddies which are of a similar scale to the cell, or slightly smaller, will however impart motions of various different intensities to regions of the cell wall. This will in turn produce a pressure difference across the wall. If this exceeds the cell wall strength, then the cell will disintegrate. However, cell wall strength is generally unknown, so Doulah (1977) assigned a surface tension type force, s, to represent it.

$$E_{sur} = \frac{\theta . s}{d_e} \qquad \textbf{(1.2)}$$

where E_{sur} = cell surface energy (J)

θ = cell shape factor (-)

d_e = cell equivalent spherical diameter (m)

Using this relationship a largest stable cell size, d_m, can be determined as a function of the energy dissipation rate. This model was found to illustrate the dependence of the degree of disruption on cell size which had been shown experimentally, however the use of the cell wall strength analogy to surface tension is now considered

fundamentally unsound (a cell wall is a structural component and as such gains its' rigidity from it's chemically bonded nature, whereas surface tension is caused by the lower potential energy of a solvent molecule when in the bulk solvent compared to that in a gaseous state or an immiscible solvent, caused by attractive forces and hydrogen bonding between the molecules). Another problem with the adaptation of the drop break-up mechanism is that when a droplet is broken a number of chemically identical entities are formed. This is clearly not the case with cells, as has been shown by transmission electron microscopy (Harrison, 1990).

Ultrasonic Cavitation

Ultrasonic vibrations are those covering a frequency range extending from 20kHz upwards. As the power input increases, pressure fluctuations are set up within the liquid, intermolecular cohesive forces cannot be maintained and cavitation results. This cavitation has been found to be both frequency and intensity dependent, and requires a pressure fluctuation within the fluid greater than the hydrostatic pressure (Greguss, 1963).

This technique has long been established as a laboratory scale technique for cell disruption. Studies on brewer's yeast have shown that protein release on exposure to 20kHz vibration at a power of 200 acoustic watts is independent of biomass concentration up to 600g/l wet weight, and is in fact almost proportional to acoustic power in the range 60-195 watts (Wang *et al*, 1978). Wase and Patel (1985) have subsequently shown that irrespective of culture conditions, the single most important factor determining the susceptibility of a cell to ultrasonic disintegration is the mean cell volume, although disruption is also dependent on the growth phase (and thus the cell wall strength) (Cumming, Tuffnel *et al*, 1985).

Although in principle ultrasonic devices could be scaled up and operated continuously, they are not found industrially at present. There are two major factors that make them extremely difficult to apply. Firstly, they require a relatively large amount of energy and thus running them at large scale is prohibitively expensive. Secondly, and perhaps

even more importantly, most of the acoustic energy absorbed by the cell suspension is subsequently converted to heat. Because of the adiabatic compression of the suspension by the acoustic radiation, localised extremely high temperatures can occur (in the order of 250^0C). This leads to rapid deactivation of enzymes (Lilly & Dunnill, 1969) and thus significant loss of product yield. This effect is further enhanced by the non-spherical geometry of cavities produced by ultrasound: their subsequent collapse will cause a discharge owing to the asymmetrical distribution of electrons and damaging ionisation. A final problem is the very fine cell debris that ultrasonication produces, the removal of which causes further processing problems (Chisti & Moo-Young, 1986).

Hydrodynamic Cavitation

If a cell suspension is pumped through a constriction a local increase in fluid velocity occurs and hydrodynamic cavitation can result. A study involving the passing of *Alcaligenes eutrophus* through a partially closed valve under conditions at which cavitation had been shown to occur generated substantial cell disintegration (Harrison, 1990). Furthermore, such breakage was mostly produced on a single pass, and, as can be expected, was enhanced under conditions which would increase the cavitation (raising the temperature or increasing the pump discharge pressure). Because of the reduced energy required for hydrodynamic cavitation, and the corresponding reduction in temperature elevation, this is currently felt to be a better disruption technique than ultrasonic cavitation.

Desiccation

Desiccation, in all its forms, is one of the oldest methods of cell disruption employed although it is now generally redundant due to the length of time it takes. Such treatment causes the permeabilisation of the cells whilst leaving them generally intact (Felix, 1982). This greatly simplifies the subsequent debris recovery. Slow drying in air, drum drying, use of a desiccant or a dehydrating solvent have all been shown to be

effective and subsequent extraction of the microbial powder in a buffer allows product recovery, although only at low levels (Engler, 1985, and Hughes, Wimpenny *et al*, 1971). Hence this technique is only applicable to low value bulk products. Freeze drying has been found to be even less effective; however, if frozen slurries of cells are forced through restrictions the shear effects of the ice particles in the slurry can cause significant disruption. In addition to this the freeze-thaw action of the ice particles causing significant volume changes is believed to contribute to the overall effect, termed the freeze-press. Chisti and Moo-Young (1986) in addition state that the cell remains relatively intact during this process, and again downstream processing problems are simplified. This technique is, however, scarcely used on a commercial scale and is reserved for the laboratory.

Osmotic Shock

Osmotic shock for microbial disruption is based on the rapid dilution of a cell suspension of high osmotic pressure (circa 20% sucrose) or the rapid re-suspension of cells in a solution of high salt content. At present this method has been shown to have only a small effect on microbial cells, an effect that is even further reduced in cells in the stationary phase due to thickening of the peptidoglycan layer (Felix, 1982). It is based on the rapid motion of intracellular liquid. In the first case suspension of the cells in the sucrose solution results in the movement of intracellular water from both the periplasm and the cytoplasm to outside the cell. Upon dilution water re-enters the flaccid cell resulting in it's rapid swelling. This technique is sufficient to release some periplasmic products from the Gram-negative cell envelope, especially if used in conjunction with lysozyme treatment. However, to release cytoplasmic contents, the cell wall must first be weakened using another technique. The second strategy relies on purely the initial exit of intracellular water from the cell rupturing the membranes. Although this method works extremely well with fragile cells, such as mammalian cells, the desirability of contaminating the product stream with large concentrations of salt should also be considered (Engler, 1985; Hughes, Wimpenny *et al*, 1971; Wang *et al*, 1978).

Temperature Extremes

As has already been stated, freezing and thawing of a cell paste can cause disruption through the formation and subsequent melting of ice crystals. Gradual freezing, which results in the formation of the largest ice crystals, has been shown to cause the most damage. Cell breakage can be enhanced with simultaneous grinding. However, this technique is costly and has so far been restricted to laboratory scale. It is also gives low yields (Sikyta, 1983, Stanbury & Whitaker, 1984) and the loss of product enzyme activity has been reported (Kula & Schutte, 1987).

At the other extreme investigations of the thermolysis of *E.coli* K12 over the temperature range 30-90^{0}C have shown significant protein release occurs after a twenty minute treatment at 90^{0}C. This apparently gave better release than an exposure to lower temperatures (30-70^{0}C) for longer periods (approximately 1 hour). However, although electron microscopy clearly showed large amounts of cell debris after treatment at 90^{0}C, because of the change in protein solubility observed at these temperatures (Harrison, 1990) no quantitative measure of release is possible.

In addition to these extreme conditions, it has been shown that exposure of *E.coli* to a temperature of 55^{0}C in a 50mM Tris-hydrochloride buffer for 2 hours results in the release of up to 50% of the cells alkaline phosphatase, a wholly periplasmic enzyme (Tetsuaki *et al*, 1985). Although at present this is merely a reported finding, it is felt likely that for thermo-stable periplasmic products a release strategy could be developed which at least partially utilises this technique. In general, however, it is hard to utilise elevated temperature as a disruption technique due to the intolerance of most biological products to such temperature extremes.

1.3.1.1.2 Chemical Disruption

There are three basic approaches to cell disruption by chemical means. These are by exposure of cells to extremes of pH, the use of chaotropic agents, or the exposure of the cell to detergents.

pH Extremes

6M Hydrochloric Acid has been shown to hydrolyse dried *Candida lipolytica* cells (Hughes, Wimpenny *et al*, 1971). This is however, a slow process and one which also causes the hydrolysis of proteins into their constituent amino acids. Because of this, and the fact that the treatment also causes the precipitation of many cellular macromolecules, it is not applicable where the aim is to release an intact and active product.

At the other extreme an alkaline treatment of pH 11.5-12.5 for only 30 minutes has been shown to cause cell lysis (Stanbury & Whitaker, 1984). A process improvement was reported (Wade, 1968) when mechanical disruption was replaced by alkaline treatment in excess of pH 9 whilst working with the extraction of L-asparaginase from *Erwinia*: furthermore the enzyme was released in a soluble form. Similar results have been found with the release of PHB from *Alcaligenes eutrophus* (Harrison, 1990). Again, however, a major problem with such extractions is the inability of most proteins to tolerate such conditions and it is difficult to recover an active product in this manner.

The Use of Chaotropic Agents

Chaotropic agents, such as guanidine hydrochloride and urea, have been shown to aid cell lysis (Becker, Ogez, *et al*, 1983 and Hettwer & Wang, 1989). They are thought to solubilise the outer membrane proteins of Gram-negative micro-organisms by altering the hydrophobicity of the surrounding aqueous medium. They may also enhance

further recovery steps by encouraging the dissociation of nucleic acids from microbial products (Damodaran & Kindella, 1983). However, these methods are currently confined to enhancing disruption on a laboratory scale.

Use of Detergents

Treatment of cells with sodium dodecyl sulphate (SDS) is used as a standard method for releasing cellular components in the microbiological laboratory (Glass, 1982). The effect of detergents in solubilising membrane proteins, and destroying the important structural protein-lipid bonds, is reviewed by Helenius and Simons (Helenius & Simons, 1975).

The effects of different detergents depend upon the conditions of treatment, and crucially on the presence of the membrane stabilising divalent cations. *E.coli* studies show the varying susceptibility of the outer membrane, the cell wall and the cytoplasmic membrane to treatments with both anionic detergents such as SDS and non-ionic detergents such as Triton X-100. In the presence of Mg^{2+} ions the action of Triton is restricted to the inner membrane, and although SDS is still fairly effective at solubilising both the outer and inner membranes it will not disrupt the peptidoglycan layer (Filip *et al*, 1978). Membrane removal has been reported as independent of detergent concentration in the range 0.5-2.0% (w/w), although some enhancement is found increasing the temperature between 4-37^{0}C (Schnaitmann, 1971).

Because of the highly selective nature of these detergents it should be possible to use them to release a microbial product in a highly specific manner, particularly in conjunction with another method, such as a chaotropic agent. However, generally speaking they are not used on an industrial scale. This is due to the undesirability of contaminating a product stream with a detergent which must then be removed during subsequent processing.

Ethylenediaminetetraacetic acid (EDTA)

Divalent cations, and crucially Mg^{2+}, are essential to stabilise the outer membrane of Gram-negative bacteria such as *E.coli*. EDTA will chelate these cations, and cause the outer membrane to become unstable: in particular it disrupts the permeability function of the outer membrane and thus allows access for other agents such as Lysozyme or detergents. *E.coli* has been shown to lose up to 50% of it's lipopolysaccharide content during treatment by EDTA, as well as small amounts of protein and phospholipid (Felix, 1982). In *E.coli* EDTA has also been shown to increase autolysis: in other Gram-negative bacteria it merely increases the permeability of the outer membrane.

1.3.1.1.3 Biological Disruption

At first sight the use of enzymatic cell lysis is very appealing to the process engineer. It is highly specific (enzymes tend to only cause lysis to a specific group of bacteria, thus any contaminating growth remains intact and can be excluded at this stage), requires very mild operating conditions, has low energy and capital investment requirements (this method is generally performed in a simple stirred vessel at around room temperature), and avoids harsh physical conditions such as high shear forces associated with mechanical disruption, thus safeguarding the product.

Three types of bacteriolytic enzymes have to date been identified: glycosidases (they split the polysaccharide chains of the peptidoglycan backbone), acetylmuramyl-L-alanine amidases which cleave the polysaccharide-polypeptide junction, and endopeptidases, which split polypeptide chains within the peptidoglycan (Andrews & Asenjo, 1987).

Of these the most popular example is hen egg white lysozyme, a glycosidase, the only bacteriolytic enzyme currently available commercially for large scale use. This enzyme works by attacking the β-1,4 linkages of the polysaccharide chains of the peptidoglycan layer, which, as has already been stated, falls between the outer and cytoplasmic membranes of Gram-negative organisms, and is responsible for providing

the cell's rigidity. Without the petidoglycan layer the outer membrane in particular is extremely sensitive to any other disruption technique. Although *E.coli* is directly susceptible to the action of this enzyme, to obtain a substantial effect it is first necessary to treat the cells with EDTA or Triton-X100, in order to permeabilise the outer membrane and expose the peptidoglycan layer to the enzyme. Once this has been achieved, 20-30 minutes at pH 6-7 and a temperature of 25-35^{0}C is sufficient to break effectively the peptidoglycan layer (Andrews & Asenjo, 1987). If the cell is subsequently exposed to an osmotic shock the outer membrane will rupture and fall away, leaving the cytoplasmic membrane intact as a spheroplast cell. This has been confirmed by transmission electron microscopy (Andrews & Asenjo, 1987).

At first glance this may appear the perfect strategy for release of a periplasmically expressed product from a bacteria. However, there is a major problem associated with it. For this treatment to work well all the cells in a harvested suspension must come into contact with the enzyme. Because of it's expense, in order to be economically viable, the enzyme can only be added in very low quantities (in the order of 500μg/ml).Thus the efficiency of mixing in the lysis vessel at a microscopic level becomes crucial. To date it has proved difficult to spheroplast more than 70-80% of cells in a suspension using this technique, probably due to insufficient mixing. This is an unacceptably high loss of yield before purification begins. There is also the additional processing requirement of removing the lysozyme at a later stage. However, the advantages of accurately rupturing just the outer membrane to release a periplasmic product, and thus leaving the bulk of the cell, and it's contents, intact are obvious, particularly as the spheroplast remainder can then be removed easily in a centrifugation or microfiltration step.

1.3.1.2 Mechanical Cell Disruption

1.3.1.2.1 Liquid Shear Devices

As the name suggests, liquid shear devices achieve their disruption through the shearing action of the liquid surrounding the cells. In general, despite the high capital

investment and energy costs associated with this type of equipment, the advantages of ease of use and control have made them by far the most usual method employed in industrial cell disruption. As such there are three equipment designs applicable for this task: the dispersion or colloid mill, the bead mill, and the high pressure homogeniser, machines which have all been developed from an original role of particle reduction or emulsion formation in traditional industries.

Dispersion and Colloid Mills

Dispersion and colloid mills were originally developed for both the disruption of lightly bonded agglomerates and emulsion formation. They consist of a smooth or grooved rotor in the shape of a cone or disk. This rotates at speeds of approximately 3600rpm. The rotor is surrounded by a casing (the stator) at a distance of around 50μm. Because of very rapid non-uniform acceleration of the fluid in the mill large liquid shear forces are set up which have been demonstrated to be capable of cell disruption (Wang *et al*, 1978). Very high throughputs are also obtainable (10 m^3/h) and the machine can be operated continuously. However, this technique is not generally employed for microbial disruption because of the heating effect produced when large amounts of energy are dissipated in the form of heat, which is sufficient to denature the protein product (Wang *et al*, 1978). Rotor wear is also a problem.

Jet Impingement

Cell disruption in a jet impingement device is again due primarily to liquid shear. Jets of cell suspension are projected at high velocity, either at a solid surface, or in a counter-current model, at each other. The fluid stream is extremely turbulent, causing both liquid shear disruption and the cells to grind upon each other (Snow *et al*, 1988). The impingement on the solid surface or the other jet is also thought to play a major role in the disruption obtained with these devices. Engler and Robinson (1981) demonstrated the disruption of *Candida utilis* using a high velocity jet impinging on a

stationary plate while Becker, Ogez & Builder (1983) have shown it to be a first order process in respect of the number of passes, not dissimilar to the high pressure homogeniser. Morphology of the micro-organism, nozzle geometry, jet velocity and number of passes have all been shown to influence disruption, and counter-current designs are now available which compare favourably to the homogeniser. Disruption of up to 95% for recombinant *E.coli* in a single pass has been reported.

High Pressure Homogenisation

High pressure homogenisation, or HPH, is the best known and most widely used method of large scale cell disruption currently available. It works using a valve and impactor arrangement, whereby the cell suspension is pushed by a positive displacement pump through a non-return valve and into the main homogeniser cylinder. The piston then forces the suspension through the adjustable annular gap of the discharge valve where it impinges on an impact ring. The discharge pressure is regulated by a spring loaded valve rod which moves the valve in relation to the valve seat, and is typically up to 1200 bar.

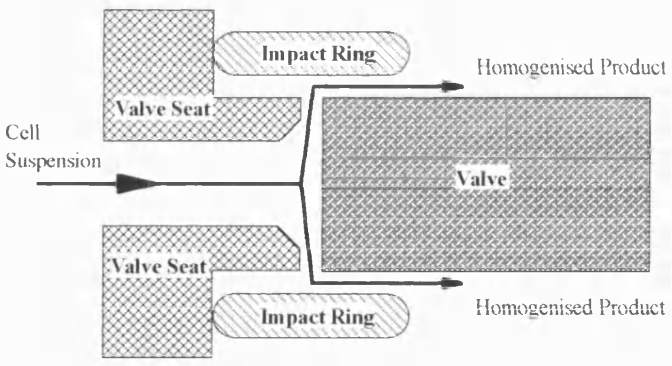

Figure 1.3: The High Pressure Homogeniser

Most of the work seeking to characterise the high pressure homogeniser has been carried out using yeast (Engler & Robinson, 1981; Follows, Hetherington *et al*, 1971a; and Follows, Hetherington *et al*, 1971b). From a study conducted using

Saccharomyces cerevisiae (Follows, Hetherington *et al*, 1971b), the following relationships have been demonstrated:

- Protein release, and thus cell disruption, is temperature dependent and increases with it.
- Protein release is independent of biomass in the range 84-170 kg/m^3 dry weight, although it exhibits a dependence at higher concentrations
- Enzymatic activity does not generally decrease with homogenisation, although enzymes may become deactivated due to temperature rises (Follows, Hetherington *et al*, 1971a)
- The rate of specific enzyme release with respect to total protein release is independent of homogenisation pressure, but is dependent on the location of these enzymes within the cell: periplasmic enzymes are most readily released, followed by cytoplasmic enzymes. Most difficult of all are membrane bound enzymes (Follows *et al*, 1971a).
- Protein release R is first order with respect to the number of passes N

$$-\frac{dR}{dN} = k^a R$$

- The dependence of protein release on operating pressure can be expressed as a function of the pressure. Therefore, the above equation becomes:

$$\ln\left(\frac{R_m}{R_m - R_h}\right) = kNP^{a_h} \qquad \textbf{(1.3)}$$

where R_h = protein released (kg protein/kg biomass)

R_m = maximum protein available (kg)

k = rate constant (-)

P = pressure (bar)

a_h = exponent (-)

N = number of passes (-)

These relationships have subsequently been confirmed for Gram-negative bacteria (Harrison *et al*, 1990). It has, however, been observed that the pressure dependence virtually disappears at very high pressures (in excess of 50 M Pa), when disruption becomes entirely independent of biomass, allowing very high cell concentrations to be used (Engler and Robinson, 1981).

This relationship has been studied further by Siddiqi who developed the following equation to relate particle size to both homogeniser pressure and the number of passes the feed suspension is exposed to;

$$\log_e\left[\frac{1}{(d_{50})}\right] = k_D N^{\beta} \Delta P^{\alpha} \qquad \textbf{(1.4)}$$

where ΔP = $P-P_{th}$ (barg)

k_D = breakage rate constant ($barg^{-\alpha}N^{-\beta}$)

P_{th} = threshold pressure (barg)

d_{50} = mean particle diameter (m)

Siddiqi found that for yeast a value of $\beta = -0.4$, $\alpha = -1$ and $k_D = 670$ $barg^1$ $pass^{0.4}$ when used in the above equation provided an accurate model of disruption in the homogeniser (Siddiqi, 1997).

Keleman and Sharpe (1979) used a homogeniser with a ball and seat valve, (the Stansted disrupter) to deduce the relative force required to disrupt a range of micro-organisms. All that were investigated showed a sigmoidal disruption profile with respect to disruption pressure: little disruption was observed below a threshold pressure. However, distinct differences in the ease of disruption appeared, with Gram-negative bacteria the easiest to disrupt, followed by Gram-positive and filamentous fungi. Most difficult were yeast cells. Again, the ease of disruption can be related to cell wall strength, with factors such as composition, growth-phase, size and shape being important (Harrison *et al*, 1990).

There is currently no uniform view as to the precise mechanism of disruption which occurs in a homogeniser, with high shear conditions, sudden decompression causing cavitation, turbulence and impingement all believed to exist within the machine.

Ayazi-Shamlou, Siddiqi and Titchener-Hooker (1994) developed a model based on disruption through elongational shear and dependant on the level of energy dissipation within the valve as turbulent eddies of a scale smaller than the yeast cells studied. This leads to fluctuating pressure differences acting on the surface of the cell, causing elongational shear and disruption in the high shear stress areas close to the valve rod and the impact ring. They subsequently found that experimental data fitted the model very well, although they were unable to relate this to proposed strength data on the organism obtained using micromanipulation (Roberts *et al*, 1994).

Conversely, by modifying the impact ring and particularly increasing the distance before it, Keshavarz-Moore *et al*, (1987), have demonstrated that disruption decreases drastically with increasing impact distance, a finding that led them to conclude that up to 80% of the disruption obtained in the machine was due to impingement. However, it is worth noting that the increase in impact distance also significantly increases the volume over which power is dissipated within the machine, and thus would significantly decrease the shear stresses developed.

Whatever the precise disruption mechanism, it seems certain that all these methods play a part in the disruption obtained, although as yet it is not clear which is the major factor responsible for it.

The homogeniser does tend to be an "all or nothing" tool, however. It is used industrially to break open the entire cell. Thus any purification advantage obtained by Gram-negative periplasmic expression is lost by not being able to disrupt the outer membrane only, although partial success in releasing only periplasmic contents using mild disruption conditions (2 passes at 200 bar) has been reported (Harrison, Ukar *et al*, 1994).

1.3.1.2.2 Solid Shear Devices

High Speed Bead Mills

Most popular of all the solid shear disruption devices available are the high speed bead mills. They provide grinding and dispersion through the motion of glass (or sometimes plastic) beads which are accelerated by rotating disks or impellers contained within a horizontal or vertical grinding chamber. The chamber must be cooled, usually by a jacket, to remove the heat generated and avoid deactivation of enzymes: the beads are retained within the grinding chamber by a sieve plate.

The effect of high speed bead mills, originally developed for the paint industry, has been studied on yeast (Currie, Dunnill & Lilly, 1972; Hedenskog, Mogren & Enebo, 1970; and Schutte *et al*, 1983) and both Gram-negative and Gram-positive bacteria. The disruption is obtained through an extremely complex process involving the number and energy of the impacts, the energy transfer to the grinding beads, liquid shear, mixing and general hydrodynamics. The process parameters concerned are bead diameter, loading and density, feed suspension concentration and flow rate, agitator speed and configuration, and grinding chamber geometry. As always, the residence time, cell wall structure, size, shape and state of the organism are also factors.

It has been found that small beads are generally more effective, although larger beads can be employed to release preferentially periplasmic enzymes (Schutte *et al*, 1983). Total disruption of bacteria requires very small beads (they occupy only approximately 1% of the volume of a yeast cell) and this has reduced the use of bead mills in this application (small beads have a tendency to float). This necessitates an increased residence time and a large number of passes for complete disruption to be obtained.

First order kinetics can be used to model breakage in a bead mill, with the rate of protein release directly proportional to the amount of unreleased protein. For a batch reactor this is described by the equation

$$\ln\left(\frac{R_m}{R_m - R}\right) = k_b t_b \qquad (1.5)$$

where R_b = protein released (Kg protein/Kg biomass)

R_m =maximum protein available for release (Kg)

k_b = first order rate constant (-)

t_b = residence time (s)

Similar expressions exist for continuous operation, viewing the mill as a series of continuous stirred tank reactors (CSTR).

Bead mills offer very real advantages when seeking to release a granular product, in that the granules will be thoroughly separated from any membrane association which may otherwise exist. However, for bacterial disruption the long residence times, very small bead sizes, the danger of ground bead chippings contaminating the product stream, and the micronisation of the cell debris, all combine to make the bead mill an unattractive choice.

Having considered the primary methods employed for cell disruption in the bioprocess industries we now turn to the other focus of this thesis, that of solid-liquid separation. Again, although the unit operation studied in detail is high speed disk stack centrifugation it is useful to present a summary of the other methods available, and alternative designs of centrifuge in particular.

1.4 Solid-Liquid Separation in Biotechnology

In the bioprocessing industries there are currently two basic techniques employed to separate solids (whole cells, cell debris, flocs and precipitates) from the suspending liquid streams. These are filtration (cross flow microfiltration and ultrafiltration, or simple depth filters) and centrifugation. Although more novel techniques, such as the

application of magnetic particles, are beginning to be investigated they are not expected to make a major impact on industrial processes in the near future.

A centrifuge has a "one off" purchase cost in comparison to a membrane, which must be renewed on a regular basis. Because of this it is generally considered most cost effective to employ a centrifugal separator in large volume or high throughput applications, where a large membrane area would be needed. This is provided that the centrifuge will perform satisfactorily (centrifugal separation operates on particle size and density difference (between particle and surrounding liquid (see Chapter 3)) and thus is subject to operating limits that membrane systems do not suffer). However, both centrifuges and membrane-based systems may offer complications from a regulatory perspective which must be considered by the process designer. This thesis focuses on a specific type of centrifuge, the high speed intermittent discharge disk stack centrifuge, and the disruptive forces associated with it. A short introduction to the types of centrifuge available and their differing applications will now be given.

1.4.1 Centrifuge Selection

Industrial centrifuges can be subdivided into two major categories; clarifiers and separators. Clarifiers are used to separate two or more liquid phases from each other. More common in the bioprocessing industries are separators, which are used to remove solid particles from liquid streams. As such this introduction will focus on this type of machine.

Separators can be divided into two basic designs; those capable of solids discharge during operation, and more basic non-discharging models. The complicated designs necessary to eject solids during operation usually result in a reduction in the speed of rotation and hence centrifugal force. Therefore the designs which offer the best clarification frequently operate in a batchwise manner. Every time the solids capacity is reached they must be taken off-line and manually cleaned. Machines capable of discharge are frequently not capable of removing very fine particles (such as cell debris downstream of a homogeniser) without the use of very low volumetric throughputs;

furthermore, frequent discharge may lead to a loss of supernatant with the solids which could produce an unacceptable yield over the unit operation. Thus solids loading must also be considered when selecting a centrifuge for a specific application. Below is a discussion of the most common designs of centrifuge and examples of their industrial application.

1.4.1.2 The Tubular Bowl Centrifuge

The simplest of all centrifugal separators is the tubular bowl centrifuge. This design is based on a high speed rotating tube into which a feed stream is introduced through a nozzle which is used to distribute the flow evenly around the cylinder. Extremely high relative centrifugal forces can be achieved in this type of separator because of it's simple design (up to 38,000 G on a pilot scale or 17,000 G in a full scale model). However, this high separating force is somewhat negated by an intrinsically short residence time as the length of the cylinder is limited by the mechanical stresses imposed when driving it at such speeds. Furthermore the conventional tubular bowl centrifuge cannot be discharged during operation, requiring a time and labour consuming strip down and manual solids removal ("dig out") which presents both biosafety and product handling difficulties. Because of this they are commonly utilised only when such high G forces are required for satisfactory separation, or where a low solids content is present in the feed suspension (1-5%). This has lead to them finding specialist applications in the blood processing industry, and for fine debris separation after homogenisation.

It is worth noting that a new company, Carr Powerfuge™, have just entered the market with a design of tubular bowl centrifuge which *is* capable of solids discharge during operation. Although the machine is considerably more complicated than the standard design it is still capable of generating high G forces. It is beginning to find a use in blood fractionation but has yet to attain general acceptance in a notoriously conservative industry.

1.4.1.3 The Multichamber Centrifuge

The next most complicated design is the multichamber centrifuge. This is basically an improvement on the tubular bowl with the aim of increasing the separating area, residence time and solids capacity. It consists of a series of nested cylinders, each with a slightly larger radius than it's inner neighbour, forming chambers. Fluid enters through the centre of the machine and flows through each chamber in turn until finally being discharged after passing through the outer-most chamber. Pilot scale machines will typically contain four chambers, whilst larger industrial separators will contain 8-10 such segments. In this manner the flow path of liquid through the machine is extended, along with the residence time and solids holding capacity. However the more complex design, with the need for the dividing cylinders to be firmly held in place, reduces the maximum rotational speed available with between 8000 and 12000 G being typical relative centrifugal forces.

Again it is not possible for such machines to be discharged during operation, and the increased complexity of design and solids holding capability makes the strip down and dig out of a multichamber centrifuge more complicated and time consuming than that of a similar scale tubular bowl design. However, this is counterbalanced by the increased solids capacity which allows larger or more concentrated batches to be processed. Multichamber centrifuges are found extensively in the blood processing industries and are used in general bioprocessing applications where one or several such machines have sufficient capacity to process a complete batch without the need to remove solids from the bowl.

1.4.1.4 The Disk Stack Centrifuge

The disk stack centrifuge is considerably more complicated than either type so far discussed. It exists in two basic formats; the nozzle separator, where the solids are continually ejected from the periphery of the bowl, and the intermittent discharge design, where solids are ejected in discrete batches when required.

Separation in both designs occurs between a stacked series of conical disks. Because flow is evenly divided between all the disks in a stack a large area for separation can be contained in a low footprint machine. Typically an industrial separator contains up to 250 disks, and a pilot scale machine 50. The disks are separated by as little as 1 mm in order to minimise the distance a particle must migrate under the action of centrifugal force to be separated from the liquid stream.

Both the nozzle and the intermittent discharge variants are capable of solids discharge during operation. In both cases the solids are separated to the outside of the bowl whilst liquid is discharged through a centripetal pump at the centre of the machine. The nozzle separator discharges solids under centrifugal force continuously as they arrive at the periphery of the bowl. In the more common intermittent discharge machine the solids ejection ports are uncovered to allow solids discharge only when the bowl is full; the desludging operation is triggered by an operator, a timer or a reduction in supernatant quality.

The theory and operation of the disk stack centrifuge is explained in greater detail in Chapter 3.

Because of the complicated design of such machines again speeds of rotation are restricted, with pilot scale machines designed to operate at relative centrifugal forces of up to 10,000 G but industrial separators often developing lower G forces. However, because of the use of close fitting disks very high residence times and separating areas are achievable. Also the ability of such designs to release collected solids during operation means that theoretically no limits as to batch size or solids concentration are imposed. In practice, however, this is not the case. Disk stack centrifuges have only a limited solids capacity, and the processing of solids streams containing more than 10-20% (intermittent discharge) or 20-30% (nozzle) solids (v/v) is not recommended because of the short length of time between discharges (intermittent type) or problems with nozzle blockage (nozzle type). However, for many bioprocessing operations, particularly cell harvest and precipitate/floc removal, such machines are the perfect choice, with the capability to operate all day processing large batches with minimal operator intervention. In addition, modern disk stack centrifuges are manufactured to

allow the validateable CIP and SIP procedures vital for modern biopharmaceutical manufacture.

1.4.1.5 The Scroll Decanter Centrifuge

The last major type of separator in use in the bioprocess industries is the scroll decanter. This design again is capable of solids discharge during operation but operates in a radically different manner to the disk stack centrifuge.

Fluid is introduced into a horizontal rotating cylinder and solids are separated to the outside of the drum. Within the cylinder is an Archemedian screw rotating at a different speed. This has the effect of transporting the collected solids along the drum towards the solids discharge point. Solids are driven out by the screw after passing up a "beach" which allows dewatering of the stream. Liquid is discharged at the other end of the rotating drum.

Such machines are not capable of rotating quickly enough to generate high relative centrifugal forces, with 5,000-6,000G being typical values. However, they are capable of processing streams containing up to 80% solids, a far higher figure than any other common design. The low RCF and high solids handling capacity means that scroll decanters are often not suitable for biopharmaceutical processes; they are, however, extremely common in waste processing, particularly in sewage and industrial sludge applications. Because of this they are available at a very large scale capable of processing many hundreds of m^3 per hour.

1.5 Typical Periplasmic Process

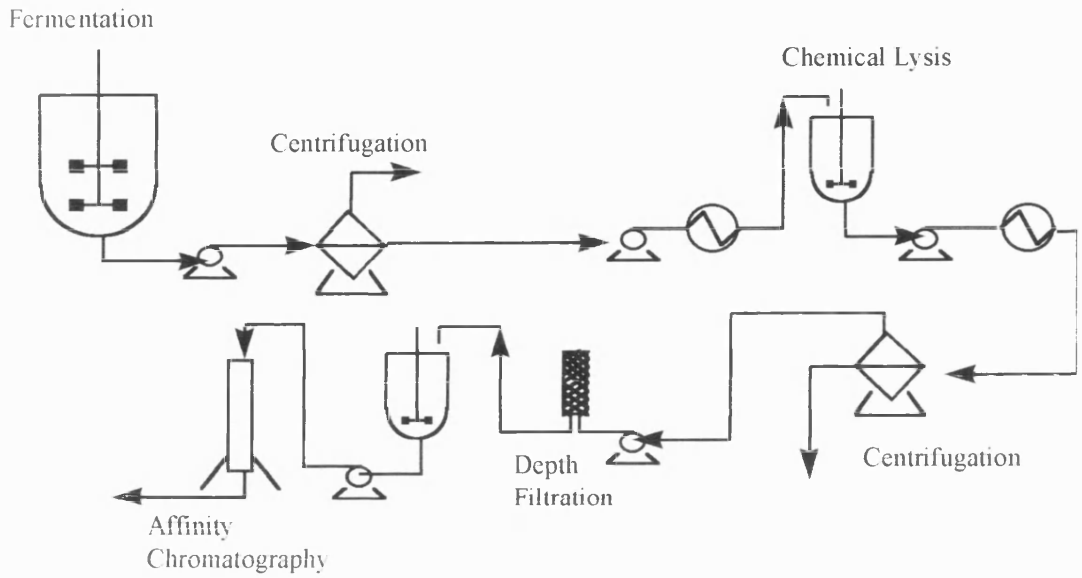

Figure 1.4: Flowsheet of a typical process for recovering a periplasmically expressed product

Figure 1.4 above shows a typical recovery chain designed to capture and purify a target protein that has been expressed to the periplasmic space of a Gram-negative organism, typically *E.coli*. After the upstream fermentation there is a cell harvest step to concentrate the biomass and reduce the volumes passed down the processing chain. This will typically be accomplished using a disk stack centrifuge and achieve a ten-fold concentration. Next a chemical lysis is employed to rupture the outer membrane, releasing the product whilst leaving the inner membrane intact as a spheroplast. This is usually performed at a given temperature (either elevated in the case of EDTA or reduced when working with lysozyme) and thus heat exchangers are necessary. The final primary step is to remove the spheroplasts intact before passing the liquid stream to chromatographic purification. This can be accomplished using a high G-force centrifuge at a low volumetric throughput (tubular bowl designs are particularly suited to this) or a open ultrafiltration membrane. Finally a depth filter may be employed as a final polishing step to avoid fouling of the chromatography column.

1.6 Thesis Layout

The following chapters present the experimental work, results and conclusions obtained during the course of this project. Each chapter is essentially self-contained, with an introduction containing necessary background information and theory, materials and methods, results and discussion, and conclusions. Chapter 2 covers the fermentation development and characterisation conducted as part of this work. Chapters 3 and 4 deal with the interaction between a pilot scale high speed intermittent discharge disk stack centrifuge and both whole cell *E.coli* fermentation broth and polyethylene glycol precipitates of yeast homogenate respectively. Chapter 5 deals with a theoretical estimate of the destructive forces generated within such centrifuges and the application of laboratory scale mimics to reproduce such forces. Finally Chapter 6 summarises the effects observed both in the pilot plant and the laboratory, and draws conclusions as to the causes of disruption to biological particles observed and methods of operation of such machines to minimise yield loss during processing.

1.7 Aims of Thesis

This thesis sets out to establish;

- A well characterised and reproducible large scale *E.coli* fermentation.
- The disruption caused to both whole cell *E.coli* and polyethylene glycol 8000 precipitates of yeast homogenate during passage through a high speed disk stack centrifuge.
- The regions of the centrifuge responsible for such disruption and the mechanisms causing it.
- Laboratory scale mimics of these disruptive regions as a tool for rapid bioprocess development.

2.0 FERMENTATION

2.1 Introduction

This chapter describes the techniques used to produce whole cell feedstock for the pilot scale centrifugation trials of Chapter 3. Section 2.2 covers the details of strain selection, and some of the previous work undertaken using *Escherichia coli* JM107 pQR126. Section 2.3 contains a review of factors affecting product expression and plasmid stability. The protocols and materials used during the fermentations are given in 2.4, and results are given in Section 2.5. Finally, a review and discussion are presented in section 2.6.

2.2 *Escherichia coli* JM 107 pQR 126

2.2.1 Choice of Organism

The microbial system used in this study was chosen to meet several key parameters;

- ability to measure cell breakage and to distinguish between partial and total disruption
- compatibility of fermentation with current industrial practice
- fast production of biomass
- reproducibility
- ability to scale up to 150L scale and still operate "single handed".

Of these conditions the first two were most important; unless the cells could be used for centrifugation trials quantifying disruption under varying conditions, (Chapter 3), the fermentation would be of no use. Similarly, unless the cells were produced in a

realistic manner the centrifugation results could not be guaranteed relevant. The second three points were also highly desirable. The faster the biomass could be produced, the more experiments could be conducted. The more reproducible the fermentation, the easier it would be to compare downstream processing performance between batches. Finally, production of 100-150L of broth per batch would allow a range of centrifugation conditions to be examined utilising the same feed stock.

In order to reduce fermentation development time, it was decided that a system already in use at UCLACBE should be employed. Several appropriate systems were available, however the system that was most widely researched and fulfilled all of the above needs was that of an α-amylase producing *E.coli*.

A series of genetically modified *E.coli* K12 strains were available within the department. The plasmid added to the cells encoded for the production of periplasmic α-amylase (for the commercial advantages of periplasmic expression, see Chapter 1) originally cloned from *Streptomyces thermoviolaceus* CUB 74 within UCL's Department of Biochemistry and Molecular Biology (Bahri and Ward, 1990, and French, 1993). α-Amylase is a thermostable endoamylase which hydrolyses α-(1⇒4)-glycosidic linkages of amylose and amylopectin molecules of starch. It is widely used in the paper, textile, starch, distillation and brewing industries for the liquefaction of starch (Mukhopadhyay, 1992). There were a number of different strains available but the one most studied and showing the highest overall level of α-amylase production was JM107 pQR126 (French, 1993, and Turner, 1993).

E.coli is a rapidly growing Gram-negative bacteria, capable of reaching cell densities in the region of 10-14 gL^{-1} (dry cell weight) within 24 hours in a batch mode. This corresponds to 2-3% solids on a volume-volume basis, making the cell suspension very suitable for recovery in a disk stack centrifuge (Chapter 3). Furthermore, in comparison to a *Streptomyces* type organism, which may take up to a week to produce through fermentation, the system met the requirement that biomass must be produced for further experimentation quickly.

Previous work had shown the presence of the enzyme α-amylase in the media, the periplasmic space, and the cytoplasmic region of such cells (French, 1993, Turner, 1993, and Fisher, 1997). Although the genetics of the system were not targeted specifically for the secretion of α-amylase into the media, the permeability of the outer membrane (particularly in genetically modified organisms), the limited capacity of the cell periplasm for heterologous protein and the lysis of a proportion of the cell population during a fermentation cycle were believed to be responsible for the presence of extracellular enzyme. Similarly, any α–amylase detected in the cytoplasmic fraction of the cell after a chemical release of the periplasmic contents was thought to have been retained in the complex structure of the peptidoglycan layer (see Chapter 1) part of the periplasm (Turner, 1993). This was because the enzyme was produced with a terminal signal peptide that rendered it inactive. This peptide was only cleaved off on passage through the cytoplasmic membrane. Therefore, it was not possible for active enzyme to exist in the cytoplasm of a cell without having passed back through the cytoplasmic membrane, an action which was believed to be impossible. By using a sensitive assay it would be possible to detect release from the periplasmic space of the cell by looking solely at changes in α-amylase titre. In addition, there were many other well defined assay techniques available for detecting wholly intracellular *E.coli* enzymes also enabling release from the cytoplasm to be quantified purely on enzyme titres. Thus the organism met the requirement for use to measure cell disruption accurately during processing.

The plasmid has a high copy number and expression is under the control of the *lacZ* promoter. Much reduced levels of repressor are present when a suitable carbon source is chosen, thus induction is unnecessary; the product is constitutively expressed. It also contains a gene for kanamycin resistance, which allows cell selection (a cell without a plasmid would die in the presence of the antibiotic) and served as an extra precaution against contamination during fermentation.

2.2.2 Fermentation Development and Choice of Protocol

French (1993) developed a range of K12 *E.coli* hosts for the pQR126 plasmid, as well as a quick and simple technique for fractionation of the cells, and a robust assay for the measurement of the heterologous α–amylase subsequently produced. Small pilot-scale complex medium fermentations were performed, and the fractionation technique scaled to allow the recovery of the periplasmic product.

Turner (1993) used JM107 pQR126 as the test system for the on-line analysis of fermentations. As part of the work Turner developed protocols for defined media fermentations including both batch and fed-batch techniques. Galactose was used as the carbon source in preference to glucose as the *lac* operon is subject to catabolite repression in the order;

gluconate>glucose>fructose>maltose>lactose>galactose>glycerol>succonate

(Dawes and Sutherland, 1992).

Fisher (1997) and Pierce (1997) subsequently used the same organism in a range of downstream processing studies, and continued the development of both the fermentation medium and the operational protocols best suited to the cell. As part of this work the carbon source was altered to glycerol, a cheaper and even less repressive chemical than galactose. Full fed-batch and complex medium protocols were also developed.

Having selected the test organism there still remained the decision on which fermentation strategy would be employed in this work. Two choices remained, complex or defined media and batch/fed-batch fermentation strategy.

Table 2.1 overleaf summarises the advantages/disadvantages of a defined medium over a complex medium. Not all points are strictly relevant to the decision made with this system, however they are significant industrially and as such are included.

Factor	Defined medium	Complex medium
Cost	Not dependant on seasonal or climatic factors. Cost optimisation possible-multicomponent.	Seasonal and climatic factors alter cost and quality of product.
Component quality	Less variation, generally more controllable, can specify requirements more clearly.	If using by-product from another process then this can cause variability.
Batch variation	Usually many components, care to ensure correct medium make-up (use medium concentrate)	More variation due to changes in component quality.
Sterilisation	Salt precipitation may require separate sterilisation: often need to sterilise the carbon source separately.	Normally the complete medium is sterilised in place: insoluble material present may cause problems.
Contamination (due to holding)	Not likely-add carbon source immediately before inoculation.	Likely if sterilisation imperfect as all growth components in place.
Cell yield	Potentially higher, can develop fed-batch protocols.	Difficult to identify limiting factor giving lower cell yields.
Fermentation monitoring	On-line monitoring techniques more easily applied (HPLC etc.)	Higher protein/amino acid content make monitoring difficult.
Fermentation predictability	Prediction is generally possible using standard models.	Growth information more difficult to obtain thus modelling imprecise.
Downstream processing	Only fermentation by-products, no "unnecessary" foulants.	Contains many potential foulants.
Product quality	"Clean" product.	Contaminating protein may be difficult to remove.
Product stability	May have lower stability as cells utilise the heterologous product when other nutrients are depleted.	More stable, evidence that less periplasmic material is leaked into the medium (Harrison *at al*, 1996).

Table 2.1: Advantages/disadvantages of defined versus complex medium (after Fisher, 1997).

The table shows that overall defined medium is clearly the strategy of choice, and industrially most biopharmaceutical processes, where quality control of feed stocks is essential for FDA approval, and cost of feed stock is not necessarily the overriding issue, are turning to defined systems to gain the measure of control and reproducibility necessary in a licensed process. Therefore, the use of a defined medium was adopted for this work.

The final choice was between batch and fed-batch growth techniques. Turner (1993), Fisher (1997) and Pierce (1997) had successfully developed fed-batch fermentation protocols for *E.coli* JM107 pQR126, as well as a standard batch growth protocol. Fed-batch fermentations, where a limiting substrate, usually the carbon source, is fed to the fermenter during operation offers several key advantages over a batch growth strategy. Firstly it is possible to obtain very much higher biomass concentrations than are achievable through a more traditional approach. Most organisms suffer from growth inhibition in the presence of large quantities of carbon source. By feeding on a "just in time" approach biomass concentrations as high as 35-50 gL^{-1} (DCW) are typically attainable. This contrasts to the 10-14 gL^{-1} that can be reached using a batch approach (Harrison, 1996). Furthermore the feeding operation offers an opportunity to control growth rate which can lead to higher product expression levels (see following section). These factors are making fed-batch fermentation increasingly the industrial approach of choice. However, fed-batch operations are inherently more complex, requiring a high degree of system characterisation and reliable automation if the strategy is to be successful with minimum "hands-on" operator input. Because the purpose of the fermentation in use here was simply to produce biomass for downstream processing experimentation, and the need therefore to use as simple as possible a protocol, it was decided to operate a batch-growth technique.

2.3 Factors Affecting Product Expression

A bacterial cell can be regarded as an extremely complicated self-replicating factory producing a useful product (either a naturally occurring protein or chemical, or a heterologous foreign protein produced via genetic manipulation of the organism). As such the precise biochemical mechanisms responsible for cell growth and particularly foreign protein formation are extremely complex. Understanding has increased dramatically over the past several decades, particularly in well studied systems such as *E.coli*, but there are still many uncertainties leading to a need for extensive pilot experimentation whenever a new organism is cultured.

There are, however, several factors that are widely recognised to effect production of a target protein in *E.coli*, and a brief review of these is presented below.

2.3.1 The Crabtree Effect

When *E.coli* is grown on certain carbon substrates (such as glucose) in fully aerobic conditions acetic acid is produced as a by-product. This occurs under two different, but very closely related, conditions. Firstly when the growth rate of the organism is too high, and secondly when the concentration of carbon source in the medium exceeds a characteristic threshold level (Luli and Strohl, 1990). It is this that is known as the bacterial Crabtree effect. This was first identified in yeast, where excess glucose under aerobic conditions leads to overproduction of ethanol. There are several reasons given for this effect. Firstly, it may be caused as a result of the limited capacity of oxidative metabolism (and perhaps the TCA cycle) being exceeded (Han *et al*, 1992). Secondly, the formation of TCA cycle enzymes are repressed resulting in a high intracellular $NADH + H^+$ concentration (Doelle *et al*, 1982 and Rinas *et al*, 1989). Although the pathways leading to the production of acetate are energetically unfavourable it does give rise to a faster growth rate (Han *et al*, 1992). *E.coli* may therefore have evolved to produce acetate to enable faster growth (Holms, 1986).

Acetate production in *E.coli* has also been found to be effected by the type of medium used. Han *et al* (1992) found that small amounts of yeast extract added to defined medium cultures reduced the production of acetate by lowering the specific glucose uptake rate (through lowering the cells anabolic requirements). However, changing to a full complex medium resulted in acetate production at lower specific growth rates than in a defined system, and a maximum production rate approaching twice that attained with a defined medium (Meyer *et al*, 1984).

2.3.2 Affects of Acetate Production

There are four main reasons why the production of acetic acid in *E.coli* is undesirable. The first and most obvious is that the diversion of carbon source to this pathway is inefficient, utilising nutrients that could be employed in useful biomass or product formation. Secondly, above a concentration of 1.2-1.4 gL^{-1} (Landwall and Holme, 1997 (a) and (b)) dependant on strain, acetate actually inhibits cell growth through an uncoupling of the cell's metabolic processes. This effect has been found to be most pronounced in recombinant organisms, which are already under metabolic stress producing foreign protein (Koh *et al*, 1992). Thirdly it is well documented that the presence of a high concentration of acetate in recombinant *E.coli* fermentations can have a major effect on the production of recombinant protein. This is caused by the uncoupling of the cell's metabolism in the same manner as that responsible for the above effect, which will have an impact on all cellular processes including that of product expression. It has been observed in many systems including β-galactosidase and human growth hormone production (Shimizu *et al*, 1988, and Bech, Jensen and Carlsen, 1990). The final reason is that excess acetic acid reduces the pH of the culture and necessitates the addition of alkali to maintain the culture pH. If the controlling agent is ammonium hydroxide, this has been shown to be inhibitory to cell growth at very low concentrations (Thompson *et al*, 1985). If the alkali is salt based, such as sodium hydroxide, then excess salt concentrations have been shown to reduce the expression of recombinant protein (Bech Jensen & Carlsen, 1990).

These different mechanisms are all implicated in reducing product production in the presence of acetate so it is clear that any growth conditions leading to an increase in the levels of acetic acid in an *E.coli* culture are undesirable.

2.3.3 Specific Growth Rate

Controlling the specific growth rate (in a fed-batch fermentation) or the dilution rate (in a continuous culture) to a low level has been observed to improve yields of a recombinant protein (Fu *et al* 1993, Brown *et al* 1985, Turner 1993). Similarly, specific growth rates decrease linearly with increasing concentrations of both intracellular plasmid contents and recombinant protein i.e. higher plasmid copy numbers reduce specific growth rate (Summers, 1991), probably because of the high levels of protein being manufactured. Cells producing high levels of recombinant protein can suffer severe stress and in extreme cases die (Kim and Ryu, 1991). Plasmid concentration in turn will effect production of recombinant protein (Zabriskie and Arcuri, 1986) although regulatory mechanisms may impose an upper limit, and promoter strength may have a greater influence (Kim and Ryu, 1991). Therefore, it can be seen that generally a low specific growth rate will result in increased production of recombinant protein, and many researchers conducting fermentations at such growth rates to avoid acetate production may also have seen productivity benefiting from the above effects (Turner, 1983).

2.3.4 Plasmid Stability

Another important issue effecting production of recombinant protein in genetically modified organisms is that of plasmid stability, a function of plasmid genetics strongly influenced by the genetics and physiology of the host organism (Zabriskie and Arcuri, 1986). Another factor is the type of plasmid present, e.g. low or high copy number.

Productivity of a recombinant plasmid has been observed to fall with age of culture (Nam *et al*, 1987). This is believed to be due to the mechanism of structural instability, the process of insertion, deletion and rearrangement of DNA within a plasmid over generations (i.e. mutation). This is inherently difficult to detect as it results in cells with the same growth characteristics and phenotype as those carrying perfect plasmids. It has, however, been linked to the growth environment of the cells (particularly glucose-limiting conditions (Zabriskie and Arcuri, 1986)).

A second and more common problem is that of segregational instability. This results from defective partitioning during cell division, and has been shown to increase at high specific growth rates (Warnes *et al*, 1991). Wild type, low copy number plasmids generally show excellent stability in contrast to high copy number recombinant plasmids (such as employed in the organism used in this study) which all tend to shed plasmid over the course of a fermentation. Obviously, cells containing fewer plasmid copies will have a competitive growth advantage over those containing many copies (because of the extra resources that are necessary to maintain the plasmid copy number). Over the course of a fermentation plasmid copy numbers per cell tend to fall in fast growing cultures because of the lack of sufficient time for each daughter cell to return to a full complement of plasmid copies before the next division cycle begins. Thus segregational instability leads to a reduction in plasmid copy number over time. Cells containing no plasmid at all will have the biggest advantage, having no extra replication to undertake before entering the next division cycle. Obviously, these effects will lead to substantially reduced product expression, or eventually to none at all.

Segregational instability is commonly improved by including the resistance marker for an antibiotic on the plasmid and the inclusion of the antibiotic in the fermentation medium. Thus cells containing no plasmid will not be able to survive. This technique has the obvious drawbacks of introducing an antibiotic into the medium, which must be removed from the product stream in subsequent downstream processing operations, and exposing workers to quantities of a biologically active chemical during the preparation of the medium. Another selective approach which has proved successful is therefore to include the coding for an essential chemical, usually an amino acid, on the

plasmid. This achieves the same result without the use of potentially hazardous material. These techniques, however, are not active in maintaining plasmid copy number. This problem can be corrected for genetically using a plasmid that has been altered for "runaway replication" which produces good plasmid stability and high productivity.

The organism in use in this study uses resistance to the antibiotic kanamycin to prevent total plasmid loss. However, all studies conducted using the organism have shown that it suffers from segregational instability, and that specific product levels therefore decline with time (Turner, 1993, Fisher, 1997 and Pierce, 1997).

2.3.5 Growth Temperature Effects

E.coli is a bacteria that is found extensively in nature in the digestive tract of mammals. As such the traditional growth temperature employed in fermentation strategies tended to be 37 ^{0}C as this mimics the conditions where the organism evolved. However, work by Schein and Noteborn (1988), showed that considerable advantage can be gained by reducing the growth temperature. Specifically, they found that the tendency of over-expressing recombinant organisms to form insoluble aggregates (inclusion bodies) was substantially reduced (by up to 90% in the systems under test) when growth was carried out at 23-30^0 C. Furthermore, this effect was independent of protein concentration suggesting that it was due not to fundamental solubility issues, but to biochemical issues within the cell.

This obviously has the effect of simplifying recovery processes and in a case where the product is assumed to be entirely soluble, such as the organism in use here, may increase yields by preventing some protein from forming insoluble intracellular inclusion bodies rather than passing through to the periplasmic space. Since this was discovered it has become more normal industrial practice to carry out *E.coli* fermentations at lowered temperatures, typically 30 ^{0}C. This also carries the advantage of reducing specific growth rates. It has been reported that it can also lead to reduced leakage from recombinant cells into the surrounding fermentation medium (personal

communication, Dr. W. Cook, DISTA Products Ltd., 1997), another source of product loss when the first recovery stage is a cell harvest step.

2.3.6 Effects of Yeast Extract Addition to a Defined Medium

The use of a small amount of yeast extract in a defined medium to reduce acetate production in *E.coli* has already been discussed (see section 2.3.1). However, this is not the only advantageous effect that has been observed using this nutrient rich complex medium component.

Matsui *et al* (1990) described the effect of the addition of 2 gL^{-1} of yeast extract to a minimal medium on the production of tryptophan synthase in recombinant *E.coli*. They found that this drastically increased plasmid stability and hence product expression. They then considered the effect of individual components within the yeast extract and found that vitamins and nucleic acids, two of the major components, were found to have little effect. However, amino acids, a third major component, were remarkably effective in improving plasmid stability over the 20-30 generations involved in a typical fermentation. Amongst these the greatest effect was seen with glutamic acid. They discovered that with the organism under test, this effect was further enhanced by glutamic acid's ability to increase tryptophan synthase production independent of plasmid stability.

Similarly, Kawabe *et al* (1992) demonstrated an increase in plasmid stability with the addition of 5 gL^{-1} of yeast extract to a defined medium in a culture of *E.coli* producing xylose isomerase. They noted, however, that increasing the levels of yeast extract to above 10 gL^{-1} caused inhibition of product expression.

The precise mechanism that causes the increase in stability and, in some cases, product expression, still remains in doubt. However, it seems likely that such a rich source of so many nutrients, vitamins and crucially amino acids is supplying an extra, easily absorbed and metabolised, source of essential chemicals to the cell. As this is far less stressful to the organism than manufacturing them "in-house" it should ease some of

the strain that the cell is under replicating foreign plasmids and proteins continuously whilst growing and dividing at a rapid pace.

To this end work is currently underway at UCLACBE to investigate other, linked effects that yeast extract addition may have. Chief amongst these is an increase in cell strength. A major expenditure of energy and materials by a cell during rapid fermentation is that involved in forming the cell wall, membranes and peptidoglycan layer. Indeed, it is well known that the strength-giving peptidoglycan layer increases in thickness rapidly during stationary phase, and that rapidly fermented recombinant organisms tend to be structurally weaker than their wild-type counterparts (see Chapter 1). It is believed that a small amount of yeast extract added to a defined medium may increase cell strength and possibly reduce the tendency of recombinant organisms to suffer frequent lysis and leakage (personal communication R. Sheridan, University College London, 1996).

2.4 Materials and Methods

2.4.1 Fermentation Protocols

The fermentation protocols used for this work were established by Turner (1993) and further developed by Fisher (1997).

2.4.1.1 Glycerol Stock Preparation and Maintenance

Glycerol stocks of *E.coli* JM107 pQR126 for fermentation were prepared as follows.

Minimal media agar plates were prepared as per the defined media recipe (see Appendix 4) except for the following alterations:

Chemical	Supplier	Grade	Concentration ($g\ L^{-1}$)
Glycerol	Merck Ltd.	-	4
Kanamycin A	Sigma-Aldrich Company	78%	0.02
Agar Bacteriological (No.1)	Oxoid Ltd.,	-	10
Soluble Potato Starch	Sigma-Aldrich Company	98%	10

Table 2.2: Alterations to defined medium recipe for production of glycerol stocks.

Cells were then applied to the plates in a standard three way streak, and incubated at 37^0C for 24 hours. At the end of this time, several lines of colonies were aseptically removed and suspended in 3 mL of 50% (w/v) glycerol which had previously been autoclaved at 121^0C for 20 minutes to insure sterility. These stocks were then batched into two groups and frozen at different temperatures: -70^0C for the immortal cell line to be used for re-culturing fresh working stocks, and -20^0C to be used for fermentation. The working stocks had a three month life span, after which the cells degraded to such a degree that subsequent growth in a fermenter was observed only after a 24 hour lag phase.

Note: the starch was added to the agar plates to enable selection for colonies of cells containing the plasmid in high copy numbers: production of α-amylase degrades the starch in the plates leaving visible "clear" spots around the colony.

2.4.1.2 Production of Seed for Shake Flasks

Cells to inoculate shake flasks were prepared from -20 ^{0}C glycerol stocks. Nutrient agar plates (Oxoid No.2, Oxoid Ltd., UK) containing 1% soluble potato starch and 0.02 gL^{-1} kanamycin to select for cells harbouring the plasmid (both Sigma-Aldrich Company) were inoculated from a single stock with a standard three-way streak. The plates were then incubated for 24 hours at 37^{0}C in a standard microbial incubator (New Brunswick Scientific Ltd., New Mimms, UK).

2.4.1.3 Shake Flask Culture

An inoculum solution was made up to the defined medium recipe (see Appendix 4) with the exception of glucose addition at 4 gL^{-1}, in a two litre side arm flask with needle attached to a maximum volume of 500 mL. If more inoculum was required then additional two litre flasks were used, the contents being transferred aseptically to the side arm flask immediately prior to inoculating the fermenter. Total volumes of inoculum for each fermenter used are shown in Table 2.3 below.

Fermenter	Working Volume (L)	Inoculum Volume (L)
LH7L03/LH7L01	5	0.1
LH20L01/LH20L02	14	1.00
LH42L02	30	2.00
LH 150L	100	5.00 (from LH7L seed vessel)

Table 2.3: Inoculum volume used with each fermenter

The shake flasks were autoclaved (Denley 200M) at 121^{0}C for 20 minutes to insure sterility (Denley Instruments Ltd., Billinghurst, UK). They were then inoculated by aseptically transferring 3 mL of liquid from the shake flask onto a freshly grown

nutrient agar plate (see above). The plate was then scraped with a sterile inoculating loop to remove the cells, and the liquid pipetted aseptically back into the shake flask. The culture was then grown for 23 hours in an orbital shaker (New Brunswick Scientific Co. Ltd., New Mimms, UK) at 37^0C and 200 rpm.

2.4.1.4 Fermentation

Four scales of fermenter were used in total for this work; 42L and 20L scale vessels for the initial establishment of an operating protocol, and 7L and 150L scale vessels for production of material for centrifugation experiments (the 7L was used as a seed vessel for the 150L). All fermenters were supplied by LH Fermentation (Inceltech UK Ltd., Pangbourne, UK).

pH and Dissolved Oxygen Tension (DOT) (Ingold, Leicester, UK) probes were calibrated and positioned within the main fermenter package. The fermenter was then filled to working volume allowing for additions with defined media (see Appendix 4 for recipe). The fermenter was sterilised as near as possible to inoculation time to minimise any risk of contamination. After sterilisation the DOT and pH probes were checked and recalibrated as necessary. pH was then adjusted to 7 and controlled throughout the fermentation by automatic addition of 4M NaOH (Sigma-Aldrich Company, Poole, UK, >97% purity). Temperature control was established and set to 37^0C +/- 0.5. The chemical antifoam addition system was set up and the line primed (25% w/v polypropylene glycol ((PPG), Merck Ltd., Lutterworth, UK) with timers set for 10 second slugs with a 4 minute interval. Initial air flow rate was set to approximately 0.5 vessel volumes per minute (vvm) and the agitator speed to approximately 40% of the rated maximum for the fermenter. These were then increased throughout the fermentation to maintain the DOT at 30% or above, below which the cells ceased to grow and entered stationary phase. Oxygen starvation can rapidly lead to cell lysis and death in fast growing *E.coli* cultures. Finally the offgas stream from the fermenter was connected to a mass spectrometer (MM8-80S, VG Gas Analysis Ltd., Winsworth, UK) and the data acquisition/ logging system initialised (RT-DAS, Acquisition Systems Ltd., Sandhurst, UK). This enabled logging of pH, DOT, agitator speed, air

flow rate, pressure, temperature, oxygen uptake rate (OUR), carbon dioxide exhalation rate (CER), and respiratory quotient (RQ), throughout the fermentation. Control of pH, temperature, air flow rate and agitator speed was provided by proportional integral derivative control loops (PID), supplied by LH Fermentation (Inceltech UK Ltd., Pangbourne, UK).

For inoculation the air flow rate was first reduced as necessary to allow gravity fed additions. Next the kanamycin and thiamine were filter sterilised (Whatman Scientific 0.2μm syringe filter) into the glycerol and magnesium salt solution. This was then added aseptically to the fermenter, immediately followed by the inoculum itself. Finally the air flow rate was restored to initial levels and a sample taken for optical density analysis.

The fermentation was continued until an optical density of 24-28 units mL^{-1} was reached, corresponding to a dry cell weight of 10-12 gL^{-1}. Throughout the fermentation samples were taken at intervals for dry weight, optical density, α-amylase, G-6-PDH and total protein analysis. The fermentation was carefully monitored to make sure no foaming took place, and to insure a DOT of above 30% was maintained. Once an OD of 24-28 units mL^{-1} was obtained, corresponding to carbon source limitation, crash cooling to 10-20 ^{0}C was applied immediately prior to harvest. In fermentations where yeast extract ("Yeatex", Bovril Food Ingredients Division, Esher, UK) was added to lengthen the stationary phase before cell death and lysis, the addition was made at this point. The cells were then drained into a container for harvest by disk stack centrifuge.

The 7L and 150L fermenters are pictured overleaf.

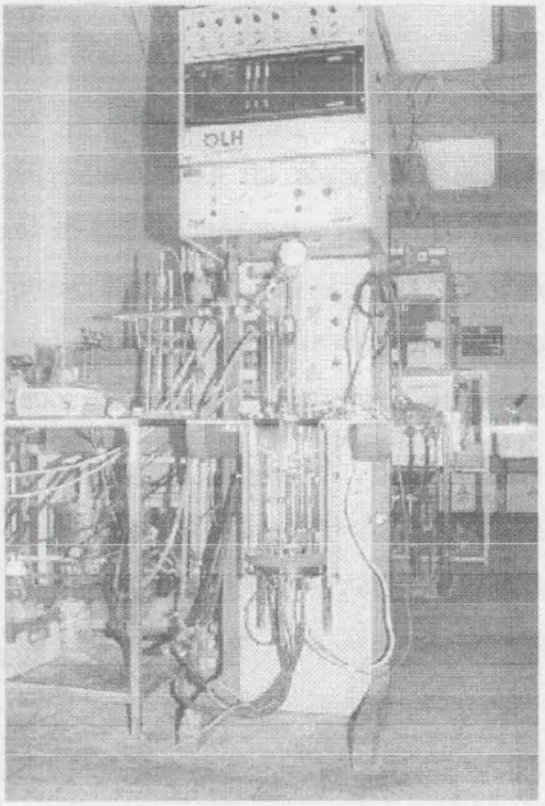

Figure 2.1: LH 7L fermenter (Inceltech UK Ltd.)

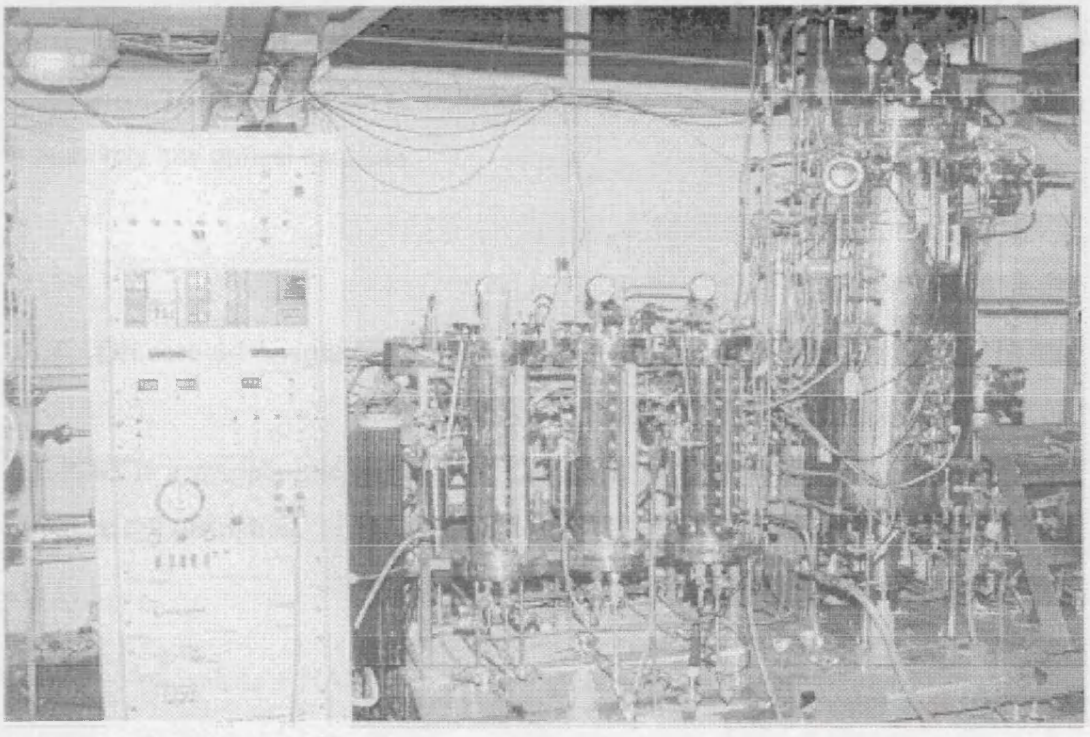

Figure 2.2: LH 150L fermenter (Inceltech UK Ltd.)

2.4.2 Optical Density

Optical density was determined using the absorbance of a sample at 600 nm, as measured against a blank of HPLC grade water (produced using a Maxima water unit, Elga Ltd., High Wycombe, UK) using a Uvikon 922 spectrophotometer (Kontron Instruments Ltd., Watford, UK). Samples were diluted as necessary with HPLC grade water to limit absorbance to below 1 optical unit (the limit of linearity of the spectrophotometer).

2.4.3 Dry Cell Weight

Between 1 and 10 mL of sample was filtered through a 0.2 μm filter (Whatman Scientific Ltd., Maidstone, UK) which had been dried for 24 hours at 105 ^{0}C and pre-weighed. The filter was then washed with twice the sample volume of HPLC grade water. It was then dried at 105^{0}C for 24 hours, and the dry weight of the sample determined. This method proved accurate enough to obtain an error of +/- 10% even at relatively low optical densities.

2.4.4 Glucose-6-Phosphate Dehydrogenase (G-6-PDH) Assay

G-6-PDH is a cytoplasmic enzyme in *E.coli* and as such was used as a marker for complete cell disruption.

Reaction:

Glucose-6-phosphate + $NADP^+$ $\Leftrightarrow$ 6-phosogluconolactone + NADPH + H^+

Reaction mixture (Bergmeyer, 1983)

Glucose-6-phosphate (Sigma-Aldrich Company, 33 mmol L^{-1}), $NADP^+$ (Sigma, 3.8 mmol L^{-1}), $MgCl_2$ (BDH, 0.63 mmol L^{-1}), Tris/HCl (0.5 mol L^{-1}, pH 7.5)

Procedure: Samples were spun down in Eppendorfs for 15 minutes at 12400G to remove any particulate matter (GS-15 benchtop centrifuge, Beckman Instruments, High Wycombe, UK). 50 µl supernatant was then added to 1 mL assay mix at 25^0C, and the rate of absorbance change recorded at 340 nm using a Uvikon 922 spectrophotometer (Kontron Instruments, Watford, UK). One unit of enzyme activity reduces 1 µmol of $NADP^+$ per 60 seconds at 25^0C.

2.4.5 Total Protein Assay

Protein concentration was determined using the colorimetric assay of Bradford (1976), using the Bio-Rad™ Protein Assay Reagent. Bovine Serum Albumin (Sigma-Aldrich Company, Poole, UK), was used to construct a calibration curve in the range 0.1-1.0 mg ml^{-1}. Samples were spun down in Eppendorfs for 15 minutes at 12400G to remove any particulate matter (GS-15 benchtop centrifuge, Beckman Instruments, High Wycombe, UK). 40 µL of sample supernatant was then added to 2 mL of assay reagent and the absorbance at 595 nm measured using a Uvikon 922 spectrophotometer (Kontron Instruments, Watford, UK). The protein concentration was then obtained from the calibration curve. This technique produced an error of +/- 5%.

2.4.6 α-amylase Assay

The α-amylase assay employed was performed on micro-titre plates and was based on the colour change of an iodine-potassium iodide complex when exposed to starch. 0.5% w/v soluble potato starch (Sigma-Aldrich Company, Poole, UK) was dissolved in 15 mM phosphate buffer at pH 5.8 by mixing well and heating in a microwave until the solution was just boiling to solubilise the starch. This solution was then filtered through a Whatman No.1 filter paper (Whatman Scientific Ltd., Maidstone, UK). The starch solution was made fresh every day.

The assay mix itself was prepared as follows:

Assay Solution A:	2.2% w/v I_2 (Sigma) and 4.4% w/v KI (Sigma) dissolved in HPLC grade water.
Assay Solution B:	2% w/v KI (Sigma) dissolved in HPLC grade water.
Assay Solution C:	1 mL A + 500 mL B. Assay solution C was stable in light for one day.

300mL of solution C was then pipetted into wells A to G down a microtitre plate, and across the plate for as many assays as were to be performed. A minimum of three repeats was performed on each sample.

0.2 mL of starch was then added along a row on another plate for as many wells as there were assays to be performed. To another line of the same plate the samples were added. These were first spun in a microfuge at 12,400 G relative centrifugal force to remove particulate matter. The supernatant from this preparation was then used for the assay. The sample volume used was between 10 and 50 μL, which was then diluted to a total volume of 150 μL with 15 mM phosphate buffer (pH 5.8). If the sample needed diluting further, this was performed with HPLC grade water (if the sample volume loaded was outside the range specified above it altered the buffering capacity of the phosphate solution).

The plate containing starch and sample/buffer solution was then incubated in a water bath at a temperature of 50^0C for at least ten minutes to allow the temperature to equilibrate.

At the start of the assay 150 μL of starch from the wells on the plate were added to the row containing samples. A stopwatch was started and at 30 seconds, 2.5 minutes and at 2.5 minute intervals for a total of 15 minutes, 15 μL aliquots of starch/sample mix were taken and added sequentially to rows A-G on the plate containing assay mix.

At the end of 15 minutes the absorbance of the wells on the plate containing assay mix was measured at 620 nm. using a microtitre-plate reader (MultiSkan Plus Mk II, Life Sciences International (Europe) Ltd., Runcorn, UK)

A linear regression was then performed by computer package and the slope calculated (A620 against time in minutes). The α-amylase activity was then calculated as follows:

$$a = \left[\frac{\text{slope}}{\left(\frac{V_{sa}}{0.3} \right)} \right] \qquad \textbf{(2.1)}$$

where a_a = α amylase activity (units min^{-1} mL^{-1})

V_{sa} = sample volume (mL)

This technique yielded an error of +/- 10% and thus multiple repeats were utilised to allow increased confidence in the result.

2.4.7 Homogenisation

To determine the protein, amylase and G-6PDH levels of any given fermentation sample it was necessary to first disrupt the cells. This was conducted using an APV Manton Gaulin Lab 40 high pressure homogeniser (APV, Crawley, Sussex, UK) operated at 1200 bar pressure, one pass, which was sufficient to obtain 100% cell disruption. The homogeniser required 40 mL of sample.

To assess the cell strength from any given fermentation against other batches, samples were homogenised at 250, 600, 1000 and 1200 bar pressure, one pass. The homogenate was then retained for total protein, G-6-PDH and α-amylase analysis. In this manner a homogenisation profile of the fermenter broth was developed.

2.5 Results

The first work undertaken was to characterise the fermentation profile on a small scale and compare fermentation performance to that obtained historically with the same organism. To this end a number of 7L scale (5L working volume) fermentations were undertaken.

A typical data profile for this standard batch fermentation carried out on a defined medium is shown overleaf (Figure 2.3). This follows a standard pattern of *E.coli* growth. There was an initial lag phase whilst cells coming from the shake flasks in stationary phase adjusted to the different conditions found in the fermenter. This period of little or no growth lasted approximately 300 minutes (5 hours). After this time period the cells accelerated into the growth phase, which is described by the exponential increase in carbon dioxide exhalation rate (CER) and oxygen uptake rate (OUR). The respiratory quotient observed during full exponential growth was approximately 0.7 (a typical value for *E.coli* metabolising glycerol in a defined medium environment). The operation of the majority of these fermentations to a time scale suitable to produce cells for downstream processing experimentation precluded in-depth study of α–amylase production rates and specific growth rates throughout the course of the fermentation. However, Table 2.4 shows final α-amylase levels, dry cell weights and optical densities obtained during these early characterisation experiments.

It can be seen that the biomass levels were fairly reproducible. However, the α-amylase expression levels, and crucially the fraction that leaked into the surrounding medium, was much more variable. This was consistent with historical data (Turner, 1993, and Fisher, 1997) in that precise expression levels had always proved difficult to control with the organism, and leakage of approximately 50% on average into the surrounding medium was not unusual.

Specific growth rates increased throughout the fermentation. However, the characteristic measurement, that of the culture in full exponential growth, was

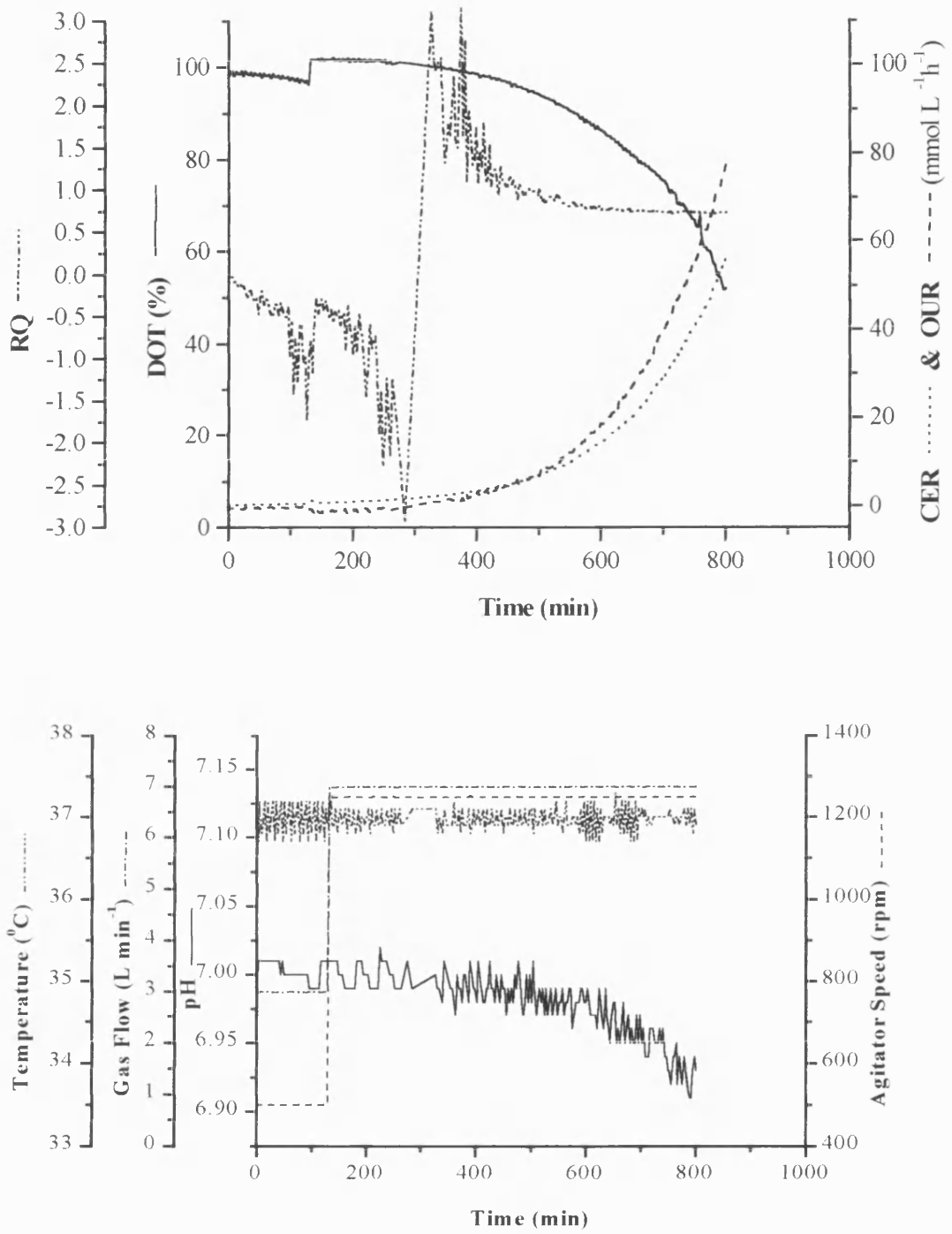

Figure 2.3: Typical growth profile for E.coli JM107 pQR 126 grown on defined medium. Trace shown is biological properties (top) and physical properties (bottom) from fermentation NJMC01, 7L scale.

Run	OD_{600}	d.c.w. ($g\ L^{-1}$)	α–amylase I.U. $min^{-1}\ mL^{-1}$		
			Total	Ex	Peri
NJMA01	25.4	8.6	20.4	6.9 (34)	13.5 (66)
NJMB01	21.5	7.9	8.5	6.4 (75)	2.1 (25)
NJMC01	26.1	9.5	18.4	5.3 (29)	13.1 (31)
NJMD01	24.6	9.3	25.4	10.7 (42)	14.7 (58)
NJME01	22.6	7.5	17.1	9.8 (57)	7.3 (43)

Table 2.4: Dry cell weights and product expression levels obtained with *E.coli* JM107 pQR 126 on defined medium (7L scale). Ex= extracellular Peri= periplasmic. Numbers in brackets indicate percentage of total.

0.36 h^{-1} corresponding to a cell doubling time of approximately 2 hours. This led to a total fermentation time of around 15 hours. The fermentation was ended whilst still in exponential growth rather than waiting for carbon source depletion and stationary phase. This was predominantly because of oxygen transfer limitations in the fermenter, however carbon source limitation has been shown to be reached at approximately 14 gL^{-1} (Turner, 1993).

It was decided that the α-amylase expression levels were too low to provide an easy target enzyme for centrifugation experiments. Of particular worry was the high proportion of enzyme which leaked into the medium during the course of the fermentation. It was decided to try and improve the yield. To this end yeast extract at a concentration of 10 gL^{-1} was added to the defined medium recipe.

Two trials were carried out utilising two identical 7L scale fermenters: one with yeast extract added to the medium, and one without. The medium (with the exception of the yeast extract) was made up as a batch and then split prior to sterilisation, and the two vessels were inoculated from the same seed. In this manner it was intended to keep all conditions in both vessels identical with the exception of the yeast extract.

The results are shown in Table 2.5;

Run	OD_{600}	d.c.w. ($g\ L^{-1}$)	α–amylase I.U. $min^{-1}\ mL^{-1}$		
			Total	Ex	Peri
NJMF01 (+yeast ex)	22.4	8.3	45.6	19.2 (42)	26.4 (58)
NJMF02 (-yeast ex)	25.6	9.0	17.5	6.7 (38)	10.8 (62)
NJMG01 (+yeast ex)	27.8	10.1	36.8	18.8 (51)	18 (49)
NJMG02 (-yeast ex)	21.6	8.0	24.6	12.1 (49)	12.5 (51)

Table 2.5: Effect of addition of 10 gL^{-1} yeast extract to defined medium on amylase production in *E.coli* JM107 pQR 126 at 7L scale.

It can be seen that the yeast extract clearly increased α-amylase expression levels, from an average of 20 I.U $min^{-1}\ mL^{-1}$ to 40 I.U. $min^{-1}\ mL^{-1}$. However, it did not appear to effect significantly the amount of product leaking into the medium from the cells during the course of the fermentation. Neither were the physical characteristics of the fermentation physically altered, with time of growth and logged fermentation characteristics not differing significantly from those already reported.

It seemed clear that the yeast extract was beneficial to the process, so the next stage was to scale up the fermentation to the 150L fermenter (100L working volume) for production of cells for use in the centrifugation experiments. This was undertaken using the 7L (5L working volume) fermenter to provide the inoculum for the 150L. Again, runs were conducted with and without the addition of yeast extract to the medium.

A typical fermentation profile obtained in the 150L fermenter (without yeast extract) is shown overleaf in Figure 2.4.

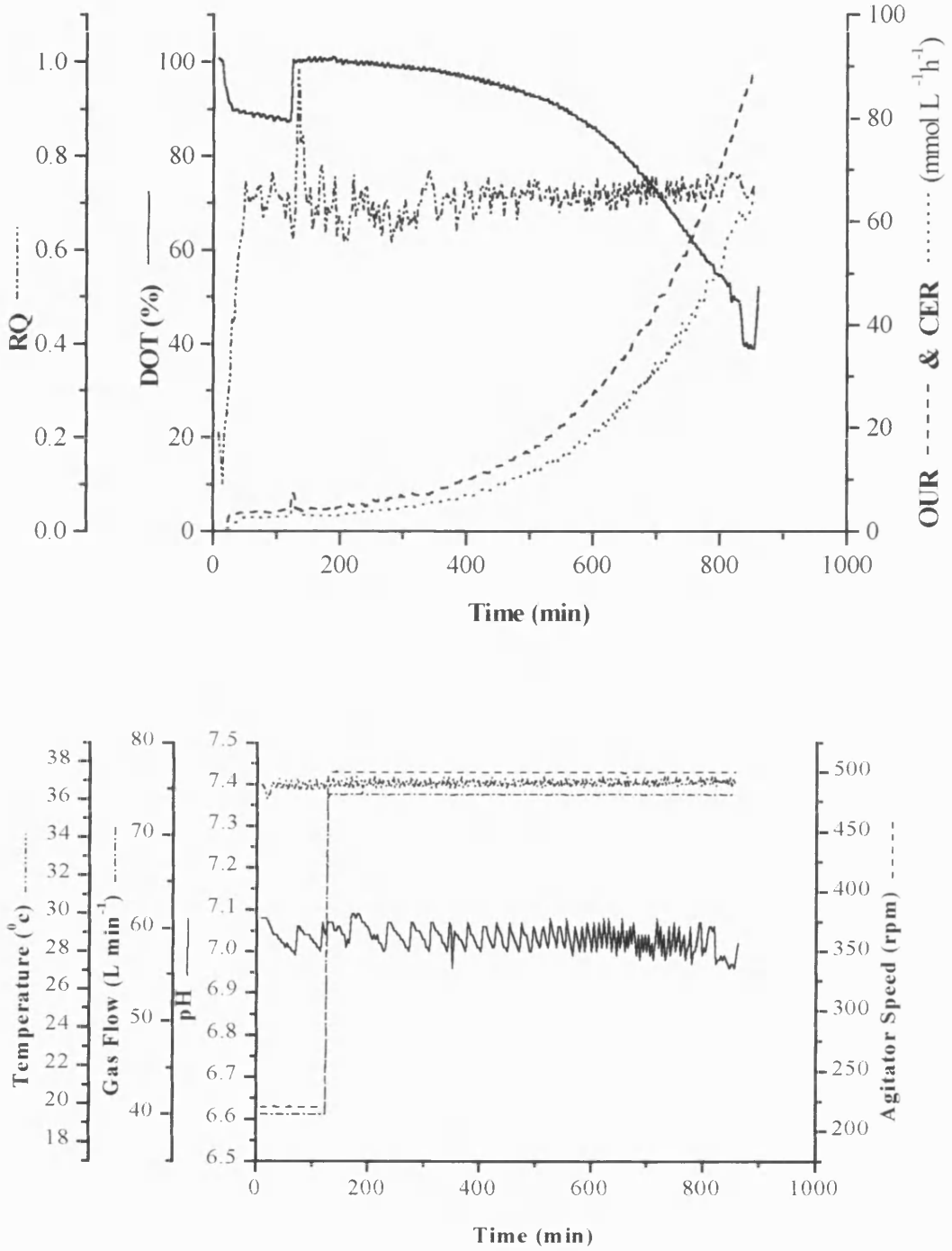

Figure 2.4: Typical growth profile for E.coli JM107 pQR 126 grown on defined medium. Trace shown is biological properties (top) and physical properties (bottom) from fermentation NJMH02, 150L scale.

The profiles shown follow almost exactly those obtained using the 7L seed vessel. The major difference is the lack of an initial lag phase at the beginning of the fermentation. The overall growth time was slightly shorter than that for the seed vessel (12.5-13.5 hours): however, the initial optical density was lower in the 150L fermenter (typically 0.07 rather than 1.4 a.u.). The cells were seen to enter exponential growth almost immediately, with a growth rate equivalent to cell doubling every 2 hours attained within 2 hours of the start.

Table 2.6 below shows the product expression levels attained at the 150L scale both with and without yeast extract present in the medium.

Run	Scale	OD_{600}	d.c.w. ($g\ L^{-1}$)	α–amylase ($I.U.\ min^{-1}mL^{-1}$) Total
NJMH01 (-yeast ex)	7L	25.6	9.2	18.6
NJMH02 (-yeast ex)	150L	22.1	7.7	5.6
NJMI01 (+yeast ex)	7L	24.3	8.6	41.8
NJMI02 (+yeast ex)	150L	20.8	7.8	27.3

Table 2.6: Effect of addition of 10 gL^{-1} yeast extract to defined medium on α-amylase production in *E.coli* JM107 pQR 126 at 150L scale.

Again, the pattern of increased α-amylase levels are seen with the addition of yeast extract to the medium. In both cases the levels of product in the production fermenter were lower than those in the seed fermenter. However, without yeast extract the reduction is large (70%) whereas the addition of yeast extract seemed to have a stabilising effect, and the α-amylase levels in the production fermenter declined only 35%.

A suitable growth protocol had now been established with one exception; the total fermentation time was only approaching 30 hours. However, the best "end point" for the production fermenter, bearing in mind it's purpose as a feed stock for substantial pilot scale downstream processing experimentation, was 7-9 a.m. This would have led to an extremely inconvenient fermentation time-schedule. It was therefore necessary to experiment with holding the seed fermenter "in stasis" for up to 8 hours between the end of one fermentation and a convenient start time for the next, an effect that was achieved by crash cooling the fermenter to 10^0C and holding it there until the inoculation of the production vessel.

At this point another alteration was made to the medium recipe. As it was not necessary to produce extra α-amylase in the seed fermenter, only the production vessel, it was decided to only add yeast extract to the production medium. Furthermore, literature surveys revealed that probably only trace amounts of the organic component were necessary, so it was decided to reduce the concentration to 0.5 gL^{-1} and observe any change in product levels. It was also decided that the required quantity of yeast extract (50 g) should be added *to the seed vessel* at the time of temperature reduction; this was to ensure that, even if growth of the bacteria continued at this much reduced temperature there would be sufficient nutrients present to support life.

Another unwanted effect was the tendency of the cells to lyse rapidly upon removal from the 150L fermenter, an effect that was attributed to the need to drain the fermenter during exponential growth due to insufficient oxygen transfer in the vessel. Therefore it was decided to also add yeast extract (at 5 gL^{-1}) and crash cool at the end of the production fermentation in order to assess any increase in stability that may have been attained.

Growth profiles for the seed and production fermenter under these conditions are shown overleaf as Figures 2.5 and 2.6. There are several points of interest. Firstly considering Figure 2.5 (the seed vessel) it can be seen that as soon as the yeast extract is added (at the time of crash cool) there is an immediate, if small, rise in pH.

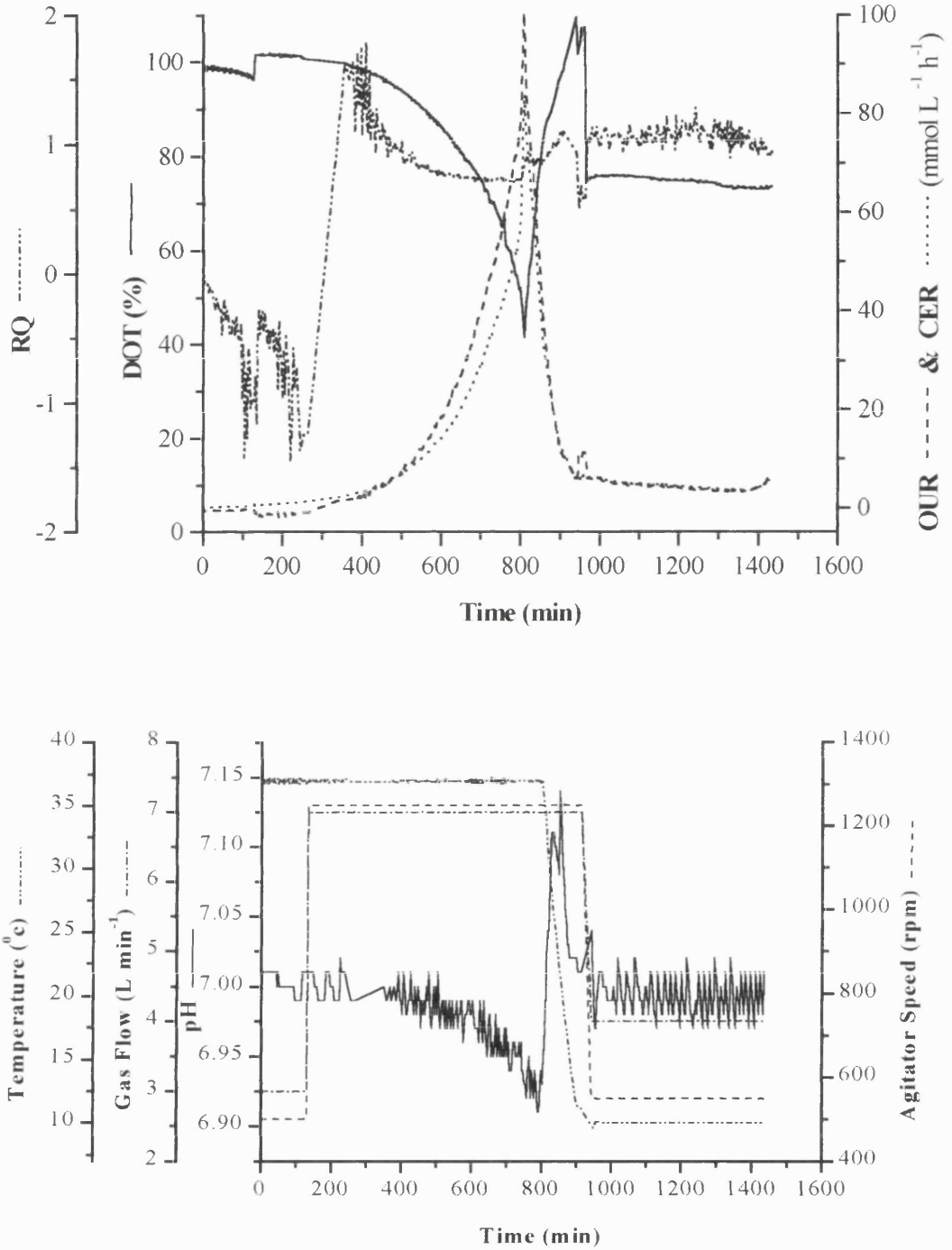

Figure 2.5: Growth profile for E.coli JM107 pQR 126 grown on defined medium. Trace shown is biological properties (top) and physical properties (bottom) from fermentation NJMJ01, 7L seed for 150L fermenter. Note, 50g yeast extract added upon crash cooling to 10°C.

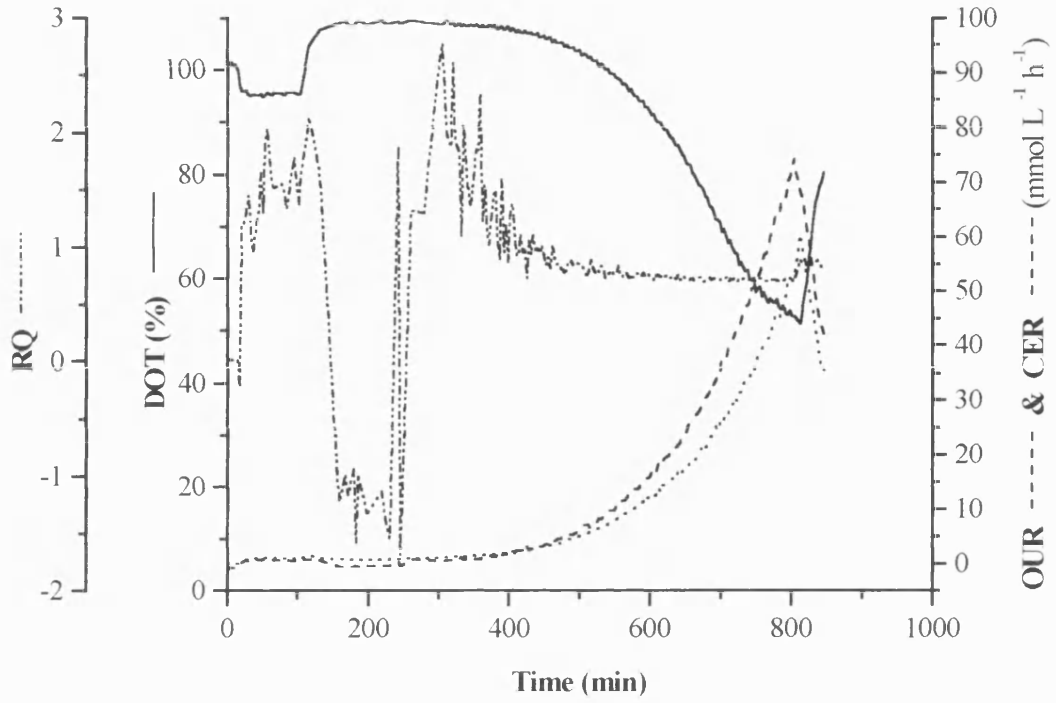

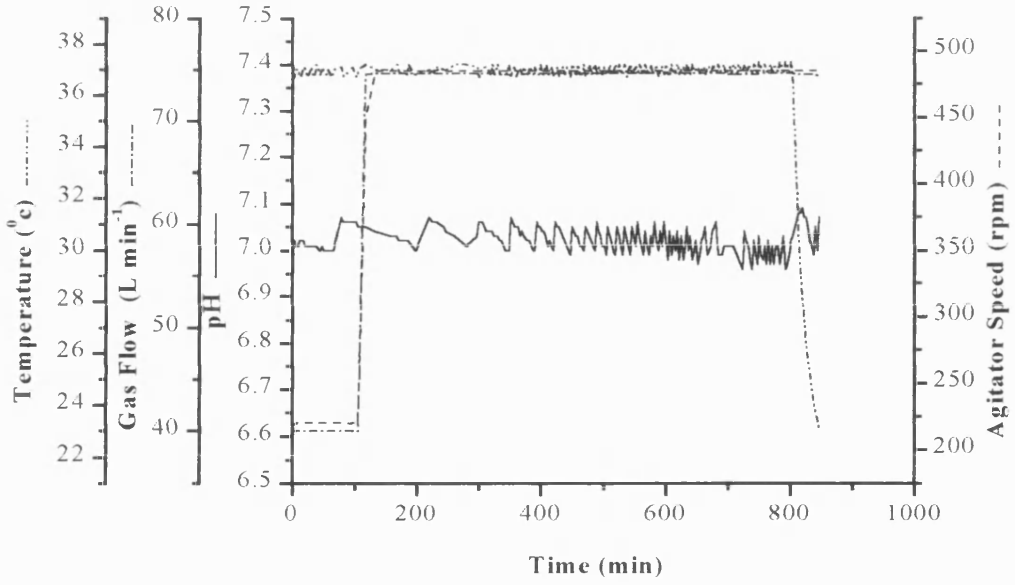

Figure 2.6: Growth profile for E.coli JM107 pQR 126 grown on defined medium. Trace shown is biological properties (top) and physical properties (bottom) from fermentation NJMJ02, 150L fermenter. Note, 500g yeast extract added upon crash cooling to 10^0C.

This continued for approximately 45 minutes (there was no acid feed to correct the problem) after which the culture naturally returned to requiring alkali for pH control. The crash cooling immediately reduced the cells' oxygen demand, with a sharp drop in both OUR and CER observed. Thereafter the fermentation remained static, with an increase in O.D. over the next 6 hours of only 1.5 a.u (note that the respiratory quotient reached a relatively stable level much higher than that associated with growth on glycerol (above 1)).

Upon inoculation of the 150L fermenter an immediate and rapid drop in dissolved oxygen in the fermenter was observed. There followed approximately 30 minutes of rapid growth. However a large reduction in growth rate was then observed (the trend shows the DOT actually going up during this time) as the cells entered a lag phase. After 3-4 hours normal exponential growth resumed and the fermentation ran to completion as expected. Again, upon crash cooling and addition of yeast extract to the vessel prior to harvest a characteristic pH rise was observed (an increase from the set point of 7.0 to 7.19 units) before a return to normal control.

It should be noted in both cases that although little or no growth was observed at below 20 ^{0}C, the oxygen demand on the vessel remained high.

Most surprising, however, was the resulting α-amylase levels, shown in Table 2.7 overleaf. It can be seen that adopting this approach to the fermentation resulted in an increase in α-amylase levels over the simple inclusion of yeast extract as an integral part of the medium. This was considered sufficiently interesting to run several additional fermentations to try and separate the potential effects of the "crash cool and hold" in the 7L vessel from the inclusion of yeast extract at lower levels in the 150L scale vessel.

Table 2.8 summarises the results obtained when attempting to isolate the cause of this further increase in product levels.

Vessel	Time	$O.D._{600}$	α-amylase ($I.U.\ min^{-1}mL^{-1}$)
7L	ferm end, pre-yeast extract	23.2	18.4
7L	ferm end, prior to 150L inoculation	24.4	15.6
150L	Ferm end., pre-yeast extract	22.5	79.4
150L	Ferm end	25.8	86.8

Table 2.7: α-Amylase production using "crash cool and hold" protocol, 7L seed vessel, 150L production vessel (Fermentations NJMK01 & NJMK02).

Run	Crash Cool?	Y.E.?	pH rise?	150L Lag?	$O.D._{600}$	α-amylase ($I.Umin^{-1}mL^{-1}$)
NJMN	✓	X	X	X	24.1	9.4
NJMM	X	✓($0.5\ gL^{-1}$)	✓	X	28.4	24.1
NJMT	✓	✓($1.0\ gL^{-1}$)	✓	✓	25.7	69.4
NJMS	✓	✓($0.5\ gL^{-1}$)	✓	✓	27.9	102.8

Table 2.8: Effect of variation of yeast extract levels and crash cool on final production vessel product levels. Y.E.=yeast extract added to end of seed vessel (conc. is that in 150L vessel assuming full carryover), pH rise= pH rise upon addition, 150L lag=observed lag phase at beginning of 150L fermentation.

It can be seen that the addition of yeast extract at the end of the seed fermentation was sufficient to cause the transient pH rise in the vessel. However, only when yeast extract was added and a crash cool and hold carried out did the product levels increase substantially from the normal amounts. Also, the induction of a lag phase in the 150L fermenter was crucial in order to produce the increased levels of product. The product levels did not seem to be influenced by the amount of yeast extract added in the limited range investigated.

The specific product levels throughout the course of both a seed and production fermentation are shown in Figure 2.7 overleaf. The plots show α-amylase per unit of optical density, and therefore give an indication of how much product each cell is producing on average.

Both fermentation courses followed similar patterns, with an initial drop in production levels followed by a large increase during the lag phase of growth. During exponential growth the levels decreased in both fermenters, however the rate of decrease in the seed fermenter, without the stabilising influence of yeast extract, was much greater than that in the production fermenter. The product level per unit OD in the production fermenter also reached higher concentrations than in the seed fermenter (4.5 as opposed to 3.2).

A final variation that was tested was to grow the cells at a temperature of 30^0C. Several technical difficulties with the equipment were experienced during these runs leading to a failure to produce a representative batch. However, the overall trend was to a decrease in the levels of α–amylase leaking into the medium indicating the production of a stronger cell. The growth time was increased to approaching 24 hours, and the total product levels fell quite dramatically (by 33-40%), which led to this strategy being abandoned without further investigation.

The final fermentation characteristic which was examined was the finished product cell strength, and the stability of the cells over three hours in a stirred tank (the length of time needed to conduct a successful centrifugation experiment).

Figure 2.8 shows homogenisation profiles for fermentation broth. The top graph shows the variation of strength between fermentation batches, with open symbols indicating the use of yeast extract in the production fermenter medium as described. It can be seen that there was a substantial variation between batches, particularly at the intermediate levels of disruption (approaching 20% at 250 bar).

Overall the cells were easily disrupted, with 80% release achieved at pressures of below 500 bar. The presence of yeast extract made no significant difference to the strength of the cells.

The lower plot shows release from the periplasmic space (α-amylase) and the cytoplasm (total protein and glucose-6-phosphate dehydrogenase) as a function of homogenisation pressure. The significant point in this figure is the ease with which α-amylase was released, with 75% of the total present released into the broth at a pressure of 250 bar. This was in contrast to the intracellular enzyme and total protein markers, where significantly higher pressures were required to achieve the same level of disruption (note that the intracellular G-6-PDH and the total protein release follow each other closely. This was as expected since the periplasmic space contains only approximately 3% of the cell's total protein. Therefore, disruption leading to significant total protein levels will also release the G-6-PDH).

Figure 2.9 shows the effect of yeast extract addition at a concentration of 10 gL^{-1} to the medium at the end of the 150L production fermentation, accompanied by a crash cool to 15 ^0C (the lowest achievable) for 1 hour prior to removal to a stirred cooled tank for centrifugation trials. This work was conducted because the organism was known to suffer from poor stability whilst awaiting processing, with the cells displaying a tendency to lyse and/or leak product into the medium with time. The fermentation was grown as normal, utilising yeast extract and a crash cool at the end of the seed fermenter. At the end of the production fermentation the 150L vessel was cooled (either with or without yeast extract addition) and left for 1 hour. The broth was then transferred to a 120L stirred baffled tank, where glycol cooling was used to cool it to 5^0C (a temperature commonly employed industrially to inhibit the action of proteases). Samples were taken over the next three hours in order to track change in cell strength (using homogenisation profiles) and leakage of both product and total protein into the medium.

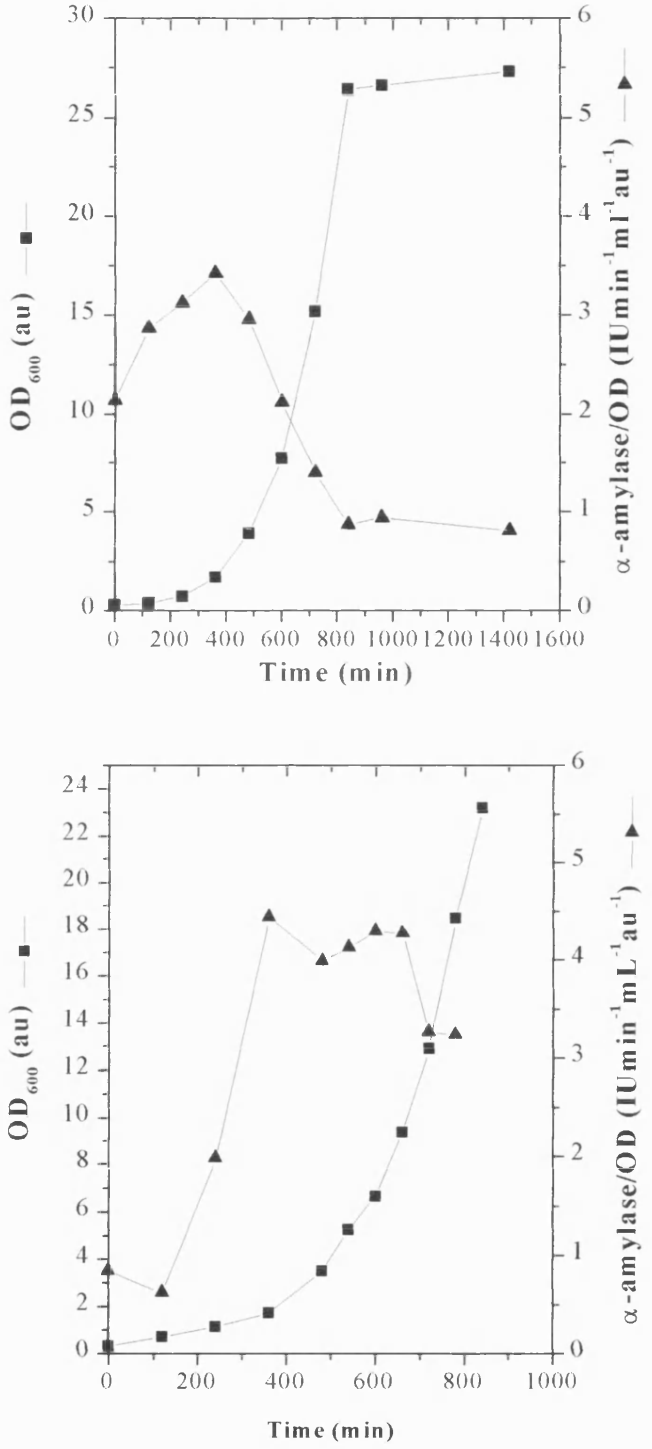

Figure 2.7: Specific product levels throughout fermentation time course of (top) 7L seed fermenter (bottom) 150L production fermenter, Protocol adopted was yeast extract addition to seed fermenter and crash cool. Fermentation: NJMBBY & NJMSCY.

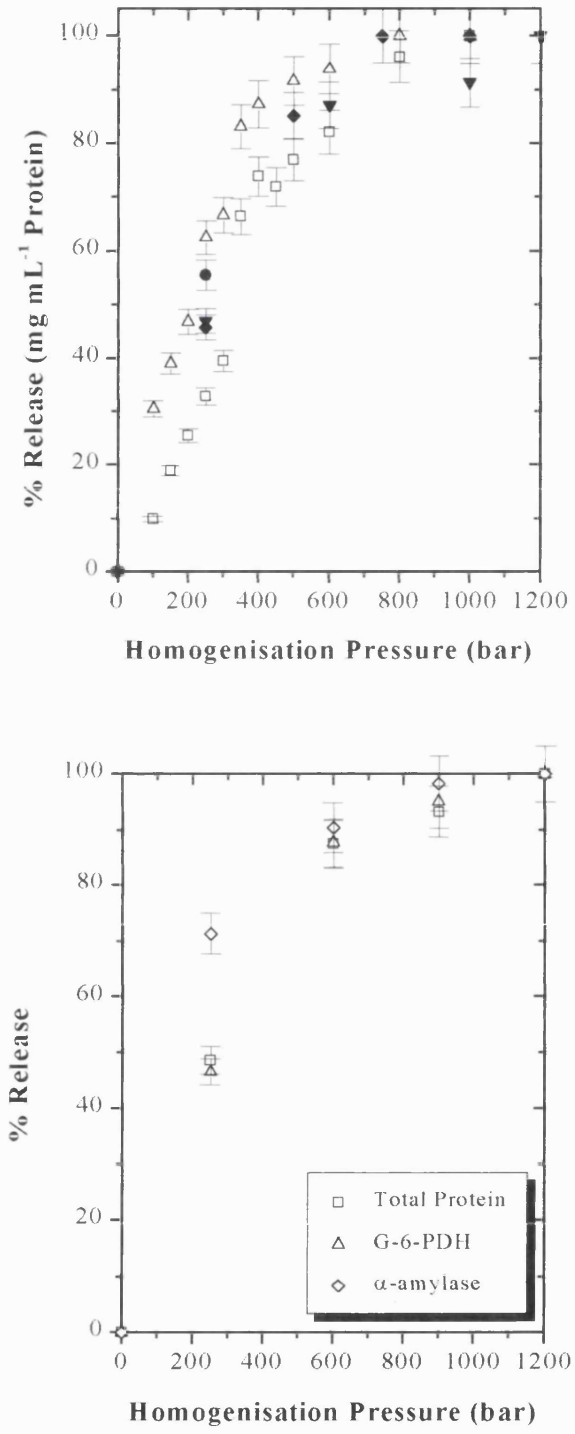

Figure 2.8: % Release as a function of homogenisation pressure. Top shows variation between batches, bottom shows release as function of detection method. Open symbols show fermentation utilising yeast extract in the production fermenter medium.

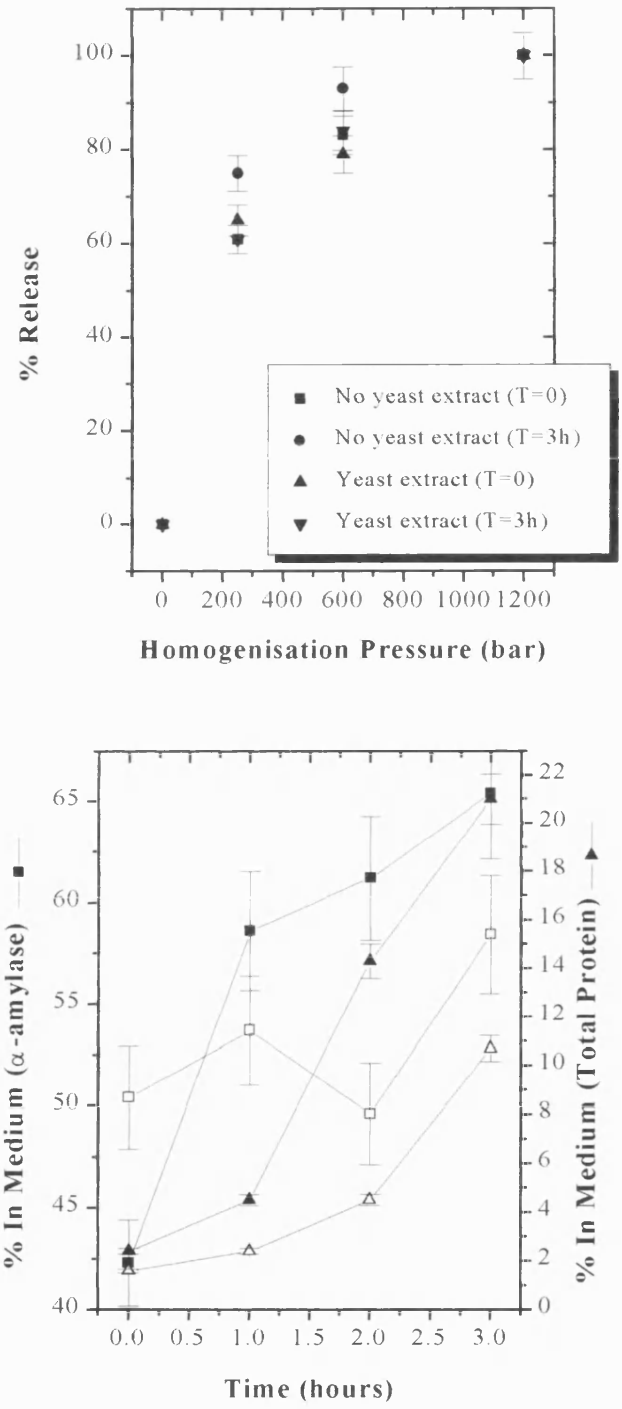

Figure 2.9: Cell strength (top) and % in medium (bottom) as a function of time and yeast extract addition at end of production fermentation. Top graph: points show α-amylase. Bottom graph: open points show yeast extract addition, closed points show no yeast extract addition.

Considering the top graph first, it can be seen that with no yeast extract added, the strength profile of the cells in terms of product release changed with time, with release at 250 bar pressure increasing from 60 to 78% over three hours. The yeast extract, however, proved to have a stabilising effect on the cell population, and no significant change in homogenisation profile was observed with time when yeast extract was added to the end of the production fermentation.

More significant is the change in % marker in the medium over time, shown in the bottom diagram. This will be indicative of both total cell lysis with time, and the effect of any inherent leakiness of the cells. This is plotted both in terms of total protein and α-amylase. The figure shows that there was an increase in the presence of both total protein and α–amylase in the medium with time. The protein figure, for the reasons explained previously, is indicative of complete disruption of the cells and is thus likely to track cell lysis. Without yeast extract the % of total in the medium increased from 3% to 21%, indicating a substantial amount of cell lysis. With yeast extract added to the medium this reduced significantly, with an increase to only 10%. The same pattern was repeated when considering product release with the percentage of α-amylase in the medium increasing from 42 to 65% without yeast extract, and from 50 to 57% with the addition. As the increase of both markers with time was approximately the same, it was felt that the α-amylase release was also due to complete cell lysis, rather than the leakage of the periplasmic contents into the medium with time.

Finally the viscosity of the whole cell broth was measured. This is an important parameter when calculating shear rates and was needed for the whole cell centrifugation analysis (see Chapter 5). Results are shown in Figure 2.10. It can be seen that the viscosity may be considered constant with shear rate and equal to 2.0 cP, or twice that of water. The measurement was taken using a cup and bob viscometer (Rheomat 115, Contraves Industrial Products Ltd., Ruislip, UK) (for details of operation see materials and methods, Chapter 4).

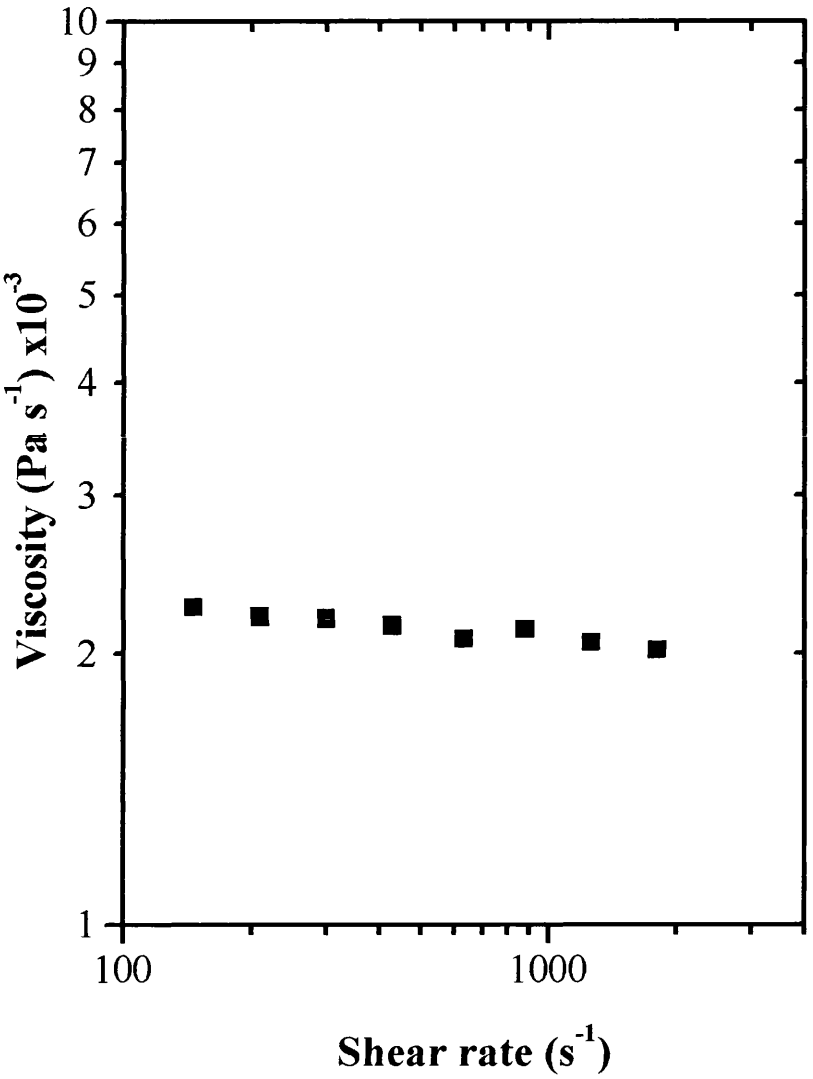

Figure 2.10: Viscosity of whole cell E.coli broth. Viscosity measured with cup and bob viscometer (Rheomat 115, Contraves Industrial Products Ltd., Ruislip, UK).

2.6 Discussion

The results from the trial fermentations described in this chapter clearly show that the addition of the organic yeast extract component to the defined medium in use increased the levels of α-amylase produced during the fermentation dramatically, from 10-15 units mL^{-1} using the standard protocol to 30-40 units mL^{-1} utilising yeast extract within the medium. However, it was possible to enhance the product levels even further, up to 80-100 units mL^{-1} when yeast extract was added to the end of the seed fermenter during a period of no growth caused by the use of low temperatures (10 ^{0}C). Under these circumstances a lag phase was induced in the production fermenter during which the specific α-amylase levels increased dramatically.

It seems clear that several effects working together caused these results. Product expression can generally be considered proportional to plasmid copy numbers. Figure 2.7(a) shows the specific α–amylase levels attained through the course of a seed fermentation without yeast extract in the medium. It can be seen that the specific levels increase during the initial lag phase but decline very rapidly throughout the period of exponential growth of the cells. Figure 2.7(b) shows the same plot for the 150L production vessel, incorporating yeast extract at 0.5 gL^{-1} in the medium. It can be seen that during the period of exponential growth under these circumstances there is also a drop in specific activity. The reduction, however, is less pronounced than without the yeast extract. This would seem to indicate that the yeast extract is stabilising the plasmid copy number to some degree, and thus total product levels are higher with the inclusion of a small amount of yeast extract in the medium. The cell is known to suffer from a high level of plasmid instability (Turner, 1983 and Fisher, 1997) and specific α-amylase levels have historically always declined throughout the course of the fermentation. This effect is most pronounced in the use of a seed and production fermenter where, without the use of yeast extract and crash cooling, the production fermenter always showed lower product levels than the seed. This is because the cell population is in continual exponential growth for roughly twice as long when employing a two stage fermentation, thus the loss of plasmid is higher than in a one stage fermentation.

This high degree of instability is believed to be linked to the rapid growth of the cell. Turner (1993) investigated the ideal specific growth rate for *E.coli* JM107 pQR126 on this defined medium and found that at any rate higher than 0.2 h^{-1} product levels decreased significantly. The fermentations conducted during this work have been characterised by a specific growth rate approaching 0.4 h^{-1}. This rapid growth rate is too fast to allow the maintenance of the high plasmid copy number essential for reasonable product expression levels. Furthermore the effect becomes worse with time; as copy number falls then specific growth rate will actually increase as the cell has less to reproduce during division. This was observed during the work, with the cell doubling time shortening as the exponential growth phase progressed.

Yeast extract has been shown to have an impact on the production of acetic acid during fermentation and the product expression rates (see section 2.3.6). The specific production rates shown in Figure 2.7 indicate that a higher rate was indeed obtained in the presence of trace amounts of yeast extract. Which of the two mechanisms is responsible for this observation is impossible to tell.

As was previously discussed (section 2.3.6) there are several possible reasons why the addition of yeast extract improves plasmid stability and product expression levels, which can be summarised in two arguments. Since the organic substrate is a rich source of amino acids, vitamins and nucleic acids, it is possible that it provides, in trace amounts, some chemical which the cells need for successful growth and expression of heterologous protein. It is also possible that by providing chemicals "pre-synthesised", rather than the cell having to manufacture them from the basic constituents of a defined media, the overall stress on the cell is reduced and thus it is less likely that plasmid numbers will fall. The evidence in this case points to the latter as the more likely explanation.

The second, and more dramatic, result observed during this work was the much greater increase in α-amylase levels when yeast extract was added to the seed fermenter during a "crash cool and hold" period of up to 8 hours. A subsequent lag

phase was then observed in the production fermenter which was never seen without the use of both yeast extract and a holding period. In this manner specific product levels were improved to 80-100 units mL^{-1} compared to 10-15 units mL^{-1} with no yeast extract and 30-40 units mL^{-1} with yeast extract integrally part of the medium. This is believed to be a result of the establishment of a diauxic growth pattern in the production fermenter.

When the yeast extract was added to the seed fermenter a temporary pH rise was observed despite the fact that the solution had a pH below the control point. This is clearly indicative of a switch in metabolism, and is probably caused by the cells' starting to metabolise the yeast extract and hence release amino acids contained within the compound free into solution. This study has produced some evidence that the organic compound is metabolised by *E.coli* either as a carbon or nitrogen source in preference to the defined medium substrates, and yeast extract based complex media's are generally recognised as producing healthier, faster growing cells. There will, at this stage, also be far more yeast extract than defined medium components in the fermentation broth (the defined components are nearly exhausted and the yeast extract is added to a final level of 0.5 gL^{-1} *in the production fermenter* assuming 100% carryover. This corresponds to a concentration of 10 gL^{-1} in the seed vessel). Whatever the precise nutrients that were being derived from the yeast extract, the cells were held in this environment for a substantial period of time during which the low temperature insured that no significant increase in biomass occurred, and hence no major utilisation of the substrates within the yeast extract occurs. Cells contain many complicated systems for ensuring that the production of intermediates in a biochemical pathway only takes place when the pathway is in use. Therefore those intermediates associated with yeast extract utilisation will be manufactured during this time, and those needed for growth on the minimal defined medium decline.

When the 150L was inoculated with cells in this state a short period of rapid growth was observed, followed by a lengthy lag phase. This is a phenomenon known as diauxic growth, and is observed when an organism changes growth substrate. It is the time necessary for the majority of the cells to manufacture new intermediates and enzymes associated with the utilisation of a new substrate. It seems very likely that this

is what is happening in this case. The yeast extract, which has been being utilised by the majority of cells as a major substrate, is diluted 20 fold when the 150L is inoculated and very rapidly exhausted. The cells must then swap back to metabolising the defined medium and this provokes the lag phase. Figure 2.7 shows that it was during this lag phase that the specific α-amylase levels increased dramatically. This again is believed to be linked to plasmid stability.

During the exponential growth of the seed fermenter the average plasmid copy number will fall. During the period the cells are cooled at the end of this fermentation no real growth takes place but neither will the copy number increase significantly as temperatures are too low to allow biological activity. However, during the diauxic lag which is subsequently induced shortly after inoculation of the 150L fermenter conditions will enable plasmids to be replicated, hence the average copy number will increase towards that encoded for on the plasmid. It is this effect that is believed to be responsible for the expression levels obtained utilising this fermentation strategy. Only when a crash cool and hold is employed are the cells exposed to the yeast extract for long enough to switch metabolism to utilising yeast extract. This accounts for the lack of a lag phase or increase in product levels in the 150L fermenter when simply yeast extract was used. Similarly, exposure of the cells to a substantial time at low temperature does not, by itself, prevent exponential growth being achieved rapidly in the 150L fermenter. Only using both establishes the diauxic growth pattern and associated lag necessary for plasmid copy numbers to increase sufficiently to boost product levels.

A similar effect was observed in the seed fermenter, with specific product levels increasing during the initial lag phase. This is believed to be because the plasmid copy number falls during the shake flask stage of inoculum preparation, through what is likely to be a lengthy period of oxygen starvation. This view is reinforced by the very low levels of product observed in the shake flasks during this work. Studies elsewhere (Fisher, 1997) have indicated that full growth is attained in the shake flasks after 10-12 hours. Although taking the cells at this point leads to the use of an exponentially growing, and thus healthier, cell population in the inoculum it is not possible to predict

accurately when the required biomass concentration will be reached in the flask. Hence with no fixed fermentation start time it is nearly impossible to control the end time. Therefore this technique was not adopted here.

The other effect that yeast extract produced was an increase in cell stability after the end of the fermentation, causing both a reduction in the shift of the cell strength and the amount of cell lysis observed in a stirred tank over three hours. This is believed again to be because of its benefits as a rich source of "total nutrients". The exposure of the cells to such easily utilised nutrients during the hour long hold period at the end of the fermentation allows the cell walls to thicken and the membranes to become less leaky, leading to a healthier population of cells. Hence the cells produced in this manner are better able to withstand prolonged periods of agitation and are less likely to die and lyse immediately in a stirred tank. This was highly desirable as the faster the cells lysed, the less opportunity for centrifugation experimentation there would be. However with the inclusion of yeast extract in the production fermenter medium there was no general increase in the cell strength as tracked using homogenisation profiles, indicating the yeast extract provided no nutrient essential for the manufacture of a healthy cell wall that could not be derived from the basic defined medium. Neither was there a change in product partitioning between the fermentation broth and the periplasm, indicating the overall leakiness of a cell's outer membrane was not decreased and again showing that no essential component was provided by the yeast extract. Indeed, leakage into the medium remained high with up to 50% of the total product lost in this manner. This was disappointing, and it is felt that further fermentation development work should be aimed at reducing the leakage from the cell. It was also observed that the homogenisation profile varied substantially between batches, with a change in release at 250 bar of up to 20%. However these differences between batches did not appear to alter cell disruption during centrifugation significantly. All fermentations used for centrifugation research were profiled in this manner, and any that fell outside the range indicated Figure 2.8 were discarded.

The leakiness of the outer membrane was also reflected in the homogenisation profiles when it was observed that the periplasmic product was released into the medium at much lower pressures than the cytoplasmic markers. This could be explained by the

disruption of the outer membrane alone, releasing the contents of the periplasm and leaving the cytoplasmic membrane intact. The trouble with this view is that the periplasm contains the peptidoglycan layer, the structural component of the cell wall which is traditionally thought to give it it's strength and rigidity (see Chapter 1). This is closely associated with the outer membrane, and therefore any disruptive mechanism sufficient to break open the periplasm and release it's contents must also be capable of disrupting the cytoplasmic membrane. It is therefore more likely that the pressures within the homogeniser were causing product to pass through the already leaky membrane, even in cells that were fundamentally strong enough to withstand the conditions without breaking. This effect was also observed during centrifugation trials (see Chapter 3).

Both these advantageous protocols were adopted during the production of cells for centrifugation trials; the first to boost product levels, and hence make monitoring cell break-up during recovery easier, and the second to increase the stability of the cells during the course of the centrifugation experiments. Over subsequent fermentations the increase in product levels was found to be maintained consistently. However, as with the simple batch fermentation product levels were found to be variable, from 75-145 units mL^{-1} .

These effects would clearly be advantageous during an industrial process. However, despite the many documented benefits of low levels of yeast extract it is not thought likely that this will become a standard industrial technique. This is because of the lack of reproducibility of the feed stock discussed in section 2.2.1. Because of it's organic nature it cannot be guaranteed in the same way as a chemical, and thus is not attractive as a medium component for a controlled process. However, it seems likely that with extensive research the components of most benefit could be identified and included in a defined medium. Similarly, in cases such as this where a diauxic growth profile is desirable it should be possible to identify other substrates to use in conjunction with glycerol to produce the same effect, thereby retaining the benefits of this growth profile without the disadvantages of organic medium components.

Fermentation science is extremely complex involving the consideration of engineering, biochemistry and microbial genetics. The work contained in this chapter describes effects that were observed during the establishment of a reproducible fermentation protocol for the reliable production of a feed stock for downstream processing experimentation. As such it was impossible to extend the study to further investigate the effects of yeast extract upon the organism, as the fermentation had to be "locked" to prevent upstream conditions effecting downstream research. It is felt that these findings are positive enough to warrant further research into the effects of such organic nutrients on product levels within a genetically modified cell.

The final fermentation protocol adopted is shown below in Figure 2.11.

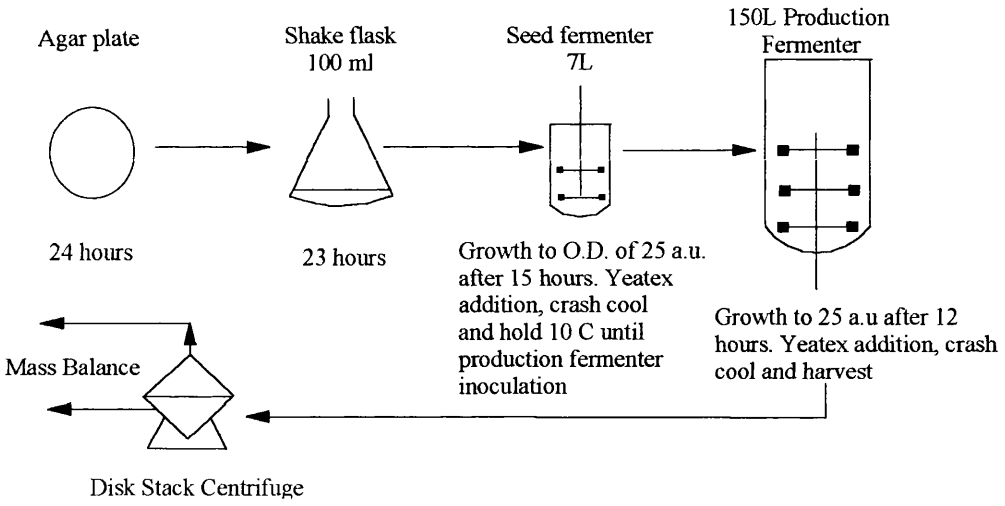

Figure 2.11: Fermentation protocol adopted for production of E.coli JM107 pQR126 expressing α-amylase to the periplasmic space for centrifugation experimentation.

2.7 Conclusions

A fermentation protocol has been established for the production of whole cells for downstream processing experiments. This utilises the addition of yeast extract to the medium to increase plasmid stability and the induction of a diauxic growth-associated lag phase to increase plasmid copy number. These effects have led to a 5 fold increase

in product levels over those achieved using a simple defined medium. Addition of yeast extract to the end of the production fermentation also increases the stability of the cells whilst awaiting downstream processing. Despite these improvements, overall product yields were still found to be variable (+/- 50%).

3.0 CENTRIFUGATION OF WHOLE CELLS

3.1 Introduction

This chapter of the thesis deals with a whole cell harvest process studied using a genetically modified organism, (*Escherichia coli* JM107 pQR126) expressing an active enzyme (α-amylase) to the periplasmic space. Details of the organism and the fermentation conditions used to produce the feed stock can be found in Chapters One and Two respectively. Details of biological assays and reagents used in this work can also be found in Chapter Two. Section 3.2 of this chapter provides an introduction to the recovery of biological solids in a high speed disk stack centrifuge while Section 3.3 outlines the problems of shear disruption in a disk stack centrifuge and details the differences between the standard semi-hermetic (high shear) bowl and the soft-shear hydro-hermetic bowl used in this work. Section 3.4 covers the experimental techniques used in this work. The release studies of both periplasmic and cytoplasmic enzymes during cell harvest are presented in Section 3.5, and finally conclusions are drawn in Section 3.6.

3.2 Recovery of Biological Solids in a Disk Stack Centrifuge

The most widely used method of solid-liquid separation for both cell harvest and cell debris recovery is centrifugation. Several different designs of such machine exist. For a typical cell/broth separation, however, the intermittent discharge disk stack centrifuge (DSC) is most commonly employed. This design is effective at cell recovery, easily obtaining greater than 99% recovery if operated correctly (although many industrial processes would accept a reduction in efficiency to 98% to increase throughput (Rehm and Reed, 1991)). It is also able to operate in a truly continuous manner with respect to both solids and supernatant, with collected solids discharge, or de-sludging, triggered during operation either by timer or turbidity sensor. The solids themselves have a relatively high liquid content due to the frequency of discharge and the

relatively small residence times and acceleration forces within the centrifuge. Solids can therefore be easily pumped through to the next processing stage without need of operator intervention. One potential disadvantage of the design is that only feed suspensions of up to 10% solids content by volume can be handled efficiently (Brunner and Hemfort, 1988). However, unless a fed-batch fermentation strategy has been employed to obtain very high biomass concentrations this is not recognised as a problem. One significant problem with DSC's is the high levels of shear and other disruptive forces which can be developed within them: these may be sufficient to disrupt whole cells (Datar and Rosen, 1987). A cells' strength is dependant on the fermentation history i.e. specific growth rate, stage of development, growth medium and growth phase, as well as genetic type (wild type or recombinant). Such forces certainly cause significant difficulties when recovery is of biological flocs or precipitates. It is understanding these disruptive forces and their effects on recovery that is the main focus of this thesis.

3.2.1 Principles of Centrifugal Recovery

Centrifugal solid/liquid separation is a process which may be considered exactly analogous to sedimentation, the process whereby solids "settle out" of a liquid stream under the action of gravity. Thus Stokes Law (Stokes, 1851) is still the main method of describing sedimentation in a centrifuge.

$$V_g = \frac{(\rho_S - \rho_L) d_S^2 g}{18\mu} \qquad \textbf{(3.1)}$$

where
- V_g = settling velocity under gravity (m s^{-1})
- ρ_S = density of the particles (Kg m^{-3})
- ρ_L = density of the suspending fluid (Kg m^{-3})
- μ = suspension dynamic viscosity (N s m^{-2})
- d_s = diameter of particle (m)
- g = acceleration due to gravity (m s^{-2})

For separation in a centrifugal field the acceleration the particle experiences under gravity is replaced with that due to centrifugal force. The settling velocity V_Z is therefore given by;

$$V_Z = \frac{(\rho_S - \rho_L) d_S^2 \omega^2 r}{18\mu} \qquad \textbf{(3.2)}$$

where V_Z = settling velocity in a centrifugal field (m s^{-1})

ω = angular velocity of the centrifuge (rad s^{-1})

r = radial position of particle (m)

Stokes Law is only strictly applicable to a system of dilute spherical particles under laminar flow conditions in a Newtonian fluid: there are therefore four key causes of deviation from equation 3.2

- non-spherical particles (biological solids can be highly irregular in shape)
- non-Newtonian rheology (many broths are highly non-Newtonian)
- hindered settling (non-dilute system)
- non-laminar flow (flow in key areas of a DSC is certainly non-laminar)

These issues will be addressed later in this chapter.

3.2.1.1 The Equivalent Settling Area (Sigma) Concept

The most common method of comparing the performance of different scales or designs of centrifuge is to use the concept of "Sigma factor" developed by Ambler in 1952, which defines the relationship between centrifuge performance, total volumetric flow rate and scale of equipment.

The force operating on a particle in a centrifugal field is given by;

$$F_P = (m_S - m_L)\omega^2 r \qquad \textbf{(3.3)}$$

where F_P = Force acting on particle (N)

m_s = mass of the particle (Kg)

m_L = mass of liquid phase displaced by the particle (Kg)

If the particle is considered to be a sphere then equation 3.3 becomes;

$$F_P = \frac{\pi}{6}(\rho_S - \rho_L)d_S^3\omega^2 r \qquad \textbf{(3.4)}$$

Opposing this is the resistance of the liquid phase to motion through it, given by Stokes Law;

$$F_L = 3\pi\mu d_S \upsilon \qquad \textbf{(3.5)}$$

where F_L = resistance of liquid phase to particle motion (N)

υ = kinematic viscosity of fluid ($m^2\ s^{-1}$)

At equilibrium, i.e. the particle reaches a constant velocity V_Z and

$$F_L = F_p \qquad \textbf{(3.6)}$$

Hence the velocity of the particle settling under a centrifugal field at equilibrium, V_Z is given by;

$$V_Z = \frac{(\rho_S - \rho_L)d_S^2\omega^2 r}{18\mu} \qquad \textbf{(3.7)}$$

Combining equations 3.1 with 3.7, it can be seen that the relationship between V_Z and the settling velocity under gravity V_g is simply;

$$V_Z = V_g \frac{\omega^2 r}{g} \qquad \textbf{(3.8)}$$

If the simplest design of continuous centrifuge is then considered, the tubular bowl centrifuge (effectively a rotating cylinder with capped ends), with feed suspension fed continuously in at one end and removed at the other, and liquid in the bowl behaving as a thin layer of thickness S against the wall of the bowl, then the residence time of any particle in the centrifugal field is given by;

$$\tau = \frac{V_e}{Q} \qquad \textbf{(3.9)}$$

where τ = residence time (s)

V_e = effective volume of centrifuge (m^3)

Q = volumetric flow rate through the centrifuge ($m^3\ s^{-1}$)

If the liquid layer within the bowl is thin, then it can be assumed that the sedimentation velocity of a particle within the centrifuge will be approximately constant. The distance travelled by such a particle within the centrifuge is therefore given by;

$$X = V_Z \tau \qquad \textbf{(3.10)}$$

where X = distance travelled by particle of diameter d_s in centrifugal field (m)

An obvious consequence of this that if X is greater than the distance separating the particle from the bowl wall it will be recovered, otherwise it will remain suspended in the feed liquid and exit with the supernatant. If an ideal system is examined, being

operated under the condition that 50% of particles of diameter d_S are recovered (the "cut point") i.e. $X=S/2=X_{50}$ then the flow rate Q is given by;

$$Q = 2V_g \cdot \frac{\omega^2 r}{g} \cdot \frac{V_e}{X_{50}} \qquad \textbf{(3.11)}$$

Re-arrangement and expansion of equation 3.11 enables us to find the critical diameter at a given flow rate d_c, i.e. the diameter of particle which will just be removed by the centrifuge;

$$d_c = \sqrt{9\mu Q \frac{X_{50}}{V_e \omega^2 r}} \qquad \textbf{(3.12)}$$

Equation 3.11 can be re-written as;

$$Q = 2V_g \Sigma \qquad \textbf{(3.13)}$$

where Sigma is given by

$$\Sigma = \frac{V_e \omega^2 r}{g X_{50}} \qquad \textbf{(3.14)}$$

It can be seen in equation 3.13 that V_g depends entirely on the physical characteristics of the particle and liquid system, whilst Σ depends entirely on the centrifuge design. Sigma can be shown to be analogous to the area of a gravity settling tank equal in separating performance to the centrifuge and so has the units of area (m^2).

From equation 3.13 it can be seen that

$$\frac{Q_1}{\Sigma_1} = 2V_g = \frac{Q_2}{\Sigma_2} \qquad \textbf{(3.15)}$$

i.e. any two centrifuges operating on the same feed material will recover particles with identical efficiency if the ratio of flow rate to Sigma factor for both machines is identical. This is used as the basis for scale up between centrifuges, and as a major design factor when specifying a machine for a given task. It may also be used to compare the performance of different types of centrifuge: however, care must be taken as all specific formulae describing Sigma factor for a given design of centrifuge involve the implicit assumption of ideal flow through the machine. This is never entirely accurate, but the non-ideality varies between type and this has led to the use of empirically derived correction factors. The following section will develop the equations/analysis for a disk stack machine. Similar analysis for other centrifuges can be found elsewhere (Rehm & Reed, 1991).

3.2.2 Separation in a disk stack centrifuge

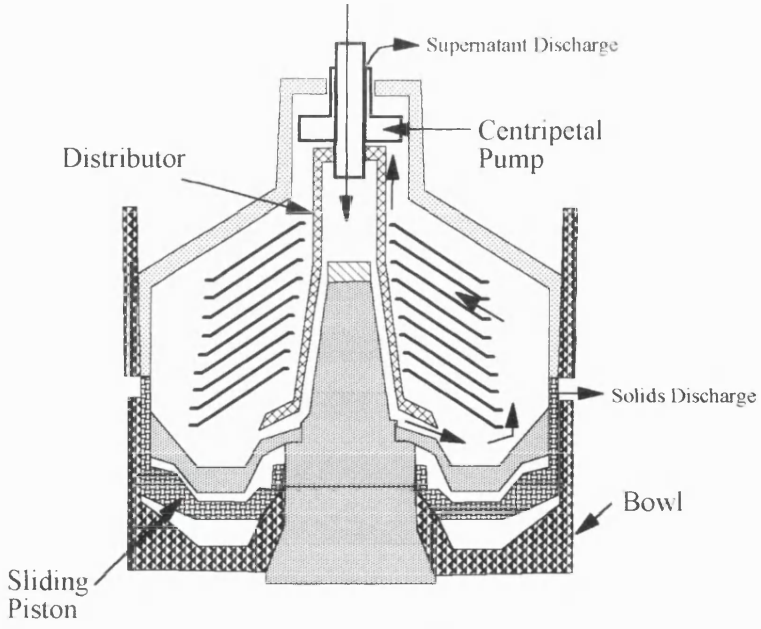

Figure 3.1 The internals of a disk stack centrifuge

Figure 3.1 overleaf shows the internal structure of a standard disk stack centrifuge. Feed suspension enters through the central pipe of the centripetal pump, which is held stationary in the centre of the rotating bowl. It then flows down into the distributor, where it is accelerated to the speed of the bowl, before flowing through six evenly arranged channels into the disk space, where separation itself occurs. The flow is divided equally between all the conically shaped disks in the stack, which are held a small distance apart from each other (typically 1-2 mm depending on the solid being separated) by six caulks or spacer ribs on the surface of each disk. The number of disks employed in the stack varies with scale from about 50 in a pilot scale machine to more than 250 in an industrial separator (Mannweiler, 1990).

When considering separation in a DSC, it is assumed that flow between the disks is laminar and therefore of a pattern where flow rate is at a maximum half-way between 2 disks, and zero at the surface of either disk (Figure 3.2).

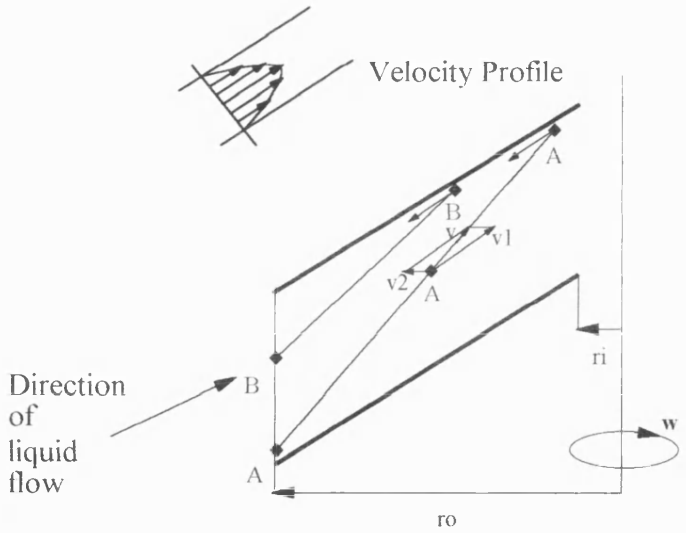

Figure 3.2: Separation between the disks

Particle A enters the disk space at the left hand side of the diagram: it will then move upwards between the disks under the influence of velocity component v_1 (parallel to the disks), and outwards under the influence of centrifugal force (component v_2). It is the resultant velocity v which determines the motion of the particle.

The diagram shows particle A as sufficiently large and dense to reach the surface of the top disk before leaving the disk stack. The velocity component v_1 is zero here, and thus all particles settling on the surface of the upper disk will eventually slide down the surface of the disk and collect at the periphery of the rotating bowl, in the solids holding space.

Smaller less dense particles will be less influenced by centrifugal force. Depending on the position at which they enter the centrifuge they may still be collected as solids (particle B Figure 3.2). However, other particles which enter the disk space sufficiently close to the lower disk will escape at the axial end of the disk space and flow out of the machine in the clarified liquid discharge stream.

This demonstrates an important concept in the operation of such machines: centrifugal separation does not give rise to a defined "cut-off" point, whereby all particles of larger than a certain size are removed and all particles of smaller than a given size are passed through in the liquid stream. Rather, the concept of grade efficiency is used to assess centrifuge performance (Svarovsky, 1990). The grade efficiency function will have a value of 100% if all particles of a given size are removed, and 0% if no particles of that size are removed. This concept will be further examined in Chapter 4.

Clarified supernatant flows into the centripetal pump chamber, above the disk space. Because the centripetal pump is stationary and the fluid is rotating, slots cut into the pump are able to scoop up the supernatant, converting approximately 50% of it's rotational energy into a pressure head, which is used to pump the supernatant out of the centrifuge. The pressure produced is a function of rotational speed of the bowl, the external diameter of the centripetal pump and crucially the depth of immersion of the pump into the rotating liquid circle. As throughput increases, the depth of immersion also increases: this illustrates the important point of this system of supernatant removal, that it is, within limits, self leveling. However an increase beyond the maximum throughput of the machine (about 400 L h^{-1} in the standard pilot model used in this work) results in the pump being unable to cope and flooding out of the centripetal pump chamber into the solids collection space. To suppress foam formation

in the supernatant discharge line which results from the centripetal pump chamber containing air a throttle valve, or on more modern machines a compressed air supply, is included in the discharge line to enable a backpressure to be applied. The amount of pressure that can be used is limited by the occurrence of centripetal pump overflow.

When the solids holding space becomes full solids will be re-entrained with fluid entering the disks as quickly as particles are separated, resulting in a drop in clarity of the supernatant. This is the "breakthrough" point at which the centrifuge must be discharged. To achieve this process water is allowed into the space between the bottom of the distributor and the top of the sliding piston. This forces the sliding piston down and uncovers six evenly spaced slots in the periphery of the bowl. Solids are then discharged from the centrifuge under centrifugal force. There are two types of discharge that can be performed; full and partial. A full discharge involves opening the bowl for a time sufficient to remove the entire contents of the bowl. Since only about 1/2 of the volume of the bowl will be occupied by solids when the centrifuge reaches it's capacity this mode of operation gives rise to a "wet" solid (about 25% solids on a dry weight basis). A partial discharge entails holding the bowl open for only the time it takes for the sedimented solids to flow out. Typically this is between one and two seconds as opposed to 10 seconds for a full discharge. Normal operation uses a combination of the two, with four partial discharges followed by a full discharge being standard.

When the required discharge has been performed the supply of process water to the bowl is shut off, and the remaining water drains back through slots to underneath the sliding piston, which rises back up under centrifugal force to re-cover the discharge ports in the bowl.

3.2.3 Deviations from Stokes Law

As has been stated, there are several major causes of deviation from Stokes Law of sedimentation which effect industrial separators (Section 3.2.1);

Obviously, when assessing shear break-up effects on the performance of a disk stack centrifuge, it is important to understand reasons for deviation from theoretical performance other than those due to shear forces. It is easy to measure the viscosity of a solution as an indicator as to whether or not it is Newtonian. Similarly the shape of particles being recovered may be examined under a microscope: the *E.coli* used as a test system in this chapter are approximately spherical, having average dimensions of one by two microns. However, the problems of hindered settling and non-laminar flow have been shown to have a large effect on theoretical recovery, and thus bear closer examination.

3.2.3.1 Hindered Settling

Hindered settling is the phenomenon whereby as the concentrations of particles in a feed stream increases, so the average distance between particles decreases and they begin to interfere with each other in such away as the sedimentation velocity of each particle is generally reduced. Stokes Law strictly only applies to suspensions where the particles are separated from each other by a large enough distance that each may be considered entirely independent of the next. However, most biological systems in use contain a much higher solids loading than this, very artificial, "ideal" suspension and therefore much work has been done in the field of hindered settling (Barnea and Mizrahin, 1973, present a thorough review). The most widely used correlation to account for hindered settling is that derived empirically by Richardson and Zaki (1954)

$$V_g^* = V_g\left(1 - C_v\right)^{\sigma_p} \qquad \textbf{(3.16)}$$

where V_g^* = hindered settling velocity under gravity (m s^{-1})

C_v = concentration of solids (ratio, volume basis)

σ_p = particle geometric factor (-)

For mono-sized spherical particles σ_p has a value of 4.6. However, for non-spherical particles σ_p can vary between 10 and 100, very much increasing the effect. Hence Stokes Law can very much overestimate the separation ability of an industrial separator.

When considering, however, the whole cell test system in use for this work such a problem cannot be viewed as so serious for two reasons. Firstly as was explored in Chapter 2, the fermentation was operated to produce a feed stock of about 10 g L^{-1} dry cell weight, an insufficient concentration of solids (about 2% on a volume basis) to move far into the region of hindered settling (Mannweiler, 1990, worked with 1% polyvinylacetate suspensions to eliminate such effects). Furthermore, suspensions within a centrifuge tend to become more dilute with time as particles separate out leading to falling concentrations of particles with passage through the machine (Baron and Wajc, 1979). Secondly this work revolves around a methodology of comparing the performance of two similar disk stack centrifuges directly to each other using the same feed suspension. Any deviation in performance due to hindered settling will therefore be expected to be equal in both machines.

3.2.3.2 Flow through the Disks

As has already been stated, Stokes Law of sedimentation only applies in laminar flow fields (i.e. in flows with $Re_p<0.5$). For turbulent flow regimes, alternative equations have been derived by Sokolov (1971) and Hsu (1981).

Sokolov gave three main reasons for deviation between the ideal disk stack centrifuge described by Stokes Law and a real disk stack centrifuge. These are:

- Flow through the disk space is not necessarily laminar over the whole gap width and radius
- Particle sedimentation is not irreversible

- Solids loading at the entrance to the disk is not even, and disproportionate fluid flow within the disk spacing can occur

It has been shown that the velocity profile across the disk spacing in fact depends on a dimensionless number λ which accounts for Coriolis and shear force effects (Sokolov, 1971, Brunner and Molerus, 1979, and Zastrow, 1976):

$$\lambda = h\left(\frac{\omega \sin\theta}{\nu}\right)^{\frac{1}{2}} \qquad \textbf{(3.17)}$$

where h = disk spacing (m)

θ = half the disk angle (degrees)

υ = fluid kinematic viscosity ($m^2\ s^{-1}$)

ω = angular velocity (rad s^{-1})

If λ is smaller than π then the flow between the disks is parabolic, as assumed in the theoretical description of flow in a disk stack centrifuge. The value of λ in industrial separators is, however, between 5 and 28. Brunner and Molerus (1979) calculated flow profiles for such machines and found that the relative circumferential velocity increases from the disk surfaces to the centre of the disk gap, and at large λ values may approach values λ times larger than the average radial velocity. They argued, therefore, that at large λ values this velocity component will split into two thin layers, one near to each disk surface. Within these layers both the velocity and the thickness of the layer will increase with increasing λ: hence the Reynolds number will also increase and transition to turbulence can take place (caused by an interplay between Coriolis, frictional and centrifugal forces).

This behaviour was studied by Willus and Fitch (1973) who studied flow patterns in a simulated disk fitted with six long radial spacing ribs rather than the traditional point spacers. They showed that the parabolic flow profile seen in non-rotating systems does not hold true in rotating systems, where Coriolis and incremental centrifugal forces act on particles impelling them at right angles to their local directions of motion. The spacer ribs, however, suppressed the transition from laminar to turbulent flow by

preventing circumferential flow and vortex formation (Brunner and Molerus, 1979). This has lead to modern centrifuges all utilising a spacer rib or caulk design, as opposed to point spacers.

The other cause for deviation given by Sokolov was uneven solids loading through the centrifuge. Skvortsov in 1984 examined the role of the solids holding space, and found that extremely coarse particles may have already sedimented into the solids holding space, giving rise to such uneven loading. However, without converting to a full nozzle discharge machine, it is difficult to do without a significant solids holding volume, because of the increase in the number of discharges that a reduction would entail, and the corresponding increase in wetness of solids (see section 3.2.2).

Again, however, within the experimental system used here these effects should not produce differences in performance between the two machines studied as the design of the disks and the solids holding space in both the semi-hermetic and the hydro-hermetic designs is identical.

3.2.4 Sigma Factor for the Disk Stack Centrifuge

In 1962 Trowbridge provided the theoretical equations needed to calculate Σ factor for a range of different centrifuge designs. The equation for a disk stack centrifuge is given below;

$$\Sigma = \frac{2}{3g}\pi Z_s \omega^2 \cot\theta\left(R_o^3 - R_i^3\right) \qquad \textbf{(3.18)}$$

where Z_s = number of disks in the disk stack (-)

θ = half the conical disk angle (rads)

R_o = outer disk radius (m)

R_i = inner disk radius (m)

In modern centrifuges the disks are usually held apart from each other using a number of evenly spaced caulks or ribs along the surface of each disk, as opposed to point spacers, to aid suppression of transition to turbulent flow. These obviously occupy area within the disk stack and reduce the equivalent settling area of the machine. To take account of this a multiplier is applied to equation 3.18;

$$F_1 = 1 - \frac{3Z_c b_c}{4\pi R_o} \cdot \frac{\left(1 - \left[\frac{R_i}{R_o}\right]^2\right)}{\left(1 - \left[\frac{R_i}{R_o}\right]^3\right)} \qquad \textbf{(3.19)}$$

where F_1 = Σ correction factor to account for disk caulks (-)

Z_c = number of caulks per disk (-)

b_c = caulk width (m)

A further error is introduced by the assumption implicit in this equation of ideal flow and adherence to Stokes Law, something which in practice is never achieved. Different designs of centrifuge, however, will deviate by different amounts. To compensate for this error, a series of correction factors have been empirically derived to correct sigma factor calculations for different separator designs, benchmarked on the assumption that a laboratory scale bottle centrifuge is 100% efficient (i.e. is an ideal "Stokes" separator). The efficiency factor employed for the disk stack centrifuge is 40%. However, as this work will compare only one design of disk stack to another, use of the efficiency factor is not necessary (Kirk-Othmer, 1992). (The calculation of Σ factors for the machines in use in this work can be found in Appendix 1.)

3.3 Breakage of Biological Solids in the Disk Stack Centrifuge

There are many problems associated with the centrifugal recovery of biological solids; small particle size, low density difference between the solid and liquid phases, high suspension viscosity, and the sensitivity of biological particles to shear-associated

break-up effects. Of perhaps the greatest concern is particle degradation and product loss within the separator (any reduction of particle size prior to separation will obviously make such a particle harder to recover; and disruption to a particle such as a whole cell which entails product release will result in yield loss when only the solid fraction is retained). However, the exact nature of the mechanisms causing concern, and the level of breakage seen, will depend to a large extent on the nature of the solids being processed. In the bio-processing industries these can be split into four main categories:

- whole cells
- cell debris
- protein precipitate particles
- inclusion bodies

Of these categories the work in this thesis examines two in detail; whole cell processing in this chapter, followed by the processing of polyethylene glycol precipitates of proteins released from homogenised yeast in Chapter Four. However, some examples of the different concerns raised by different solids are that when processing cell debris the target enzyme has already been released into the liquid stream being processed. Therefore any air/liquid interfaces seen in a turbulent area of a centrifuge would be expected to be extremely harmful to such a protein: however, such interfaces are unlikely to have any effect on whole cells. Similarly, whole cells may be expected to be much tougher than protein precipitates, and therefore be damaged only by higher destructive forces within a separator than those necessary to destroy protein precipitates. They are, however, usually of a different size to such precipitates, and this may approach an order of magnitude. This will clearly have an impact on the way such disruptive forces interact with the particles to be processed.

When considering fluid flow through a DSC, with particular reference to areas where breakage of biological solids may occur, it is possible to divide the centrifuge into three major areas:

- Discharge
- Disk Space
- Feed Zone

3.3.1 Breakage upon Discharge

Cells being discharged from a disk stack centrifuge undergo a large pressure drop and rapid acceleration as they are thrown out at high velocity through the discharge ports; furthermore they will then suffer a mechanical impact on the walls of the solids collection chamber. In addition, as the solids are approximately ten-fold more concentrated than the feed suspension, the viscosity of the discharging solution will be high, giving rise to high theoretical shear rates. However, although theoretically this could form an important site for disruption, it must be born in mind that the vast majority of biological solids have extremely little mass, being very small. This gives rise to low momentum values even when the material is travelling at high speed. This makes impact damage of the type postulated during discharge unlikely. Also, when considering cell harvesting, disruption at this stage becomes almost irrelevant: the cells have already been separated from the fermenter broth and the next stage will inevitably be a release step to enable further processing. It is nevertheless important to establish whether the discharge process leads to product release in order to aid our understanding of the overall effect of passage through a disk stack centrifuge on a solid. This has been investigated as part of the experimental work within this chapter.

3.3.2 Breakage in the Disks

Any disruption occurring to particles in the disk spaces prior to separation will obviously have a negative impact on the ease of separation of such particles. As has already been stated flow through the disks is theoretically laminar and thus may be considered non-disruptive. However, under certain circumstances it can become turbulent (see section 3.2.3.2). Despite this, the disk region is generally considered

non disruptive for two important reasons. Firstly, centrifuges are rarely operated under throughput conditions where flow in the disk spaces could become turbulent. This is because of it's high negative impact on the separation ability of the machine, and because biological particles are generally difficult enough to recover that most machines have to be operated under relatively low throughput conditions to obtain satisfactory clarification. Secondly, any forces that could theoretically be generated in the disk spaces by such a transition are very much smaller than those experienced in both the feed zone and upon discharge. For these reasons it will be assumed that no disruption occurs in the disk spaces throughout this thesis.

3.3.3 Breakage in the Feed Zone

The most important region to consider when examining disruption in a disk stack centrifuge is the feed zone. This is for two reasons. Firstly any disruption here occurs before separation and thus will cause yield loss, and secondly, this is the area where maximum shear conditions in an industrial centrifuge can in theory be developed.

The feed zone is the area that accelerates the fluid from stationary to the angular velocity of the rotating bowl, and within it fluid is subjected to a sudden increase in both radial and tangential velocity. This is the area which is considered responsible for most protein aggregate break-up when a disk stack centrifuge is employed in such recovery (Bell, 1982, and Mannweiler, 1990).

It is composed of two parts: a stationary cylindrical feed pipe formed by the bottom section of the centripetal pump, and a flow distributor. Feed suspension flows into the rotating bowl via the feed pipe and is then tangentially accelerated in both the distributor neck (the cylindrical section), and the conical distributor foot. As the feed reaches the bottom of the distributor foot it is passed out at the rotational speed of the bowl through six evenly distributed channels onto the disks.

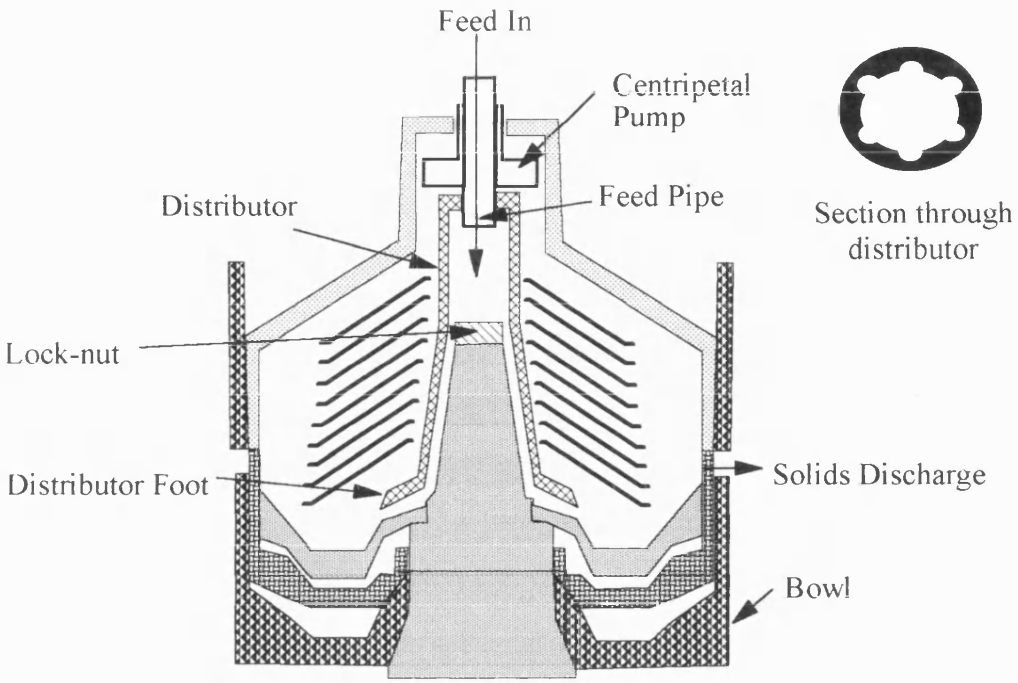

Figure 3.3: The Semi-Hermetic Disk Stack centrifuge

Figure 3.3 shows a semi-hermetic disk stack centrifuge; this is the standard design in use today and is so called as it is only hermetically sealed with respect to the clarified liquid discharge stream. Several other designs are now becoming available (most notably the hermetic and hydro-hermetic) and this thesis will compare the functioning of the hydro-hermetic design with the semi-hermetic, which has previously been shown to cause the most damage of all three to protein precipitates (Mannweiler, 1990).

5 key locations have been identified in the feed zone of such a machine which may be important when considering damage to particles in the suspension (Van der Linden, 1987).

- Primary contact between the centrifuge and the feed suspension occurs at the lock-nut; this deflects the liquid flow which has been ejected from the feed pipe out onto the walls of the distributor. Owing to the short contact time little angular momentum is expected to be transferred; however, high radial shear rates will be generated at the surface of the lock-nut.

- The distributor is fitted with acceleration ribs (see section in diagram 3.3) which both aid acceleration and guide fluid through the channels at the base of the distributor foot and thus out onto the disks. However, intensive contact between the distributor and the feed suspension will occur here.
- The trajectory in between the distributor rib and the liquid surface, at the pressure side of the guiding rib.
- The inner wall of the distributor where axial shear can become predominant when flow rates are low resulting in a thin liquid layer.
- The conical distributor foot, where high shear rates may occur during flow through onto the disks.

In practice particle damage is probably due to a combination of all five factors. However, of particular importance when considering cell wall breakage are the effects of shear and cell impingement on the distributor ribs; both these mechanisms are thought to be responsible for cell disruption in the high pressure homogeniser (Ayazi Shamlou *et al*, 1994.

There are several different techniques which have been used to estimate the shear rates that particles will be exposed to in the feed zone of a centrifuge. Chief amongst these are the theoretical consideration of the centrifuge as a spinning disk, which effectively seeks to model the initial contact of the feed suspension with the centrifuge lock-nut, and an overall consideration of power dissipation. This can be used to calculate a generalised shear rate associated with passage through the feed zone. These will be considered in detail in Chapter 5 where laboratory scale mimics of the feed zone are designed and evaluated.

3.3.3.1 Operational considerations of the Semi-Hermetic Feed Zone

When considering the feed zone of the standard semi-hermetic disk stack centrifuge one key feature of the machine's hydro-dynamics bears closer examination. This is the depth of flooding in the distributor.

The depth of flooding will depend on four factors:

- Level of backpressure on supernatant discharge line
- Hydraulic resistance of distributor foot to flow through and onto the disks
- Hydraulic resistance of disk stack
- Throughput

The level of backpressure in use on the supernatant discharge line will effects the amount of liquid held up in the centrifuge as a whole, as it serves to increase the resistance to flow of the bulk of the throughput, in the form of supernatant, out of the machine. However, as has already been pointed out the centripetal pump itself is to a certain extent self-controlling, and the backpressure applied will have a much greater effect on the level in this chamber than on the flooding depth in the distributor. To overcome any such effects in this thesis however, the backpressure employed was held constant when considering effects such as throughput and rotational speed of the bowl.

The hydraulic resistance of both the distributor foot channels and the disk stack is obviously a major influence, and indeed is a key design parameter for disk stack centrifuges. However, as this is obviously a constant and a function purely of the machines design, we can ignore this here.

This leaves hydraulic throughput as the most important parameter. At low flow rates there will be very little liquid resident in the feed zone of the semi-hermetic design of

disk stack centrifuge: such liquid as there is will be resident entirely in the flow channels between the distributors acceleration ribs. As throughput increases, the volume of liquid held up in the feed zone will increase, and the liquid layer distributed around the outer wall of the distributor foot will become thicker. This will give rise to a longer residence time for particles in the feed zone, which may be counter-acted by the higher throughput reducing it. It will also decrease the specific power input per unit volume and thus the bulk shear rate. Eventually the throughput exceeds the hydraulic capacity of the feed zone, and the distributor passes feed suspension directly into the centripetal pump chamber as an overflow mechanism (distributor overflow).

3.3.3.2 The Hydro-Hermetic Feed Zone

Figure 3.4 overleaf shows the hydro-hermetic (soft-shear) design disk stack centrifuge. This incorporates several key differences in feed zone design to reduce damage to biological solids being processed.

The most significant alteration is in the level of liquid held up inside the distributor foot. The channels that the feed suspension must flow through out of the distributor foot and onto the disk stack have been slightly altered to produce an increase in resistance to flow. This in turn partially floods the distributor foot, with the limiting condition being a liquid level just sufficient to immerse the hydro-hermetic disk, a circle of metal attached to the base of the feed pipe. At the scale used for this work, this occurred at a flow rate of approximately 50 L h^{-1}.

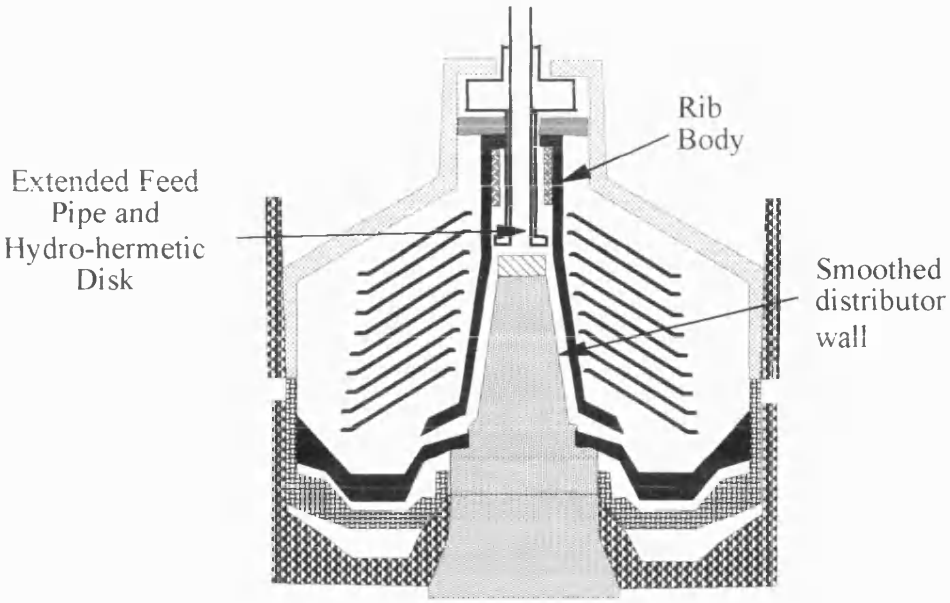

Figure 3.4: The Hydro-hermetic (soft shear) design disk stack centrifuge.

This has two effects. Firstly, the power that is input into the liquid in the distributor foot is distributed over a much greater volume (approximately 30 mL as compared to 1 mL in the standard semi-hermetic feed at low flow rates). The physical meaning of this is at the same flow rate, particles are resident in the hydro-hermetic feed zone longer than in the semi-hermetic feed. This means that angular acceleration within the hydro-hermetic feed zone is reduced (the limiting condition is obviously all liquid must be at the rotational velocity of the bowl as it exists the distributor foot), which would be expected to translate to a large reduction in the shear forces developed in the feed zone. Secondly, and potentially of equal importance, primary contact between the bowl and the feed suspension is no longer at the lock nut; instead it is introduced into a rotating core of fluid. Thus there is no potential impact site with this design of machine and further more, the majority of particles will no longer flow through the high shear region above the lock-nut.

No acceleration ribs exist within the upper section of this design of distributor foot, only at the base where the feed suspension is already at a similar velocity to the bowl. Here they serve more to guide the feed suspension into the channels through which it

flows onto the disk stack. Thus impact damage caused by collision with the acceleration ribs in a standard design is negated.

There is, of course, no air-liquid interface present within the bulk of the feed zone. Although such interfaces are not thought important in terms of whole cell disruption, they can damage protein precipitates or soluble enzymes. This design therefore should show improved characteristics over the semi-hermetic feed when handling such a feed solution.

One draw back with this design is, however, the rib body at the top of the distributor. This consists of six equally spaced ribs rather like the acceleration ribs in the standard design. At feed flow rates higher than 50 L h^{-1} the depth of flooding of the feed zone increases as with the standard semi-hermetic design, until at a flow rate of approximately 250 L h^{-1} the feed zone of the pilot-scale machine floods out into the supernatant discharge: at some point between these two flow rates the rib body becomes flooded. This will act as a high speed impeller, impinging rapidly upon cells in the region and thus could act as an extra source of disruption. However, at steady state it is believed that there should be little re-circulation of flow up over the hydro-hermetic disk into the rib body, even when fully flooded. Therefore, only a small fraction of the feed will interact with the rib body.

A further disadvantage is, of course, the much reduced operating throughput range available. For the two equivalent scale bowls used in this experimentation, the standard semi-hermetic bowl was able to operate in the range 0 to approximately 400 L h^{-1} with no significant problems. The hydro-hermetic, however, was limited to the region 50 to 250 L h^{-1}. This, of course, reduces the machines versatility and may lead commercial processors to have to invest in several centrifuges if different feed suspensions are to be processed, where formerly they could have used one.

3.4 Materials and Methods

3.4.1. Preparation of Feed Suspension

Feed suspension was batch-grown *E.coli* JM107 pQR126 (see Chapter 2).

3.4.2 Biological Assays

For details of the biological assays performed (those for α-amylase, glucose-6-phosphate dehydrogenase and Biorad™ total protein) see Chapter 2.

3.4.3 Homogenisation

100 % release levels of enzyme were established using an APV Lab 40 high pressure homogeniser (APV Manton Gaulin, Derby, UK).as described in Chapter 2.

3.4.4 Clarification Efficiency

Clarification efficiencies were based on optical density of sample read by a spectrophotometer (Uvikon 922, Kontron Instruments Ltd., Watford, UK) at 600 nm. The instruments limit of linearity was 1.0 a.u. The procedure used was as follows:

1. The optical density of a representative sample of supernatant from the process centrifuge was measured.
2. The optical density of a representative sample of feed solution was measured.
3. A sample of feed suspension was centrifuged in a microfuge at 12,400 G for 30 minutes (GS-15 benchtop Centrifuge, Beckman Instruments,

UK). The optical density of this sample was then measured and used as a background control.

4. The clarification efficiency was then calculated as follows;

$$C_e = \frac{(O.D.\,feed - O.D.\,control) - (O.D.\,sup\,erna\,tan\,t - O.D.\,control)}{(O.D.\,feed - O.D.\,control)} \quad \textbf{(3.20)}$$

where C_e = clarification efficiency (%)

3.4.5 Centrifugation

Two pilot scale disk stack centrifuges were employed during this experimentation, the

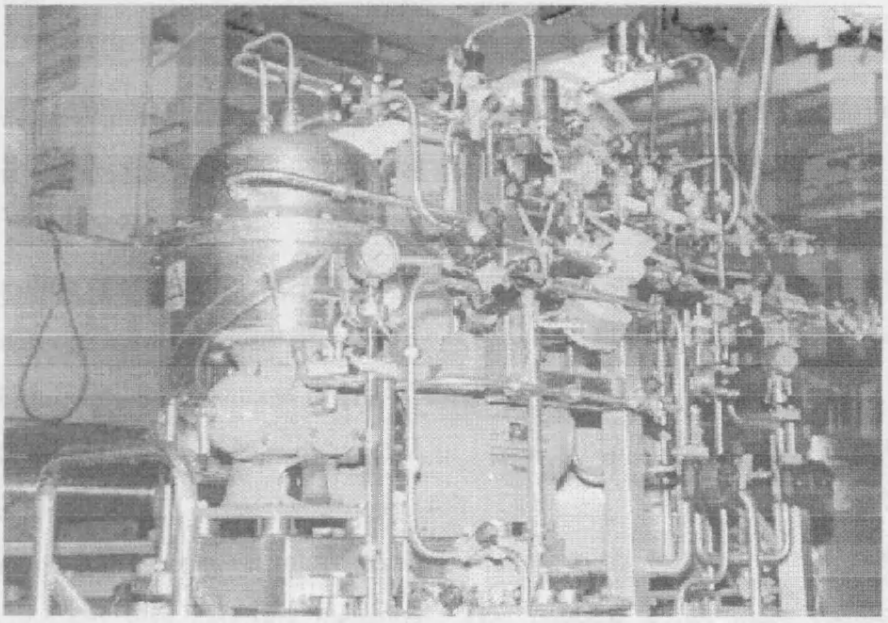

Figure 3.5: Westfalia Separator CSA-1 Disk Stack Centrifuge

SAOOH with semi-hermetic bowl, and the CSA-1 variable speed steam sterilisable model with both hydro-hermetic and semi-hermetic bowl, (Westfalia Separator Ltd., Milton Keynes, UK). The CSA-1 separator is shown above. Both machines were of the same scale (0.6 L total bowl volume) and of identical design (excepting feed zone difference between the semi-hermetic and hydro-hermetic designs), with the key

difference being the amount of automation and control available on the newer CSA-1 model (a photograph of the CSA-1 control panel is shown below). This enabled

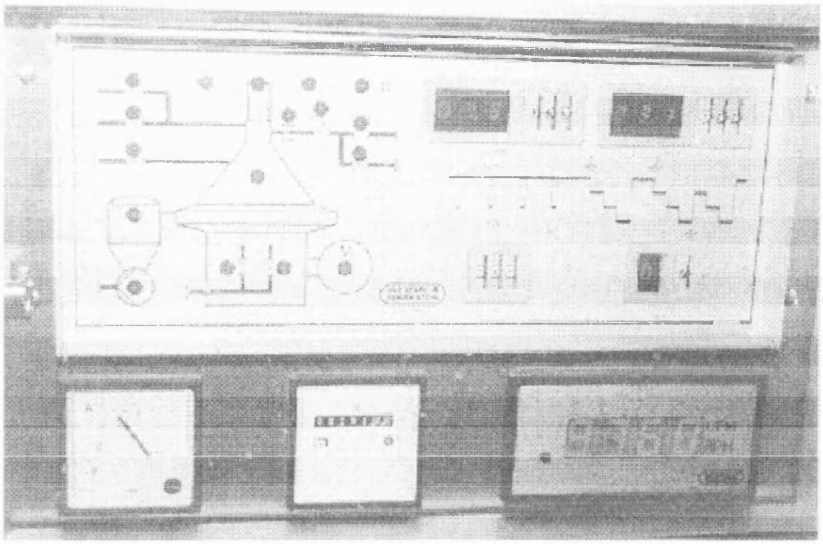

Figure 3.6: Control panel of CSA-1 Disk Stack Centrifuge (Westfalia Separator, Milton Keynes, UK)

more precisely timed discharges, better flow rate control and the effect of varying bowl rotational speed to be examined.

All operation conditions were examined in a batch-wise manner, with the batch unit being one centrifuge bowl full of solids i.e. at each condition the feed suspension was pumped through the machine at a set flow rate using a Watson Marlow 605 Di peristaltic pump (Watson Marlow Ltd., UK) until solids breakthrough occurred. The collected solids were then discharged (full discharge), with a sample of both the supernatant and the solids retained for analysis. Also, the volume of supernatant and solids collected was carefully measured. This enabled a full mass balance to be conducted as follows:

Condition	I.U. mL^{-1} enzyme in solids	I.U. mL^{-1} enzyme in supernatant	Volume of solids (mL)	Volume of supernatant (mL)	Total enzyme solids	Total enzyme supernatant
1	a	b	x	y	xa	yb
2						

Table 3.1: Sample mass balance on centrifuge

This information was then used to establish the level of release that has occurred during passage through the centrifuge as shown below

$$\text{Total Release} = xa + yb \quad \textbf{(3.21)}$$

$$\text{Total Volume} = x + y \quad \textbf{(3.22)}$$

$$\text{Therefore the target enzyme concentration} = \frac{xa + yb}{x + y} = E_R \quad \textbf{(3.23)}$$

The background level of enzyme in the feed suspension (E_0) and 100% release (E_{100}) from the feed suspension was established using a high pressure homogeniser (see Chapter 2). Therefore;

$$\% \text{ Release} = \frac{E_R - E_0}{E_{100} - E_0} * 100\% \quad \textbf{(3.24)}$$

Where E_R = Target enzyme concentration after passage through centrifuge (I.U. $m L^{-1}$)

E_0 = Background level of target enzyme in feed suspension (I.U. $m L^{-1}$)

E_{100} = 100 % release of target enzyme from feed suspension (I.U. $m L^{-1}$)

Obviously a further breakdown, that of percentage of released enzyme in the supernatant fraction and percentage of released enzyme in the solids can also be calculated from this information.

If such detailed information was not required the mass balance was simplified by collecting supernatant from a batch and then discharging the separated solids into the collected supernatant, followed by gentle mixing by hand. In this manner target enzyme levels in the pooled supernatant/solids were directly comparable to those in the feed suspension.

The experimental approach is summarised in Figure 3.7 below.

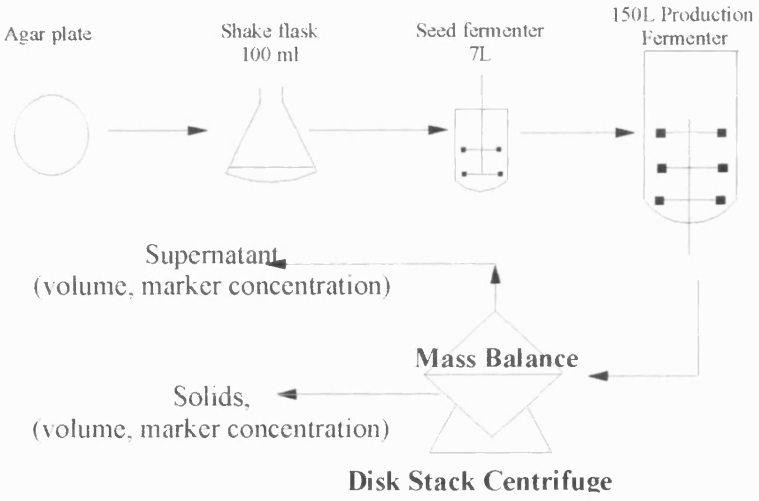

Figure 3.7: Summary of experimental procedure employed to study the effect on whole cell E.coli of cell harvest by high speed disk stack centrifugation.

3.4.6 Estimation of solids loading

In order to assess the level of release generated by the discharge process it was necessary to calculate the solids loading on a volume basis of any given stream. This was achieved by subjecting a known volume (100 mL) of solids/liquid suspension to a high G force spin (15,000 G) for a substantial length of time (2 hours) in a laboratory scale centrifuge (Beckman J2-M1, Beckman Instruments, High Wycombe, UK). The

supernatant was then poured off and measured and the volume of the compacted solids calculated. By measuring the solids content of any stream under the same conditions, an accurate comparison can be drawn regardless of the degree of centrifugal de-watering and compaction attained in the laboratory centrifuge.

3.5 Results

The first work undertaken was to establish the reproducibility of the basic experimental protocol, i.e. the batchwise mass balance approach described in the last section. To achieve this first a flow rate was established that gave reasonable solids recovery. Using the CSA-1 centrifuge fitted with a hydro-hermetic (soft feed) bowl, feed suspension was processed at the machines top rotational speed (9810 rpm) and a range of flow rates. It was determined that a volumetric throughput of 60 L h^{-1} gave very good recovery (99% clarification efficiency on an optical density basis), with the bowl taking approximately 4 minutes to fill at this flow rate. Several batch runs were then repeated under these conditions to check reproducibility. This was then repeated in the SAOOH centrifuge with semi-hermetic feed bowl, where again adequate clarification was achieved at 60 L h^{-1} (93%) and a processed volume of 4 litres was sufficient to fill the bowl.

A mass balance in terms of total protein (mg mL^{-1}) was calculated for each feed zone design. To confirm the accuracy of this technique the processed supernatant and solids fractions were recombined in the correct ratios to recreate the original feed suspension in terms of solids concentration ("reconstituted broth") and the total protein levels in this suspension compared to those calculated using the full fraction technique outlined in the previous section. Because any release caused purely by exposing cells to high g-forces was also of interest, a control was established whereby a sample of feed suspension was spun in a laboratory scale bottle centrifuge (J2-M1, Beckman Instruments Ltd., UK) at 10,000 G for 4 minutes (the longest any cells were exposed

to such a force in the pilot scale machines) and this sample was also assayed for release.

Finally the whole process was repeated on a different fermentation broth to check for effects of variability of feed suspension. The results are shown overleaf in Figure 3.8.

It can be seen that the hydro-hermetic feed zone caused almost no disruption to whole cells being processed at this throughput, releasing only 1.8% (+/- 0.2%) of the total protein present. It can also be seen that these levels of release were similar to those seen in both control experiments, and thus that this disruption level could simply be caused by the exposure of whole cells to significant centrifugal fields. The semi-hermetic feed however, disrupted a much larger percentage of cells, releasing 13.7% of all protein available (+/- 1.5%). It should also be noted that the reproducibility of the experiment was excellent, with a relative error of +/- 10% being attained, that variation between batches was negligible, and that physically reconstituting the broth mirrored results obtained using the fractional mass balance technique.

The next stage involved repeating the experiment utilising three rate assays to examine release. Total protein work was continued, but supplemented by both α-amylase (the target periplasmic "product" enzyme), and glucose-6-phosphate dehydrogenase, an entirely cytoplasmic enzyme, analysis. In addition, the opportunity was taken to utilise the CSA-1 semi-hermetic bowl rather than the SAOOH, to ensure that both machines did behave identically when fitted with the same design of feed zone.

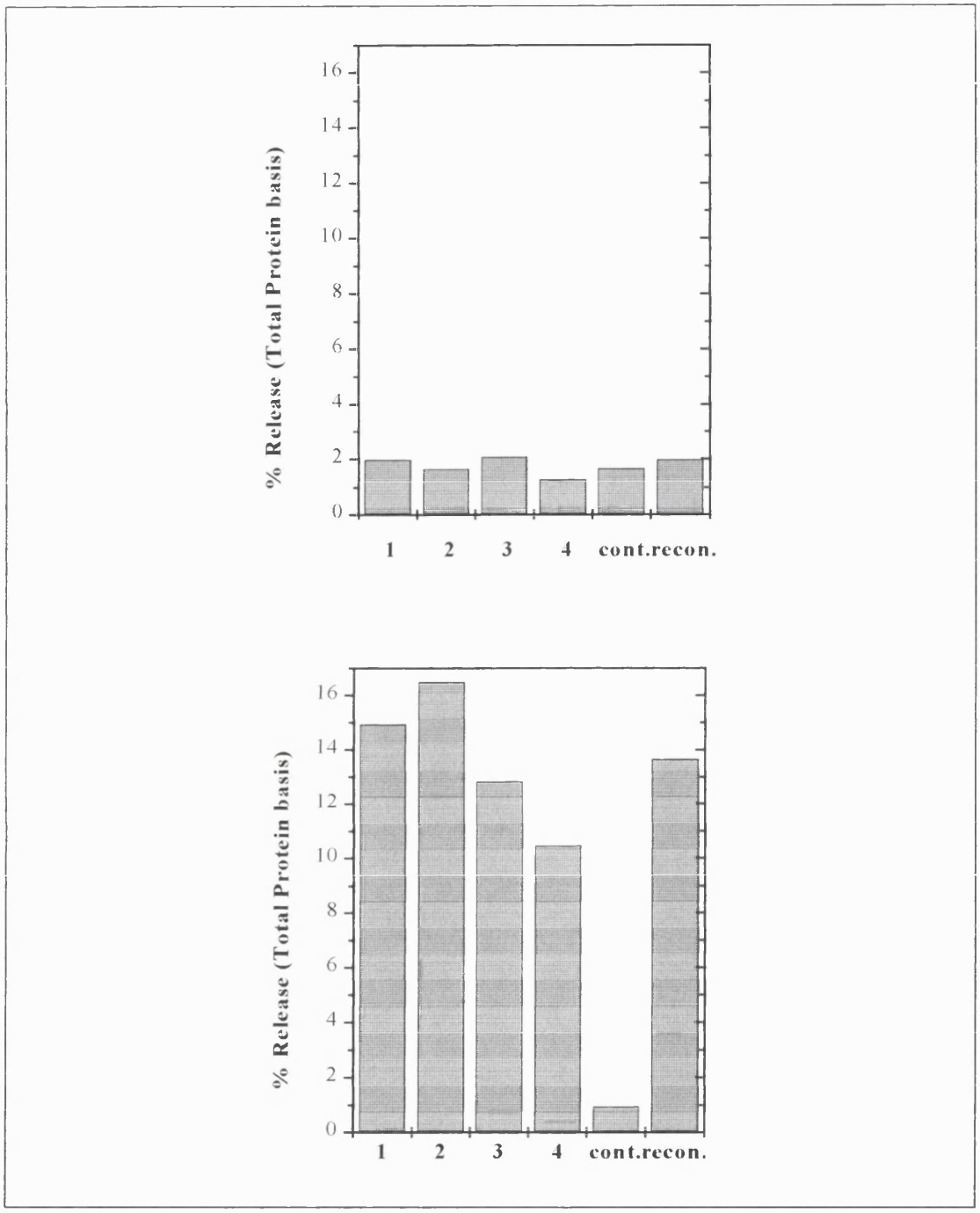

Figure 3.8 shows % release of total protein from whole cell fermentation broth upon passage through a hydro-hermetic feed zone (top) and a semi-hermetic feed zone (bottom). Biorad™ total protein assay used. 0% release is background total protein level in unprocessed cells, 100% release is total protein level after 1 pass, 1200 bar in a high pressure homogeniser. Control (cont.) is sample spun in bottle centrifuge at 10000G for 4 minutes, reconstituted broth (recon.) is feed suspension reconstructed from solid and supernatant fractions after processing. 1-4 show repeat experiments

The results of the work are shown overleaf in Figure 3.9. Firstly it should be noted that again both the glucose-6-phosphate dehydrogenase (G-6-PDH) and α-amylase release levels showed excellent reproducibility during processing in both the hydro-hermetic and the semi-hermetic bowl. When considering first the semi-hermetic configuration, it can be seen that the CSA-1 semi-hermetic configuration matches closely the release seen with the SAOOH semi-hermetic centrifuge:- although the two machines are very similar there were some differences in the discharge mechanism which therefore apparently had no effect on cell disruption during processing, and this will be considered in greater detail in the discussion of this chapter. Also, the glucose-6-phosphate dehydrogenase release is shown to mimic closely that of total protein: as discussed in Chapter 2, this is to be expected as approximately 97% of the total protein in the cell is cytoplasmic, as is the G-6-PDH marker. Therefore when one is released, so will be the other one to the same degree.

It can also be seen that release of α-amylase from the periplasmic space was very much higher than release from the cytoplasm, 22.8% as opposed to 13.5%. Again, the error on the G-6-PDH and α-amylase reproducibility is within 10%, and as such this level of error will be assumed on all further processing experiments.

The release of α-amylase under the controlled spin conditions was again seen to be higher than that of the G-6-PDH and total protein, at 4.5%. This was no doubt due to the inherent leakiness of the outer membrane in this cell strain, as discussed in Chapter 2.

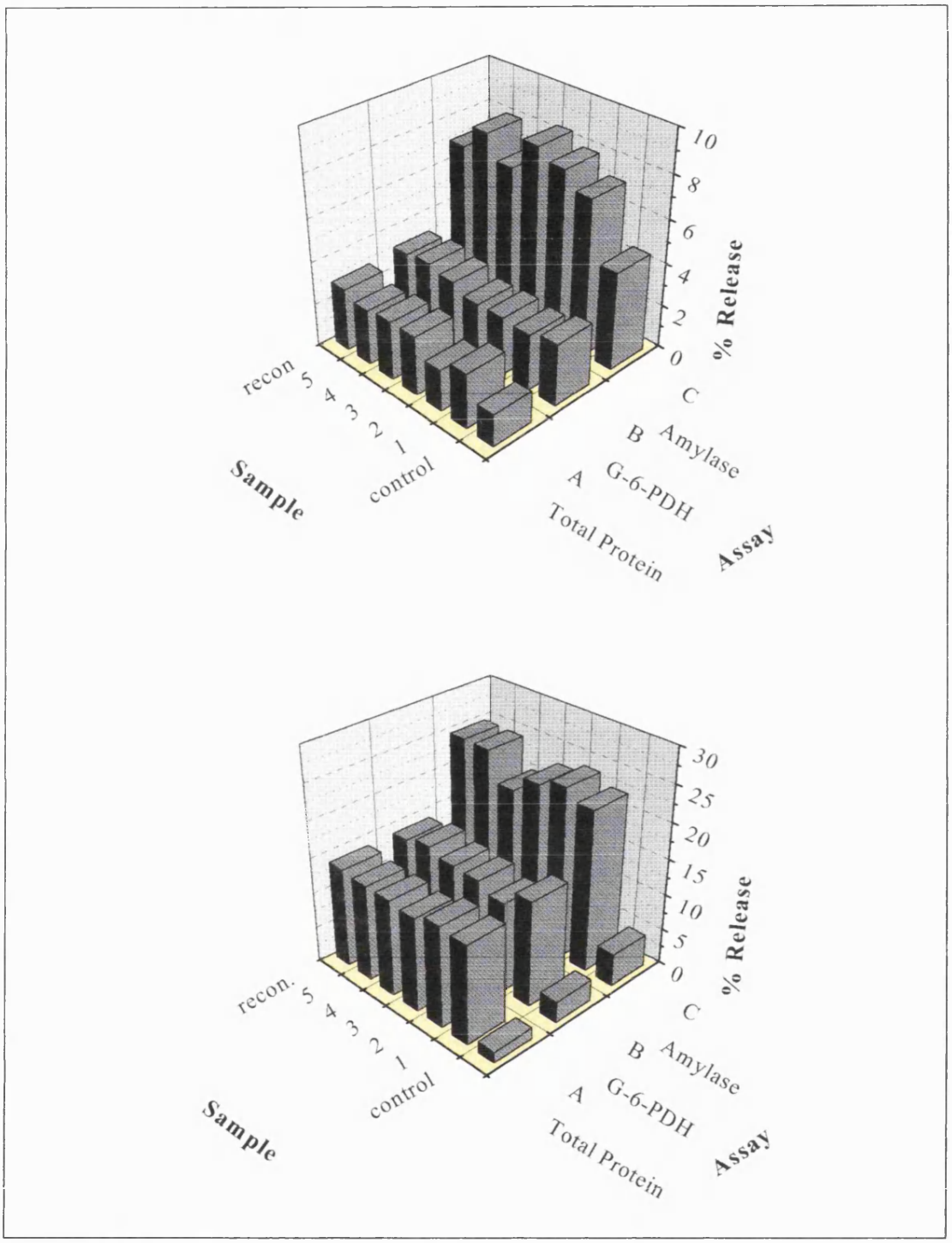

Figure 3.9 shows % release of total protein, α-amylase and glucose-6-phosphate dehydrogenase from whole cell fermentation broth upon passage through a hydro-hermetic feed zone (top) and a semi-hermetic feed zone (bottom). 0% release is background levels in unprocessed cells, 100% release is levels after 1 pass, 1200 bar in a high pressure homogeniser. Control (cont.) is sample spun in bottle centrifuge at 10000G for 4 minutes, reconstituted broth (recon.) is feed suspension reconstructed from solid and supernatant fractions after processing. 1-5 indicate repeat experiments.

The hydro-hermetic feed zone also released more α–amylase than G-PDH or total protein (7.7% release as opposed to 1.8%) and so can be seen to again out-perform the semi-hermetic design. However, unlike the total protein and G-6-PDH release, which was similar in both the control and the processed broth, the α-amylase levels clearly increased more when processed through the centrifuge than when merely exposed to the control centrifugal field. This indicates again that although the disruptive forces in the centrifuge were not great enough to disrupt cells totally (except for that percentage of cells which were weak enough to be damaged by the centrifugal field); they were however great enough to cause release from the already leaky periplasm.

As release was clearly somewhat effected by exposure to a centrifugal field during processing, and the three biological assays used all involved a microfuge spin step to remove debris, it was decided to investigate any possible effect the process of assaying might have had on the data. This was conducted by processing feed suspension through a centrifuge fitted with semi-hermetic feed zone (i.e. one that would cause the maximum amount of damage to the cells), again at 60 L h^{-1} throughput, pooling the solids and supernatant fraction to reconstitute the suspension, and then conducting the spin step of the assay at a range of g-forces and spin times. In addition, a sample was also filtered to remove solids through a 0.2 μm filter paper (Whatman Scientific Ltd., UK) and then assayed (thus forming a control). It was found that neither microfuge spin speed or residence time had any significant effect on either cytoplasmic or periplasmic release, validating the experimental approach used for the work. This also indicated that the release seen in the laboratory scale bottle centrifuge used as the process control, and the corresponding release which should occur in the process scale centrifuges, also due to centrifugal force, was occurring very quickly after first exposure to the centrifugal field, and that length of time of exposure would have very little effect. Therefore any cells being processed that were sensitive to a centrifugal field would be damaged quickly, and no others would be affected.

The results are summarised in Table 3.2 (a)-(c) below.

	Time (min)		
Centrifugal force (G)	**15**	**10**	**5**
12400	13.9	15.0	12.0
8000	13.7	13.5	13.0
3815	14.0	13.5	14.1

Release when sample clarified by filtration = 13.34 %.

Table 3.2 (a) Release measured using Total Protein

	Time (min)		
Centrifugal force (G)	**15**	**10**	**5**
12400	13.6	14.0	13.2
8000	13.7	13.9	12.9
3815	13.8	14.9	12.8

Release when sample clarified by filtration = 14.25%

Table 3.2 (b) Release measured using Glucose-6-Phosphate Dehydrogenase

	Time (min)		
Centrifugal force (G)	**15**	**10**	**5**
12400	22.8	20.4	24.0
8000	22.4	24.9	23.2
3815	23.3	22.5	21.4

Release when clarified by filtration = 24.35%

Table 3.2 (c) Release measured using α-amylase

Table 3.2 (a)-(c): Release quantified by total protein, α-amylase and glucose-6-phosphate dehydrogenase markers. Feed suspension was processed through a disk stack centrifuge equipped with semi-hermetic feed zone and then clarified pre-assay in a microfuge at a range of centrifugal forces and for different times. Control was sample clarified using a 0.2 μm filter. 0% release was marker background levels in unprocessed cells, 100% release was levels after 1 pass, 1200 bar in a high pressure homogeniser.

The next process variable investigated was the effect of centrifuge throughput on the cytoplasmic and periplasmic release of cells being processed through a disk stack

centrifuge with both semi-hermetic and hydro-hermetic feed zone. The results are shown in Figure 3.10 overleaf.

Considering firstly the standard semi-hermetic design bowl (open points) it can clearly be seen that initially from 50-150 Lh^{-1} the levels of release both from the periplasm (α-amylase marker) and from the cytoplasm (G-6-PDH and total protein markers) increase rapidly with throughput, from 21% and 11% respectively at low flow rates to a peak of 40% and 27% respectively at 150 Lh^{-1}. From here, however, as throughput continues to increase the levels of release fall. The periplasmic release reduces to a level of 28% at 350 Lh^{-1}: more dramatic however is the reduction of cytoplasmic release down to 3.5% at the top flow rate tested.

The centrifuge when equipped with a hydro-hermetic bowl (closed points), however, behaves somewhat differently, with only a slight rise and fall in the release of both periplasmic and cytoplasmic markers from their starter levels of 7.5% and 1.78% respectively.

Figure 3.11 shows the clarification efficiencies achieved with the two designs of feed zone plotted as a function of equivalent settling area and throughput. It can be seen that two distinct lines are shown on the graph, indicating that the semi-hermetic bowl under-performs the hydro-hermetic design. If both feed zones had the same effect on the feed suspension then these lines would overlay each other (see Section 3.2.4). The two lines indicate that passage through the semi-hermetic bowl was in some manner making the whole cells harder to recover than processing through the hydro-hermetic. This could only be explained by a percentage of the cells being disrupted in the semi-hermetic feed zone, releasing debris which was not recovered at the throughput being examined. This issue will be addressed further in the discussion.

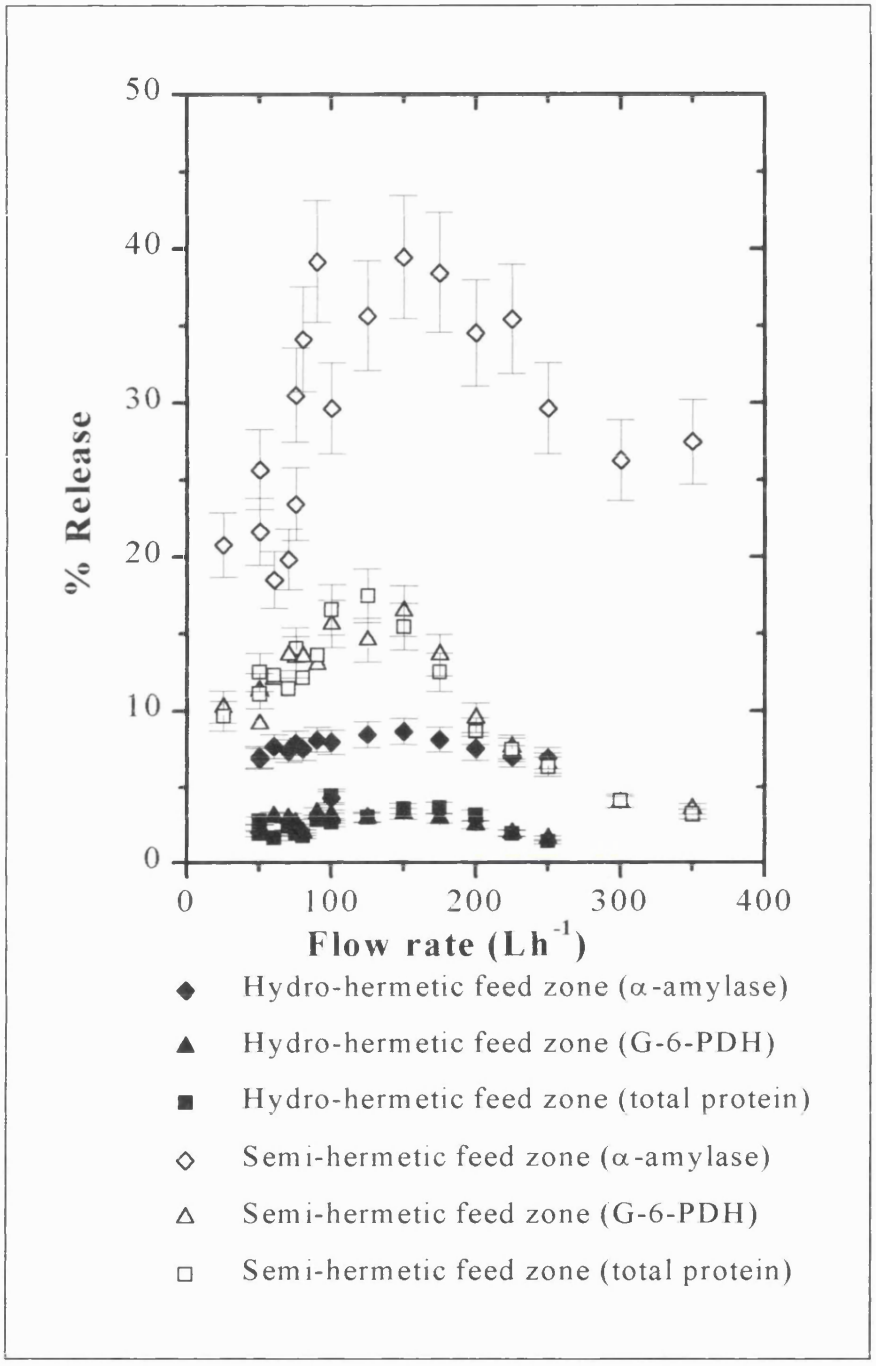

Figure 3.10 shows the effect of centrifuge throughput on release of both a cytoplasmic (G-6-PDH) and a periplasmic (α-amylase) marker. Experiments were conducted over the standard operating range of 50-350 L h^{-1} (CSA-1 equipped with semi-hermetic feed zone bowl) and 50-250 L h^{-1} (CSA-1 equipped with hydro-hermetic feed zone bowl) and are based on solids/supernatant mass balances on the unit operation. 0% release was marker background levels in unprocessed cells, 100% release was levels after 1 pass, 1200 bar in a high pressure homogeniser. The experiment was duplicated to confirm results lay within 10% error margins previously established.

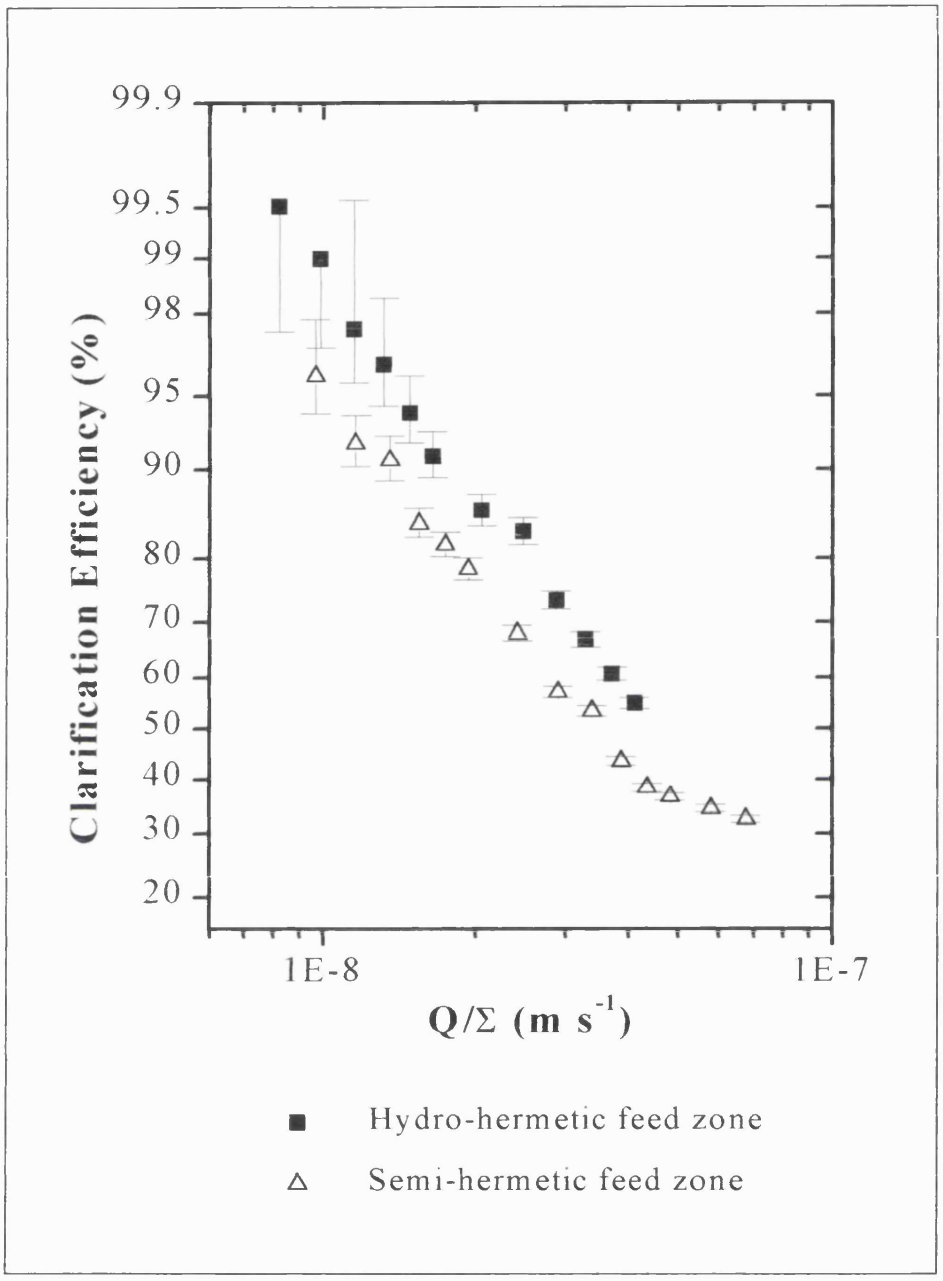

Figure 3.11: Variation of centrifuge clarification efficiency with throughput shown over operational range for both semi-hermetic feed zone (50-350 Lh^{-1} and hydro-hermetic feed zone (50-250 Lh^{-1}). Feed suspension was whole cell E.coli, clarification determined on an optical density basis (600 nm). Error shown at 2% based on repeat sampling and duplicate experiment.

The data gained when conducting the above experiments was then further analysed to uncover the mass balance "split" of the released markers i.e. what percentage was exiting the centrifuge in the supernatant, and what with the solids stream.

Figures 3.12 and 3.13 overleaf show the release broken down into solids and supernatant fraction in terms of cytoplasmic release (3.12) and periplasmic release (3.13), with the top graph in each figure showing results with the hydro-hermetic feed zone, and the bottom for the semi-hermetic.

When considering cytoplasmic release, at low total throughputs (60 Lh^{-1}) where recovery was excellent (90% clarification and above) both feed zones produced an approximate 70/30 division, with 34% of released protein exiting the centrifuge in the solids when in hydro-hermetic format, and 31.5% when in semi-hermetic format. In both machines this reduced with throughput, to 18.4 % at the top throughput (250 Lh^{-1}) in the hydro-hermetic, and the much lower 6.5% utilising the semi-hermetic design. This pattern was repeated when considering the periplasmic release of product (α-amylase), (Figure 3.13): the hydro-hermetic carried slightly less periplasmic than cytoplasmic release in the solids stream at the low flow rate, 29%, dropping to 16% at the top throughput, and the semi-hermetic repeating the trend with solids fraction release falling from 25.2% to 4.8% respectively with increasing throughput.

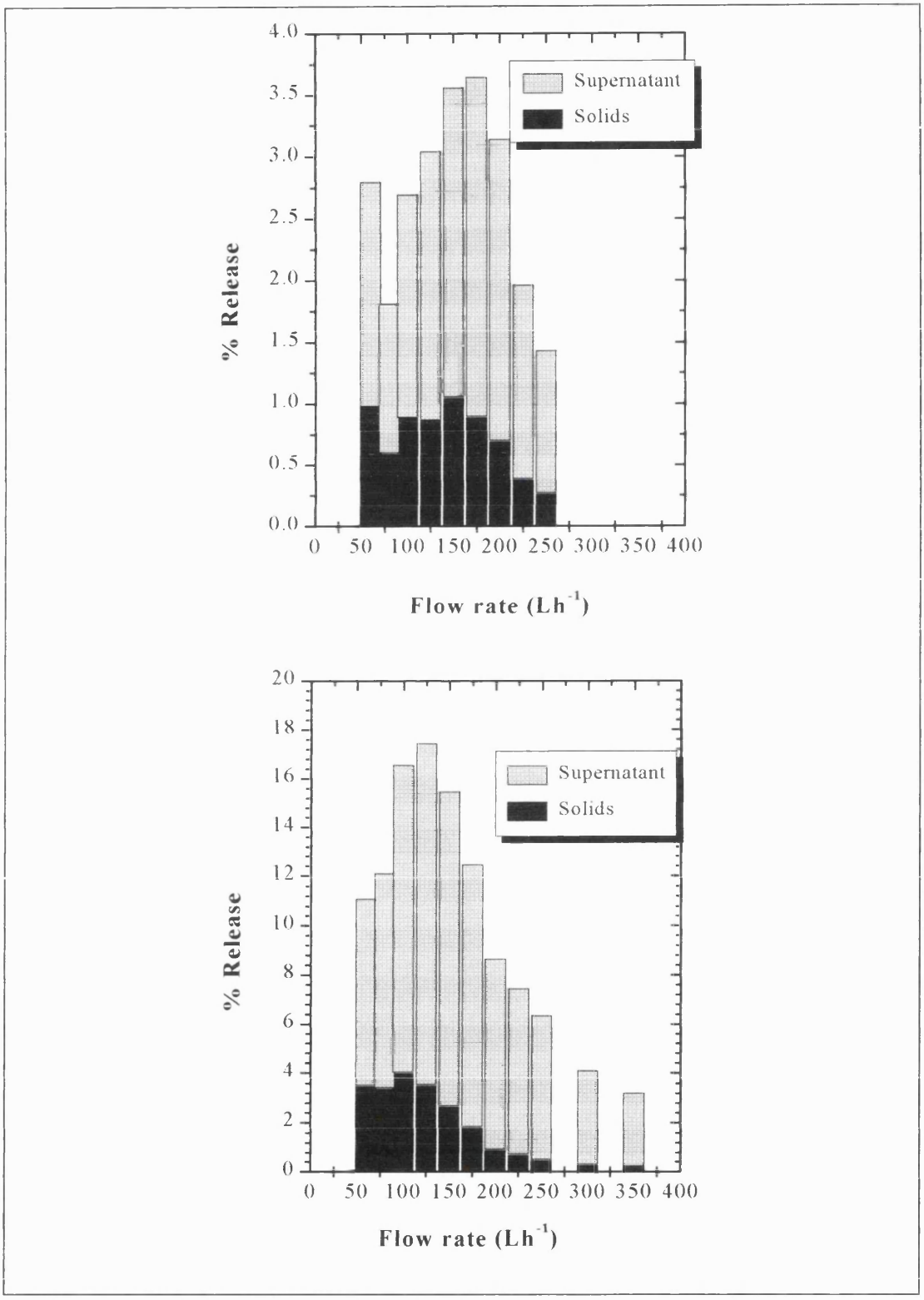

Figure 3.12: Release of cytoplasmic marker (total protein) with throughput shown with fractionation (supernatant/solids stream) information. Top graph shows information for hydro-hermetic feed zone, bottom for semi-hermetic.

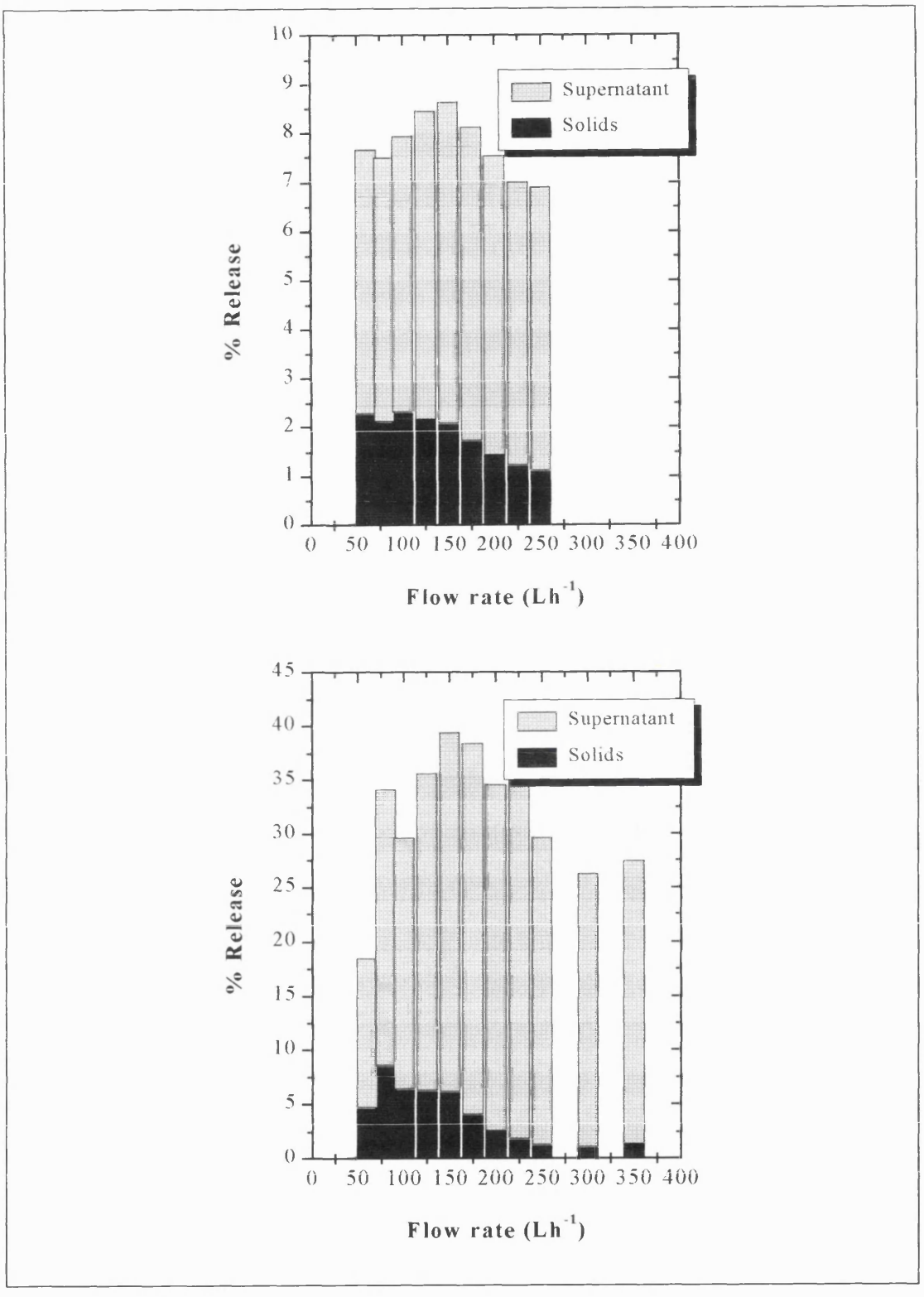

Figure 3.13: Release of periplasmic marker (α-amylase) with throughput shown with fractionation (supernatant/solids stream) information. Top graph shows information for hydro-hermetic feed zone, bottom for semi-hermetic.

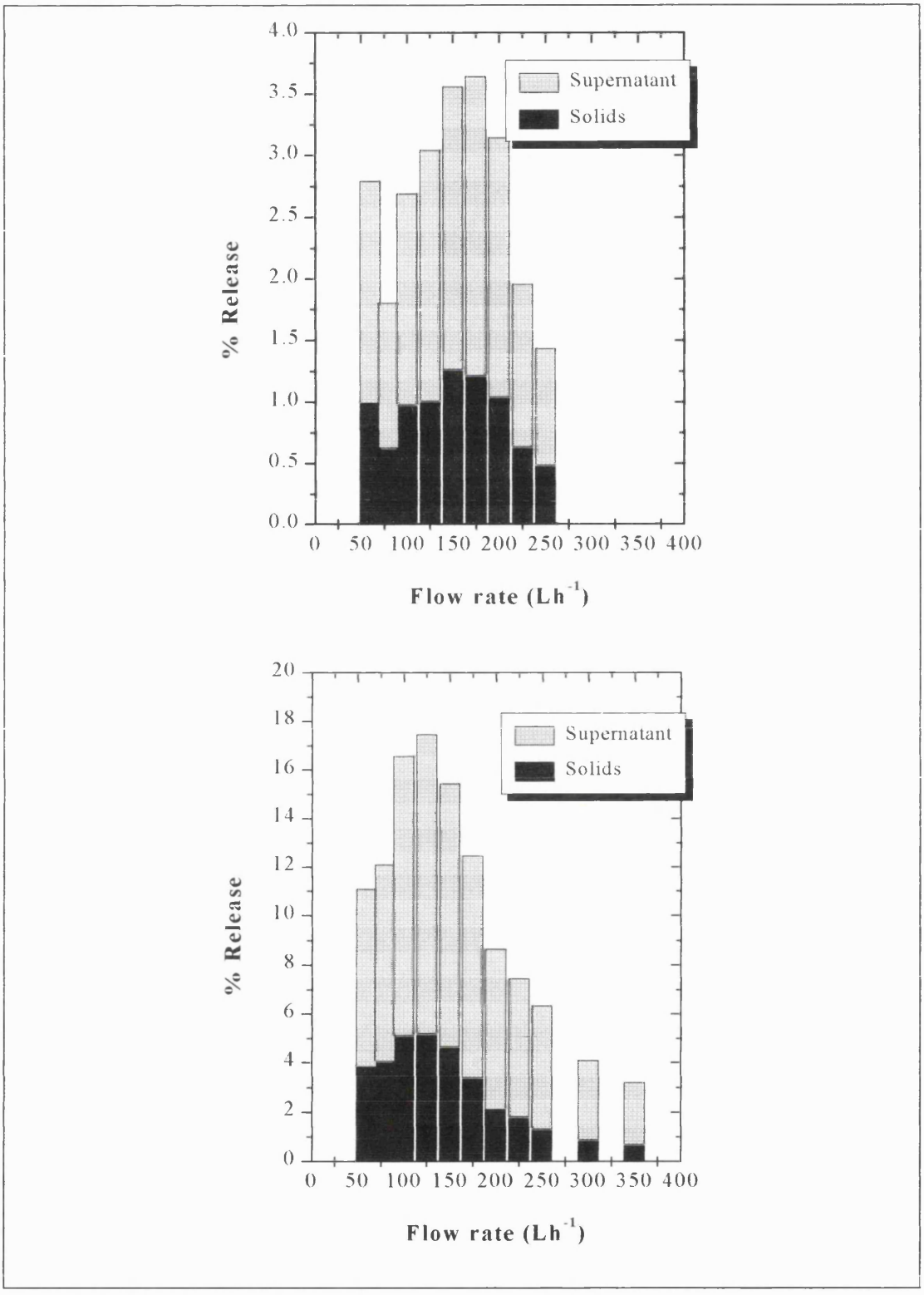

Figure 3.14: Release of cytoplasmic marker (total protein) with throughput shown with fractionation (supernatant/solids stream) information, adjusted for clarification efficiency. Top graph shows information for hydro-hermetic feed zone, bottom for semi-hermetic.

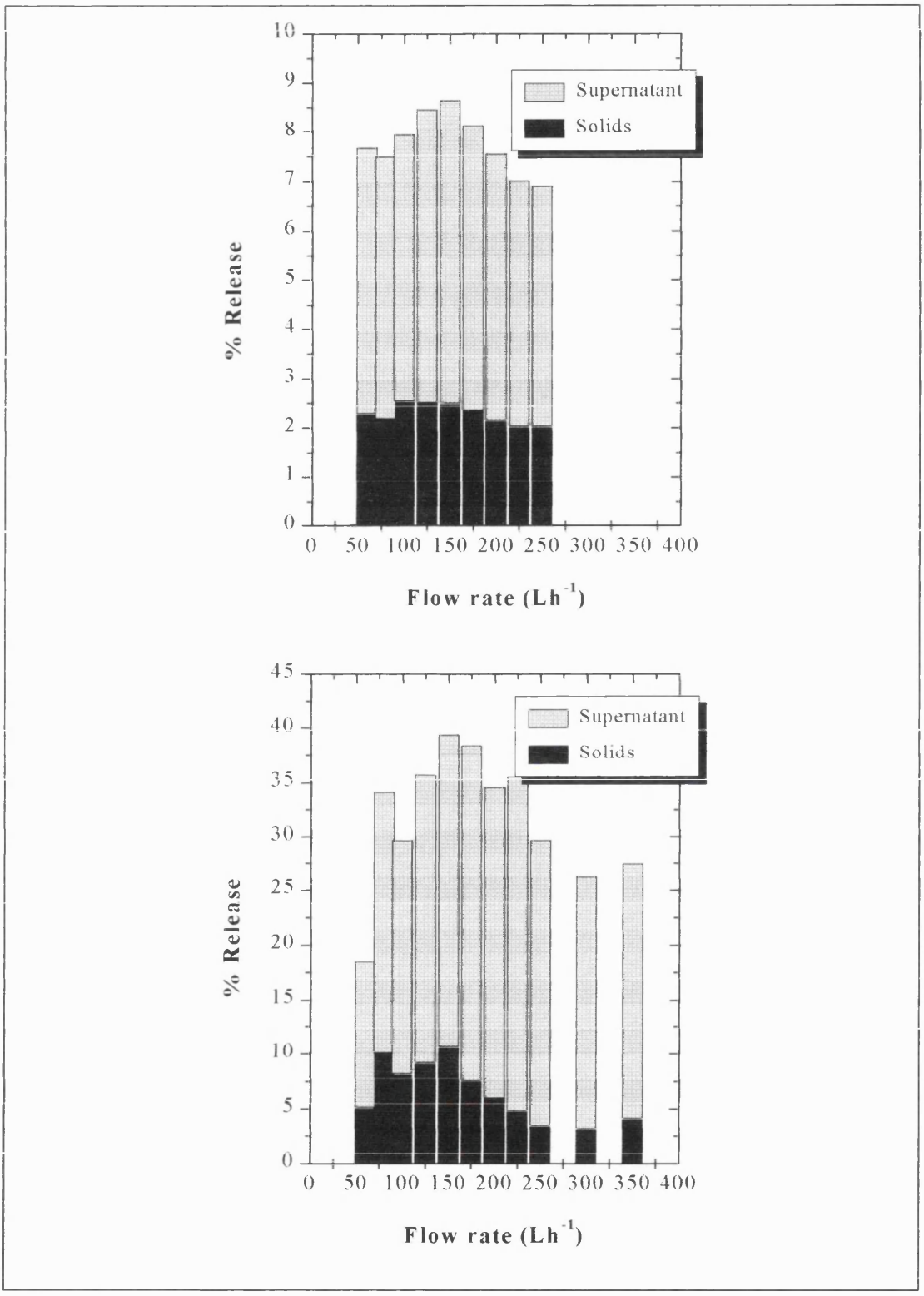

Figure 3.15: Release of periplasmic marker (a-amylase) with throughput shown with fractionation (supernatant/solids stream) information adjusted for clarification efficiency. Top graph shows information for hydro-hermetic feed zone, bottom for semi-hermetic

However, these results do not take into consideration the falling clarification efficiency and thus the decreasing fraction of total cells processed that are exiting the unit operation in the solids stream. Figures 3.14 and 3.15 therefore show the same information adjusted by a scaling factor to account for this (i.e. scaled to 100% solids recovery). This information is summarised in Figure 3.16 below.

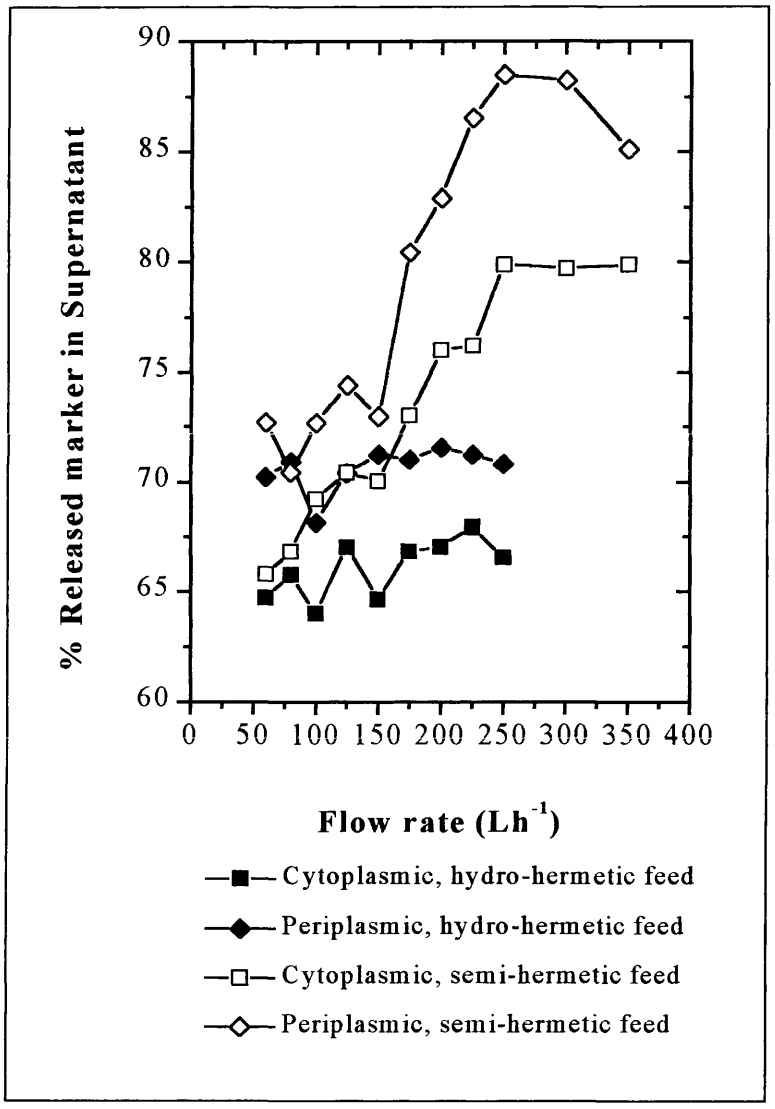

Figure 3.16: Percentage of released periplasmic and cytoplasmic marker exiting centrifuge in supernatant stream as a function of feed zone design and throughput.

It can be seen that the percentage of marker released exiting the machine when fitted with a hydro-hermetic feed zone remained constant with throughput, with 65% of the cytoplasmic marker exiting in this stream, and 70% of the periplasmic product. The semi-hermetic design, however, showed a clear change in the supernatant/solids division with flow rate for both cytoplasmic and periplasmic release; 65% of cytoplasmic release exits in the supernatant stream at low throughputs, rising to 80% at the top flow rate examined. Similarly, the periplasmic release rose from 72% to 85%. Applying the standard 10% error established for the mass balance and assay system, both these increases are significant.

The observation that a significant fraction of released protein and α-amylase was exiting the unit operation in the solids stream with both designs of centrifuge feed zone suggested that some disruption was possibly occurring during the discharge process, where solids are removed in a concentrated, and thus viscous, stream through six small ports in a very short time; conditions which should generate significant shear forces.

The throughput which contained the maximum level of marker release exiting with the solids stream with both designs was the lowest, 60 Lh^{-1}. Therefore this was the flow rate chosen to examine this effect.

Feed suspension was processed through the centrifuge fitted with semi-hermetic feed zone at 60 Lh^{-1} as normal, until the bowl was full, when the machine was discharged and the release of both periplasmic and cytoplasmic markers assessed as normal. This was then repeated, but when the machine was full it was stopped and dissembled. A sample of solids from the internals was then taken and assessed for release. Because, as was explained when considering the operation of the disk stack centrifuge (section 3.2.2), solids are mixed with liquid from the bowl during the discharge process it was necessary to dilute this sample with supernatant to the same solid content by volume as that of the normally discharged sample. This was achieved by measuring the solids content of both the discharged and the "stopped full" stream using the technique outlined in the materials and methods section of this chapter. The "stopped full"

sample was then diluted back to the solids content of the discharged stream using supernatant, which was assumed to have a negligible solids by volume content.

This process was then repeated using the hydro-hermetic feed zone design centrifuge bowl. The results are summarised in table 3.3 overleaf. It can clearly be seen looking at the overall release levels that for the two feed zones and both cytoplasmic (total protein) and periplasmic (α-amylase) markers the overall release levels were very similar. It appeared to make very little difference whether the solids are discharged by the normal route or removed by hand from the disassembled centrifuge, and certainly when applying the error of 10% (and it may well be higher in this experiment because of the need to conduct the solids balance) there was no statistically significant difference. This indicated that neither centrifuge disrupted cells in the solids stream when they underwent discharge.

The final experiment undertaken was to vary the rotational speed of the centrifuge during processing. This was undertaken with the semi-hermetic (standard) bowl only as the total release when utilising the hydro-hermetic feed zone at maximum revolutions (9810 rpm) was already very low (below 2% cytoplasmic release) and it was not felt any variation with rotational speed could be easily detected.

The experiment was undertaken at a constant throughput of 120 Lh^{-1} as this was a condition that still offered reasonable clarification whilst approaching the maximum level of disruption. The experiment was performed in the standard discharge-based batch mass balance manner, with rotational speed varied from the top 9810 rpm down to 7080 rpm. To highlight further the effect of the discharge mechanism, the discharge of solids from the centrifuge was approached in two ways. Firstly the centrifuge was discharged at the rotational speed the solids had been collected at. Then the process was repeated but now discharging the centrifuge at full speed (9800 rpm). In this manner any shear based disruption taking place upon discharge should have been indicated by producing a difference in total release between the two conditions. The results are shown in Figure 3.17.

Condition	Level supernatant	Level solids	Volume supernatant (mL)	Volume solids (mL)	% solids in solids stream (by volume)	Level solids adjusted for "stop full"	**% Release**
HH, normal discharge **PROTEIN**	0.433	0.527[-1]	3550	600	25.52	-	**1.924**
HH, "stop full" **PROTEIN**	0.433	0.589[1]	3550	600	46.76	0.518	**1.89**
HH, normal discharge **AMYLASE**	33.23	35.65[1]	3550	600	25.52	-	**4.52**
HH, "stop full" **AMYLASE**	33.23	33.03	3550	600	46.76	33.13	**3.74**
SH, normal discharge **PROTEIN**	0.781	1.585	3820	600	24.45	-	**13.57**
SH, "stop-full" **PROTEIN**	0.781	2.20	3820	600	49.21	1.63	**13.73**
SH, normal discharge **AMYLASE**	40.77	53.80	3820	600	24.45	-	**23.52**
SH, "stop-full" **AMYLASE**	40.77	49.02	3820	600	49.21	49.23	**22.20**

Table 3.3: Key mass balance components and overall release levels for both hydro-hermetic and semi-hermetic feed zones, normal discharge or "stopped full". HH= hydro-hermetic, SH= semi-hermetic. Units for protein levels, mg mL^{-1}, units for α-amylase levels I.U. $min^{-1}mL^{-1}$

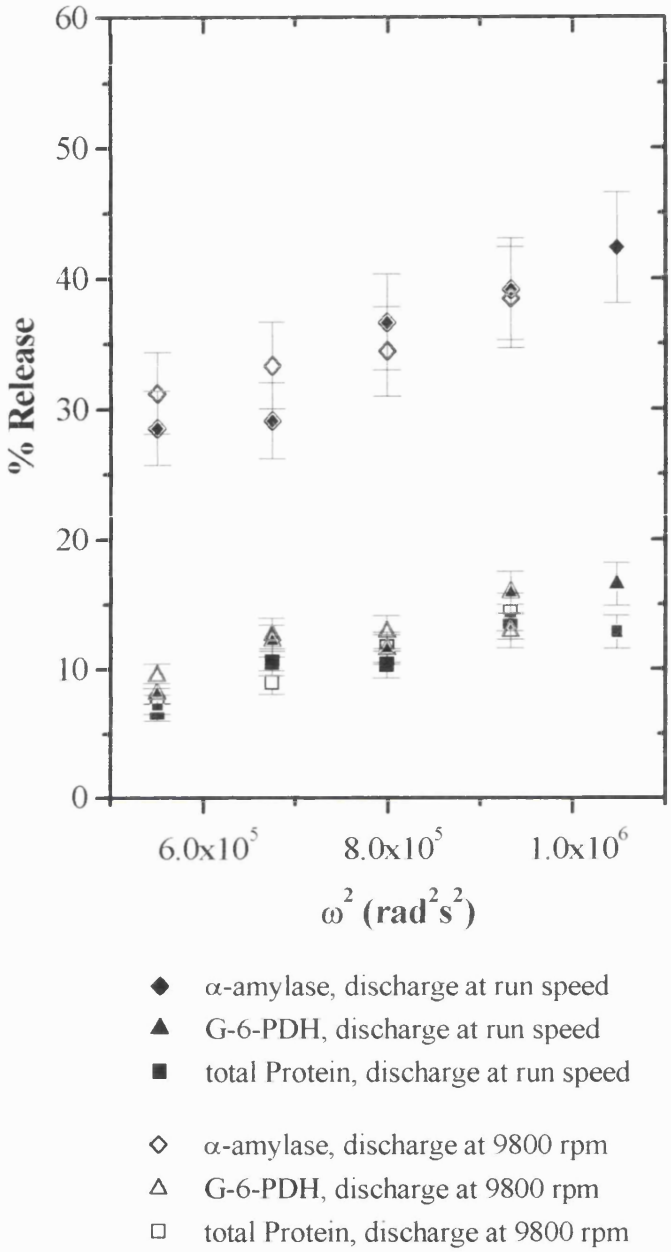

Figure 3.17: Release of periplasmic and cytoplasmic markers as a function of centrifuge rotational speed (semi-hermetic bowl fitted). Discharge at run speed is release when discharge took place at the rotational speed used for separation; discharge at full speed is discharge at 9800 rpm. Angular velocity range corresponds to 9800 rpm to 7080 rpm. 0% release was marker background levels in unprocessed cells, 100% release was levels after 1 pass, 1200 bar in a high pressure homogeniser The experiment was duplicated to confirm results lay within 10% error margins previously established.

It can clearly be seen that the angular velocity of the bowl, which ought to be a key factor in the shear rates developed within the feed zone, (see Chapter 5), had an effect on both periplasmic release and cytoplasmic release, with a significant reduction in disruption at lower angular velocities (15% cytoplasmic release at 9810 rpm reduced to 9% at 7080 rpm, and 42% periplasmic release reducing to 30%. The rotational speed of solids discharge however appeared to have no significant effect on the extent of release observed across the range of flow rates studied. This offered further evidence that the discharge process is not significant when considering release during processing through a disk stack centrifuge.

3.6 Discussion

There are several key points when considering disruption of whole cells during passage through a disk stack centrifuge that are indicated by results presented in this chapter, and although a more exhaustive discussion on centrifuge hydro-dynamics and operation will be presented in Chapter 6 (considering also the laboratory scale mimics which were designed and tested, theoretical shear forces and mechanisms of disruption, and the processing of a second test system (polyethylene glycol precipitates of yeast homogenate)), it is worth highlighting these at this point.

Firstly it is clear that the semi-hermetic (standard) design of feed zone does indeed disrupt many more cells than the hydro-hermetic (soft-feed) bowl. The 13.7% release of total protein and 22.8% release of the periplasmic α–amylase at the most efficient volumetric throughput of 60 Lh^{-1} is indicative of a large amount of damage to the cells, especially when compared to the 1.8% release of protein and 7.7% release of product seen with the hydro-hermetic feed. The key questions of interest to both a process engineer and a centrifuge manufacturer are what causes the disruption (and thus the difference), and how can a centrifuge be operated to minimise such disruption.

At this point it is useful to recap on the sites considered responsible for the disruption of biological solids in the standard design disk stack centrifuge. These are as follow;

- Primary contact between the centrifuge and the feed suspension occurs at the lock-nut; this deflects the liquid flow which has been ejected from the feed pipe out onto the walls of the distributor. Owing to the short contact time little angular momentum is expected to be transferred; however, high radial shear rates will be generated at the surface of the lock-nut.
- The distributor is fitted with acceleration ribs which both aid acceleration and guide fluid through the channels at the base of the distributor foot and thus out onto the disks. However, intensive contact between the distributor and the feed suspension will occur here.
- The trajectory in between the distributor rib and the liquid surface, at the pressure side of the guiding rib.
- The inner wall of the distributor where axial shear can become predominant when flow rates are low resulting in a thin liquid layer.
- The conical distributor foot, where high shear rates may occur during flow through onto the disks.

(J.P. Van der Linden, 1987)

The data presented in this chapter enables this list to be narrowed down somewhat by assessing the changes made to the hydro-hermetic bowl.

The first information to consider is the alteration of release levels with throughput. The hydro-hermetic centrifuge releases approximately 2% of the total protein present in the feed stream (i.e. disrupts 2% of cells being processed totally, or significantly damages a higher proportion of them to a lesser degree). However, this is equal to the level of release seen by simply exposing a sample of feed suspension to the centrifugal field generated in the centrifuge (approximately 10000G) for the maximum length of time solids would be resident in the disk stack machine. Furthermore, very little variation is seen with changing flow rate. This is surprising when it is considered that the rib body at the top of the hydro-hermetic feed zone may cause an increase in disruption levels at

flow rates high enough to bring it into contact with the feed suspension (i.e. as flooding of the distributor approaches). From these results either it has no effect, or mixing within the feed zone is poor, therefore very little of the feed suspension transiting the feed zone comes into contact with the rib body even when liquid hold-up levels are high.

Also of interest is the release of the periplasmic marker. As was discussed in the cell strength studies contained in Chapter 2, the outer membrane of *E.coli* JM107 pQR126 is naturally leaky, and it is not surprising that exposure to the control centrifugal field results in higher release levels than those of total protein, the majority of which must also pass through the inner membrane. What is surprising, however, is that the hydro-hermetic centrifuge releases 7.7% of α-amylase compared to the 4.5% released by the control, indicating that the process centrifuge is increasing the disruption levels over those generated by the simple centrifugal field. This implies that the disruptive mechanisms seen in the hydro-hermetic feed zone are sufficient to disrupt the outer membrane and peptidoglycan layer in cases where they leave the inner cytoplasmic membrane intact. As the mechanical strength and rigidity of the *E.coli* cell wall is considered to be associated with the peptidoglycan layer (Thwaites and Mendelson, 1985) it seems unlikely that this could happen. It is more likely that the outer membrane is being subjected to a disruption mechanism which is tearing holes in it; then, when the cell is subjected to the intense centrifugal forces during it's passage through the machine the leakage from the periplasmic space is increased.

The semi-hermetic feed zone, however, shows a strong relationship between release and throughput. The release of both the periplasmic and the cytoplasmic marker rises sharply from a throughput of 50 Lh^{-1} to a throughput of 150 Lh^{-1} (from 21% to 40% and 11% to 27% respectively). From then on, however, the level of disruption observed falls dramatically with flow rate, to 28% periplasmic release at 350 Lh^{-1} and only 3.5% cytoplasmic release. This offers some strong indications as to what mechanisms in the feed zone are responsible for the damage.

An increase in the volumetric throughput of the centrifuge results in an increase in the amount of liquid contained in the feed zone also. At low flow rates, it is estimated that as little as 1 mL of feed suspension may be present in the semi-hermetic feed zone (based on the geometry of the distributor and the assumption that at minimum the guide channels must be full of liquid). The increase in this volume clearly will reduce the specific power input per unit volume and thus the shear rates. However, this is counter-balanced by the increase in flow rate, which will tend to lead to a lower residence time and thus an increase in the power per unit volume necessary to accelerate the feed suspension to the rotational velocity of the bowl before passage out onto the disks. Clearly, the length of time a cell is exposed to a given shear force may well have an impact on the level of disruption, but in this case it is the increase in power per unit volume that appears to have the greatest effect. It should be noted that as flow rate increases the layer of liquid on the distributor wall will thicken, resulting rapidly in a situation where an ever decreasing fraction of the feed suspension will come into direct contact with the acceleration ribs unless a high degree of mixing is present. This appears to have little direct effect on the system studied here, and would suggest that the two mechanisms postulated which involve interactions with the ribs are not sufficient to explain the observed release alone.

Mannweiler (1991) also reported an increase in disruption of Soya protein precipitates with flow rate when working with a semi-hermetic feed zone centrifuge, an observation that agrees with the data discussed here.

This leaves the key question of what happens to the flow within the feed zone at approximately 150 Lh^{-1}. The most obvious answer is that the flooding depth within the distributor reaches the point where the lock-nut is covered over. As has been stated, running un-flooded the first point of contact between the feed suspension and the centrifuge is the lock-nut. As will be shown in Chapter 5, high shear forces will be generated in the liquid at the surface of the nut. These will persist in a layer only several millimetres thick; however, at low flow rates, the majority of the feed suspension will pass through this region. As this fraction will not change with increasing throughput until the lock-nut becomes covered, and results show that the disruption level does increase, clearly this mechanism is not sufficient to explain the full

levels of release seen. However, it is likely that it is responsible for some release, and, by "pre-shearing" the feed suspension probably renders the cells more sensitive to disruptive forces experienced further down the distributor. Then, at approximately 150 Lh^{-1} the lock-nut surface becomes covered. From this point on, the proportion of material passing through the disruptive zone above the surface of the lock-nut will decrease with flow rate (as the depth of flooding continues to increase), and a corresponding total reduction in release is seen. As one of the key differences between the hydro-hermetic and the semi-hermetic design is the constant immersion of the lock-nut in the former, this suggests that the interaction with the lock-nut is key. However, it must be considered that the hydro-hermetic design contains a second disk which will generate shear in a similar way to the lock-nut (the hydro-hermetic disk at the base of the feed pipe: it's held stationary whilst the liquid around it rotates so the net effect is the same). If the disruptive mechanism were purely lock-nut based then under conditions where both the semi-hermetic and the hydro-hermetic feed zones were operating at the same level of flooding then the two machines would perform equally or the hydro-hermetic, in fact, worse due to the presence of the extra disk. This doesn't happen and this could be due either to the much higher throughputs needed to attain the same degree of flooding in the semi-hermetic compared to the hydro-hermetic or to further interactions with the distributor ribs within the semi-hermetic distributor. The former would increase the specific power input and thus shear forces in the semi-hermetic design and the latter would suggest that the total release seen must be a combination of several factors in the feed zone design, all of which are important.

The bottom of the distributor, and the flow channels through onto the disks, is similar in both designs. This means that an equal contribution to any disruption will be made by this section in both designs. Since the release levels observed are radically different between the machines this in turn implies that this site does not play a significant role in causing release.

No disruption during the solids discharge process was observed with either feed zone, despite the fact that a significant proportion (30% at low flow rates) of total protein release exited in the solids stream. This is contrary to the findings of Rosen and Datar

(1986) who studied the cell harvest of an *E.coli* expressing the enzyme β-galactosidase to the cytoplasm. They showed that as much as 10% of the total enzyme was released during the solids discharge process. However, as was discussed in Chapter 2 the precise growth process of a cell is very important when determining it's strength characteristics. In addition, the discharge ports and mechanism on both the semi-hermetic and hydro-hermetic centrifuges are identical. Disruption during solids discharge therefore cannot explain the observed differences in the two designs' performance.

The presence of a significant proportion of the total release of both periplasmic and intracellular marker in the solids stream despite the lack of disruption directly attributable to the discharge process can be considered as further evidence of the nature of disruption. It is very possible that a cell that has suffered damage which increases the leakiness of the outer and inner membranes will then only finally release it's contents into the free suspending solution after exposure to a "squeeze" such as that provided by a centrifugal force. The whole cells, when recovered, spend a significant length of time exposed to just such a force in the solids holding space: furthermore this is a stagnant area and, because the degree of centrifugal de-watering seen in a disk stack is not high, will contain much trapped fluid. Any proteins coming free from the cells in this manner will therefore remain in the solids stream. However, the mixing involved in the analysis of the "stopped full" solids stream will also allow these proteins to become free, and thus be detectable by assay, hence the release levels seen are identical. The increase with throughput in the fraction of release exiting the semi-hermetic centrifuge in the supernatant stream after adjusting for clarification efficiency is suggestive of a change in the mechanism by which cells are disrupted. At higher flow rates, even though the total release is reduced, those cells which are being affected are disrupted to a higher degree, releasing both periplasmic and cytoplasmic markers directly into the surrounding liquid without the "squeeze" mechanism of the solids holding space.

The similarity of the clarification versus Q/Σ plots for the two designs of feed zone is also suggestive of a disruption mechanism which ruptures the membranes of the cells

rather than totally breaking them up as in a high pressure homogeniser. Although there is a distinct difference in the data (which is clear evidence of disruption occurring before passage through the clarifying disk section of the centrifuge), the difference is not big enough to account fully for the decrease in clarification which would occur if a significant fraction of the cells were being smashed into small debris particles by passage through the semi-hermetic feed zone.

Finally, the reduction in release of both periplasmic and cytoplasmic markers with rotational speed of the centrifuge is as expected. Such a reduction will lower both the total power input to the fluid in the feed zone, the shear forces surrounding the lock-nut and the speed of any impact between the distributor ribs and the cells in the feed suspension. Furthermore, it will reduce the centrifugal force on the liquid at the base of the distributor, and thus liquid will flow through and onto the disks less readily, resulting in an increase in flooding level in the distributor. Therefore it is difficult to infer much about the disruptive mechanisms involved from this result.

All these issues will be further examined in Chapter 6.

3.7 Conclusions

The semi-hermetic feed zone causes significant disruption to cells being accelerated within it. This doubles from 13.7% of total protein being released at low flow rates to 27% at a throughput sufficient to just cover the lock-nut. From this point release reduces until, at the maximum volumetric throughput 3.5% of all protein in the feed suspension is released. Periplasmic release follows this pattern though with even higher levels. The disruption is believed to be due to a combination of the shear forces generated by the power input necessary to accelerate the feed suspension to the angular velocity of the bowl, and the region of high shear found around the lock-nut itself. However, not all of the released protein from either the cytoplasm or periplasm of the cell becomes free during this process, and thus exits in the supernatant. Approximately 30% at low throughputs remains associated with the cells and exits

with the solids stream, falling to 15% at higher throughputs. This reduces the scale of the product loss problems associated with such disruption.

The hydro-hermetic feed zone inflicts negligible disruption on cells passing through it (approximately 2% of total protein is released) although product loss from the periplasmic space is higher (7.7%). There is little change with flow rate and the fraction exiting with the solids stream remains constant with throughput at 30%.

No disruption was found to be associated with the discharge process itself.

4.0 CENTRIFUGATION OF POLYETHYLENE GLYCOL PRECIPITATES OF YEAST HOMOGENATE

4.1 Introduction

This chapter deals with the formation of polyethylene glycol (PEG) precipitates of protein released from a homogenised yeast suspension; the physical property measurements of the suspension, and the pilot scale centrifugation trials conducted on the suspension utilising both semi-hermetic and hydro-hermetic design feed zone disk stack centrifuges (see Chapter 3). Section 4.1 provides an introduction to the formation of such precipitates, 4.2 an explanation of centrifugal grade efficiency theory, used to evaluate the differing performance of the centrifuge with varying conditions, and an introduction to the issues surrounding recovery of precipitates using high speed disk stack centrifugation. Section 4.3 covers the materials and methods used for this section of the work. Section 4.4 describes the physical properties of the PEG precipitate used for centrifugation trials and details the results obtained with the pilot scale centrifuges. Finally section 4.5 provides a summary of the results, and draws key conclusions.

4.1 Formation of Protein Precipitates.

4.1.1 Introduction to Precipitation

A good general review of the precipitation of biological solids is presented by Bell, Hoare & Dunnill (1983).

Protein precipitation and the subsequent recovery of the precipitate from suspension represents a major unit operation both industrially and at laboratory scale, found widely in the majority of the biotechnology industry, from food products through brewing to biopharmaceuticals and blood fractionation. In many cases it is operated by adding a reagent in such a manner as to recover a protein or proteins in an unchanged

molecular form using a reversible precipitation reaction. Such an approach, however, is also a powerful technique when used to remove contaminating proteins leaving the product suspended in the liquid stream. The most important methods of bringing about such precipitation are summarised below;

- "Salting out": the addition of high concentrations of neutral salts, which generally decrease protein solubility
- Isoelectric point precipitation:-the extent of ionisation of the weakly acid or alkali side-chains of a protein molecule are highly sensitive to pH. Solubility is a strong function of the net charge of these groups, and adjustment of the pH to a point where the net charge is zero will bring about a reduction in solubility.
- Solvent precipitation:-reduction of the dielectric constant of the aqueous medium by the addition of a miscible organic solvent will enhance the electrostatic interactions between protein molecules and hence produce precipitation.
- Non-ionic polymer precipitation:- addition of such a polymer brings about a reduction in the amount of water available for protein solvation, and hence precipitation.
- Use of charged polyelectrolytes :-these will bring about precipitation by acting as flocculating agents at the correct pH.
- Polyvalent metal ions:-in cases where the ion interacts directly with the protein, these have proved very valuable in inducing reversible precipitation.

(Bell, Hoare and Dunnill, 1983)

However, it is also possible to precipitate protein from suspension by coagulation, drying or temperature reduction to near 0^0C (cryo-precipitation).

The use of such techniques to remove selectively a target protein from solution is still technically difficult, frequently requiring much experimentation and optimisation work.

The majority of proteins' solubility is determined by their polypeptide structure, which can be very similar, and thus it is sometimes small differences that must be exploited during precipitation.

There are also a number of biochemical engineering aspects to precipitation which must be considered when designing a process. Localised high concentrations of the precipitating agent may cause significant damage to a target protein. During and after precipitate formation, growth and shear-associated break-up of the particles will be dependant on the conditions they are exposed to. Proteins can be irreversibly damaged by the presence of gas-liquid interfaces, particularly in the presence of foaming. The density difference between the precipitate and the liquid tends to be low, and the particles small, and this, together with the precipitates' sensitivity to size degradation in the presence of shear, can lead to significant problems in the recovery of such precipitates. It is the recovery of such precipitates by disk stack centrifuge, and particularly the effect of feed zone design on this unit operation, which is the focus of this chapter.

Polyethylene glycol is a non-ionic polymer, widely used as a highly selective precipitation agent. It is this precipitation that will be examined in this work.

4.1.2 Polyethylene Glycol Precipitation

Polyethylene glycol precipitation is an example of precipitation using a non-ionic polymer as the precipitating agent. PEG is the most popular agent utilised for this type of operation, although dextrans are also employed.

Laurent and Iverius (1967) and Ogsten (1970) suggested that the precipitation is driven by the polymer excluding proteins from part of the solution, and thus the amount of water available for protein solvation is effectively reduced. This mechanism

can be considered analogous to the formation of liquid-liquid two phase systems from mixtures of aqueous polymers first studied by Albertsson (1970) and later by Kula and Kroner (1978).

For polyethylene glycol precipitations of yeast intracellular protein, Foster *et al* (1973) developed the following equation to describe the precipitation process;

$$\ln S_p + f_p S_p = X_p - aC_p \qquad \textbf{(4.1)}$$

where S_p = protein solubility (Kg m^{-3})

f_p = protein self-interaction coefficient (-)

a = polyethylene glycol interaction coefficient (-)

C_p = polyethylene glycol concentration (Kg m^{-3})

and X_p is given by;

$$X_p = \frac{\left(\mu_j - \mu_j^0\right)}{RT} \qquad \textbf{(4.2)}$$

where μ_j = chemical potential of component j (J mol^{-1})

μ_j^0 = standard chemical potential of component j (J mol^{-1})

R = universal gas constant (J mol^{-1} K^{-1})

T = temperature (K)

The protein self-interaction coefficient term has been shown to become significant at higher protein concentrations (greater than 10 mg mL^{-1}) and at pH levels away from the isoelectric point. pH, temperature and ionic strength can also have a marked effect on protein solubility (Miekka and Ingham, 1978). In addition the presence of cell debris in a precipitation batch can have a marked effect on the size and density of the particles produced. This will be discussed in greater detail later.

It has also been reported that high concentrations of polyethylene glycol are required to precipitate proteins of low molecular weight, and vica versa. In addition, the higher the molecular weight of the precipitating agent, the greater its effect, up to a limiting value (approaching 10,000 in the case of PEG). Such observations are consistent with the proposed mechanism of protein exclusion from part of the hydrating solution similar to that utilised in gel filtration. In the former case however it is not necessary to have two visibly distinct phases.

Ingham (1978) observed that the minimum solubility of the protein albumin in the presence of PEG occurred at the protein's isoelectric point. He also observed very little variation with temperature, which leads to the advantage that such precipitations may be operated at room temperature. This is believed to be due to a stabilising effect that non-ionic polymers have on proteins.

Precipitation using this technique generally occurs at reagent concentrations of below 20% by volume. Furthermore, whereas salts used during salting out must be removed from solution before any form of ion exchange chromatography can be undertaken, non-ionic polymers will be carried straight through such a column and thus will be separated from a target protein during the binding of the protein to the matrix. It has, however, been shown that the use of high concentrations of PEG can greatly reduce the performance of some exclusion chromatography media. The simple addition of 0.4M phosphate is sufficient to force the PEG to become a separate phase, with the protein partitioned mainly in the aqueous phase (Busby & Ingham, 1980).

4.1.3 Kinetics of Protein Precipitate Growth

Smoluchowski (1917) developed the theory most commonly used to describe the kinetics of protein aggregate growth. It involves the division of the process into two stages controlled by distinct mechanisms. Perikinetic growth is the process of precipitate nucleation. The other mechanism, orthokinetic growth, describes the process of particle growth by aggregation.

Smoluchowski's theory when applied to perikinetic growth describes the initial rate of decrease of particle number concentration. This nucleation stage involves the removal of any barrier to molecular aggregation to allow particle growth to proceed at a rate controlled by both particle number concentration and diffusivity. The equation governing this stage of precipitate formation for a mono-sized dispersion is given below;

$$-\frac{dN}{dt} = K_A N^2 \qquad \textbf{(4.3)}$$

where N = particle number concentration (No. μL^{-1})

K_A = Rate constant ($m^3\ s^{-1}$)

The rate constant K_A is in turn controlled by the diffusivity and particle diameter;

$$K_A = 8\pi D_f d \qquad \textbf{(4.4)}$$

where D_f = diffusivity ($m^2\ s^{-1}$)

d = particle diameter (m)

This equation, however, is somewhat deficient in that it doesn't take into account the presence of electrical barriers around the particle, which will decrease the rate of aggregation. In 1964 Fuchs proposed the following equation to account for this;

$$-\frac{dN}{dt} = \frac{K_A}{W} N^2 \qquad \textbf{(4.5)}$$

where W is the stability ratio, and is defined by the following equation;

$$W = d\int_0^\infty \frac{\exp\left[\frac{\phi(h)}{K_B T}\right]}{(h_p + d)^2} dh \qquad \textbf{(4.6)}$$

where h_p = particle separation distance (m)

K_B = Boltzmanns constant ($J\ K^{-1}$)

$\phi(h)$ = potential energy of interaction between two particles (J)

The stability ratio W, however, is frequently difficult to evaluate. Neither does the above equation allow for the presence of a hydration barrier of associated water around the molecule, or the fact that protein association may not be the limiting step in precipitation, where removal of hydration or electrical barriers can be very slow.

After nucleation and initial perikinetic growth, the presence of hydrodynamic shear within the precipitation vessel will cause particles larger than a certain size to collide. These collisions give rise to an overall increase in particle size. Smoluchowski gives the rate of decrease of particle number concentration in a uniform shear field as;

$$-\frac{dN}{dt} = \frac{2}{3}\alpha_c G_p d^3 N^2 \qquad \textbf{(4.7)}$$

where G_p = uniform shear rate (s^{-1})

α_c = collision effectiveness factor (-)

There are, in practice, a number of deviations from equation 4.7. Two particles on a direct collision course will tend to follow the streamlines around each other, reducing the actual number of collisions. Estimations of the shear rate are frequently difficult. In laminar systems the actual shear will vary with position so an average is used. In turbulent systems, however, there is a non-uniform and variable shear field. This is frequently described by the Kolmogorov scale of microturbulence (KSM, see Chapter 1), which estimates the size of the smallest eddy which will exist before the energy contained within it is dissipated to heat (the higher the energy input to the liquid, the smaller the value of the KSM);

$$\eta = \left(\frac{\nu^3}{\varepsilon}\right)^{\frac{1}{4}} \qquad \textbf{(4.8)}$$

where η = Kolmogorov scale of microturbulence (m)

υ = suspension kinematic viscosity ($m^2\ s^{-1}$)

ε = energy dissipation per unit mass of fluid ($W\ Kg^{-1}$)

The following equation was proposed by Saffman and Turner (1956) to describe the decrease in particle number concentration N of neutrally buoyant particles in a homogeneous turbulent flow field.

$$-\frac{dN}{dt} = \frac{1.294}{8}\left(d_1 + d_2\right)^3\left[\frac{\varepsilon}{\nu}\right]^{\frac{1}{2}} N_1 N_2 \qquad \textbf{(4.9)}$$

where d_1 and d_2 are particle diameters (m).

Camp and Stein (1943) suggested that the average shear rate in use in Smoluchowski's equation can be estimated on the basis of power dissipation per unit volume;

$$-G_p = \left[\frac{\varepsilon}{\nu}\right]^{\frac{1}{2}} \qquad \textbf{(4.10)}$$

Thus utilising equation 4.9 and applying to a monosized suspension of particles;

$$-\frac{dN}{dt} = \frac{2}{3} d^3\left[\frac{\varepsilon}{\mu}\right]^{\frac{1}{2}} N^2 \qquad \textbf{(4.11)}$$

where μ = suspension dynamic viscosity ($N\ s\ m^{-2}$)

Camp and Stein also proposed the dimensionless Camp number, Ca;

$$Ca = G_p t \qquad (4.12)$$

where t = time (s)

This theory has now been used successfully to model growth of precipitate over the first few seconds of orthokinetic growth (Virkar *et al*, 1982, and Hoare, 1982). More significantly for the work presented here, the Camp number has become the scale-up basis employed when considering precipitation reactions.

4.1.4 Protein Precipitate Aggregate Breakage

An equally important concept when considering the precipitation process is that of aggregate breakage in the precipitation vessel. This will be instrumental in determining the final size of the particles, and thus the ease of solid/liquid separation. Glasgow and Luecke (1980) proposed four major aggregate breakage mechanisms;

- fluctuating dynamic pressure resulting in aggregate deformation and rupture
- hydrodynamic shear erosion of primary particles
- fragmentation due to collision
- fragmentation due to hydrodynamic shear.

Most models developed have assumed that any collisional events are negligible compared to shear induced events. Furthermore, such events appear to invoke binary breakage, as observed by Pandya and Spielman (1983) who used a population balance to observe that the average number of daughter particles produced upon rupture per floc was 2.5. Tomi and Bagster (1978 a, b) proposed that such break-up would result in the precipitate particles reaching a final, stable, maximum size. They used a force balance between aggregate strength and induced stress to give the upper size, D_{max}, as;

$$D_{max} \propto N_i^{-3\gamma} \propto \varepsilon^{-\gamma} \propto G^{*-2\gamma} \qquad (4.12)$$

where γ = 1 for $d >> \eta$

γ = 0 for $d << \eta$

γ = 0.5 for $d = \eta$

G^* = mass average shear rate (s^{-1})

η = Kolmogorov scale of microturbulence (m)

ε = energy dissipation per unit mass (W Kg^{-1})

N_i = agitator speed (RPS)

D_{max} = maximum particle size (m)

They found that this model was in close agreement with data for both ferric oxide and carbon black aggregates published by Reich and Vold (1959). However, experimental values ranging from 0.1 to 0.8 have been found for γ (Tambo and Hozumi, 1979, and Tomi and Bagster, 1978).

Bell *et al* (1983) comment that in practice, under a laminar Couette shear rate of 2000 s^{-1} breakage was to a certain extent concentration dependent (very low precipitate concentrations reduce particle/particle and particle/surface collisions).

Hoare *at al* (1982), working with isoelectric soya protein precipitate, showed that the change in particle size distribution was strongly indicative of particle breakage by fragmentation, with the particle size decreasing extremely rapidly over the initial period of shear, this process continuing until almost spherical aggregates were obtained. Further break-up observed was considered due to the erosion of these primary particles slowly with time. Final fragment size was found to be a very weak function of shear. However, the rate of breakage of aggregates (particularly the larger ones) was found to be strongly dependent on shear rate (Bell and Dunnill, 1982).

It is obviously the interaction of these shear effects with the rate of particle growth and aggregate formation that controls the final finished size distribution of precipitate particles i.e. the rate at which fragmentation occurs combined with the rate at which the protein aggregates "mop up" the fines created. Bell and Dunnill showed that, at the

high end of the size distribution, the d_{05} value showed a very strong dependence on the shear rates developed in the precipitation vessel, whereas the smallest particles (d_{90}) were almost independent of it.

Equation 4.12 therefore describes the simplest correlation which has been used to describe shear associated particle break-up of precipitates. However, generally this and many other more complex models, both theoretically and empirically derived, have not proven completely successful in predicting such effects, mainly because of the complex, and time dependent, nature of such processes. It is, however, important that a general understanding of mechanisms thought likely to cause breakage to protein precipitates is applied when assessing the impact of high speed disk stack centrifugation upon such particles.

4.1.5 Particle Ageing

The final consideration when operating a precipitation process, and the one that has a major effect on particle strength, is that of ageing. Obviously, the objective of the process after the formation of the nuclei is to form as large, dense, stable aggregates as is possible for ease of subsequent centrifugal recovery. The history of preparation influences the size, shape and degree of compactness of such particles, with manipulation of the protein concentration and reactor shear rate having been shown to be advantageous in numerous cases. An excellent review is presented by Bell, Hoare & Dunnill (1983). Essentially, a balance must be maintained between the faster rate of growth that can be obtained at higher shear rates and concentrations, against the higher rate of break-up which is also seen under these conditions. It is the second factor which is generally the more important; hence lower reactor shear rates give rise to larger particles. However, in a stirred tank reactor it is not always easy to define the shear rate as there is a difference between the mean velocity gradient and the much higher rate of shear seen in the impeller zone. As has already been stated, the Camp number, Ca, is extensively used when considering precipitation and it is the product of the mean velocity gradient, G^*, and the time of exposure which is used to calculate this, as it is the shear rate in the bulk of the suspension which is considered the most

important. Values of Ca from 10^4 to 10^5 are recommended in the water treatment field, with G^* up to 100 s^{-1}. However, much research into geometry and type of reactor has indicated that, despite this, it is important also to have the high regions of shear that exist in the impeller zone of a Rushton turbine driven STR as this promotes and enhances precipitate growth (Virkar *at al*, 1982, and Ives and Bhole, 1973). Because this plays a significant role, scale up and switches between types of reactor can be difficult to predict.

In addition, the Camp number has been shown to correlate strongly to the strength of soya protein precipitates prepared by isoelectric precipitation (Bell and Dunnill, 1982). They found that apparent aggregate strength, as measured by examining the change in mean particle diameter obtained upon exposure to a capillary shear force of 10^4 s^{-1}, increased dramatically up to a G^*t value of 10^5, after which it declined slightly. This Camp number also produced denser precipitates, a highly desirable characteristic. The effect was further investigated by Titchener (1986) who showed that the maximum aggregate size in a reactor was linked to the Camp number within it, with the PSD (Particle Size Distribution) reducing as the shear rate increased. Smaller aggregates were generally composed of fewer, more tightly packed, primary particles than larger aggregates and were thus stronger. The existence of velocity gradients within the reactor, as described above, was also considered to be a possible factor. A similar effect was noted by Kitchener and Gochin (1981), who surmised that the effect was due to the preferential survival of tightly packed nodular flocs in water treatment systems.

4.2 Recovery of Protein Precipitates by High Speed Disk Stack Centrifugation

The general problems found when recovering precipitates have already been outlined; those of low density difference between particle and fluid, small particle size, and sensitivity to shear forces. These particles are typically formed at shear rates of 100 s^{-1} or lower, and thus are unprepared to experience the shear forces found in high speed rotating machinery such as a DSC, typically several orders of magnitude higher. Indeed, a key consideration when recovering such particles utilising a disk stack centrifuge is that of shear associated particle break-up in the feed zone of the machine. Any disruption occurring within this region will result in the production of many small particles which can be extremely difficult to recover centrifugally, and drive down volumetric throughputs and recovery efficiencies. This in turn can give rise to longer residence times, and hence even longer exposure to shear forces as well as increased temperature rises which may damage target proteins (if the precipitate being removed is a waste product and the product remains in suspension). The presence of gas/liquid interfaces within the centrifuge can also denature significant amounts of soluble protein. Therefore any understanding that can be gained of the mechanisms within a disk stack centrifuge causing such breakage, and methods of reducing it, is extremely valuable, and is the purpose of the work contained in this chapter.

4.2.2 Shear based Disruption of Biological Flocs

As has been stated, shear induced break-up of protein precipitate aggregates in a centrifuge gives rise to poor clarification because of the amount of un-recoverable fines produced. As was reviewed in Chapter 3, the maximum shear field in a disk stack centrifuge is recognised to be generated in the feed zone, where particles are subjected to a rapid increase in both radial and tangential velocity components (Bell and Dunnill, 1983). A full discussion of the sites believed to cause disruption in the standard semi-hermetic feed zone of a disk stack centrifuge, as well as the differences between it and

the new hydro-hermetic feed zone can be found in Chapter 3, and an estimation of these shear forces in Chapter 5.

Bell and Brunner (1983) suggested that protein floc break-up in a disk stack centrifuge could be described by;

$$\frac{dN}{dt} = K_p \sqrt{P_d}\, t \qquad \textbf{(4.13)}$$

where N = Particle number concentration (No. μL^{-1})

K_p = rate constant (-)

P_d = power dissipation (W m^{-3})

t = time (s)

However, the proposal that the rate of floc break-up was proportional to the square root of the power dissipated was based on two assumptions;

- the density of the flocs is constant and equal to the density of the solid particles
- no significant floc disruption or aggregation occurs in the clarified liquid discharge stream.

Integrating this equation gives;

$$\ln\left(\frac{N}{N_0}\right) = K_p \sqrt{P_d}\, t \qquad \textbf{(4.14)}$$

where N_0 = Initial particle number concentration (No. μL^{-1})

In a scroll decanter centrifuge, it was shown that floc break-up was strongly dependent on both the speed of the bowl, with an increase in speed increasing break-up, and also on the location of the feed pipe. When the feed pipe was situated in the shallowest section of the pond, break-up was at it highest.

When assessing recovery in a disk stack centrifuge it is vital to be able to estimate the level of breakage occurring in the feed zone. The full recovery process can be summarised as in Figure 4.1 below.

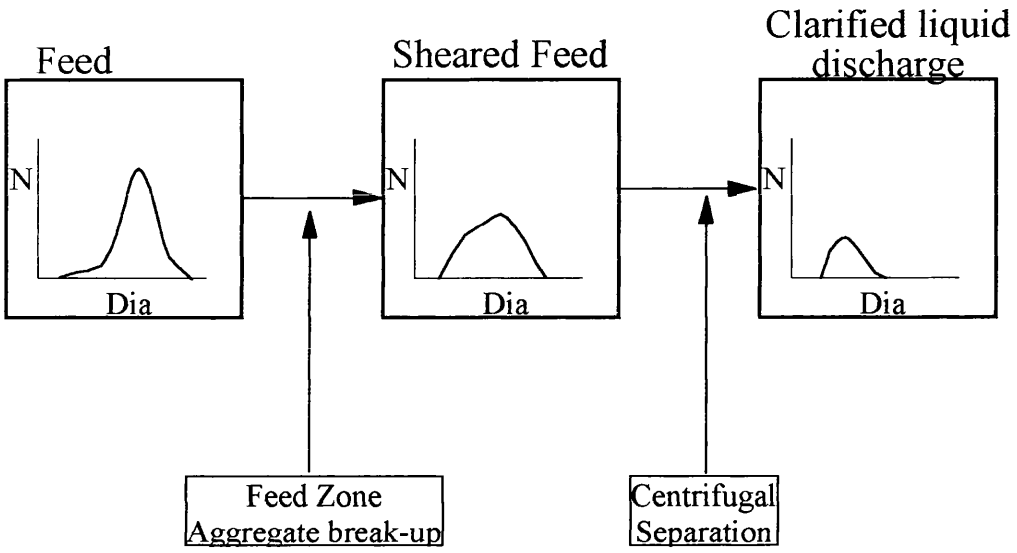

Figure 4.1: Transformation of particle size distribution due to precipitate breakage in the centrifuge feed zone and subsequent clarification (Clarkson, 1994).

Unlike the whole cell work described in Chapter 3, breakage of precipitates cannot be estimated using biological assays. The above diagram shows the transformation that occurs to the precipitate size distribution upon passage through a disk stack centrifuge. It can be broken into two distinct phases; first the initial size distribution is altered by passage through the centrifugal feed zone, where the bigger particles in the initial feed are fragmented into many smaller ones. Secondly the centrifuge recovers a percentage of the particles during clarification. A physical performance function of the centrifuge, known as the grade efficiency curve, can be used to describe the recovery obtained within a disk stack centrifuge, and this can be compared to the theoretical recovery which assumes there is no breakage of particles in the machine. Furthermore, by plotting grade efficiency curves at different flow rates, and for different feed zone designs, the change in the level of breakage can be estimated. This is the approach that will be taken in this work.

4.2.3 The Grade Efficiency Concept

As was detailed in Chapter 3, the separating ability of a centrifuge is governed by Stokes Law, and thus is highly dependant on particle size, having a different efficiency for each and every particle size in the feed suspension. For this reason, when predicting or expressing the separation efficiency of a centrifuge in terms of particle size distributions it is impossible to use one overall value, and the concept of grade efficiency must be employed instead. If the mass recovery efficiency is measured for each particle size in a feed stream then the gravimetric grade efficiency function, T(d), is obtained. This function is independent of both solids size distribution and density, and will be constant for a given centrifuge design. Grade efficiency has been used successfully together with three dimensionless numbers for the scale-up of geometrically similar disk stack centrifuges (Gupta, 1981). Mannweiler and Hoare (1992) used grade efficiency plots to scale down a pilot scale disk stack centrifuge to one tenth of it's operating capacity. With no shear associated particle break-up, therefore, both a semi-hermetic and a hydro-hermetic design DSC should yield the same grade efficiency function. Because, however, the separation efficiency is based on the ratio of particles of a given size in the feed to those in the clarified supernatant, any particle breakage will create particles which were not present initially. As these will inevitably be small and difficult to recover, they will show up in the supernatant analysis and thus alter the value of the grade efficiency function. Hence grade efficiency plots can be used to assess the level of breakage in a disk stack centrifuge.

4.2.3.1 Use of the Grade Efficiency Concept

The definition of Sigma factor (Σ) has already been given in Chapter 3. Equation 3.13 stated;

$$Q = 2V_g\Sigma \qquad \textbf{(4.15)}$$

where Q = volumetric throughput ($m^3\ s^{-1}$)

V_g = settling velocity of particle d_s under gravity (m s^{-1})

Σ = equivalent settling area of centrifuge (m^2)

However, this equation was defined in terms of recovery of 50% of all particles of size d_s (the cut point). If the volumetric throughput Q_{100} at which 100% of particles of size d_s is desired then this equation becomes;

$$Q_{100} = V_g\Sigma \qquad \textbf{(4.16)}$$

If a specific throughput q_s is defined as that at which all particles with gravitational settling velocity equal to or greater than V_g are removed, then;

$$V_g = V_{gc} = \frac{q_s}{\Sigma} \qquad \textbf{(4.17)}$$

where V_{gc} = critical settling velocity (m s^{-1})

q_s = specific throughput capacity (m^3 s^{-1})

q_s for V_{gc} can itself be obtained from Stokes Law;

$$\frac{q_s}{\Sigma} = \frac{d^2\Delta\rho g}{18\mu} \qquad \textbf{(4.18)}$$

where d = diameter of particle (m)

$\Delta\rho$ = particle-liquid density difference (Kg m^{-3})

μ = suspension dynamic viscosity (N s m^{-2})

g = gravitational acceleration (m s^{-2})

This equation can therefore be solved for the critical particle diameter d_c, the diameter of the particle which will just be recovered from solution;

$$d_c = \sqrt{\frac{18 q_s \mu}{\Delta \rho \Sigma g}} \qquad \textbf{(4.19)}$$

At throughput q_s, therefore, only particles of diameter equal to or greater than d_c will be recovered. However, as was demonstrated in Chapter 3, because particles are uniformly distributed across the disk space, and particles near the surface of an upper disk are easier to recover than those near the surface of a lower, there is a probability of separation involved. The probability of particles of gravitational settling velocity less than V_{gc} being recovered is what is defined by the grade efficiency curve, T;

$$T = \frac{V_g}{V_{gc}} \qquad \textbf{(4.20)}$$

where T = grade efficiency (-)

The value of the grade efficiency increases linearly with gravitational settling velocity V_g until V_g equals V_{gc} where the grade efficiency will reach a value of unity. Equation 4.20 can therefore be formulated as;

$$T = \left(d/d_c\right)^2 \qquad \text{for } d<d_c \qquad \textbf{(4.21)}$$

$$T = 1 \qquad \text{for } d>d_c \qquad \textbf{(4.22)}$$

4.2.3.2 Derivation of the Grade Efficiency Equation

For a centrifugal separation process, the total mass of the feed must be equal to the sum of the total masses of the products;

$$m_f = m_{sed} + m_{sup} \qquad \textbf{(4.23)}$$

where m_f = mass in centrifuge feed (Kg)

m_{sup} = mass in centrifuge supernatant (Kg)

m_{sed} = mass in centrifuge solids (Kg)

For each particle size, d, present in the feed;

$$m_f(d) = m_{sed}(d) + m_{sup}(d) \quad \textbf{(4.24)}$$

By definition the particle size distribution frequency gives the fraction of particles of size d in the sample. Equation 4.24 can therefore be rewritten as;

$$m_f \Delta F_f(d) = m_{sed} \Delta F_{sed}(d) + m_{sup} \Delta F_{sup}(d) \quad \textbf{(4.25)}$$

The total efficiency of separation E_T, or mass yield, can be defined;

$$E_T = \frac{m_{sed}}{m_f} = \left(1 - \frac{m_{sup}}{m_f}\right) \quad \textbf{(4.26)}$$

For a self cleaning disk stack centrifuge, the product of the mass flow rate and the concentration of the solids in the feed will be equal to the mass of solids in the feed. Similarly, if it is assumed that mass of fluid leaving the centrifuge through the supernatant is approximately equal to the mass of fluid entering, (i.e. fluid loss through solids discharge is negligible, valid when processing streams of low solids content) then the mass of solids in the supernatant will be equal to the product of the mass flow rate and the solids concentration in the supernatant. Therefore equation 4.26 can be written as;

$$E_T = 1 - \frac{C_{sup}}{C_f} \quad \textbf{(4.27)}$$

where C_{sup} = volume concentration of solids in supernatant (-)

C_f = volume concentration of solids in feed (-)

This means that the mass yield of the centrifuge can be directly measured either using a feed and supernatant volume based size distribution measurement, or, as optical absorbance is approximately proportional to the volume of solids in a sample, on an optical density basis.

Equation 4.25 can be re-written as;

$$\Delta F_f(d) = E_T \Delta F_{sed}(d) + (1 - E_T)\Delta F_{sup}(d) \qquad \textbf{(4.28)}$$

If the mass yield is evaluated for every particle size d, the grade efficiency curve T(d) will be obtained;

$$T(d) = \frac{m_{sed}(d)}{m_f(d)} \qquad \textbf{(4.29)}$$

or

$$T(d) = \frac{m_{sed}\Delta F_{sed}(d)}{m_f \Delta F_f(d)} \qquad \textbf{(4.30)}$$

Substituting into equation 4.26 gives;

$$T(d) = E_T \frac{\Delta F_{sed}(d)}{\Delta F_f(d)} \qquad \textbf{(4.31)}$$

The particle size distribution in use can be mass, surface area, or volume, provided they are specified on the same basis as E_T. However, it is most convenient experimentally to use volume-based size distributions, measuring both the feed and the supernatant streams and using the equation;

$$T(d) = 1 - (1 - E_T)\frac{\Delta F_{sup}(d)}{\Delta F_f(d)} \qquad \textbf{(4.32)}$$

Grade efficiency curves are by convention plotted against the dimensionless number d/d_c , and this convention will be adopted in this thesis.

4.2.3.3 Curve Fitting for Grade Efficiency

Grade efficiency curves may be accurately transformed into mathematical expressions described by only a few parameters. The Rosin-Rambler-Sperling-Bennet (RRSB) function is normally used for describing particle size distribution curves (Svarovsky, 1990). Mannweiler (1990) converted this for use with grade efficiency curves;

$$T(d) = 1 - \exp\left[-\left(k_1 \frac{d}{d_c}\right)^n\right] \qquad \textbf{(4.33)}$$

where k_1 and n are constants. This can be expressed;

$$\ln\left[-\ln\left(1 - T(d)\right)\right] = n \ln(k_1) + n \ln\left(\frac{d}{d_c}\right) \qquad \textbf{(4.34)}$$

n can therefore be found from the gradient, and k_1 is given by;

$$k_1 = \exp\left(\frac{\text{int ercept}}{n}\right) \qquad \textbf{(4.35)}$$

The curve developed by Mannweiler and Hoare (1992) using dilute suspensions of polyvinylacetate particles, (which are shear insensitive) obtained values of k_1=0.865, and n=2.08. This work was carried out on a Westfalia Separator BSB disk stack centrifuge, however, both Clarkson (1994) and Rumpus (1997) observed similar values when the above theory was applied to other disk stack centrifuges and shear insensitive solids.

It should be noted that the values quoted above do not fit the theoretical Stokes Law based grade efficiency curve: once again, deviation from Stokes Law is to be expected as flow through a centrifuge is not ideal (see Chapter 3).

4.3 Materials and Methods

4.3.1 Measurement of Particle Size Distribution

Particle size analysis was conducted using the electrical sensing zone method, utilising an Elzone model 280 PC (Particle Sizing Systems Ltd., Hereford, UK). In operation the sensing tube, complete with defined orifice of known size, is filled with and immersed in a dilute suspension of electrolyte containing a known amount (at known dilution) of the material to be analysed. A vacuum pump is used to draw suspension containing the sample through the orifice into the sensing tube. The electrical resistance across the orifice is monitored by means of immersed electrodes on either side of the tube wall. Passage of any particles within the sample through the orifice causes a change in the electrical resistance across the orifice. This is converted to a voltage pulse which is then amplified. The number of pulses is equal to the number of particles passing through the orifice, with the height of the voltage pulse being proportional to the volume of the particle. The instrument is initially calibrated with a dilute suspension of highly defined latex particles (also supplied by Particle Sizing Systems). The data is presented as count per channel with the measurement range of the machine broken into 128 channels, the total channel width being a function of orifice size, current across the orifice, and gain in the amplifier. The count is presented as volume or number of particles in each channel, with the volume measurement per channel calculated from the particle number count and relative to the total volume recorded across the instruments range. The rate of particle counting is strictly controlled (hence the need to dilute samples) to prevent several particles moving through the orifice at once, known as coincidence, which leads to inaccurate measurement.

The electrolyte used was 8% polyethylene glycol 8000, 5% sodium chloride, 0.1M phosphate buffer, pH 6.7. This was identical to the reagent solution used for precipitation and was selected so as to prevent any change in sample during measurement caused by a change in reagent concentration. The electrolyte was filtered through a 0.1μm depth filter (Whatman Scientific Ltd., Maidstone, UK) prior to use to remove any particles which may have been present and caused a background count to be registered.

A 48μm orifice was used, calibrated with 5μm, 10μm and 20μm latex standards. All samples were measured over 20 seconds, the sample dilution being adjusted to obtain a coincidence of between 0.8 and 1% (this corresponded to between 12,000-14,000 particles measured). Background counts over this time were maintained below 300 particles. All samples were analysed in triplicate and the mean count at each channel taken. Errors were low (+/- 5%) and the reproducibility high (all samples were analysed in triplicate with the total particle volume within 5% each time).

4.3.2 Disc Photosedimentation Method

As was shown in the theory section, it is necessary to know the density difference between the precipitate particles and the surrounding suspension in order to calculate the critical particle diameter, d_c. The density of the particles was measured using a disc photosedimentometer (BI-DCP 1000, Brookhaven Instruments Ltd., Stock Wood, UK).

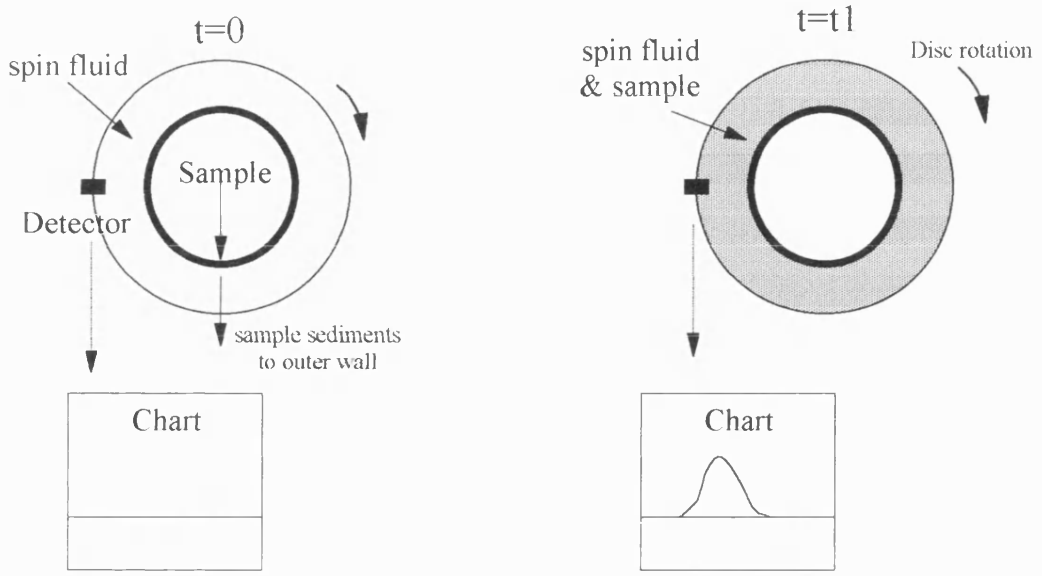

Figure 4.2: Schematic Diagram of the Disc Photosedimentometer equipment, (Middleberg and Bogle, 1990)

The rate of sedimentation of particles through a spin fluid of known viscosity and density at a specified centrifugal force is measured (see Figure 4.2 above). White light from a tungsten/halogen lamp passes through the disc and spin fluid at a known distance from the axis of rotation. This corresponds to a fixed height of liquid from the start point for a sample when a known volume of spin fluid is used. Particles in the sample travel out under centrifugal force, the larger and more dense a particle, the faster it moves. As particles pass through the light beam the light intensity is decreased due to both scattering and absorption. This intensity is measured by a photodiode, and the data presented as a plot of absorbance against time.

The centrifugal sedimentation rate at constant angular velocity increases proportionally with distance from the axis of rotation;

$$\frac{dr}{dt} = \frac{\Delta\rho d^2}{18\mu}\,\omega^2 r \qquad \textbf{(4.36)}$$

where $\Delta\rho$ = solid liquid density difference (Kg m^{-3})

d = particle diameter (m)

μ = spin fluid dynamic viscosity (N s m^{-2})

ω = angular velocity (rad s^{-1})

Integrating equation 4.36 with respect to time, from the initial radius of injected sample R_s at time zero to the radius of the detector R_d at time t gives;

$$t = \frac{18\mu \ln\left(R_d / R_s\right)}{\omega^2 d^2 \Delta\rho} \qquad \textbf{(4.37)}$$

The absorbance/time plot from the instrument can be transformed to a cumulative basis to yield a plot of cumulative fraction sedimented with time on a mass basis. By using the electrical zone sensing technique described previously a cumulative size distribution plot on a particle volume basis can also be obtained. Matching of the two distributions enables the sedimentation velocity of each particle of a given size to be determined. Using equation 4.37 it is therefore possible to calculate the density difference between the particles coming through at time t and the spin fluid. Hence a particle density distribution may be obtained.

The spin fluid used was 15 mL of 8% polyethylene glycol, 5% NaCl, 0.1M phosphate buffer, 5% sucrose, pH 6.7. Again, this was very similar to the reagent concentrations used in the precipitation, (with the addition of a small amount of sucrose to reduce the rate of sedimentation), in order to avoid fundamental changes to the sample during measurement. 1mL of "cut" fluid was also used; this was the above solution with the exception of sucrose. Because this was less dense than the spin fluid it remained suspended in a band at the point the sample is loaded (i.e. on the inner surface of the spin fluid). Immediately before loading the sample, the angular velocity of the disk was raised for one second and then lowered again. This mixed the cut fluid into the top surface of the spin fluid, creating a density gradient. In turn, when the sample was loaded this produced a "straight line start" i.e. the sample band loaded evenly around the inner surface of the spin fluid. Without the use of this technique, the phenomena of "streaming" tended to occur, whereby sample travels through the spin fluid unevenly around the disc, thus destroying the measurements. The sample volume was 1mL,

diluted to a concentration whereby the detectors maximum signal of 2.5mV was not exceeded. Details of the density calculations can be found in Appendix 2.

4.3.2 Optical Density

Optical density of feed and supernatant suspensions was measured by spectrophotometer, (Uvikon 922, Kontron Instruments, UK.) at an absorbance of 650 n.m. Clarification efficiencies were calculated from these measurements as per Chapter 3.

4.3.3 Density of Fluids

The density of the spin fluid and the precipitating reagent was measured using the specific gravity bottle technique. The bottle held an accurately repeatable volume, (approximately 50 mL). Firstly the bottle was weighed empty. It was then filled with de-ionised water and the weight measured on a 5 decimal place balance. This was repeated in triplicate. The bottle was then filled with the sample whose density was to be determined and weighed; again this was repeated in triplicate. The weight of the water contained by the bottle, together with standard density tables, enabled the volume of the bottle to be calculated accurately. Thus the density of the sample could in turn be found accurately and simply, with a reproducibility of +/-5%.

4.3.4 Measurement of Viscosity

All viscosity's were measured using a Rheomat 115 cup and bob viscometer (Contraves Industrial Products, Ruislip, UK). This operates on the principle of subjecting a sample to a known shear rate; the torque on the driving shaft at this shear rate is then measured. Using a correlation specific to the cup and bob in use, derived after testing with pure water, the viscosity of the sample under test could then be

calculated. The measurements were conducted in duplicate at a temperature of 5^0C to yield an accuracy of +/- 7%.

4.3.5 Preparation of Yeast Homogenate

DCL high activity packed bakers yeast (J.W. Pike Ltd., UK), was suspended in 5% sodium chloride, 0.1M sodium phosphate (Sigma-Aldrich Company Ltd., UK) solution at 280 g L^{-1} wet weight. The pH of the solution was adjusted to 6.7 using 4M sodium hydroxide solution (Sigma-Aldrich). Preliminary precipitation was carried out on a small scale to produce material for density and viscosity measurements. This was then disrupted using a Lab 40 high pressure homogeniser (APV Manton-Gaulin Ltd., UK) utilising 5 passes at 500 bar. On a large scale disruption was carried out by 5 passes at 500 bar pressure through a model K3 high pressure homogeniser (APV Manton Gaulin Ltd., UK), at a flow rate of 280 Lh^{-1}, sufficient to release approximately 95% of total protein present in the suspension. Homogenisation was carried out in a continuous mode at 5^0C on a large scale and in batch mode also at 5^0C on a small scale, with the temperatures maintained using ethylene glycol coolant. Finally the pH was re-adjusted to 6.7.

4.3.6 Preparation of Precipitating Agent

The precipitating agent was 50% w/w polyethylene glycol 8000 (M.W. 8000) (supplied by the Sigma-Aldrich Company Ltd., UK), 5% NaCl, 0.1M KH_2PO_4,, adjusted to pH 6.7 using 4M sodium hydroxide. This was made up at least 8 hours before use to allow the PEG 8000 to dissolve completely.

4.3.7 Clarification of Homogenate prior to Precipitation

Experimentation was carried out both with an unclarified and a clarified yeast homogenate stream. When clarification was necessary it was conducted using an Alfa-Laval AS26 Tubular Bowl centrifuge (Alfa Laval Separations Ltd., Camberley, UK) operating at a volumetric throughput of 50 Lh^{-1} and a centrifugal force of approximately 20,000G, processing a maximum of 25L of suspension per batch before removing solids from the bowl. Temperature was controlled to below 10^0C. This technique achieved a clarification efficiency of 81% on an optical density basis, approaching 90% on a solids volume basis. Clarification of the yeast homogenate stream prior to precipitation was carried out in order to reduce the solids loading on the disk stack centrifuges used for pilot scale shear studies.

4.3.8 Precipitation

Previous work at UCL (Bird, 1997 and Maybury, 1997) has shown that a concentration of 8% polyethylene glycol will act as a precipitation reagent for a suspension of 28% w/v homogenised yeast, sufficient to remove up to 65% of the total protein from suspension whilst leaving 95% of alcohol dehydrogenase, an intracellular product, in solution. The purpose of the work described here was not to study product recovery or precipitation efficiency; however, the conditions specified above were adopted for the production of feed stock for pilot centrifugation in order to utilise a realistic feed stream. The precipitation was also conducted at a controlled temperature of 5^0C and a pH of 6.7 to conform to previous protocols. The work cited above suggests that although temperature effects are not important, pH is vital to the control of the process. The only addition made was that of the 5% NaCl; this was to make the whole solution conducting, necessary for size analysis using the electrical zone sensing technique described previously (Section 4.3.1).

The precipitation was operated as a batch process, in a "dump" manner, i.e. the precipitating reagent was added to the yeast suspension rapidly (<15s). The 50% PEG

8000 solution prepared as described earlier (Section 4.3.6) was added to the yeast suspension in the ratio 1:5.25 to obtain the final concentration of 8% v/v PEG 8000.

Several sizes of precipitation vessel were used; a small laboratory sized vessel for initial production of material, and a 110L scale vessel for production of material for centrifugation studies. Both were geometrically similar, fitted with baffles and a Rushton turbine design of agitator (the dimensions of which and the details of the shear rate calculations for can be found in Appendix 3). The parameters used to define the operation and scale-up between the vessels were the bulk average shear rate G^* , and the Camp number G^*t.

The equation derived by Vrale and Jordan (1971) was used to calculate the bulk average shear rate within the reactor;

$$G^* = \left(\frac{2\pi N_i T_M}{V_v \mu} \right)^{\frac{1}{2}} \qquad \textbf{(4.38)}$$

where G^* = bulk average shear rate (s^{-1})

N_i = impeller speed (revolutions per second)

V_v = volume of precipitation reactor (m^3)

T_M = motor torque (N m)

μ = dynamic viscosity (N s m^{-2})

The motor torque can be calculated using the empirical correlation of Hill and Kime (1976);

$$T_M = 7.21 \times 10^2 N_i^2 D_i^5 \qquad \textbf{(4.39)}$$

where D_i = impeller diameter (m)

The reactors were operated at an initial shear rate of 180 s^{-1} for 5 minutes, to provide good mixing of the feed suspension and the precipitating agent. The precipitate ageing was then conducted at a shear rate of 50 s^{-1} for 30 minutes, to give a total Camp

number of 1.4 x 10^5 s^{-1}. This was in the range suggested to achieve maximum precipitate strength (Bell and Dunnill, 1982). The low level of shear rate was used to encourage the formation of large aggregates for ease of sizing and centrifugal recovery.

4.3.9 Centrifugation

A CSA-1 pilot scale centrifuge (Westfalia Separator, Milton Keynes, UK) equipped with both a semi-hermetic and a hydro-hermetic feed zone bowl was used to investigate the effects of throughput and bowl rotational speed on overall recovery and shear break-up of the PEG precipitate aggregates. The centrifuge was fed by a Watson Marlow Di 605 variable speed peristaltic pump, (Watson Marlow, Falmouth, UK). The solids breakthrough time was established using optical density measurements of the supernatant and found to be approximately 3 minutes at a flow rate of 75 Lh^{-1} when processing precipitate suspension produced from clarified homogenate, equal to a total volume processed of 3.75 L. This was then used as a performance benchmark, with samples of supernatant at each different operating condition taken for size analysis after 75% of this volume had been processed. This ensured that the centrifuge had the maximum time to reach steady state without reaching the point where excess particles passed out of the machine in the supernatant stream. For the reasons stated in Chapter 3, the centrifuge was operated at a constant backpressure of 0.5 bar (gauge).

4.4 Results

The first requirement of the work was to establish the physical characteristics of the PEG precipitate suspension.

70 mL of suspension was prepared using the laboratory-scale method (Section 4.3.8) both with and without clarifying the yeast homogenate prior to precipitation. This was then analysed to produce a particle size distribution on a volume basis, shown in Figure 4.3 below.

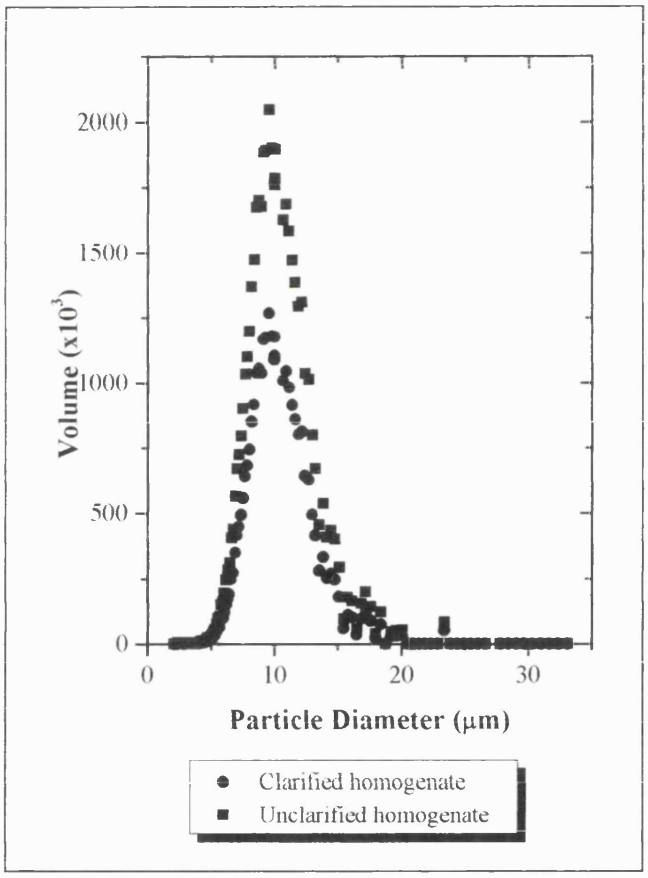

Figure 4.3: Size distribution (volume basis) of 8% v/v PEG 8000 precipitate produced from yeast homogenate showing the effect of pre-clarification of the homogenate prior to precipitation. Count is based on 1mL of undiluted sample in 50 mL instrument running buffer, count time = 20 s

This figure shows that in both cases a tight size distribution was produced, with the peak at approximately 10μm and a size range from 5μm to 20μm. The form of the distribution was identical in the case of both clarified and unclarified homogenate. However there was a substantial increase in the height of the peak when precipitation was performed on the unclarified stream, indicating an increase in the total volume of solids present.

Next the stability of the precipitate suspension was established. Because of the length of time needed to perform pilot scale centrifugation experiments (a maximum of 2 hours per batch) it was considered important to establish that the precipitate characteristics wouldn't change during this time and hence make an accurate comparison of the centrifuge feed zones difficult. The size distribution of the suspension was measured at the end of the precipitation process, (i.e. after 5 minutes high shear mixing in and 30 minutes ageing), 1 hour later and finally after another hour. During this holding time the reactor was agitated at a shear rate of 50 s^{-1}, the same as that used during ageing. The results are shown in Figure 4.4 overleaf. It can clearly be seen that there was no change in the size distribution during the holding time. Subsequent investigation of the precipitation process showed that the peak in size distribution reached 10 μm very early on in the ageing process, (within 10 minutes), after which it remained stable.

The other factor that needed to be investigated was the sampling technique. A sample of precipitate suspension should not undergo any change in size distribution with time. This is because without agitation the particles will not contact each other and hence the twin processes of aggregation and attrition will not occur. However particles in dense suspensions may interact with each other as they settle under gravity therefore creating the possibility of a change in size distribution. The dilution of a sample in precipitation reagent should therefore "freeze" the particle size distribution without altering the conditions of precipitation, by greatly reducing the number concentration of aggregates. To investigate this process a sample was taken at the end of the precipitation process and immediately diluted 1:100.

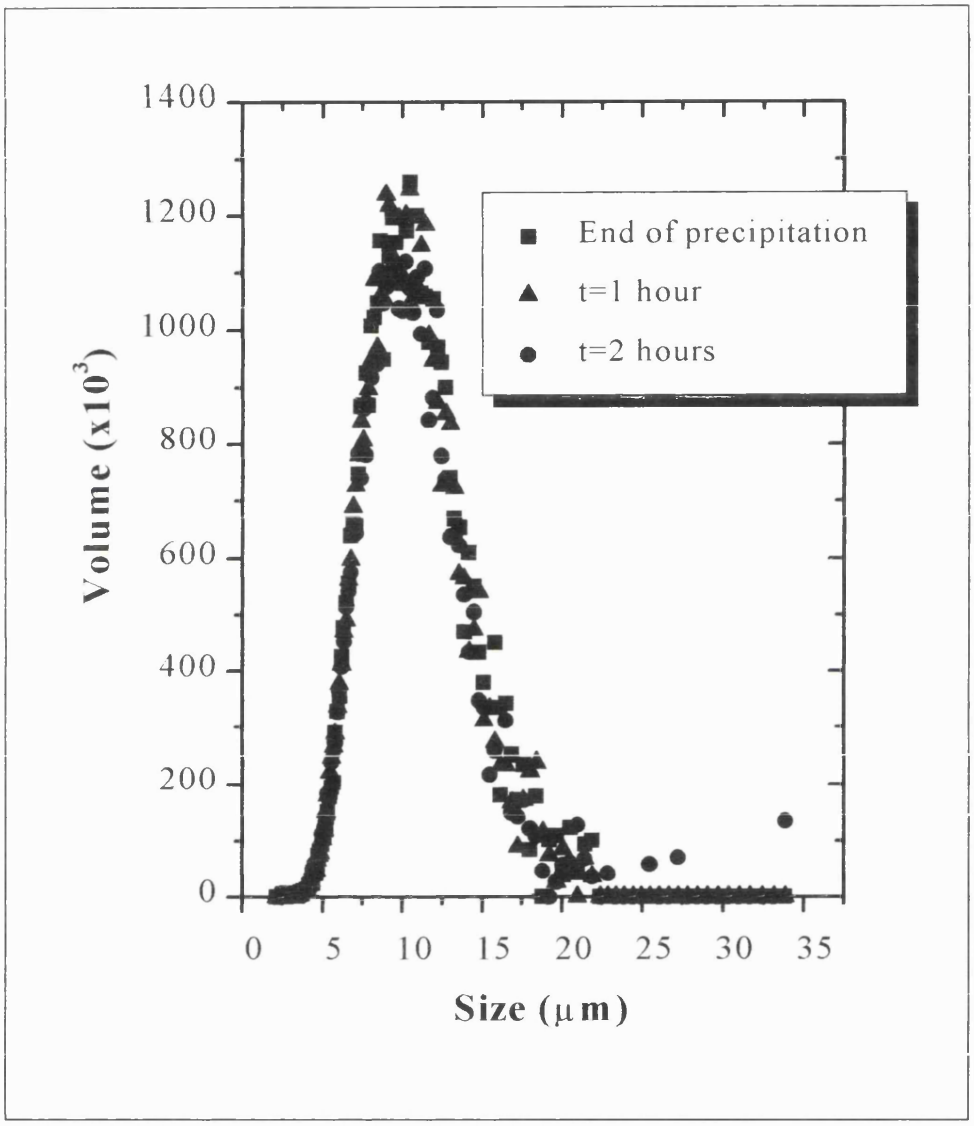

Figure 4.4: Size distribution of 8% v/v PEG 8000 precipitate of clarified yeast homogenate as a function of time after completion of the precipitation process. Reactor agitated at shear rate = 50 s^{-1} (ageing rate) for 2 hours after end of precipitation. Count is based on 1mL of undiluted sample in 50 mL instrument running buffer, count time = 20 s

The particle size distribution of this and an undiluted sample were then analysed over the next 6 hours (the maximum length of time before a sample would be analysed in an experimental day). The results are shown in Figure 4.5. Again, there was no variation in the PSD with sample age in either the diluted or undiluted system, indicating that no special care was necessary in the storage of samples.

The next information needed to perform grade efficiency-based centrifugation experiments was the density of the precipitate aggregate. Bulk density measurements of the precipitating reagent, the precipitate suspension, and the spin fluid used in the photosedimentometer were made using a 50 mL specific gravity bottle, and the results are given in Table 4.1.

Substance	Density (Kg m^{-3}) (+/- 5%)
8% v/v PEG 8000, 5% NaCl, 0.1M KH_2PO_4	1061
8% v/v PEG 8000, 5% NaCl, 0.1M KH_2PO_4, 5% Sucrose	1078
8% v/v PEG 8000 precipitate suspension	1084

Table 4.1: Density of solutions used in precipitate experimental work measured using the specific gravity bottle method.

The graphs used to calculate the density of the precipitate particles as detailed in Section 4.3.2 are shown on the following pages. Figure 4.6 shows information for unclarified homogenate and Figure 4.7 for clarified homogenate. The density distribution of precipitate suspensions prepared from both clarified and clarified homogenate are shown in Figure 4.8.

It can be seen that the precipitate suspension formed in the presence of debris from the disruption process is more dense than that which was pre-clarified. Both systems show an increase in density with size. The unclarified system, however, has a much flatter response than the clarified, only increasing from 1122 Kg m^{-3} to 1130 Kg m^{-3}

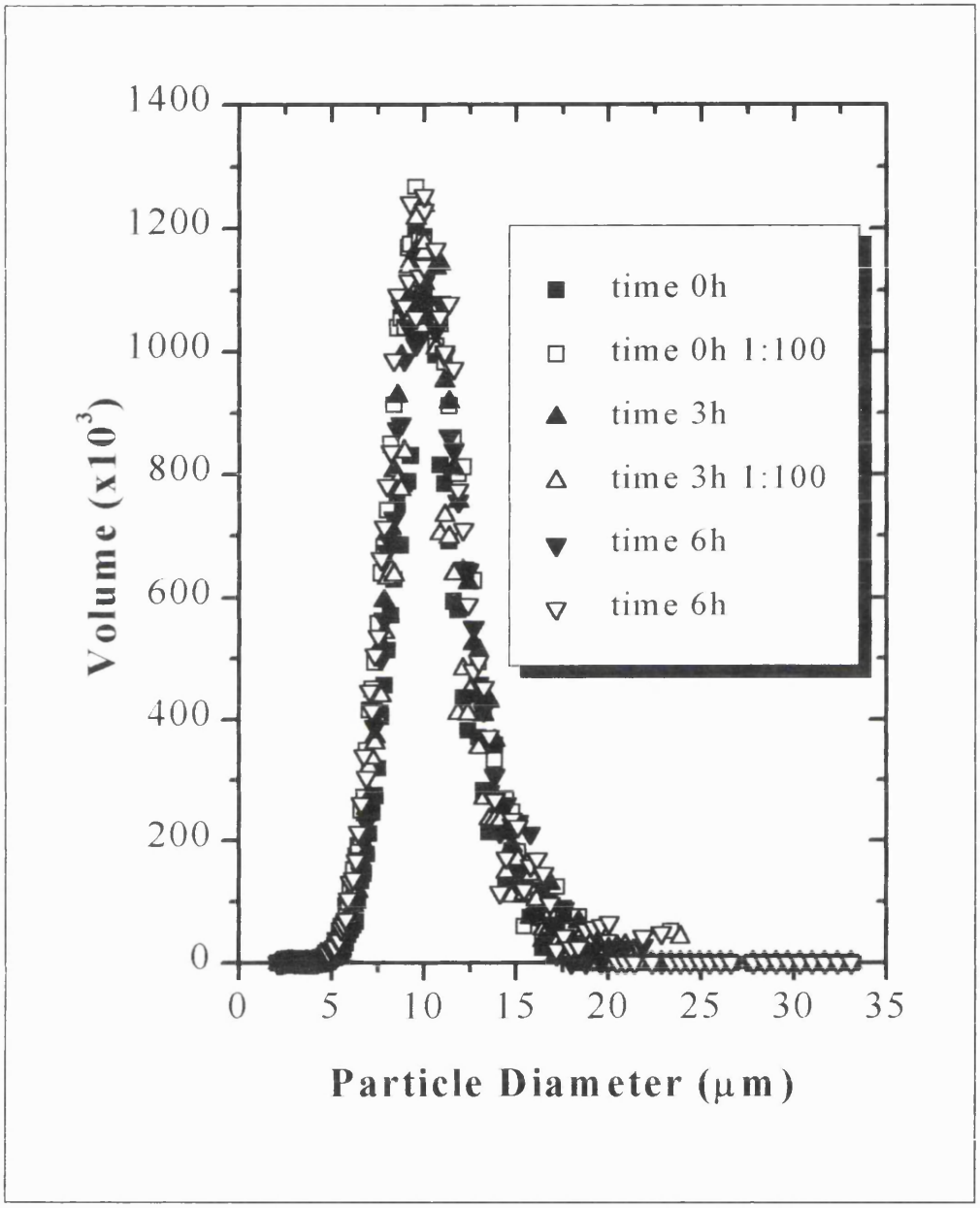

Figure 4.5: Study of particle size distribution in sample with time and as a fraction of distribution prior to analysis. 1:100 indicates 1:100 sample dilution before hold time. Precipitate is 8% v/v PEG 8000 precipitation of clarified yeast homogenate. Sample is based on 1mL of undiluted sample in 50 mL instrument running buffer, count time = 20 s

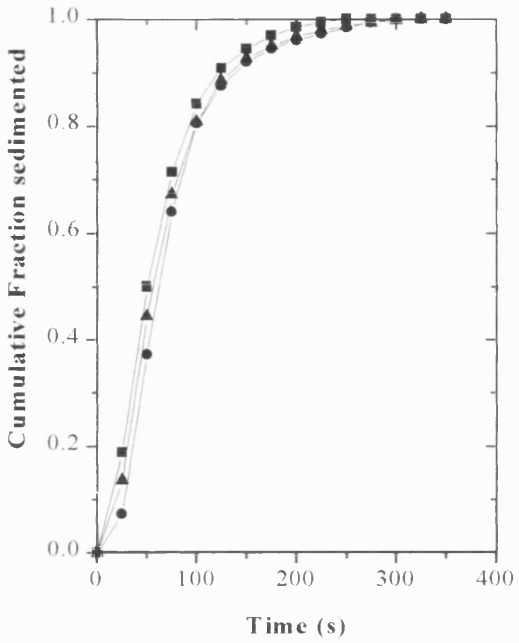

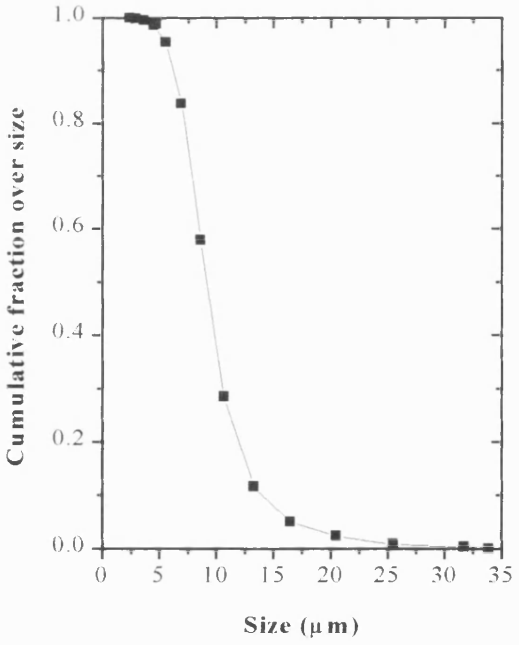

Figure 4.6: Cumulative mass and size (volume basis) distributions for 8% v/v PEG 8000 precipitates of unclarified yeast homogenate. Mass data was obtained by DSC photosedimentometer (Section 4.3.2) and size by Elzone particle sizer (Section 4.3.1). Errors +/-5%

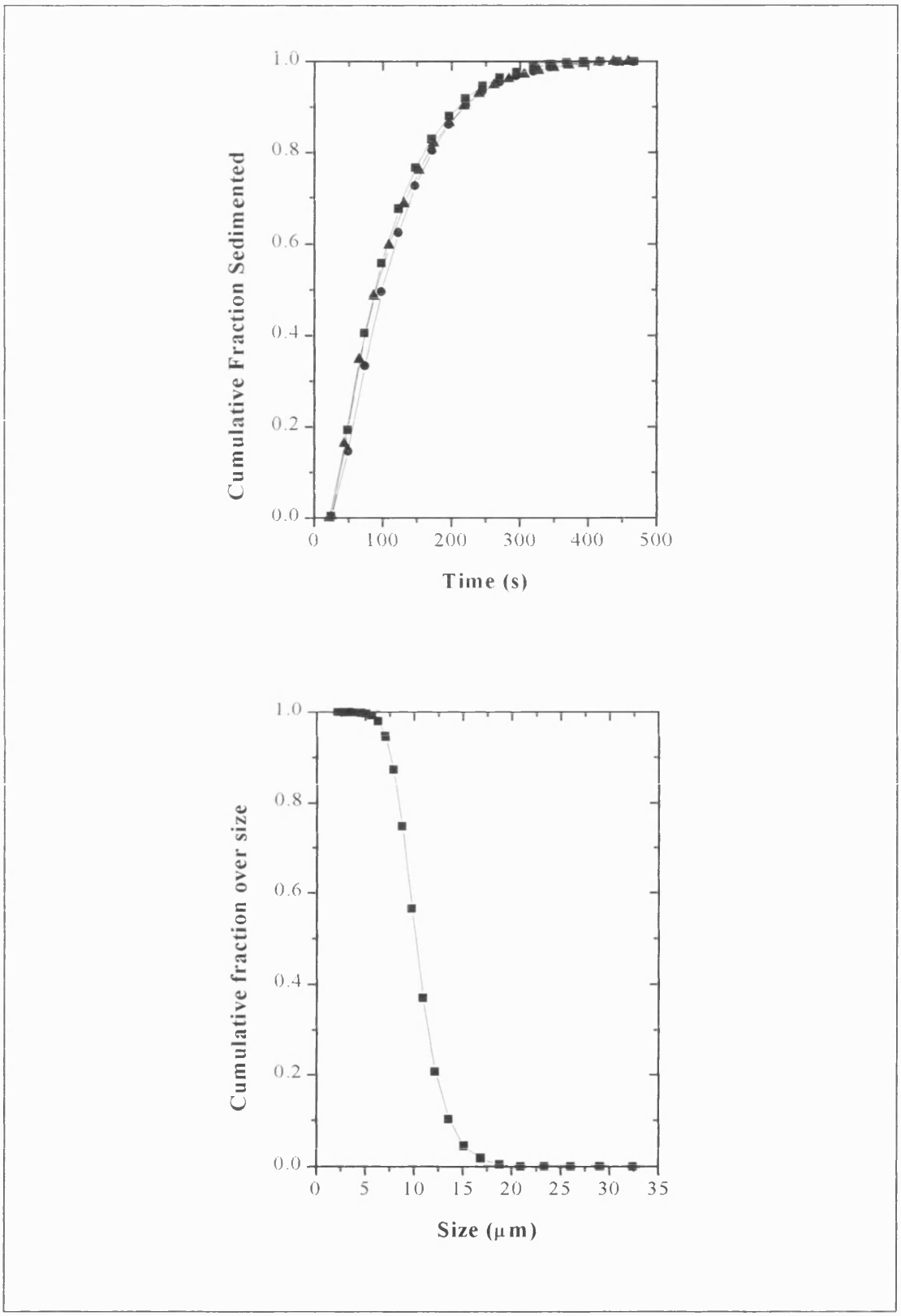

Figure 4.7: Cumulative mass and size (volume basis) distributions for 8% v/v PEG 8000 precipitates of clarified yeast homogenate. Mass data was obtained by DSC photosedimentometer (Section 4.3.2) and size by Elzone particle sizer (Section 4.3.1). Errors +/-5%

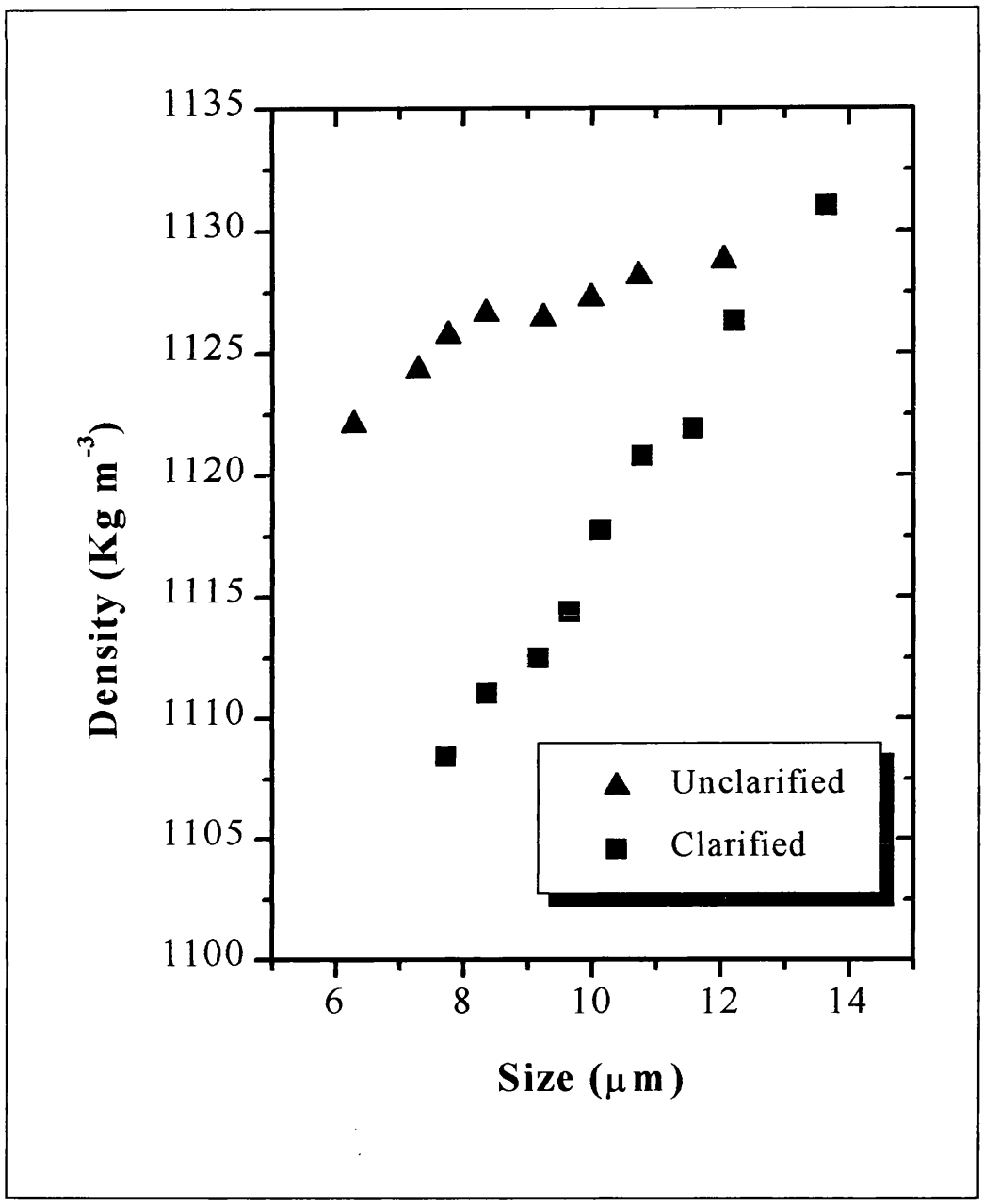

Figure 4.8: Density distribution of 8% PEG 8000 precipitate particles formed from unclarified and clarified yeast homogenate. Density is based on particle size distribution and rate of particle sedimentation.

in the size range 5-15 μm. The pre-clarified system, in contrast, showed an increase in particle density from 1107-1132 Kg m^{-3} over the same size range. All size and mass distribution measurements used to calculate this parameter were conducted in triplicate, and the process repeated with two separate precipitate batches to provide confidence in the reproducibility of the feed stock for the pilot scale centrifugation experiments. The error in any step of the procedure was no greater than 5% and the reproducibility of the density measurements indicated a total error of no greater than this.

A linear regression was used to obtain equations relating density of precipitate particles to size distribution for use with the calculation of the critical particle diameter term in the centrifuge grade efficiency function. These are given as equation 4.40 (clarified system) and 4.41 (unclarified system) below;

$$\rho_p = 1078 + 3.90 * d \qquad \textbf{(4.40)}$$

$$\rho_p = 1117 + 1.06 * d \qquad \textbf{(4.41)}$$

where ρ_p = density of precipitate particle of diameter d (Kg m^{-3})

d = particle diameter (μm)

These relationships differ substantially from the normal Vold model (Clarkson, 1994) due to the presence of debris in the homogenate stream and this will be further addressed in the discussion.

Finally, the viscosity of the precipitate suspensions formed from both clarified and unclarified homogenate was measured. The results are plotted in Figure 4.9 overleaf. The viscosity of both solutions can be seen to be high for a biological system, with the precipitate suspension in the presence of debris having a viscosity of 12 cP, and that of the pre-clarified system 10.5 cP. Both suspensions are Newtonian in behaviour, with constant viscosity. This enabled a value to be used in the calculation of critical particle diameter without the necessity of predicting a shear rate in the centrifuge feed zones.

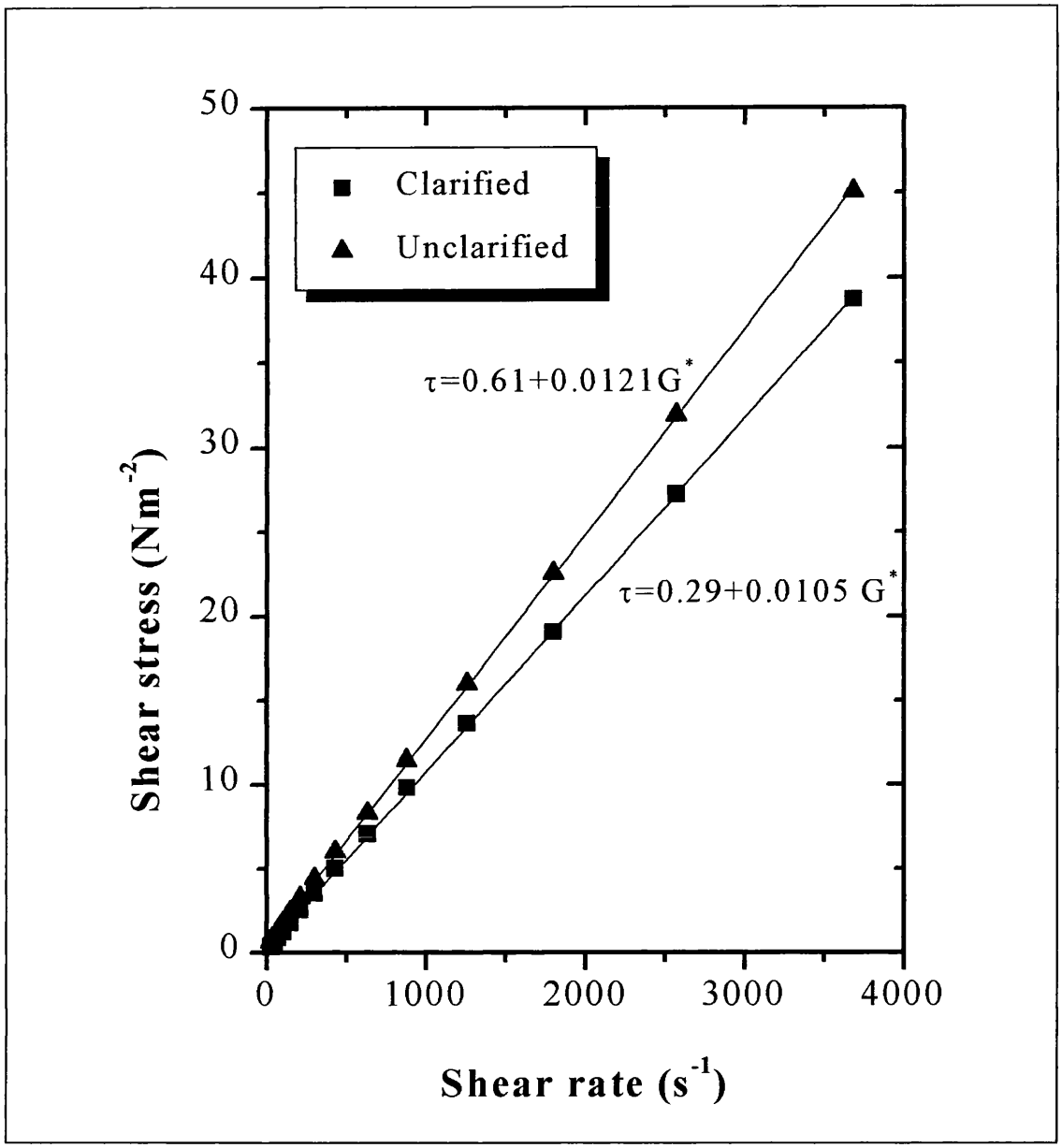

Figure 4.9: Viscosity of 8% v/v PEG 8000 precipitate suspension of clarified and unclarified yeast homogenate. Viscosity measured using cup and bob viscometer, (Contraves Rheomat 115). Equation obtained using linear regression. Errors were calculated as +/- 7%.

Next the physical property results for both the pre-clarified and unclarified systems were examined to enable a decision to be made on a system for use in the pilot centrifugation trials. Both systems yielded sharp particle size distributions, with relatively large peak particle sizes suitable for centrifugal recovery. The unclarified system produced particles of higher density at this peak size (1125 Kg m^{-3} as opposed to 1115 Kg m^{-3}). In contrast the viscosity of the pre-clarified precipitate solution was lower than that of the unclarified system. These factors suggested that the two systems were similar in terms of suitability for centrifugal recovery. However, the solids loading of the unclarified system was obviously higher than that of the pre-clarified; 280 gL^{-1} packed yeast translates to approximately 15% solids on a volume basis. Previous work has shown that a PEG 8000 precipitation of a pre-clarified system under the conditions employed in this work produces 8% solids (v/v). Therefore, the unclarified system in total consisted of approximately 23% solids, in contrast to the pre-clarified where 90% of the solids were removed prior to precipitation, giving a total solids loading after precipitation of approximately 10%. As disk stack centrifuges are considered unsuitable for the processing of streams of more than 10% v/v solids content (Belter, 1982) due to the short length of time to reach solids breakthrough at such high concentrations, it was decided to conduct the pilot scale centrifugation studies on precipitate suspensions produced from yeast homogenate which was clarified prior to the precipitation stage itself.

Figure 4.10-4.12 show the results obtained when clarifying such a precipitate suspension through a CSA-1 pilot scale disk stack centrifuge (Westfalia Separator, Milton Keynes, UK) fitted with both semi-hermetic and hydro-hermetic feed zones, at a range of volumetric throughputs. Figure 4.10 shows the particle size distributions in the supernatant after such clarification. It should be noted that the peaks in the distributions increased both in total volume of particles in the supernatant, and in mean particle size, with an increase in volumetric throughput. This corresponded to a decrease in centrifuge efficiency, as would be expected. Also, the hydro-hermetic equipped machine performed slightly better than the semi-hermetic at a given flow rate; again, as the hydro-hermetic design bowl held more disks, and therefore had a higher equivalent settling area, this was as expected.

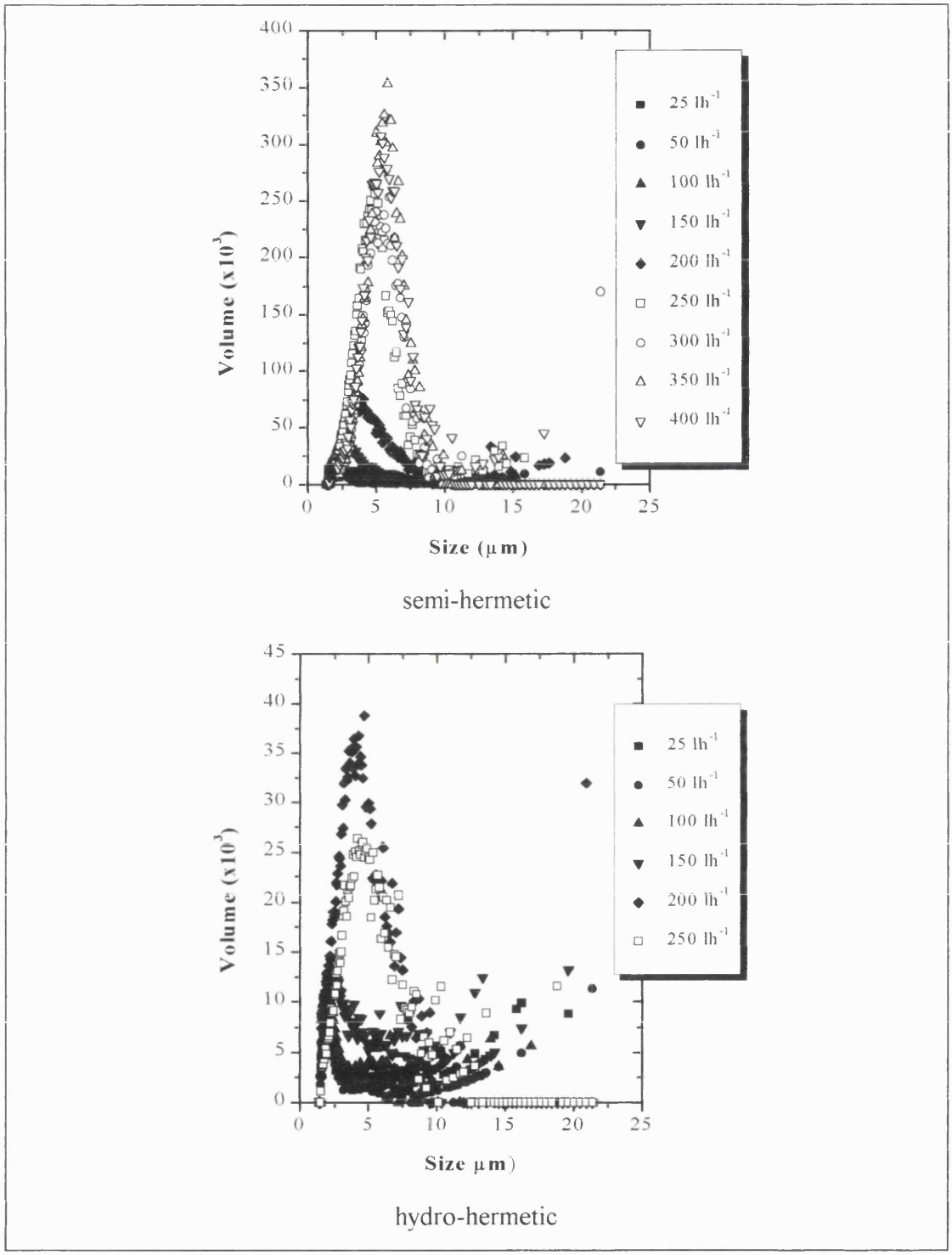

Figure 4.10: Particle size distribution of 8% v/v PEG 8000 precipitate particles of clarified yeast homogenate present in supernatant after recovery in a CSA-1 disk stack centrifuge (Westfalia Separator, UK) fitted with hydro-hermetic and semi-hermetic feed zone processed at a range of throughputs. Count is based on 1mL of undiluted sample in 50 mL instrument running buffer, count time = 20 s

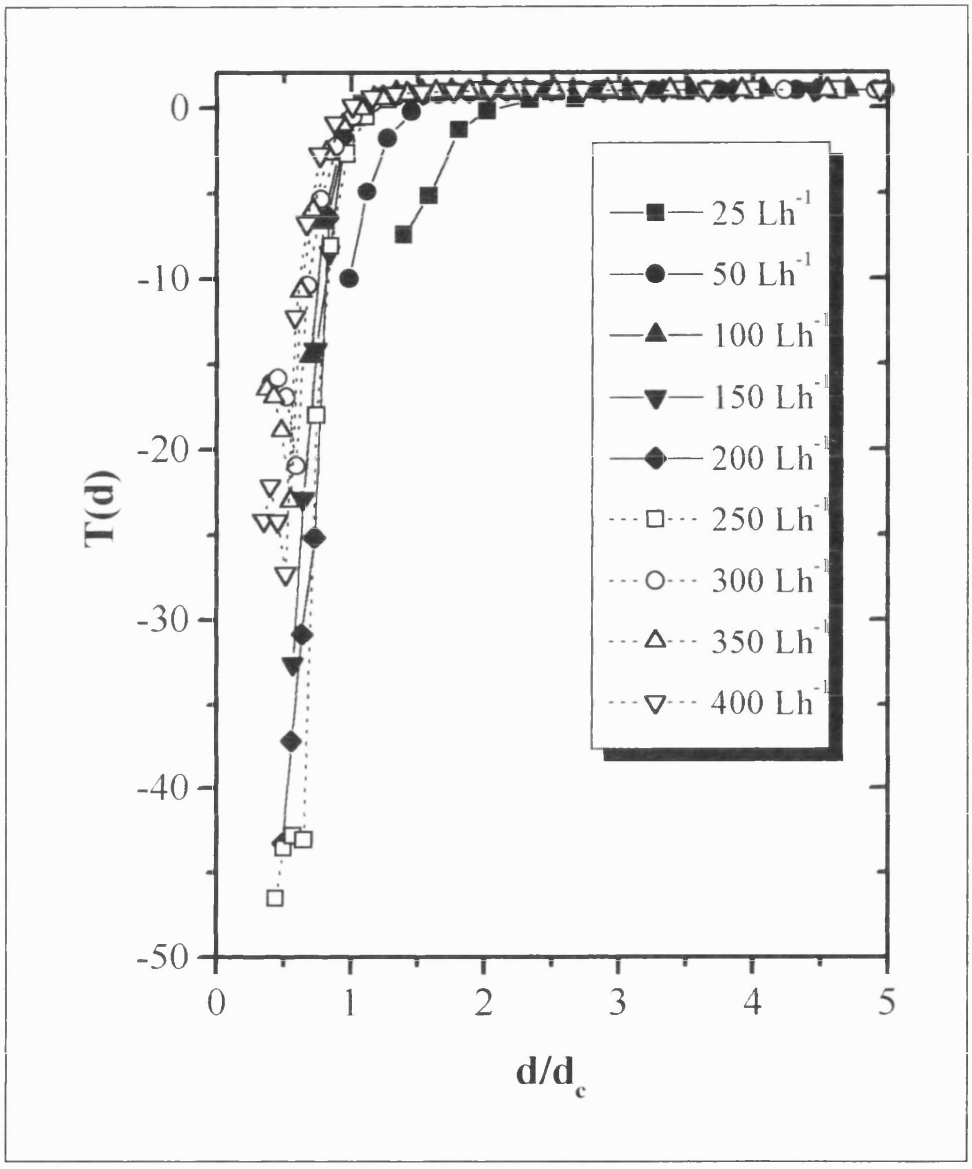

Figure 4.11: Grade Efficiency curve for CSA-1 Disk Stack centrifuge with semi-hermetic feed plotted against normalised diameter. Feed material 8% v/v PEG 8000 precipitate particles formed from clarified yeast homogenate suspension. Centrifuge operated at maximum rotational velocity (9800 rpm), Σ=1456 m^2.

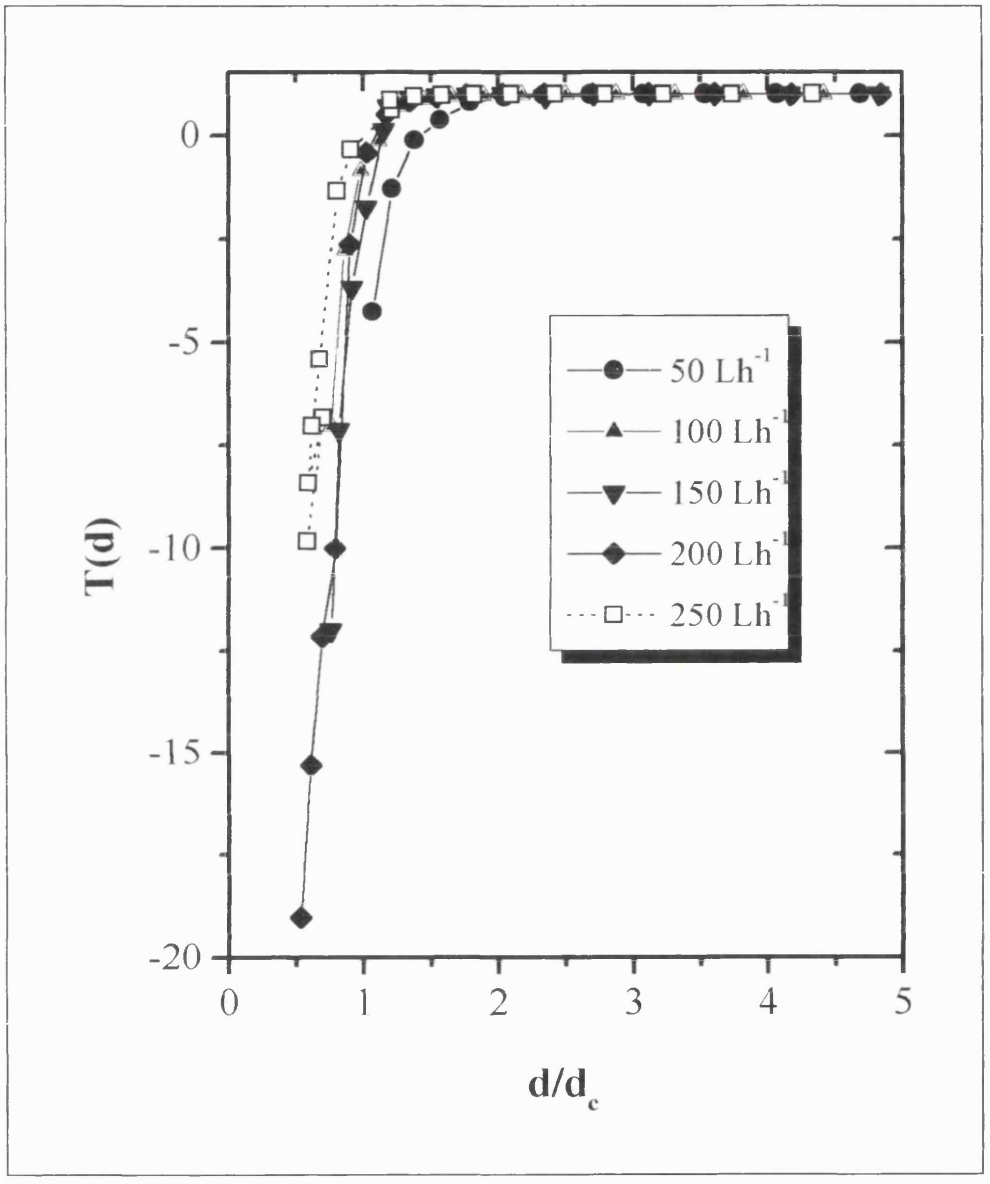

Figure 4.12: Grade Efficiency curve for CSA-1 Disk Stack centrifuge with hydro-hermetic feed plotted against normalised diameter. Feed material 8% v/v PEG 8000 precipitate particles formed from clarified yeast homogenate suspension. Centrifuge operated at maximum rotational velocity (9800 rpm), Σ=1710 m^2.

More interesting was the data expressed as grade efficiency plots against normalised diameter (d/d_c), shown in Figure 4.11 (semi-hermetic) and Figure 4.12 (hydro-hermetic). Considering the semi-hermetic feed zone first, it can be seen that the grade efficiency curve shifted to the left as the throughput increased from 25 Lh^{-1} to 100 Lh^{-1}. Thereafter the function continued to shift slightly to the left with increasing throughput; however this change was very small and probably within experimental scatter. It should also be noted that at low values of d/d_c, corresponding to the measurement of the number of small particles in the supernatant, the function took on a negative value. This became more negative with increasing throughput, it's value approaching -50.

This pattern is repeated in Figure 4.12 which shows the results of the same trial utilising the hydro-hermetic feed zone. Note that although the grade efficiency function still assumed negative values at the lower values of d/d_c, it didn't reach the extremes obtained with the semi-hermetic feed (it approached -20).

Comparisons of the grade efficiency curves attained with semi- and hydro-hermetic feeds are shown in Figure 4.13. The curves are very similar for both hydro-and semi-hermetic feed zones, suggesting a very similar separation performance. It should be noted that the semi-hermetic design produced a shift in grade efficiency to the right at a throughput of 250 L h^{-1} in contrast to the hydro-hermetic, where the function shifted to the left.

Finally the optical density based clarification efficiency with increasing throughput is plotted in Figure 4.14. The hydro-hermetic feed zone gave slightly better clarification at low flow rates than the semi-hermetic (98% as opposed to 95.7% at 50 Lh^{-1}). In both cases there was a sharp drop off in the clarification with throughput as the flow

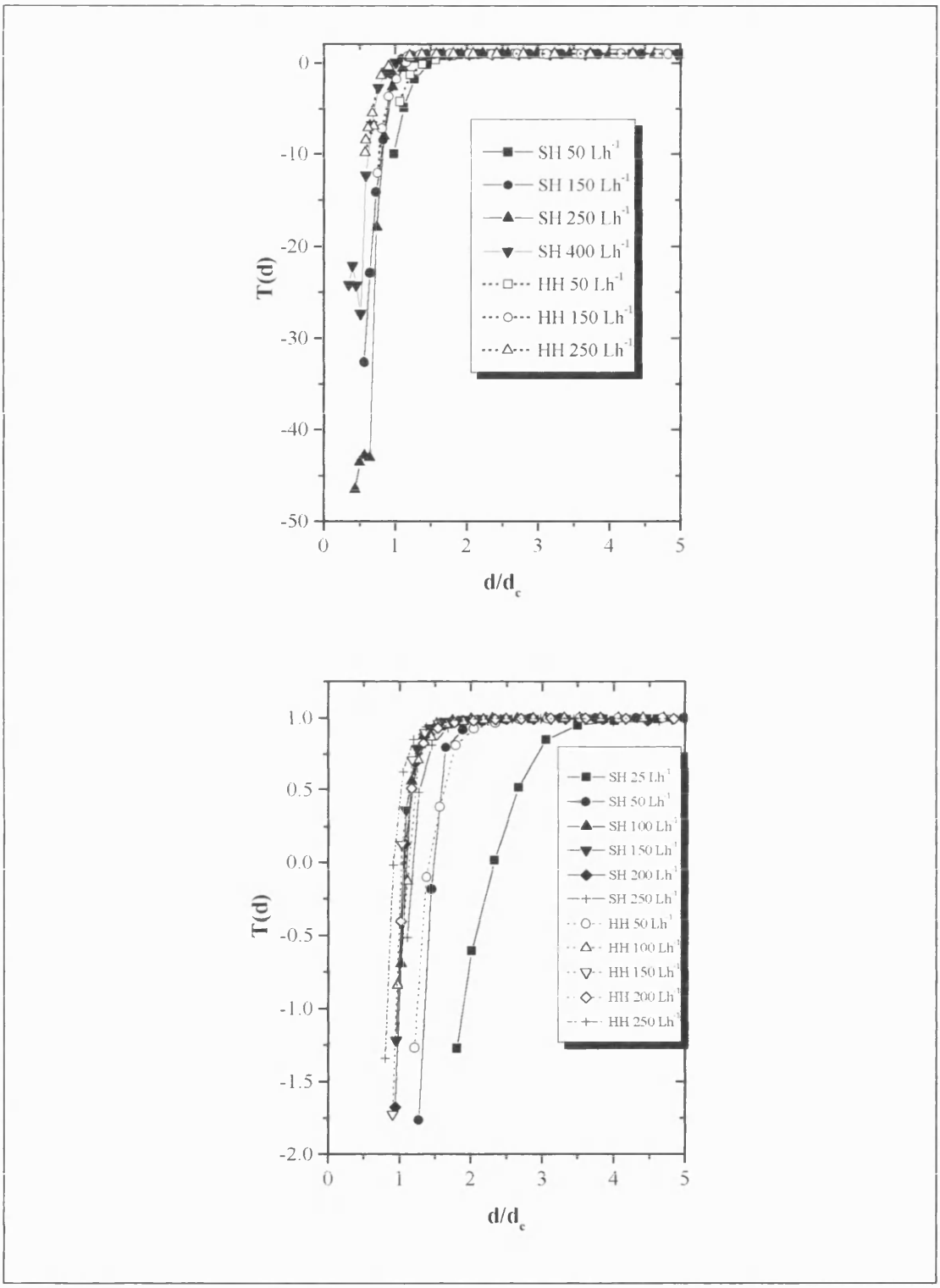

Figure 4.13: Comparison of Grade Efficiency curves plotted against normalised diameter. obtained with both semi- and hydro-hermetic feed zones. Feed material 8% v/v PEG 8000 precipitate particles formed from clarified yeast homogenate suspension. Bottom figure shows blow-up of -2.0<T(d)<1.0. SH=semi-hermetic feed, HH=hydro-hermetic feed.

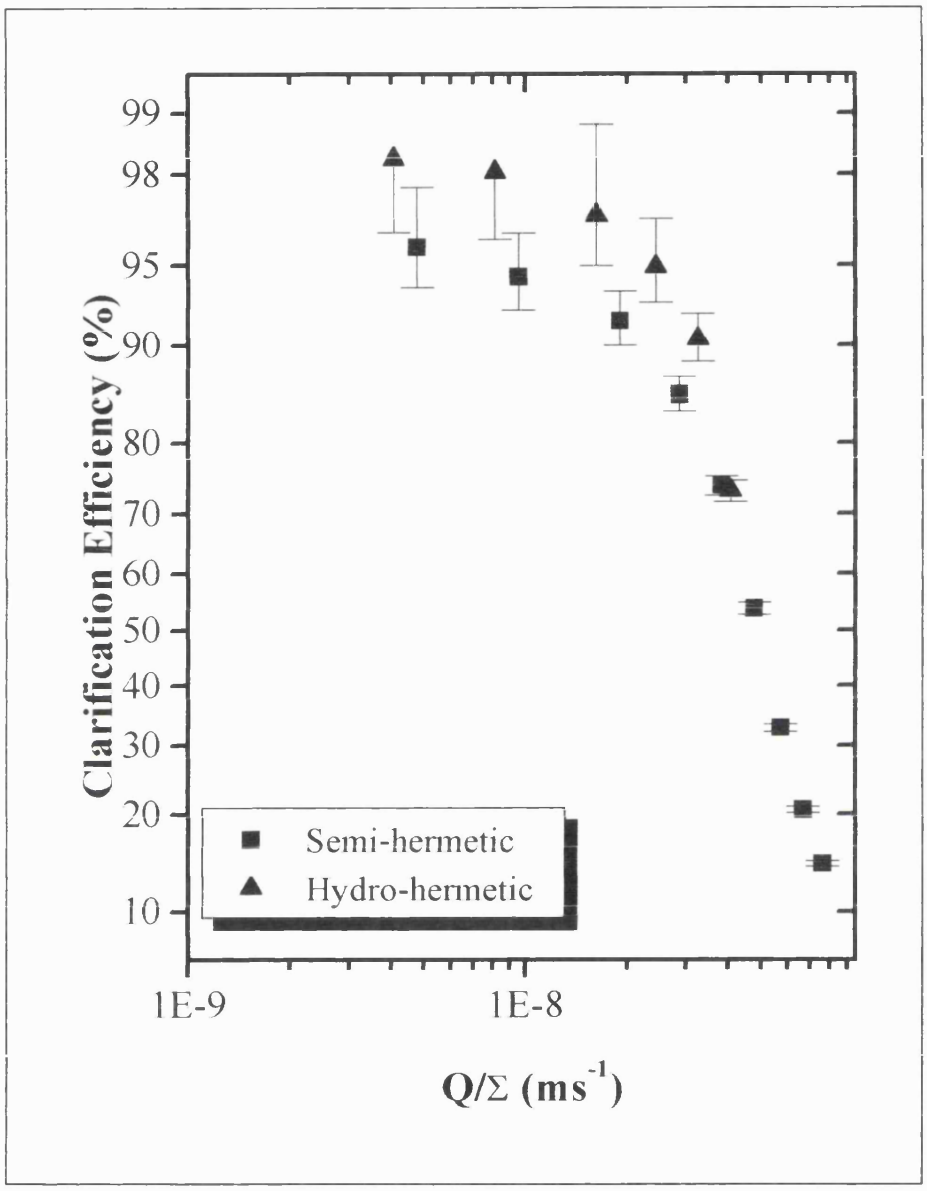

Figure 4.14: Clarification efficiency (optical density basis, absorbance measured at 650 n.m.) against throughput over equivalent settling area obtained processing clarified 8% v/v PEG 8000 precipitates of yeast homogenate through a CSA-1 disk centrifuge fitted with semi-hermetic and hydro-hermetic feed zones.

rate reached 100 Lh^{-1}.

The other effect that was examined was that of altering the rotational velocity of the centrifuge at a constant volumetric throughput of 150 Lh^{-1}. The particle size distributions of the centrifuge supernatants are shown in Figure 4.15. Again, the volume of particles exiting in the supernatant stream increased as the bowl speed decreased with both centrifugal feed zones. This corresponds to the decrease in equivalent settling area produced by the reduction in centrifugal force. Considering the semi-hermetic feed, the increase in peak particle size with the reduction in rotational speed was only small (from 2.0 to 3.5 μm across the range considered), and similarly the increase in solids volume in the peak was relatively modest (from 22,200 to 46,500 relative to the total volume in the sample). The hydro-hermetic feed zone was more sensitive to such changes, with the peak particle size shifting from 1.5 μm to 6.5 μm, and the solids volume from 2400 to 29,700. The hydro-hermetic feed zone also showed a reduction in the peak particle volume in the feed at the lowest rotational speed considered.

When considering the grade efficiency curves in the following figures (4.16-4.17), a more interesting pattern emerges. The semi-hermetic feed zone yielded a slight shift in grade efficiency to the right with decreasing rotational speed. There was, however, a much greater shift between 7070 rpm and 6120 rpm. The hydro-hermetic feed zone displayed a different pattern. There was no shift in curve between 9800 rpm and 8570 rpm. There was then a shift in curve to the right at rotational speeds of 7850 rpm and 7070 rpm, followed by a shift back to the left at a bowl speed of 6120 rpm.

Again, large negative values of the grade efficiency function were obtained. Both centrifuges showed approximately the same maximum negative value of the function, (up to -50). This value generally decreased with rotational speed when processing material through the semi-hermetic feed zone; in contrast, the hydro-hermetic feed showed a relatively constant degree of negativity.

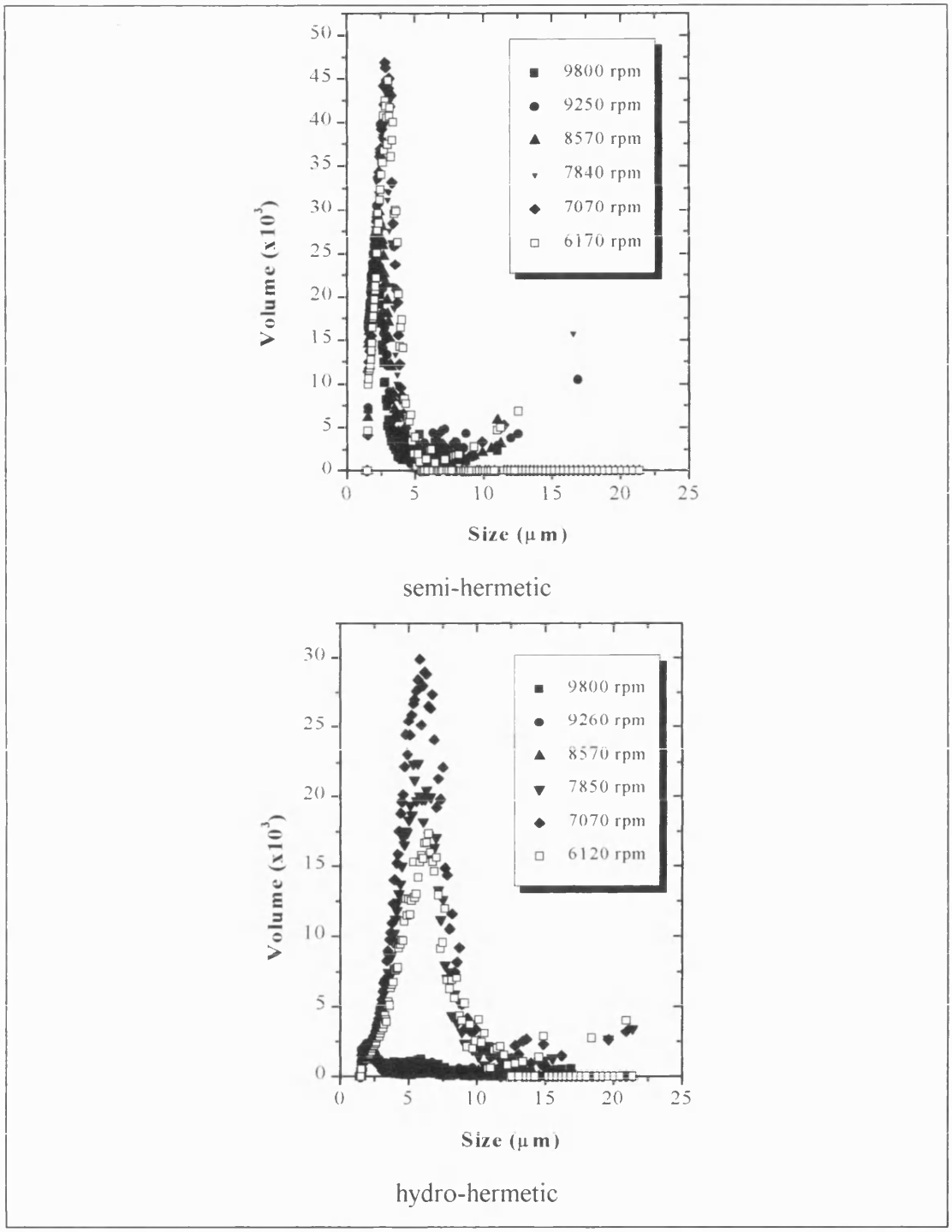

Figure 4.15: Particle size distribution of 8% v/v PEG 8000 precipitate particles of clarified yeast homogenate present in supernatant after recovery in a CSA-1 disk stack centrifuge (Westfalia Separator, UK) fitted with hydro-hermetic or semi-hermetic feed zone processed at a range of bowl rotational speeds. Count is based on 1mL of undiluted sample in 50 mL instrument running buffer, count time = 20 s

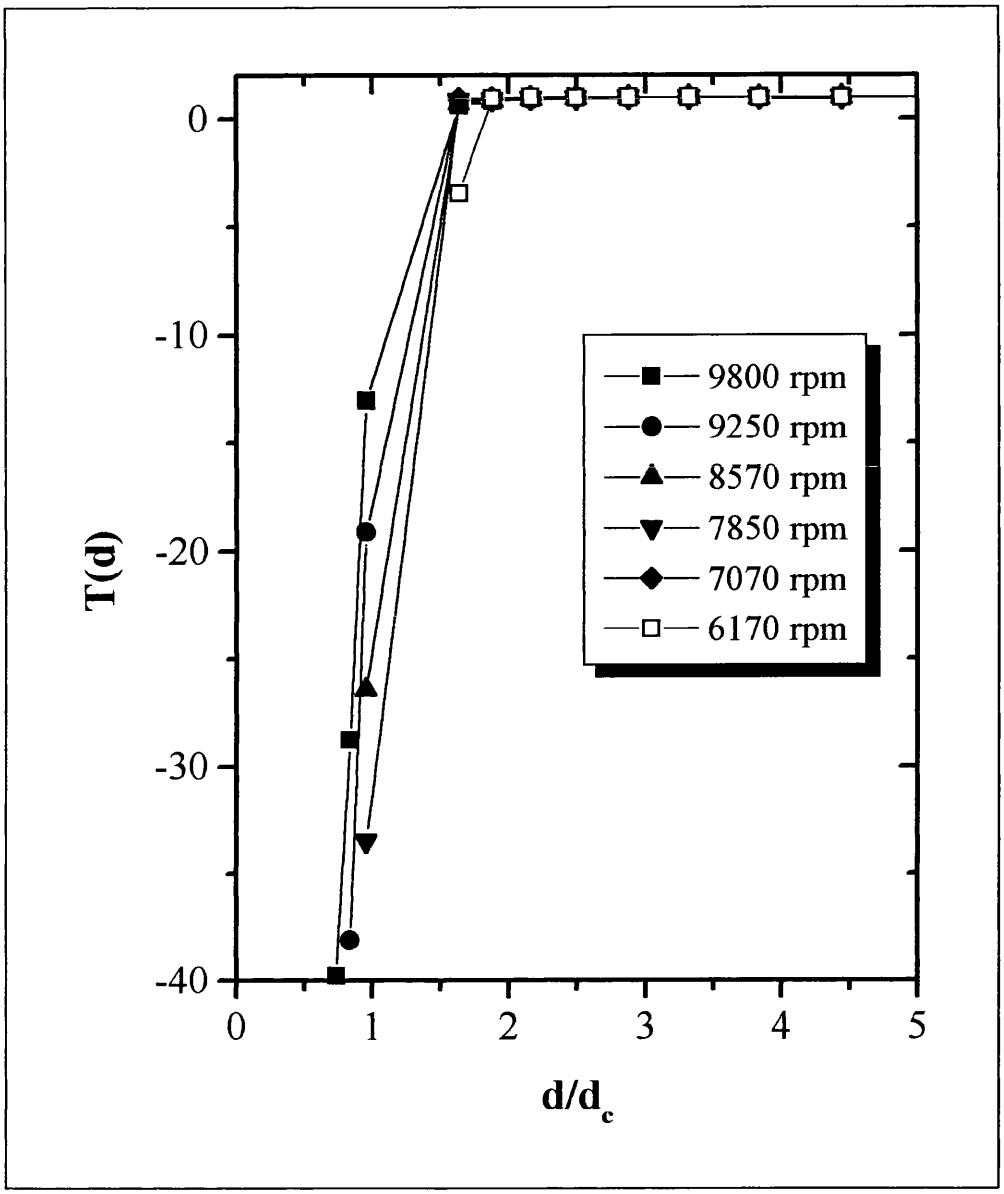

Figure 4.16: Grade Efficiency curve for CSA-1 Disk Stack centrifuge with semi-hermetic feed plotted against normalised diameter. Feed material 8% v/v PEG 8000 precipitate particles formed from clarified yeast homogenate suspension. Centrifuge operated at constant volumetric throughput of 150 Lh^{-1}.

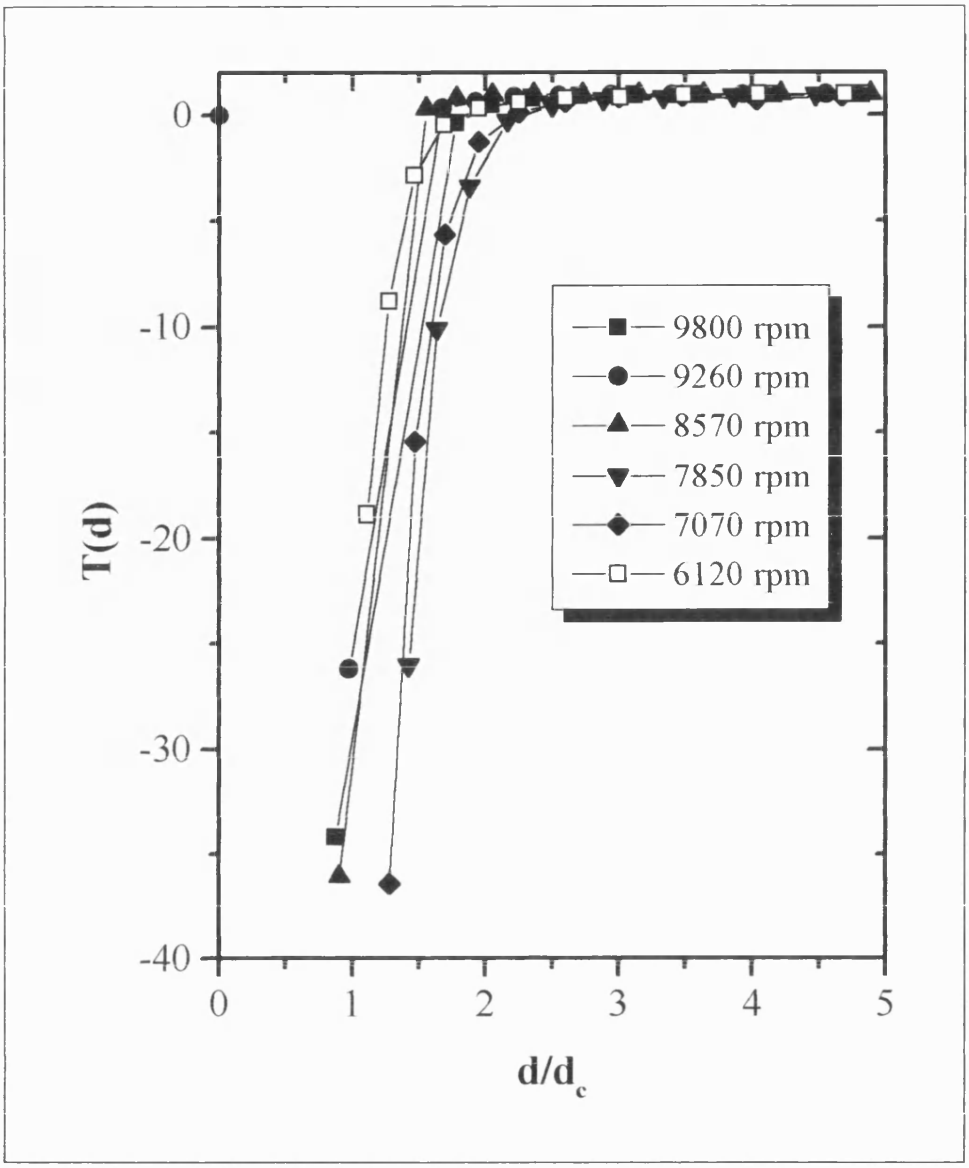

Figure 4.17: Grade Efficiency curve for CSA-1 Disk Stack centrifuge with hydro-hermetic feed plotted against normalised diameter. Feed material 8% v/v PEG 8000 precipitate particles formed from clarified yeast homogenate suspension. Centrifuge operated at constant volumetric throughput of 150 Lh^{-1}.

4.5 Discussion

The results presented in this chapter deal primarily with the processing of 8% v/v PEG 8000 precipitates of yeast homogenate by disk stack centrifuge. However, some data was presented on the characterisation of such precipitate systems and it is this information which will be discussed first.

Generally it can be seen that the polyethylene glycol 8000 precipitation process employed here provides large particles (of the order of 10 μm) with a reasonable density difference between the particle and the surrounding liquid (approximately 60 gL^{-1} in the clarified system used for centrifugation studies). These characteristics make for a relatively easily recovered precipitate, when compared for example to ammonium sulphate induced precipitation of the same system, where mean particle sizes tend to be in the 1-2μm range, with very similar density differences (Clarkson, 1994, and Varga, 1997). However, the nature of the size/density relationship measured is in contrast to that reported for other systems.

Bell and Dunnill, 1982, proposed the following aggregate density-size relationship;

$$\rho_p = \rho_L + Kd^{-n} \qquad \textbf{(4.42)}$$

where K and n are system specific constants. This equation is based on the standard Vold model where aggregate density falls with particle size as the voidage increases. This change in voidage is reflected in n which becomes increasingly negative as the voidage increases. This relationship was derived empirically for iso-electric precipitate aggregates of soya protein with n=-0.441 (Bell & Dunnill, 1982). It has also been applied successfully to ammonium sulphate precipitates of a clean (clarified) yeast homogenate suspension by Clarkson, (1994).

However, the relationship demonstrated for the polyethylene glycol precipitates investigated in this work is quite different;

$$\rho_p = 1078 + 3.90 * d \qquad \textbf{(4.43)}$$

Although it is formulated in a slightly different manner, the obvious implications are that equation 4.42 requires the precipitate aggregate density to reduce in a power relationship proportional to particle size, whereas the relationship observed in this work showed a linear increase in density with size.

This apparent contradiction clearly indicates a difference between the system in use in this work and those investigated by Bell and Clarkson. To understand what this could be one must first examine the reasons given by Bell which produce the reduction in density of particle with an increase in size. This is simply a function of the precipitation process, as outlined in Section 4.1. There are 3 distinct stages to the precipitation process; perikinetic and orthokinetic growth, to form the so called "primary particles", followed by the ageing process during which particle aggregates are formed under hydrodynamic shear conditions within the reactor. Hence, the densest particles are assumed to be the primary particles; aggregates of the primary particles are never as closely packed as the proteins in the primary particles themselves, therefore the larger the aggregates grow, the less dense they become.

One key difference between the system tested here and those of Bell and Clarkson is the presence of debris in the stream used in this work. Both Bell and Clarkson worked with systems which were very clean, containing little solids apart from precipitated protein. In the system presented here the debris clarification step removed only 80-90% of the solids, which will consist of both undisrupted whole cells and cell debris material. Figure 4.8 clearly shows that the precipitation carried out in the presence of all the debris from the homogenisation step formed denser particles than that carried out on a 80-90% clarified one. However, the increase in density with size in the unclarified system was much less steep than that of the clarified system, and indeed at the top of the size range reviewed, (approaching 14μm), the two systems converged. The implication of this is that precipitate aggregates which contained cell debris were inherently more dense than those containing none, with the larger aggregates in the

clarified system being those that did, in fact, contain debris. This in turn leads to the presumption of several species of primary particle; purely protein, purely debris, and a combination of the two. Similarly, each aggregate particle will then be made up of a varying number of variable density primary particles. Such a system could easily produce the results demonstrated.

Another consideration is also that of the precise mechanism of particle formation; it has been reported that in the case of both ionic polyelectrolyte precipitation and precipitation by non-ionic polymers such as PEG 8000 the process of flocculation is likely to play a role in addition to that already detailed in Section 4.2. Flocculation in turn involves two mechanisms, that of charge neutralisation similar to salting out, and bridging between particles by the flocculating agent (Bell *at al*, 1983).

Overall, with such a complex system containing both insoluble cellular components, and a wide range of soluble proteins, with the possibility of two fundamental mechanisms playing a part in the production of aggregates, it is perhaps not surprising that the density-size distributions obtained do not match those demonstrated for more defined systems. The system under investigation consists of true precipitate particles, cell debris and whole cells and thus the relationship derived is really a density versus size distribution for a heterogenous distribution of populations. Further work investigating the effect of changing precipitation conditions, and the level of debris, is needed to establish the precise mechanisms of aggregate formation in this case.

Turning to the pilot scale centrifugation trials, it is analysis of the grade efficiency curves which gives insight into the degree of particle breakage in the centrifuge feed zone. Because the grade efficiency function, T(d) is plotted against the dimensionless particle diameter d/d_c the T(d) curve should not shift with varying volumetric throughputs or bowl rotational speeds since these will alter the value of d_c to compensate for increased or reduced separation efficiency. The only way the curve can shift is if (a) the flow pattern through the separating area of the centrifuge alters radically under certain conditions, increasing or decreasing the deviation from Stokes Law, or (b) the centrifuge interacts to alter the physical properties of the feed suspension before separation. It is this latter effect, specifically the reduction of particle

size by disruption in the feed zone, that is generally considered to be by far the most important (Mannweiler, 1990, and Clarkson, 1994) as changes in the flow pattern are unlikely given the range of Reynolds numbers the centrifuge operates under. Disruption to the particles in the feed is generally considered to result in a shift of the grade efficiency curve to the left. This would appear to indicate an increase in the performance in the centrifuge i.e. 100% recovery of particles of a given size (T(d) = 1) is attained at a smaller value of d/d_c. In fact what is happening is the larger particles in the feed are being broken up. Thus even though 100% of them would not be recovered at a given volumetric throughput or bowl rotational speed, there are none present in the supernatant to effect the grade efficiency function as they have all been broken into smaller particles in the feed zone. This then leads to the large negative values seen at low values of d/d_c . This is indicative of the presence of a greater number of particles of a given size being present in the supernatant than were detected in the feed suspension. In this study such particles were created by the destruction of larger aggregates.

A perfect Stokes Law separator would obviously have a grade efficiency curve which reached a value of unity at $d=d_c$. However, because of the non-idealities of flow through a disk stack centrifuge discussed in Chapter 3, in practice T(d) only approaches unity when $d/d_c>2.5$ (Mannweiler, 1990). Figure 4.11 shows the variation of grade efficiency curve with volumetric throughput for the semi-hermetic feed zone design where the grade efficiency curve shifts dramatically to the left at throughputs between 25 Lh^{-1}, (the lowest tested), and 100 Lh^{-1}, which would indicate an increase in the level of breakage. Thereafter the curve continues to shift as the flow rate increases, but only by a small amount, indicating that the breakage in the feed zone is relatively insensitive to throughput in this range. Similarly the degree of negativity of T(d) at low values of d/d_c increased with increasing throughput, corresponding to the production of small particles through feed zone disruption which were not recovered in the centrifuge. There appears to be no reduction in disruption, as seen with the whole cells (Chapter 3), at a throughput of 150 Lh^{-1}, corresponding to the flow rate at which flooding over of the lock-nut occurs. There is however, a decrease in the degree of negativity of the grade efficiency function at throughputs of approximately 200 Lh^{-1}, indicating a reduction in the number of small fines in the supernatant. Because the

aggregate debris which is represented by particles of low d/d_c value does not account for a significant volume of the total mass processed, and because the overall grade efficiency is still indicating an increase in break-up, this cannot be said to represent a fall in disruption. However, it is indicative that the size of the smallest particles detectable in the supernatant increases at these higher throughputs. This would indicate that although the feed zone is breaking down a greater proportion of the particles to un-recoverable sizes, the degree of disruption is smaller than at the lower throughputs examined.

The centrifuge equipped with a hydro-hermetic feed zone (Figure 4.12), exhibited a similar pattern, with evidence of particle break-up in the feed zone increasing substantially with flow rate from 50 Lh^{-1} to 100 Lh^{-1}. Thereafter, as in the case of the semi-hermetic feed zone, breakage increased only slightly with throughput. However, a large shift in grade efficiency to the left was observed at a throughput of 250 Lh^{-1}. This flow rate is very close to the maximum achievable before flooding of the feed zone occurs. At such a flow rate then the rib body present at the top of the feed zone will be in contact with the feed suspension. The shift in grade efficiency indicates that with this material, unlike the whole cell results discussed in the previous chapter, an increase in particle break-up through impact with the rib body rotating at high speed occurs.

The comparison of the grade efficiency functions obtained with either feed zone shows that at most throughputs examined an equivalent degree of disruption occurred producing very similar grade efficiency curves. This was contrary to expectations based on the whole cell work set out in Chapter 3, which clearly showed the hydro-hermetic feed zone breaking less material than the semi-hermetic. Similarly, none of the shifts in disruption as a function of flow rate obtained with the semi-hermetic feed zone when processing whole cells were detectable when processing the PEG protein aggregates. However, it must be remembered that although the hydro-hermetic feed zone is predicted to be a much less harsh environment than the semi-hermetic, every material will have a yield stress above which it will suffer disruption, and below which it will remain intact. The results would suggest that the aggregates formed during the precipitation process are sufficiently weak that neither feed zone is "soft" enough to allow the aggregates to survive intact. Similarly, it was suggested by Dunnill and Bell

(1982) that final particle size when investigating shear disruption of precipitate aggregates is only a very weak function of shear rate which in turn implied that the aggregates tended to either break to primary particles or not break at all, with few intermediate stages of disruption. This is reflected in the relative insensitivity of the grade efficiency curves presented here to volumetric throughput.

The major difference between the two sets of curves is the degree of negativity displayed by the grade efficiency curves at low values of d/d_c. It can be seen that the hydro-hermetic does not produce as many very fine particles at all flow rates as the semi-hermetic design. Because these particles have very little volume, this does not affect the overall position of the grade efficiency curves but clearly indicates breakage to somewhat larger particles than those exiting the feed zone of the semi-hermetic centrifuge (see figure 4.18 overleaf). It is this that gives rise to the differing clarification efficiencies observed at low flow rates in Figure 4.14. The grade efficiency curves indicate that the machines performed in an almost exactly similar manner, and yet the hydro-hermetic centrifuge yielded a slightly higher clarification efficiency based on optical density than the semi-hermetic centrifuge. This may be attributed to the phenomenon of light scattering by small particles which increases the optical density of a sample i.e. a given volume of small particles will have a higher absorbance than the same solids volume of large particles. This effect is particularly pronounced in spectrophotometers measuring very small particles. Note the clarification efficiencies of the two feed zones become very similar at 250 Lh^{-1}, a throughput where the grade efficiencies indicate the hydro-hermetic feed zone was causing more particle break-up than the semi-hermetic, but the semi-hermetic was producing more very fine particles. At this point the two effects appear to cancel each other out.

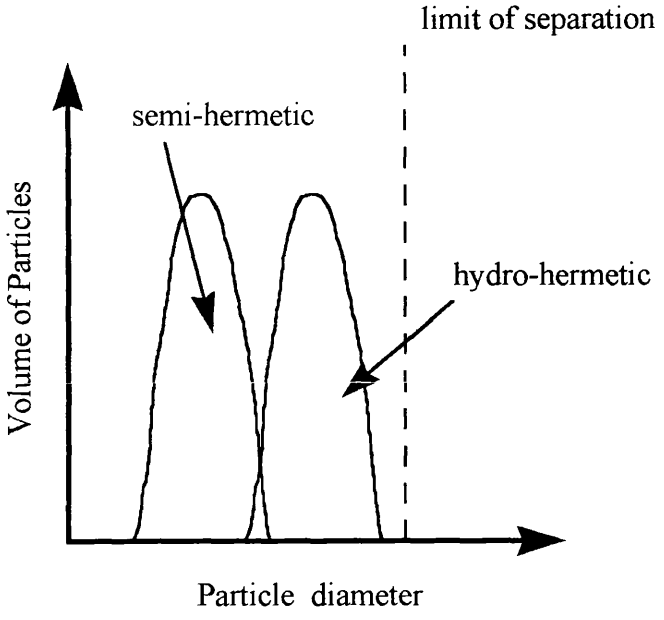

Figure 4.18: Idealised Illustration of particle size distribution present after passage through both semi- and hydro-hermetic feed zones.

The indication that feed zone break-up increases generally with flow rate fits well with similar investigations conducted by Clarkson (1994) and Mannweiler (1990) who both observed a similar trend. However, Mannweiler observed a difference in the mass yield obtained with a semi-hermetic and a hydro-hermetic feed zone, with the hydro-hermetic equipped machine performing approximately 10% better than the semi-hermetic design. These trials were conducted using an iso-electric precipitation technique on soya protein. Again when strength is so critical a different feed material is likely to yield different results.

Turning to the effect of bowl rotational speed, Figure 4.16 shows a slight decrease in disruption with bowl speed from 9800 rpm to 7070 rpm when utilising the semi-hermetic feed zone. This was as expected from the results obtained in Chapter 3. There was, however, a substantial reduction in particle break-up in going from 7070 rpm to 6170 rpm. This would suggest that this final bowl speed reduction altered the disruptive forces developed in the bowl sufficiently to have an observable effect on the material entering the separation area.

The hydro-hermetic feed zone bowl displayed similar behaviour with several notable exceptions. There was no apparent reduction in particle break-up from 9800 rpm to 8570 rpm. Then, however, there was a large reduction in disruption at 7850 and 7070 rpm, followed by an increase to the lowest rotational speed of 6120 rpm. Again, these results are indicative of the nature of the material being processed, in that the bowl speed reduction initially produced little change, but below a certain rotational speed the shear forces present dropped sufficiently to reduce significantly the particle break-up. The increase in disruption at a bowl speed of 6120 rpm is almost certainly due to interaction with the rib-body at the top of the feed zone. A reduction in rotational speed reduces the centrifugal force which is a factor in determining the flow rate out of the distributor and onto the disks. The feed zone will therefore become flooded to a greater depth at a lower rotational speed when operated at constant throughput in the same manner as was observed in the throughput studies.

Turning to the comparison of the two feed zones (Figure 4.18) it can be seen that, in contrast to operation at full rotational speed, the hydro-hermetic feed zone causes less break-up than the semi-hermetic at lower rotational speeds. This again was probably due to the specific strength characteristics of the material; it has already been shown in Chapter 3 that the hydro-hermetic centrifuge produces a lower disruptive force than the semi-hermetic. Because of the alterations to the feed zone which have produced the increase in flooding depth, the volume in the feed zone will be higher at any given flow rate or rotational speed than that in the semi-hermetic, corresponding to lower shear rates based on a power per unit volume approach (see Chapter 3). As a reduction in bowl rotational speed will significantly decrease the shear rates in the feed, it seems likely that those generated in the hydro-hermetic at full rotational speed are just sufficient to cause a large amount of disruption to the precipitate aggregates. Therefore, any reduction in bowl speed reduces the shear forces sufficiently that a change in the amount of break-up can be detected. In contrast the semi-hermetic feed zone is estimated to produce much higher shear forces when operating under the same conditions, and therefore a much greater reduction in rotational speed is necessary to bring about a measurable reduction in feed zone associated particle break-up (see Chapter 5). This argument is supported by the much bigger shift in grade efficiency curve observed with the hydro-hermetic feed zone than with the semi-hermetic. The

degree of flooding in the semi-hermetic feed zone is less than that in the hydro-hermetic until the point where flooding out of the feed zone is about to occur. This point will be reached at lower volumetric throughputs when operating at a lower speed of revolution. However, this condition was not investigated in this trial.

The major difficulty in interpreting these results is the difficulty in working back to the post-feed zone particle size distribution. Such knowledge would provide an accurate picture of the interaction of the feed zone with the protein aggregates under different conditions, though this is greatly complicated by the need also to consider recovery. With such an ability the performance of the feed zones could be accurately compared, as in Chapter 3.

Several researchers have attempted to do just this, most notably Mannweiler (1990), and Clarkson (1994). The most obvious method is to re-arrange the grade efficiency equation (equation 4.32) to predict the sheared feed distribution from the theoretical grade efficiency, the observed supernatant PSD and the mass yield. However, this approach has never proved successful because of the sensitivity of the equation to small errors in measurement of the supernatant PSD. For values of d where T(d) approaches unity the predicted sheared feed PSD will become very high if the supernatant contains more particles than theoretically possible as is the case when disruption has taken place. Therefore, a different iterative approach was taken, whereby it was assumed that the geometric standard deviation of a log-normal PSD would not alter during breakage in the feed zone; therefore, knowing the theoretical recovery characteristics of the centrifuge the transformation of the mean particle size between the feed and sheared feed PSD's could be calculated in terms of a system specific breakage constant, assuming the shape of the curve would not alter. This approach proved effective when predicting the recovery of ammonium sulphate precipitates using a disk stack centrifuge (Clarkson, 1994).

When considering the differing effects of feed zone design and operational conditions, however, such an approach is self-defeating. Assuming that the form of the feed PSD does not alter means that the effects of multiple disruption mechanisms, such as are believed to exist within centrifuge feed zones, are likely to be hidden. Furthermore, the

calculation of breakage constants in this manner from theoretical grade efficiency curves will only express the degree of particle break-up under different conditions in an alternative form to that already considered. Therefore, a different approach will be taken. Chapter 5 contains the theoretical estimations of the shear rates developed by the different feed zones under differing conditions, as well as the results of exposing a feed suspension to such shear rates in several different laboratory scale mimics. By utilising such particle size distributions as the simulated feed PSD to the centrifuge a grade efficiency curve closer to that theoretically predicted should be obtained. This technique can thus be used to establish a degree of confidence in the shear rate predictions and the lab scale mimics. Such work is presented as part of Chapter 5, and a summary of these results together with those obtained with whole cells is contained in Chapter 6.

4.6 Conclusions

Polyethylene glycol precipitation of yeast homogenate forms a suspension of particles that are relatively easy to recover centrifugally, being of moderate size with an acceptable density difference between aggregates and surrounding fluid (6%). However, they are very susceptible to aggregate break-up by the disruptive forces developed in the feed zone of a disk stack centrifuge. Such disruption increases with both volumetric throughput and rotational velocity. Both the semi-hermetic (standard) feed zone and the hydro-hermetic (soft) feed zone produce similar degrees of disruption across the throughput range investigated at full bowl rotational speed. However, as the rotational speed was reduced the hydro-hermetic feed zone generally out-performed the semi-hermetic, causing less particle breakage. This is believed to be due to the strength characteristics of the precipitate suspension. At full speed the majority of particles undergo considerable disruption at the shear rates apparent in either centrifuge. However, as the rotational speeds of the centrifuge bowls were decreased the shear rate in the hydro-hermetic bowl reduced sufficiently to drop below that required to disrupt all the particles. In contrast the semi-hermetic bowl produces a

sufficiently high shear rate to disrupt the majority of particles at all rotational speeds other than the lowest.

Finally, at high flow rates and low rotational speeds disruption in the hydro-hermetic bowl increased dramatically. This was believed to be due to interaction with the rotating rib-body at the top of the feed zone, inflicting increased levels of particle break-up through an impact-based mechanism.

Further discussion of these results can be found in Chapters 5 & 6 where an estimation of shear rates found in the centrifuge feed zones is made.

5.0 SHEAR RATE CALCULATIONS AND LABORATORY SCALE MIMICS.

5.1 Introduction

Chapters 3 and 4 of this thesis have detailed the hydro-hermetic and semi-hermetic feed zone disk stack centrifuges used to assess the break-up of biological solids during centrifugal recovery as well as the disruption measured under various processing conditions when handling both whole cells and polyethylene glycol precipitates of yeast homogenate. Chief amongst the theoretical disruptive mechanisms occurring within the machine are the effects of shear in the feed zone, and this is generally considered to be the most important factor (Mannweiler, 1990 and Clarkson, 1994). The final stage of the work described in this thesis was therefore to examine in greater detail the shear rates generated in a centrifugal feed zone, and to identify and test appropriate laboratory scale mimics of such shear forces. This chapter contains details of this work. Section 5.2 contains a review of previous approaches to calculating the disruptive forces generated within a disk stack centrifuge feed zone, as well as the development and application of such models to the system under test. Section 5.3 describes the materials and methods used with the laboratory scale mimics, as well as detailing the test rigs themselves. Section 5.4 presents the results obtained at laboratory scale, and section 5.5 a general discussion of these findings.

5.2 Disruptive Forces in the Feed Zone of a Disk Stack Centrifuge

A review of the physical characteristics of the disk stack centrifuge feed zone thought to cause disruption has already been presented in Chapter 3. In order to understand further these effects it is, however, necessary to estimate the magnitude of these forces and several authors have previously attempted this. Chief amongst these are Mannweiler (1990) and Bell (1982).

Two basic approaches may be used. The overall power dissipation in the feed zone can be estimated and related to shear force and stress, or models of specific parts of the feed zone (such as the lock-nut or the distributor ribs) can be considered.

5.2.1 Power Dissipation

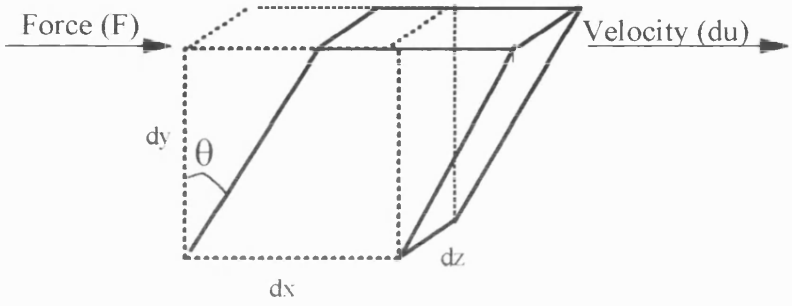

Figure 5.1: Force acting on an element of fluid.

If a force F acts on the top surface of an element of fluid dydxdz then it will cause a rotation θ over time dt (see Figure 5.1). This can be represented as follows:

Torque applied to element (T_M) = Force x distance = Fdy **(5.1)**

Shear Stress (τ) = Force/area = $\frac{F}{dxdz}$ **(5.2)**

Torque applied = $\tau dxdydz$ **(5.3)**

Power Input (P) = Torque x rate of rotation

= Torque x $\frac{d\theta}{dt}$

= Torque x $\frac{du}{dz}$

= $\tau dxdydz\frac{du}{dz}$ **(5.4)**

Shear Rate (G) = velocity gradient = $\frac{du}{dz}$ **(5.5)**

For a Newtonian fluid $\tau = \mu G$ **(5.6)**

Therefore combining equations 5.4-5.6 and simplifying;

$$G = \left(\frac{P}{V\mu}\right)^{\frac{1}{2}} \qquad \textbf{(5.7)}$$

and

$$\tau = \left(\frac{P\mu}{V}\right)^{\frac{1}{2}} \qquad \textbf{(5.8)}$$

where G = shear rate (s^{-1})

P = power (W)

μ = dynamic viscosity (N s m^{-2})

τ = shear stress (N m^{-2})

V = volume (m^3)

Equations 5.7 and 5.8 can therefore be used to relate the power dissipated in the feed zone of a centrifuge to both the shear stress and shear rate generated as long as the viscosity of the suspension is known. This is a very common technique and has been applied to estimating shear forces in a variety of unit operations from homogenisation to stirred tank reactors.

The next stage, therefore, is to estimate the power dissipated in the feed zone of the centrifuge.

For a centrifugal pump the power input required to generate a given pressure head is given by;

$$P = Q\Delta p \qquad \textbf{(5.9)}$$

where Q = volumetric flow rate (m^3 s^{-1})

Δp = change in pressure (N m^{-2})

Mannweiler (1990) used this approach to calculate the shear rates in an hermetic disk stack centrifuge. Because this design is fully flooded it was possible to measure the pressure at both the inlet and the outlet without altering flow through the machine. He assumed that the total pressure drop was the sum of that across the feed zone and the disks, and used the expression derived by Carlsson (1986) to calculate that for the disks. This yielded a specific power dissipation of 15 kW/m^3 and a shear rate of $2x10^3$ s^{-1}. However, this approach was not readily applicable to either a hydro-hermetic or a semi- hermetic design machine since these are not fully flooded making pressure drop measurements impossible to obtain. Therefore Mannweiler applied a more theoretical analysis to the problem by deriving a momentum balance across the centrifuge. He assumed that fluid entered the centrifuge with no momentum or kinetic energy and left at an "effective discharge radius" with the momentum and energy derived from the rotational speed of the bowl at that radius. Again when considering the hermetic centrifuge it was possible to measure the effective discharge radius and a specific power dissipation of 15 kW/m^3 was calculated.

This approach still contains some fundamental difficulties. Firstly the energy balance is still for the whole bowl, not the feed zone This introduces inaccuracies; calculating the "effective discharge radius" from the bowl, i.e. the radius at which the momentum of fluid leaving the bowl should be calculated, is difficult in any design other than the full hermetic because it is the centripetal pump which forms the discharge mechanism (see Chapter 3). Equally the behaviour of the fluid after it leaves the feed zone is of little interest as no disruption is believed to occur. Including the whole bowl therefore complicates and confuses the issue. Secondly, an assumption must be made about the useful power input and power input that goes to waste. It is this second term which describes the efficiency of the machine and enables an estimate of the energy that must be dissipated to heat through turbulent eddies and is thus the cause of turbulent shear.

In this thesis in order to refine the accuracy of the shear force estimate an expression has therefore been developed for the feed zone alone. It is based on the work of Gössele (1983) who calculated the power dissipated in a scroll decanter centrifuge. The approach of Gössele can be summarised as follows. Firstly the value of the torque

which must be supplied to increase the angular momentum of the incoming fluid from zero at the inlet to it's value at the bowl overflow radius is calculated. From this the power required can be found. Next the rate at which energy is carried out of the centrifuge (in the form of kinetic energy in the overflow) is calculated. The difference between the rate of energy coming in and the rate going out must be the rate at which it is dissipated within the bowl as shear stresses (which would thus appear as heat in the output stream in a full energy balance). This form of calculation proved effective when applied to a scroll decanter. Such a machine is simpler than a DSC and so an energy balance on the whole machine can be accurately carried out and pressure and torque measurements easily taken to confirm the calculations. However it is possible to apply the basic approach as follows;

ASSUMPTIONS

Fluid enters the feed zone with negligible kinetic energy and at atmospheric pressure. Radius of interest R_f is that of the inner end of the flow channels out of the distributor foot onto the disks i.e. consideration is given to the feed zone alone.

(1) Power supplied to increase fluid angular momentum (P_{am})

Change in angular momentum of unit volume= $\rho R_f^2 \omega$
of fluid.

Torque (rate of change of angular momentum) $= Q\rho R_f^2 \omega$

Power supplied = Torque x ω

Therefore;

$$P_{am} = Q\rho R_f^2 \omega^2 \qquad \textbf{(5.10)}$$

where P_{am} = Power supplied to increase angular momentum (W)

Q = Volumetric throughput of centrifuge ($m^3\ s^{-1}$)

R_f = outer radius of feed zone (m)

ω = angular velocity of bowl (rad s^{-1})

(2) Power leaving as kinetic energy at edge of feed zone P_{ke}

Tangential velocity at edge $= R_f\omega$

Kinetic energy per unit volume $= \frac{1}{2}\rho R_f^2\omega^2$

Power (the rate of energy increase) =Q x k.e. per unit volume

Therefore;

$$P_{ke} = \frac{1}{2}\rho R_f^2\omega^2 \qquad \textbf{(5.11)}$$

where P_{ke} = Power leaving feed zone as kinetic energy in fluid (W)

ρ = density of fluid (Kg m^{-3})

Equations 5.10 and 5.11 are identical to those derived by Gössele. The difficulty when considering a disk stack centrifuge comes when considering pressure forces. The fluid in a scroll decanter could, in principle, enter and leave the machine at atmospheric pressure. In a disk stack the fluid leaves the feed zone at a raised pressure due to centrifugal force, and it is likely that this term will be significant. The pressure acting on an element of fluid at radius R in a rotating cylinder of fluid is given by;

$$p = \frac{1}{2}\rho\omega^2\left(R^2 - r_0^2\right) \qquad \textbf{(5.12)}$$

where p = pressure due to centrifugal force (N m^{-2})

R = radius of element of fluid (m)

r_0 = radius of free surface of cylinder (i.e. inner wall) (m)

A pressure difference is equivalent to potential energy change per unit volume. Therefore fluid leaving the disk stack centrifuge feed zone carries potential as well as kinetic energy. This power is given by;

$$P_{pe} = \frac{1}{2} Q\rho\left(R_f^2 - r_0^2\right)\omega^2 \qquad \textbf{(5.13)}$$

where P_{pe} = Power leaving feed zone as potential energy in fluid (W)

When conducting the energy balance it can be argued that the energy required to supply the increase in potential energy must be over and above that required to raise the angular momentum. Similarly the transfer of this energy from the bowl to the fluid will not be 100% efficient. If the efficiency of this transfer is assumed to match that of angular momentum to kinetic energy (i.e. is 50% efficient) then;

$$\left(P_{pe}\right)_{in} = 2xP_{pe} \qquad \textbf{(5.14)}$$

Therefore the power dissipated in the feed zone of a disk stack centrifuge can be calculated from an energy balance;

$$P_{dis} = P_{in} - P_{out}$$

$$P_{in} = P_{am} + \left(P_{pe}\right)_{in}$$

$$P_{out} = P_{ke} + P_{pe}$$

$$P_{dis} = P_{am} - P_{ke} + P_{pe}$$

$$P_{dis} = Q\rho R_f^2\omega^2 - \frac{1}{2}Q\rho R_f^2\omega^2 + \frac{1}{2}Q\rho\left(R_f^2 - r_0^2\right)\omega^2$$

$$P_{dis} = \frac{1}{2}Q\rho R_f^2\omega^2 + \frac{1}{2}Q\rho\left(R_f^2 - r_0^2\right)\omega^2 \qquad \textbf{(5.15)}$$

Some thought must now be given to the radius of the free surface of the fluid r_0. In the case of the hydro-hermetic centrifuge where the feed zone is fully flooded this will

obviously be zero, and inspection of the equation shows that this forms an upper bound on the power dissipated;

$$P_{disMAX} = Q\rho R_f^2\omega^2 \qquad \textbf{(5.16)}.$$

The semi-hermetic feed zone, at very low flow rates, will contain a layer of fluid on the outside of the feed zone with a negligible thickness. Under such conditions the pressure term from the power dissipation equation can be ignored, and the lower limit of power dissipation is obtained;

$$P_{disMIN} = \frac{1}{2}Q\rho R_f^2\omega^2 \qquad \textbf{(5.17)}$$

Note this is seemingly back-to-front i.e. the limiting condition in the highly disruptive semi-hermetic design would indicate less shear stress than in the much gentler hydro-hermetic. However, it is power dissipation *per unit volume* that is important. The liquid volume in the semi-hermetic feed zone at low flow rates will be minuscule (as low as 1 mL) whereas the minimum volume of the hydro-hermetic at the scale tested was 30 mL. It can be seen that consideration must therefore be given to the flooding depths and physical geometry's of the two feed zones if the power dissipation approach is to be successfully applied.

5.2.1.1 Application of Power Dissipation Equation

Using equations 5.16 and 5.17 it is possible to estimate the power dissipated in the feed zones of both the hydro- and the semi-hermetic feed zones. However, to convert this to a shear rate it is necessary to estimate the volume of liquid held up in the feed zone under varying flow conditions. This is not a trivial problem as it is not possible to measure experimentally. By examining the physical dimensions of the feed zones it is possible to obtain an idea of the liquid levels they should contain.

5.2.1.1.1 Volume of the Semi-Hermetic Feed Zone.

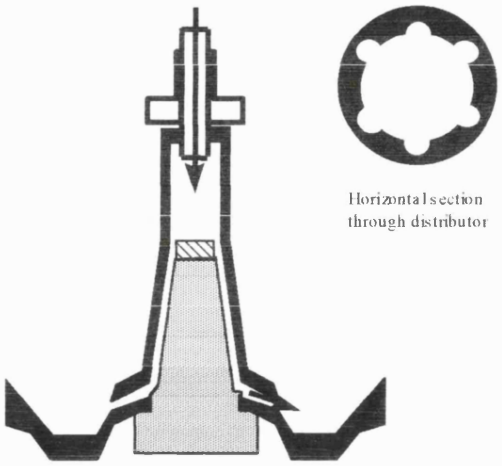

Figure 5.2: Section Through Semi-Hermetic Distributor

Figure 5.2 above shows a section through the distributor of semi-hermetic design. Feed zone flooding levels increase with volumetric throughput, with the whole feed zone becoming flooded at approximately 400 Lh^{-1}. At low flow rates there will therefore be very little liquid held in the feed zone. To estimate a lower bound for liquid hold-up, therefore, it was assumed that only the six guide channels within the distributor wall contain liquid. These can be considered as six semi-circles of radius 2.5 mm, running 43 mm from the lock-nut (where liquid is initially deflected out to the distributor wall) to the flow channels through to the disks. This gives a total volume of 2.5 mL.

The gap between the distributor wall (excluding the guide channels) and the central spindle is 5 mm. The next condition we can accurately evaluate is the point at which the lock-nut becomes covered over. Experimental evidence suggests this occurs at approximately 150 Lh^{-1} (see Chapter 3). Assuming the liquid film on the outer distributor wall must have thickened to fill the space between the distributor wall and the spindle then the volume held up in the feed zone will be 12 mL.

The final condition is as the feed zone becomes fully flooded, at approximately 400 Lh^{-1}. At this point the feed suspension leaks out of the top of the feed zone into the

supernatant discharge; therefore the entire space within the distributor must be full. This corresponds to a volume of 30 mL.

From these volume estimates the power dissipation can be calculated from equation 5.15 and the shear rate estimated from equation 5.7.

ω (rad s^{-1})	Q (Lh^{-1})	R_f (mm)	r_0 (mm)	P_{dis} (W)	Volume (mL)	G (*E.coli*) (s^{-1})	G (PEG) (s^{-1})
1026	50	17.5	15.0	3	2.5	$3.0x10^4$	$1.0x10^4$
1026	150	17.5	12.5	10	12	$2.0x10^4$	$9.8x10^3$
1026	400	17.5	0	36	30	$3.3x10^4$	$1.0x10^4$
712	50	17.5	15.0	1.38	2.5	$2.2x10^4$	$7.2x10^3$

Table 5.1: Shear rates and power dissipation generated in the semi-hermetic feed zone under a range of operating conditions (note, 1026 rad s^{-1} = 9800 rpm, 712 rad s^{-1} = 6800 rpm).

Table 5.1 shows the estimated shear rates developed in the feed zone calculated on a power dissipation basis for a range of flow rates. Several points are worth noting. When considering the *E.coli* system there is an apparent 50% decrease in shear rate between 50 Lh^{-1} and 150 Lh^{-1} followed by an increase to 400 Lh^{-1}, a trend repeated with the PEG. When considering PEG precipitates the shear rates predicted are slightly lower than those for *E.coli* due to the increase (by almost an order of magnitude) of the viscosity of the suspension. Finally, reducing the rotational speed of the bowl is predicted to have by far the greatest effect, bringing about a significant reduction in shear rates.

It must be remembered that these figures are only estimates and the volume estimation is likely to be a significant source of error. Although the flooding depths used to calculate the volumes are believed to be correct an important issue will be the rate of acceleration of the fluid. In all the calculations it has been assumed that the liquid reaches the rotational speed of the bowl as it leaves the feed zone (the limiting condition); therefore it is the entire volume of the feed zone (proportional to the depth of flooding) that has been used to calculate the shear rates. If the feed suspension is accelerated significantly over a much small section of the feed zone it is possible that

the power is being dissipated over a much smaller volume which may be much less sensitive to the throughput, and thus the shear rates will be higher. It is believed that this may become increasingly important as flow rates increase. If the majority of the liquid acceleration occurs at the top of the feed zone then the effective volume (that used for the power dissipation calculation) increase with throughput will be much reduced, giving rise to substantially increasing shear rates with flow rate. Significantly this model would suggest that instead of decreasing from 50 to 150 Lh^{-1} the shear rates would, in fact, increase.

In addition it is likely that the depth of flooding within the feed zone will increase with a reduction in rotational speed, even when the throughput is held constant. This is because a significant fraction of the force pushing liquid out of the feed zone and onto the disks is centrifugal. This will decrease the shear rate further than those calculated. However, since it is impossible to predict how bowl speed will influence flooding depth this effect has been ignored.

Despite these difficulties Table 5.1 should provide a good enough estimation of shear rates in the feed zone to allow comparison of the hydro- and semi- hermetic feed zone conditions, and sensible consideration of laboratory scale mimics.

5.2.1.1.2 Volume of the Hydro-Hermetic Feed Zone

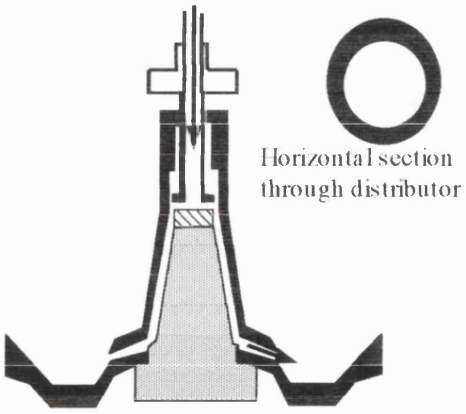

Figure 5.3: Section Through Hydro-Hermetic Distributor

Figure 5.3 shows a section through the soft-shear hydro-hermetic distributor. As was reviewed in Chapter 3, the major differences between this and the standard semi-hermetic design are the lack of flow guide channels in the main section of the distributor, and crucially an increase in the volume held up in the distributor, with the space flooded to the level of the bottom of the feed pipe at flow rates of 50 Lh^{-1} and above. As the throughput increases so does the volume held up, until the distributor floods out at 250 Lh^{-1}. This simplified flooding behaviour allows easier calculation of the liquid hold-up, and it is estimated that at 50 Lh^{-1} the distributor holds approximately 30 mL increasing to 40 mL shortly before overflowing.

This reduces the shear rate estimations significantly, and the range of values estimated are shown below in Table 5.2.

ω (rad s^{-1})	Q (Lh^{-1})	R_f (mm)	r_0 (mm)	P_{dis} (W)	Volume (mL)	G (*E.coli*) (s^{-1})	G (PEG) (s^{-1})
1026	50	17.5	0	4.5	30	$1.1x10^4$	$3.8x10^3$
1026	250	17.5	0	22.8	40	$2.2x10^4$	$7.3x10^3$
712	50	17.5	0	2.18	30	$8.1x10^3$	$2.6x10^3$

Table 5.2: Shear rates generated and power dissipation in the hydro-hermetic feed zone under a range of operating conditions (note, 1026 rad s^{-1} = 9800 rpm, 712 rad s^{-1} = 6800 rpm).

The predicted shear rates at 50 Lh^{-1} are only one third of those estimated for the semi-hermetic feed zone. As the throughput increases it can be seen that the estimated shear rate doubles. There is also a larger difference between the whole cell and PEG shear rates; because the volumes are higher the difference in viscosity between the two systems becomes more significant.

As before there are difficulties with volume estimation. However, these should not be as significant as those associated with the semi-hermetic centrifuge because the majority of the feed zone is flooded at all times. Again these estimates should be good enough to provide the basis for laboratory scale mimics.

The shear rate estimates given here will be further considered in Chapter 6.

5.2.2 The Spinning Disk Model

An alternative method of estimating the shear rates found within a disk stack centrifuge is known as the spinning disk technique. This technique was used by Bell (1982). The model assumes that the feed rate to a centrifuge is of approximately the same order of magnitude as the pumping rate developed by a flat spinning disk rotating about an axis perpendicular to it's plane. If this is so then the feed zone of a centrifuge may be considered to approximate such a disk rotating in a fluid otherwise at rest (Bell, 1982) with fluid flowing axially towards the disk turned and ejected radially by centrifugal forces.

The exact solution to the Navier-Stokes fundamental fluid flow equations for such a disk was first calculated by Cochran (in Schlichting, 1979) for an infinitely large disk, and it was this form of the solution that Bell used for his estimates. He calculated an average shear rate within the feed zone of $1x10^5$ s^{-1}, an estimate that compares well to those he obtained using a variation of the power dissipation technique. However, Bell considered the whole feed zone as a rotating disk. From the experimental investigations described in Chapter 3 it seems clear that interactions between the feed suspension and the lock-nut play a key role in causing whole cell disruption, and the lock-nut may be considered as the true "spinning disk" of known diameter (22 mm). The formula given in Schlichting has therefore been refined within UCLACBE to apply specifically to a disk of known diameter (Ayazi-Shamlou and Yim, personal communication). They conducted a thorough numerical analysis of the region around the top surface of the lock-nut and found that significant turbulent shear forces are predicted within a very thin boundary layer at the disk surface. They developed equations based on the specific Navier Stokes solution of Cochran to calculate both the layer thickness and the maximum shear force developed and these are given below;

$$G_{max} = \rho(\omega r_l)^{1.75}\left(\frac{\mu}{\delta}\right)^{0.25} \quad \textbf{(5.17)}$$

$$\delta = d_l^{0.6}\left(\frac{\nu}{\omega}\right)^{0.2} \quad \textbf{(5.18)}$$

Where δ = thickness of boundary layer (m)

ρ = suspension density (Kg m^{-3})

ω = rotational speed of centrifuge bowl (rad s^{-1})

μ = suspension dynamic viscosity (N s m^{-2})

r_l = radius of lock-nut (m)

d_l = diameter of lock-nut (m).

This enables a calculation of the maximum theoretical shear rate generated at the surface of the lock-nut. This will obviously be the same for both designs of centrifuge. For an *E.coli* suspension processed through a centrifuge running at 9800 rpm the calculated value is $6.6x10^4$ s^{-1} with a boundary layer thickness of 1.6 mm, and for PEG, $1x10^5$ s^{-1} with a thickness of 2.5 mm. When the bowl speed is reduced to 6800 rpm the *E.coli* shear rate drops to $3.4x10^4$ s^{-1} within a layer of thickness 1.7 mm, and PEG, $5.6x10^4$ s^{-1} within a region 2.7 mm thick.

What is clear from these estimates is that very significant shear forces will occur at the surface of the lock-nut and therefore this region cannot be ignored when considering the disruptive forces present within the centrifuge. Although the regions involved are small they are much larger than the size of either a cell or a precipitate particle, so a significant amount of the feed could be exposed to such forces.

Again, these estimates will be considered further in Chapter 6.

5.2.3 Kolmogoroff Scale of Microturbulence

It is widely accepted that an important parameter when considering shear-based disruption mechanisms is the Kolmogoroff Scale of Microturbulence (KSM) which predicts the size of the smallest turbulent eddy that will be present within a flow before the energy is dissipated to heat. The higher the amount of energy present within the fluid, the smaller the value of the KSM. Eddies which are of a scale much larger than a body within the fluid will tend to move it from place to place, inflicting little real damage. Eddies which are of the same scale or smaller than the body, however, will impart motions of differing intensities to different sections of the object creating a pressure difference across it, as well as shearing motions on the outside of the object (see Chapter 1). It is these effects that are acknowledged as being very disruptive to biological particles (Cherry and Papoutsakis, 1986), and play an active role in mammalian cell culture breakage and traditional cell disruption mechanisms, such as cavitation and homogenisation.

The KSM (λ) is given by the equation;

$$\lambda_k = \left(\frac{\nu}{\varepsilon}\right)^{\frac{1}{4}} \qquad \textbf{(5.19)}$$

where λ_κ = Kolmogoroff scale of microturbulence (m)

ν = fluid kinematic viscosity ($m^2\ s^{-1}$)

ε = energy dissipation rate ($J\ s^{-1}$)

$$\varepsilon = G^2 \nu \qquad \textbf{(5.20)}$$

The values of the KSM obtained with the range of shear rates predicted for the two feed zones are shown in Table 5.3;

$G\ (s^{-1})$	$\varepsilon_{PEG}\ (J\ s^{-1})$	$\lambda_{kPEG}\ (\mu m)$	$\varepsilon_{E.coli}\ (J\ s^{-1})$	$\lambda_{kE.coli}\ (\mu m)$
$6x10^4$	35280	12.8	3888	2.1
$3x10^4$	8820	18.0	927	6.1
$1x10^4$	980	31.0	108	10.4
$8x10^3$	627	35.0	69	11.6
$3x10^3$	88	57.0	10	19.0

Table 5.3: Predicted Kolmogoroff Scale of Microturbulence across the range of shear forces present in the DSC feed zone.

It can be seen that the values of the KSM approach the scale of both *E.coli* cells (1 by 2 μm) and the PEG precipitates (10 μm) and so it is expected that the shear forces predicted in the feed zones will have a disruptive effect on the particles being processed. However the KSM over the shear range does not "straddle" the size of the particles; rather the highest forces, corresponding to those around the lock-nut, produce a KSM value of the same size as the particles but this value increases rapidly and at the lowest shear rate predicted, by the power dissipation model applied to the hydro-hermetic feed zone, the KSM values are becoming sufficiently large that the particles may cease to be acted on by the turbulent eddies. This forms another important piece of information about the differences between the two feed zones and will be returned to in Chapter 6.

5.3 Laboratory Scale Mimics

Having established that, in theory, significant shear rates are generated in the feed zone of a disk stack centrifuge and these will generate turbulent eddies of the correct order of magnitude to cause damage to both the whole cell system and the PEG precipitate system the next step was to expose both test systems to defined shear fields generated on the laboratory scale and observe the degree of disruption caused. To do this it was decided to use two distinct types of laboratory system; one to create defined shear

fields in order to attempt to mimic the overall "power dissipation" effect, and one based on a rotating disk, to mimic the effect of the lock-nut. Details of these mimics are given below.

Material for shear tests was generated in an identical manner to that used for pilot scale centrifugation i.e. whole cells were generated using the standard protocol within a 150L fermenter (see Chapter 2), and polyethylene glycol precipitates were generated within the 110 L reaction vessel (see Chapter 4). This was to avoid the possibility of a change in physical characteristics of the feed suspension with scale. All disruption measurement techniques used are described in Chapter 2 & 3 (whole cells) and Chapter 4 (PEG precipitates).

5.3.1 The Capillary Shear Rheometer

Figure 5.4 shows a section through the capillary shear rheometer used in this work. The suspension under test was exposed to a defined shear field generated using a modified Instron 1141 Food Tester (Instron Ltd., High Wycombe, Bucks., UK). The capillary reservoir barrel held 15 mL of feed suspension, which was then forced through a precision bore capillary at a range of pre-selected flow rates by the Instron's piston drive. The shear rate generated within the capillary could thus be calculated.

For each shear rate and residence time selected 14 mL of test suspension was loaded into the Instron. Approximately 5 mL of suspension was allowed through the capillary in order for the machine to equilibrate, after which the remaining material was collected for analysis. Between samples the rheometer was rinsed through with HPLC grade water. All conditions were examined in duplicate.

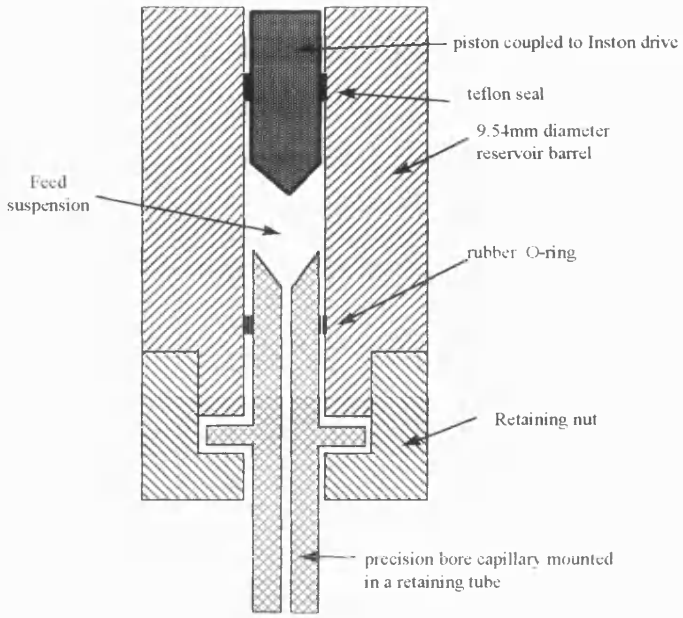

Figure 5.4: Section through the Capillary Shear Rheometer.

Because of the accuracy of the Instron drive (a "wormdrive" system), and the use of high quality capillaries, it was possible to be very confident of the shear rate generated within the instrument. The difficulty with this approach is the limited range of shear rates available and the difficulty in varying residence time independent of shear rate. It proved impossible to generate shear forces greater than 10^6 s^{-1} in this manner as the capillary necessary was too fine to withstand the high pressure drop generated. Furthermore, at a given shear rate the only way to alter the residence time under test was to lengthen the capillary in use. Because of the design of the instrument it was impractical to use lengths greater than 200 mm, which at high shear rates corresponded to a residence time of about 1000th of a second. This is approximately 100 times shorter than the residence time of a particle in the entire feed zone of a DSC at an average volumetric throughput.

Full details of the shear rate calculations and the shear rates/residence times available with the Instron capillary shear rheometer are given in Appendix 6.

5.3.4 Spinning Disk Device

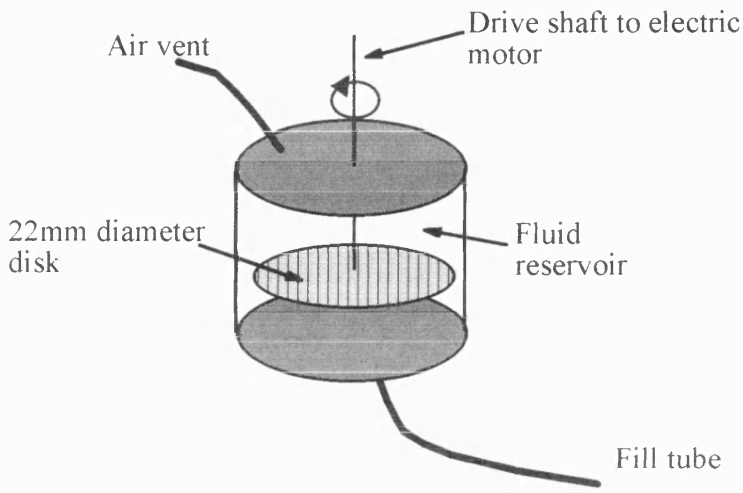

Figure 5.5: The Spinning Disk Shear Device

Figure 5.5 shows the spinning disk shear device used during this work. It consists of a flat disk the same diameter as the centrifuge lock-nut mounted within a 15 mL reservoir. This reservoir was completely filled with feed suspension to exclude all air-liquid interfaces from within the device. The disk was then rotated by an electric motor over varying time periods, and the feed suspension examined for disruption. Rotational speeds of approximately 16,000 or 24,000 rpm were available, corresponding to shear rates of approximately 1.6 $x10^5$ s^{-1} and 3.3 $x10^5 s^{-1}$ respectively . All conditions were examined in duplicate. The disk chamber was thoroughly rinsed with HPLC grade water between samples.

5.4 Results

The system tested first with the laboratory scale mimics was whole cell *E.coli*. This was produced at 150L scale just as for centrifugation experiments. Furthermore, as was explained in Chapter 2, the strength profile of the batch was examined using a high pressure homogeniser to insure a similar quality feed as that in use for pilot scale centrifuge examination.

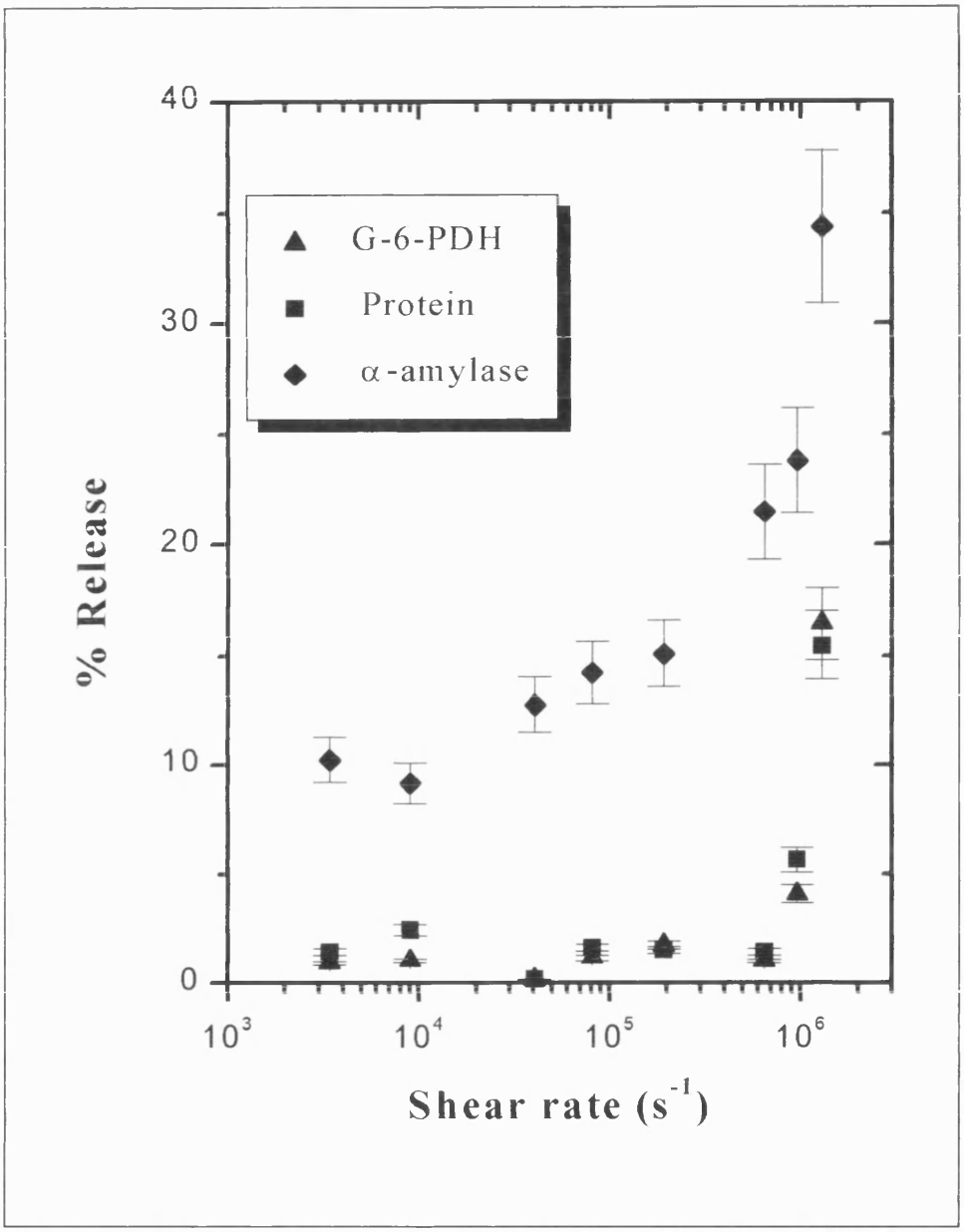

Figure 5.6: Release of periplasmic (α-amylase) and cytoplasmic markers from whole cell E.coli JM107 pQR126 when subjected to a defined shear field in the Capillary Shear Rheometer. Residence times varied between 0.1 s (lowest shear rate) and 0.001 s (highest shear rate).

Figure 5.6 gives the release observed of both periplasmic α-amylase and the cytoplasmic glucose-6-dehydrogenase (G-6-PDH) and total protein markers from whole cell *E.coli* JM107 pQR126 in the capillary shear rheometer. This shows the by now familiar pattern of the periplasmic enzyme being released at considerably higher levels than the cytoplasmic markers (10% as opposed to 2% at low shear levels, rising to 35% and 15% respectively). Of more interest is the way the observed release altered with increasing shear rate. The periplasmic α-amylase, which is already significantly released at the lowest shear rate tested showed a gradual increase in release with shear rate until approximately $3x10^5$ s^{-1}. After this the levels in the broth increased substantially until, at the highest level of shear tested ($1x10^6$ s^{-1}) 35% of the total enzyme associated with the cells was released into the surrounding liquid. This matches closely the pattern observed for cytoplasmic release, with no real release observed until a shear rate of $7x10^5$ s^{-1}, followed by a rapid increase in release to a level of 15% at $1x10^6$ s^{-1}. The similarity in disruption pattern supports further the suggested mechanism of leakiness from, rather than disruption of, the periplasm contributing to the high levels of product release observed. This will be addressed in the discussion.

An obvious difficulty with this data is the variation in time of exposure to shear across the shear rates tested. This is a problem in the design of the rheometer, as described in section 3.3.1. As a higher shear rate generally led to a lower shear time it was not possible to be confident that the effect of increasing the shear rate was not being somewhat negated. In an attempt to compensate and to examine this, the effect of increasing the residence time at a constant shear rate was investigated. It was decided to employ an intermediate shear rate ($3.6x10^4 s^{-1}$) as this offered the chance of measurable disruption whilst still allowing significant variation of the time of exposure to shear with the capillaries available. The results are shown overleaf in Figure 5.7.

It can be seen that at the shear rate examined the time of exposure to shear made no significant difference to the release of either α-amylase or G-6-PDH/protein observed. This is slightly contrary to expectations: every material is expected to have a yield stress below which it is difficult to disrupt it. However, most systems are in turn liable to "fatigue" whereby the longer they are exposed to a force, the more damage is

sustained. However, it is likely that the very limited range of residence times available with the Instron equipment simply do not allow this effect to be examined. The residence time experiment was repeated at a higher shear rate ($1x10^6$ s^{-1}), and the same result obtained.

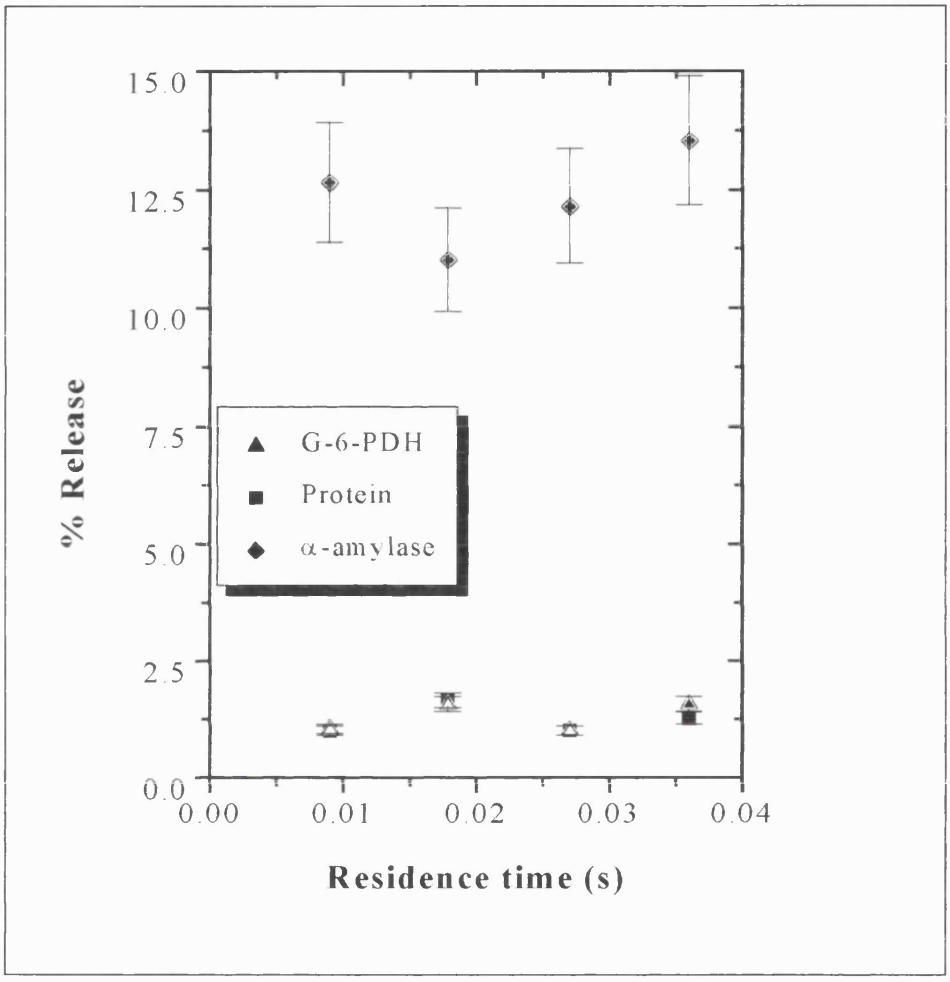

Figure 5.7: Release of periplasmic (α-amylase) and cytoplasmic markers from whole cell E.coli JM107 pQR126 when subjected to a defined shear field of $3.6x10^4$ s^{-1} in the Capillary Shear Rheometer for varying residence times.

The final experiment conducted with whole cell *E.coli* was to expose a sample to shear in the spinning disk device, at two rotational speeds and for varying residence times. The results of this trial are shown in Figure 5.8.

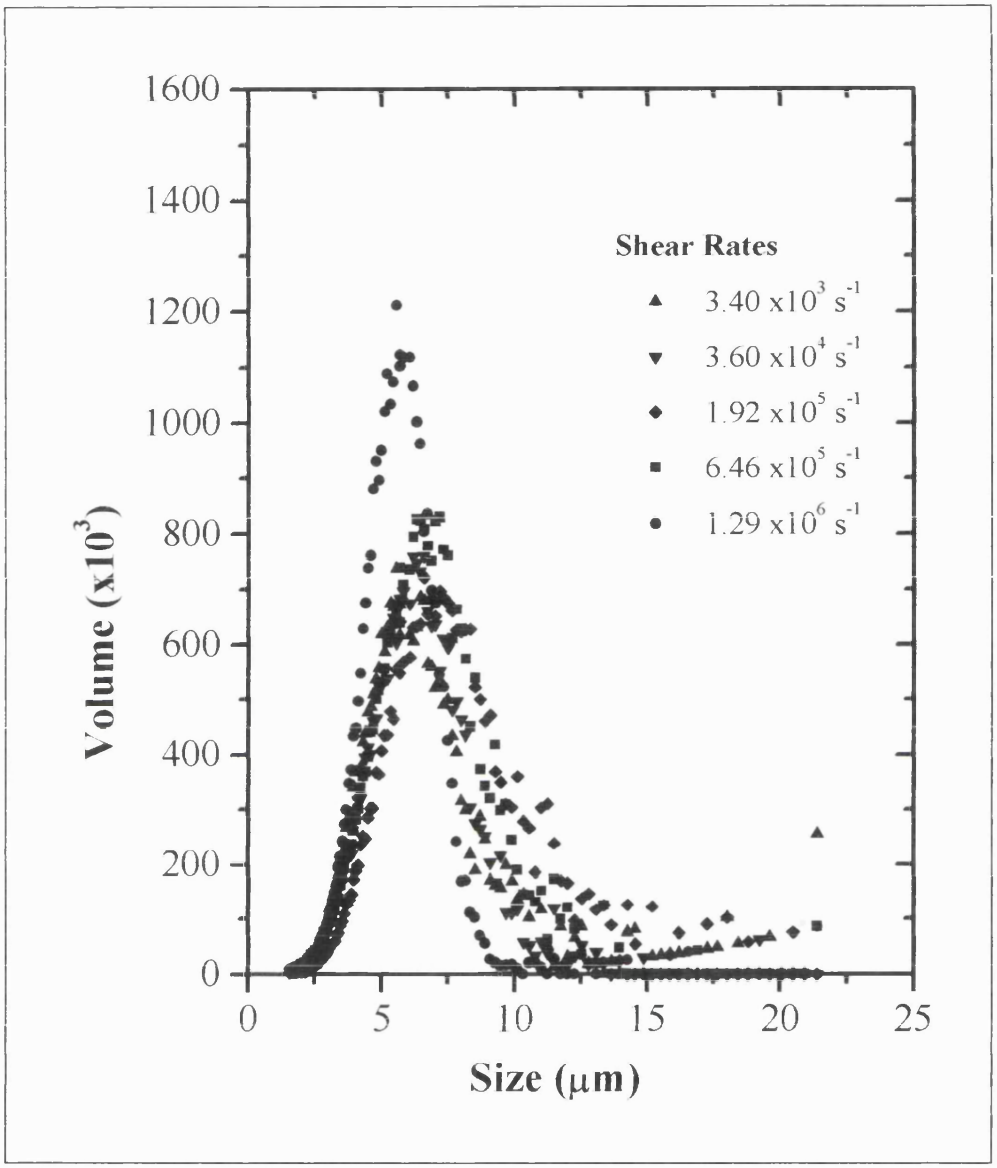

Figure 5.8: Release of periplasmic (α-amylase) and cytoplasmic markers from whole cell E.coli JM107 pQR126 when subjected to a turbulent shear field within the "spinning disk mimic". Note, shear time is the total time the mimic was in operation, not the time each cell was exposed to the shear field.

Figure 5.8 shows the release of the periplasmic α-amylase and the cytoplasmic G-6-PDH/protein with time in the spinning disk device at two different rotational speeds: 16,000 rpm corresponds to a shear rate of $1.6x10^5s^{-1}$, and 24,000 rpm which generated a shear rate of $3.3x10^5s^{-1}$. It shows that release of both cytoplasmic and periplasmic markers generally increases with shear rate, and again at both shear rates the release of α-amylase is greater than either that of G-6-PDH or protein. Generally there appeared to be little time dependence with only α-amylase levels at the lower spin speed increasing with time. Both the cytoplasmic release and that of α-amylase at the higher shear rate tested showed no time dependence, implying that all cells weak enough to be disrupted were broken very rapidly (within 5s).

The next stage of the mimic work was to repeat the above experiments using PEG precipitate suspension rather than whole cell *E.coli*. The size distribution of the feed material for these experiments is shown in Figure 5.9, along with a typical size distribution of the material used for pilot scale trials and a PSD after shearing in the spinning disk device. This can be seen to be a broad based peak with maximum particle volume at approximately 11 μm. This compared well to the feed size distribution used for the pilot scale centrifugation experiments (see Chapter 4).

The results of the capillary shear rheometer experiments are shown in Figure 5.10. The majority of shear rates tested produce similar size distributions with a peak at 7.5 μm. The peak produced is still relatively broad. However, at the highest shear rate examined, $1.29x10^6$ s^{-1}, a larger reduction in size was observed, with a narrower peak at approximately 6 μm generated.

Figure 5.11 shows the results obtained when the suspension was sheared in the "spinning disk" device. This shows slightly different results. When exposed to shear in this manner a very tight peak was produced at 5 μm. This result was obtained at both the higher and lower shear rate tested, and the device appeared to produce almost instantaneous disruption; there was no observable difference between samples that had been exposed for five seconds and 20 seconds.

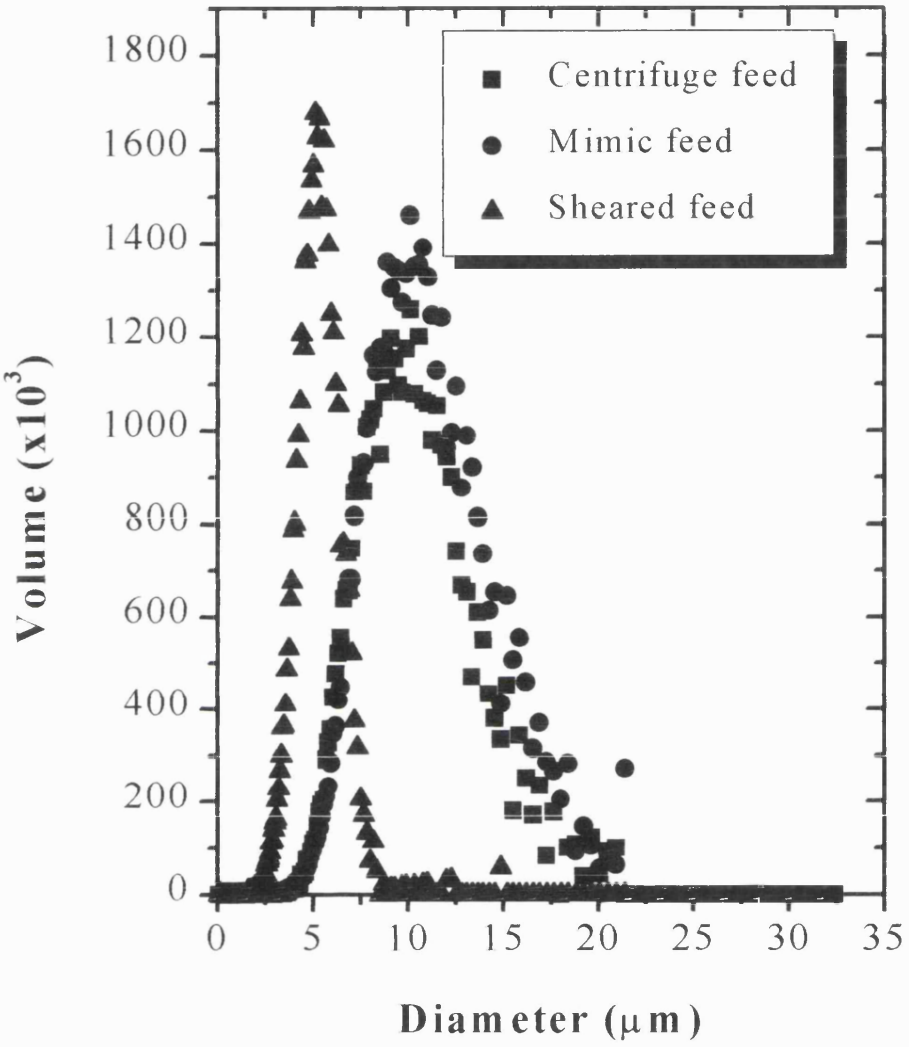

Figure 5.9: Size distribution of feed material for laboratory scale mimic experiments, original centrifugation experiments and mimic-sheared feed ("spinning disk device, 16000rpm, 20s).

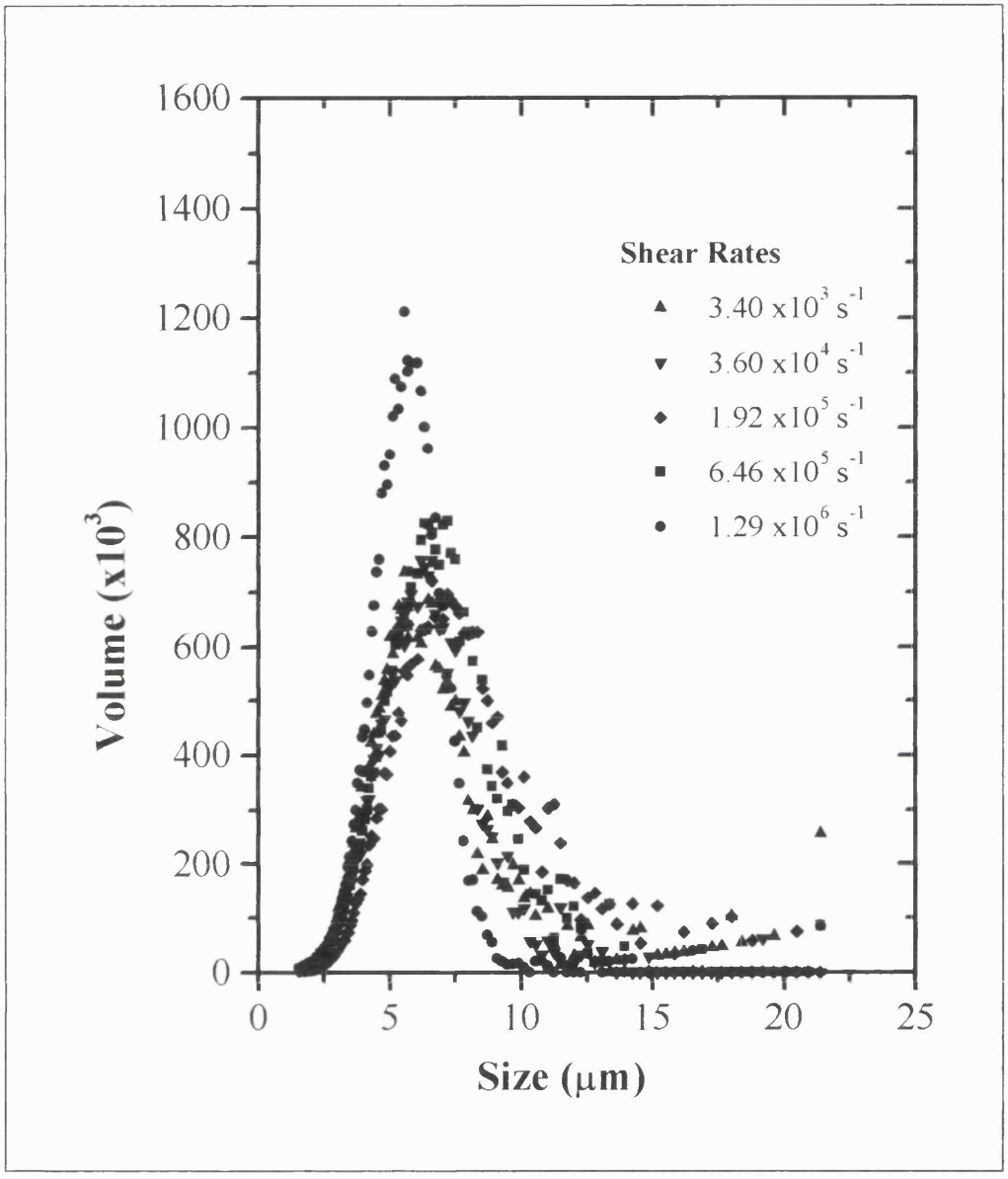

Figure 5.10: Size distribution of PEG precipitate particles when subjected to a defined shear field in the Capillary Shear Rheometer. Residence times varied between 0.1 s (lowest shear rate) and 0.001 s (highest shear rate).

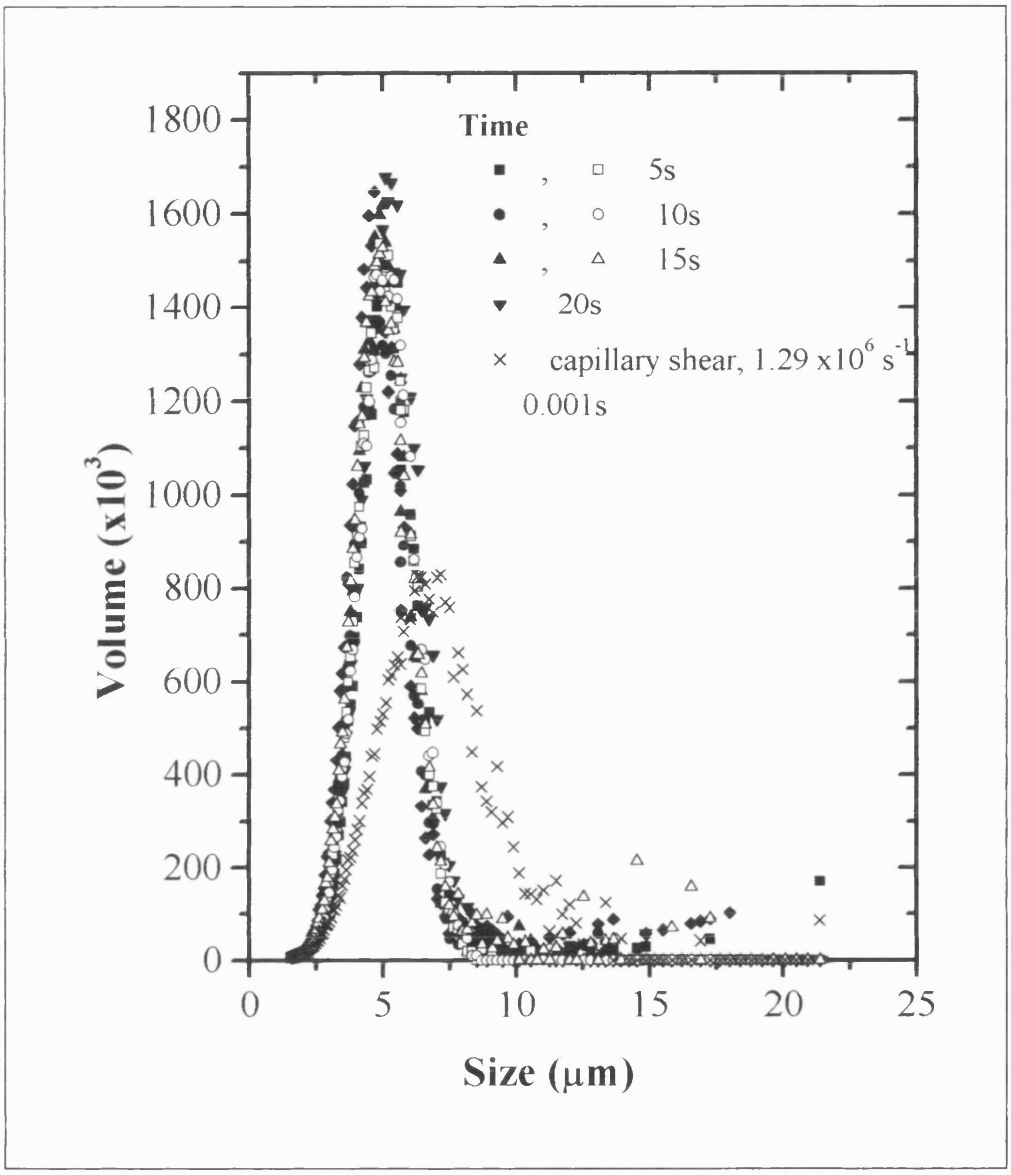

Figure 5.11: Size distribution of PEG precipitate particles when subjected to a turbulent shear field within the "spinning disk mimic". Note, shear time is the total time the mimic was in operation, not the time each cell was exposed to the shear field. Closed points show 16000rpm, open points 24000rpm.

The final analysis made with this data was to use the particle size distribution of an 8% v/v PEG 8000 precipitate suspension which had been sheared in the spinning disk device in conjunction with a pilot scale centrifuge-supernatant size distribution in the production of a grade efficiency curve. Chapter 4 showed that the grade efficiency functions of the centrifuges shifted dramatically at throughputs above 50 Lh^{-1} indicating the disruption of particles in the feed zone (see Chapter 4). This was relatively insensitive to throughput above a threshold flow rate, and similar grade efficiencies were obtained for both the hydro-hermetic and the semi-hermetic feed zones, indicating that the particle size distribution of material leaving the feed zone (either design) and entering the separation area was not effected by volumetric throughput. This further suggested that exposure to the disruptive forces found in either centrifuge feed zone was sufficient to transform the original PSD into one with a much reduced mean particle size. If the laboratory scale mimics produced *exactly* this PSD then it would be expected that a shifted grade efficiency curve would move back to fit that obtained at the low flow rates when the mimic-sheared size distribution was used in the calculation rather than the incorrect unsheared distribution.

The results of this analysis are shown in Figure 5.12. The plot shows the T(d) curve obtained with the semi-hermetic feed zone at 50 Lh^{-1} and at 150 Lh^{-1}. This shows the shift to the left characteristic of particle breakage prior to the separation stage (see Chapter 4). The modified curve obtained using a laboratory-mimic sheared feed and the supernatant size distribution obtained with the semi-hermetic feed zone at a throughput of 150 Lh^{-1} is also shown (both the typical capillary shear and typical "spinning disk" shear size-distributions have been used). Finally, the theoretical grade efficiency curve obtained by Mannweiler (1990) using shear insensitive latex particles is plotted.

It can be seen that the use of the laboratory-sheared size distribution, far from mapping the 150 Lh^{-1} experimental curve onto the 50 Lh^{-1} curve, actually shifts the grade efficiency curve the other way indicating that the mimic does not produce the same size distribution as the centrifuge feed zone. However, because T(d) curves are based on the fraction of a given size particle recovered this does not necessarily indicate that the mimic is entirely wrong. Furthermore although only T(d) values from

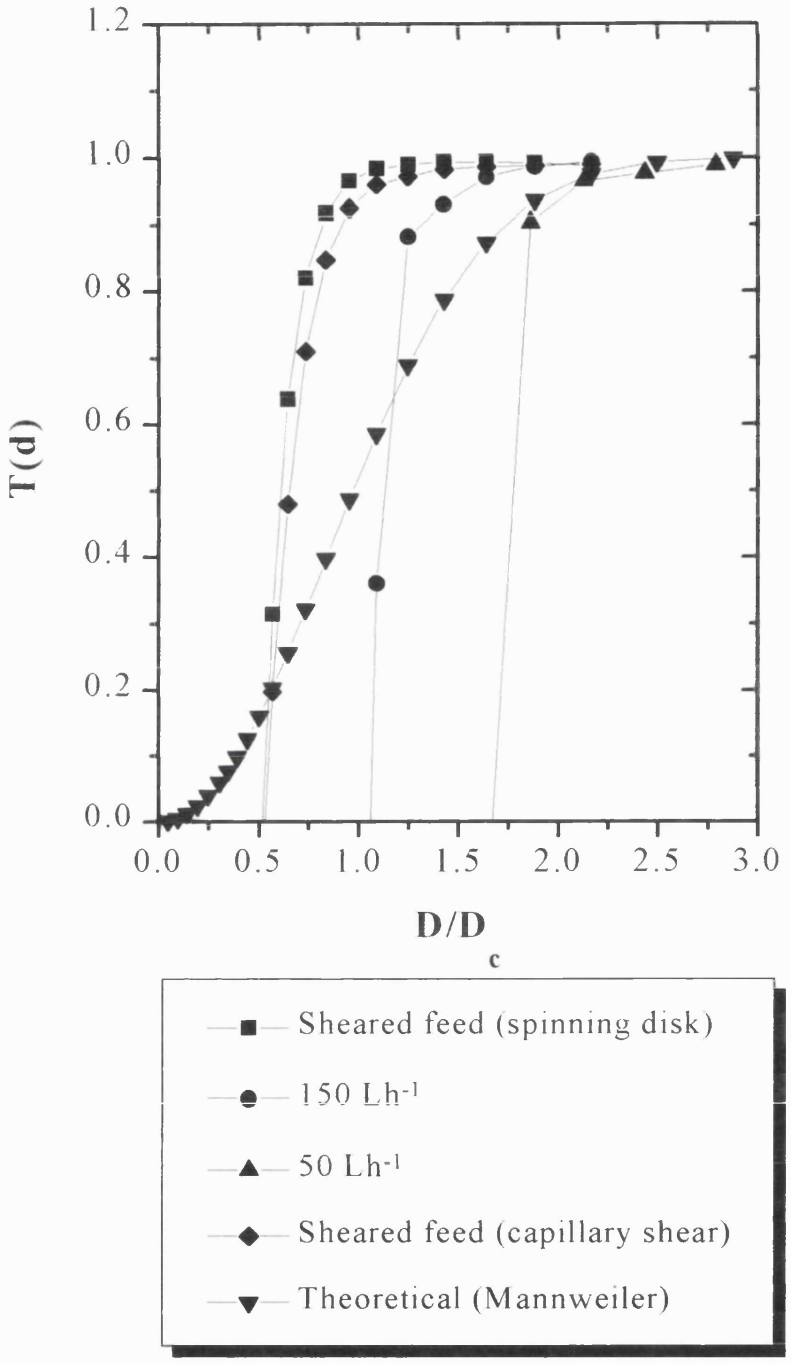

Figure 5.12: Grade efficiency curves obtained experimentally using a semi-hermetic disk stack centrifuge. Sheared curves are for centrifuge at 150 Lh^{-1} using laboratory-mimic sheared feed size distribution. Theoretical curve is that obtained by Mannweiler (1990) using shear insensitive latex particles.

0 to 1 are shown in the plot for clarity the degree of negativity of the function at low d/d_c values was very much reduced (from approaching -50 to a maximum of -1.85). This indicated that the mimic was at least producing particles as small as those created in the feed zone of the centrifuge in approximately the right number. These ideas will be explored further in the discussion.

5.5 Discussion

Because of the different behaviour of the two biological test systems in the laboratory scale mimics it is appropriate to consider them separately.

The *E.coli* system showed relatively low levels of periplasmic and cytoplasmic release in both test systems for the majority of conditions tested. The observed release in the mimics was broadly consistent with that generated within the centrifuge feed zones. The hydro-hermetic centrifuge released approximately 2% of cytoplasmic markers and 7.5% of the periplasmic α-amylase across the range of throughputs tested. The shear rate predicted for the feed zone was of the order of 10^4 s^{-1}. It can be seen in Figure 5.6 that at this shear rate disruption of approximately 2% and 10% (cytoplasmic and periplasmic) was obtained using the capillary shear device. This obviously compares favourably with that practically observed. However when considering the semi-hermetic centrifuge the mimic does not perform as well. 10% cytoplasmic and 20% periplasmic release was observed at the lowest throughput tested rising to 20% cytoplasmic and 40% periplasmic release at a throughput of approaching 150 Lh^{-1}. These levels of release could only be generated using a defined shear rate approaching $10^6 s^{-1}$, far in excess of the maximum 3 $x10^4 s^{-1}$ predicted as existing in the feed zone (on a power dissipation basis). There are two additional factors that must be considered. The first is the role of the lock-nut, and the second the accuracy of the volume estimation used to calculate the feed zone shear rate.

The results discussed in Chapter 3 show a decrease in disruption at 150 Lh^{-1}. This was attributed to the lock-nut becoming covered. This effect continued with increasing

throughput and feed zone flooding levels until at 300 Lh^{-1} release levels were approaching those observed in the hydro-hermetic feed machine. This is believed to represent the key difference between the semi-hermetic and hydro-hermetic machine since before the lock-nut becomes covered in the semi-hermetic design all of the feed material passes over it. Calculations in this chapter show that a significant shear force is present on the surface of the lock-nut (approximately $7x10^4$ s^{-1} when processing *E.coli*) but only in a very thin boundary layer (less than 2 mm). However in the semi-hermetic centrifuge significant amounts of the feed material may pass, however briefly, through this region. As the flooding depth becomes greater and the lock-nut is covered over it would be expected that proportionally less material will pass through this region. The hydro-hermetic centrifuge has it's lock-nut flooded over at any operating throughput and it appears sensible to assume that a much smaller fraction of the feed will go through this region of high shear. Since operationally this appears to be the key difference between the designs we must next consider the results from the spinning disk laboratory mimic.

Results shown in Figure 5.8 do not mimic exactly those produced in the centrifuge. However, they do indicate that the spinning disk, operating at approximately the shear rate estimated for the lock-nut region, is capable of producing significant disruption (particularly release of α-amylase from the leaky periplasm). Generally, however, the release seen with this mimic again is not high enough to represent the feed zone of the semi-hermetic centrifuge. The mimic is well mixed and the majority of material will spend a short time in the shear field produced by the disk. This does not seem to increase significantly with time, which would appear to indicate that at any given shear rate only a certain fraction of the cells present are susceptible to breakage, with the percentage increasing with shear rate.

It seems likely that in the feed zone of the semi-hermetic centrifuge it is the action of a combination of forces which gives rise to the observed disruption. Such breakage (see Chapter 3) rises to a volumetric throughput of 150 Lh^{-1} when the lock-nut becomes covered over. The lock-nut itself does not generate all of the disruption observed. The laboratory scale mimic data appears to confirm this, and certainly such a mechanism

could not cause an increase in disruption with flow rate. The lock-nut does, however, damage a significant fraction of the cells which pass through it's region of influence. Feed suspension flung off the lock-nut will still have little significant rotational speed and so will be accelerated in the feed zone, and thus come under the action of further shear forces based on a power dissipation mechanism. Again, the laboratory scale mimic shows that this shear force alone will not break up whole cells to the same degree as observed in the centrifuge. However there are two issues to consider here. Firstly the two effects will not necessarily break *the same cells* i.e. total disruption may be additive. Furthermore the effects are likely to be cumulative; cells may be weakened in the lock-nut region and then broken more easily in the feed zone, where they will be resident for much longer (and indeed longer than it has been possible to mimic using the capillary shear rheometer). Secondly the accuracy of the volume estimate of the feed zone must be questioned as discussed in the introduction to this chapter. There is no reason to assume that acceleration, and thus power dissipation, occurs over the entire flooded volume of the feed zone. This is simply the lower bound (and the only realistic estimate it is possible to make). Indeed, experimental evidence suggests this is not the case as the observed disruption in the semi-hermetic feed zone increases from 50 Lh^{-1} to 150 Lh^{-1} when, assuming dissipation over the whole of the flooded area, the shear rate should drop.

A shear based disruption mechanism here is the only possible one as the lock-nut interactions will not change over this range and impacts with guiding ribs will, if anything, decrease as the flooding depth becomes greater. The capillary shear mimic showed that an increase in shear rate of an order of magnitude from that predicted could produce a substantial increase in disruption. This could easily be obtained if the power was dissipated unevenly. Furthermore, as the lock-nut obviously plays a significant role, it can be assumed that after passage through this region of shear the increase in force necessary in the bulk of the feed zone to cause significant release would be reduced.

It therefore seems clear that disruption of whole cells is a complicated process dependant on both the power dissipated during acceleration of the fluid within the feed zone and the effect of passage through the region of high shear above the lock-nut.

Neither of these effects is sufficient to produce the observed release alone. However, assuming shear rates close to those estimated are generated in the DSC the laboratory scale mimic work has shown such a mechanism to be capable of producing the release observed. Furthermore, the mimics are capable of producing "order of magnitude" release data which could be used simply and quickly to estimate the effect of passage through a disk stack centrifuge on a given feed material. This is potentially extremely important when used in conjunction with ultra-scale down techniques as a fast process development tool. Material which is too weak to be recovered effectively in a disk stack centrifuge without high yield losses could be identified without undertaking pilot scale trials, thus saving time and money.

The second aspect for discussion centres around the effects of the laboratory scale mimics on the PEG precipitates. It can be seen that at all shear rates tested for both laboratory scale mimics a similar size distribution of "sheared feed" was generated. This is entirely consistent with what is known about breakage of precipitate aggregates when exposed to shear forces. As was discussed in Chapter 4 precipitates are formed of primary particles which are then bound together to generate the aggregates during the period of ageing. Many researchers have reported that exposure of such aggregates to shear will break them back to the constituent primary particles. However, disrupting the primary particles themselves is extremely difficult as the constituents of such primary particles are bound together much more strongly than the aggregates (Clarkson, 1994). The system under test here is slightly more complicated as it is believed that a range of primary particles or "building blocks" will exist (see Chapter 4) due to the presence of quantities of cell debris in the precipitation system and the action of flocculation mechanisms in addition to simple precipitation. However the average size of such a heterogenous mixture of primary particles appears to be of approximately the same size, hence the production of a single peak size distribution when the particle aggregates are sheared by the laboratory scale mimics (an alternative explanation is that some of the smaller aggregates survive the shear forces generated, though given the radical size reduction after shearing this doesn't seem likely). The only way to verify the accuracy of the laboratory scale mimics is to use such "sheared feed" in the grade efficiency calculation and look at the form of the altered curve. This is plotted in Figure 5.12.

At first sight this does not appear to have been entirely successful. The grade efficiency curve obtained using a sheared feed is in fact further away from the ideal curve (obtained by Mannweiler using shear insensitive latex particles) than the observed results. However, it seems likely that this is an artefact of the test. The grade efficiency curve is a measure of the ratio of particles in a given size range appearing in the supernatant to those present in the feed. Ideally, at a value of d/d_c of 1 just under 60% of all particles will be recovered. This corresponds to a particle size of 4 μm at the flow rate tested (150 Lh^{-1}). However, there are very few particles of this size present in the supernatant and therefore the sheared feed only has to overpredict the fraction of particles of this size by a small amount to have a large apparent effect on the grade efficiency function. It is this that is believed to have altered the curve in this manner. Because even relatively mild shear forces will disrupt significantly the precipitate particles the issue with the feed zones reduces to whether or not a particle is exposed to such a shear force. Both the laboratory scale mimics expose all particles to the shear force under test. If in reality even a small fraction of the feed is not exposed to such forces the form of the grade efficiency curve would be drastically altered. Furthermore the shear forces tested correspond to the range of shear projected to be present in both the hydro-hermetic and the semi-hermetic feed zone. These levels are sufficient to disrupt the feed to the same degree regardless of whether they are lock-nut derived shear forces or power dissipation derived shear forces. This may also explain why there was little apparent difference between disruption at differing throughputs, or between the feed zones designs (Chapter 4).

In the semi-hermetic feed at low throughputs the majority of the feed passes through the region of high shear above the lock-nut and is broken back to small particles. However, some feed material will escape this area and travel through to the acceleration zone of the feed zone unbroken. Within the acceleration zone the results from the whole cell work indicate that the power input to the fluid will probably not be dissipated over the whole region; rather there will be "hot spots" where the majority of the acceleration takes place. Because the power dissipation calculations contained in this chapter estimate the mean power that must be dissipated, the presence of higher

shear regions will also lead to the creation of areas of low shear in order that the mean shear rate remain constant. Therefore it is likely that a fraction of the feed particles will be exposed to lower shear forces than those tested. The capillary shear experiments show a slight tendency to less disruption at lower shear rates and it is likely that, as with the whole cells, there will be a critical value of shear rate under which disruption drops off dramatically. This effect will be enhanced when considering the Kolmogoroff scale of microturbulence; it would not take a large decrease in shear forces below those estimated to reach the point where the KSM is a sufficient amount larger than the particle size that such particles will be entrained rather than disrupted. Particles travelling through such low shear regions in the feed zone will therefore suffer much less disruption than that observed in the mimic. It is only necessary for a small fraction of the feed to survive relative to the that processed in the mimic to alter drastically the grade efficiency curve. Because both power dissipation based forces and lock-nut based forces are sufficient to disrupt fully the precipitates; and the majority of the feed will be exposed to one or both of these forces be it in a hydro-hermetic or semi-hermetic feed, and at whatever throughput, the recovery obtained under whatever condition is likely to be broadly similar, and this was in fact observed.

This does create one inconsistency with experimental observations however. Even at the lowest throughputs tested the estimated shear rates will be high enough to cause serious disruption to the feed. The pilot-scale observations, however, show that at these throughputs the disruption does not appear to be so severe, with a good agreement being obtained with the theoretical curve through some of the d/d_c range (they diverge rapidly when the experimental function becomes negative indicating the presence of numbers of particles in the supernatant which were not present in the feed i.e. particle breakage). This is felt likely to be due to the recovery pattern in the centrifuge, however, rather than greatly reduced particle breakage. At low throughputs the separation performance of the centrifuge can increase above that theoretically possible because of the high residence times and unsteady flow patterns. Both clarification in the solids holding space and a certain amount of mixing in the disks leading to an increase above theoretical residence times will take place causing the over-performance of the machine (Rumpus, 1997).

Further evidence to support the results of the laboratory scale mimics comes from the much reduced negativity of the grade efficiency function at low values of d/d_c. This indicates that the supernatant did not contain large numbers of small particles which were not present in the sheared feed. This implies that the size distribution obtained is at least similar to that generated in reality by passage through the feed zone. In addition work is ongoing at UCL to examine the utility of such mimics in reducing the recovery obtained in a laboratory scale bottle centrifuge so that it approaches that of an industrial separator (when operated at the same Q/Σ value). This is proving successful with shear sensitive precipitates indicating that the majority of particles in the feed are broken to the same extent as in the mimics.

Therefore it seems likely that the laboratory scale mimics are to a large extent accurately reflecting the breakage in a centrifugal feed zone, and deficiencies in the grade efficiency assessment can be accounted for simply by considering that a small amount of the particles will not pass through regions of significant shear in the centrifuge itself. Again this is an indicator of the difficulty of using grade efficiency to examine particle disruption in a feed zone, as the function becomes highly sensitive when there are few particles of a given size class in the supernatant.

5.6 Conclusions

The laboratory scale mimics are not entirely successful at reproducing the disruption observed during disk stack centrifugation when processing either PEG precipitates or whole cell *E.coli*. However in both cases they are sufficiently accurate to obtain "order of magnitude" data about particle breakage and enzyme release likely to occur during such processing and as such could form the basis of a valuable rapid process development tool. The observed breakage is also consistent with the differing proposed disruption mechanisms occurring in both the semi-hermetic and the hydro-hermetic feed zones and their dependence on volumetric throughput. As such, in conjunction with the shear rate estimates derived for both the overall feed zones and the region of high shear adjacent to the lock-nut the laboratory scale mimics have

provided valuable information about the behaviour of the test systems exposed to such shear rates. This information is further discussed in the following chapter which provides a summary and discussion of observed disruption in the two designs of feed zone and the conclusions drawn about the mechanisms causing this disruption.

6.0 EFFECT OF SHEAR ON THE OPERATION OF HIGH SPEED DISK STACK CENTRIFUGES

The work discussed in Chapters 3, 4 and 5 reflects the behaviour of a disk stack centrifuge on two very different feed stocks; the relatively robust *E.coli*, and the much more shear sensitive PEG 8000 precipitates of yeast homogenate. The purpose of this chapter is to pull together the results and ideas contained within those chapters and to reflect on the implications for centrifugation operations in an industrial bioprocessing environment.

It is useful to recap on the sites in a standard semi-hermetic feed zone design disk stack centrifuge traditionally believed to be responsible for damage to particles entering the centrifuge. These are;

- Primary contact between the centrifuge and the feed suspension occurs at the lock-nut; this deflects the liquid flow which has been ejected from the feed pipe out onto the walls of the distributor. Owing to the short contact time little angular momentum is expected to be transferred; however, high radial shear rates will be generated at the surface of the lock-nut.
- The distributor is fitted with acceleration ribs which both aid acceleration and guide fluid through the channels at the base of the distributor foot and thus out onto the disks. However, intensive contact between the distributor and the feed suspension will occur here.
- The trajectory in between the distributor rib and the liquid surface, at the pressure side of the guiding rib.
- The inner wall of the distributor where axial shear can become predominant when flow rates are low resulting in a thin liquid layer.
- The conical distributor foot, where high shear rates may occur during flow through onto the disks.

(J.P. Van der Linden, 1987)

Of these it seems very clear from the results set out in Chapters 3 and 4 that some regions are more critical than others. Chief amongst the disruptive areas in the centrifuge feed zone appears to be the region above the lock-nut. Shear rate estimates for the lock-nut are outlined in Chapter 5. It is estimated that shear forces of up to $1x10^5$ s^{-1} will occur in a layer several mm deep above the lock-nut when the centrifuge is operated at full speed. The semi-hermetic (conventional design) feed zone ejects the feed suspension with no radial velocity directly onto the lock-nut and thus most of the feed suspension will experience such shear forces. However, a small percentage of the feed will not pass through this region and therefore will not be affected, as discussed in Chapter 5. As the volumetric throughput of the centrifuge increases the liquid hold up in the feed zone increases proportionally and at some point the lock-nut will become covered over (in the pilot scale machines used for this work this corresponded to a flow rate of approximately 150 Lh^{-1}). From this point on until complete flooding of the feed zone occurs (at approximately 400 Lh^{-1}) a decreasing proportion of the feed suspension will pass through this region of high shear forces and indeed the degree of disruption observed to whole cell *E.coli* decreases with throughput above this critical flow rate. The flooding of the lock-nut at all flow rates is what characterises the newer hydro-hermetic design feed zone and much lower disruption levels were observed for whole cells when utilising this feed zone.

The region above the lock-nut, however, has been shown not to be sufficiently disruptive to account for all the effects observed in the pilot scale machines. The interactions with the lock-nut cannot explain, for example, the increase in disruption of *E.coli* observed with increasing volumetric throughput up to the point the lock-nut becomes covered when utilising the standard design. Therefore it is obvious that another mechanism is at work. It seems likely from the results obtained that this again is a shear force, this time related to the power dissipated in the feed zone during the acceleration of the feed suspension to the rotational speed of the bowl. This takes place rapidly in a small volume and thus the shear rates generated can reach high levels (in the order of $3x10^4$ s^{-1}, see Chapter 5). Use of laboratory scale mimics suggests that this is not sufficiently high to account for the disruption seen with whole cell *E.coli*.

However, the shear rates estimated are based on the feed suspension being accelerated over the whole of the feed zone, something that in fact seems unlikely. The behaviour of the polyethylene glycol precipitates suggests that some particles are able to transit the whole feed zone without being disrupted (see Chapter 5). If the power is dissipated evenly over the entire feed zone this is clearly not possible. However, it is entirely possible that the majority of the acceleration will occur in the top section of the distributor which will increase the power dissipated per unit volume and thus the shear forces generated. The laboratory scale mimics suggested that an increase in shear rates to a level of $1x10^6$ s^{-1} is sufficient to cause a large increase in the disruption to whole cells. Further, a percentage of the feed suspension will still be accelerated more gently over a longer time and thus a small number of particles will still not be disrupted. Such behaviour was observed with PEG 8000 precipitates of yeast homogenate (see Chapters 4 and 5).

It is possible that the acceleration ribs present in the semi-hermetic feed zone play a small role in the disruption of particles in the feed suspension. However, it seems likely that this effect is insignificant when compared to the disruption caused by the shear forces generated in the feed zone.

No disruption to whole cells occurred during the discharge process. Cells that had been damaged by passage through the feed zone, however, retained both periplasmic and intracellular enzymes which were released in the solids holding space and thus exited with the solids stream. This is due to the nature of disruption occurring in the feed zone, with the cell wall becoming more leaky rather than the majority of cells being totally disrupted as occurs in a high pressure homogeniser.

The results of the work contained in this thesis offer an important insight into the operation of high speed disk stack centrifuges in an industrial setting. Traditionally a volumetric throughput is set which allows acceptable clarification of the feed stream. This is usually obtained by pilot scale trials where a sample is processed and the flow rate reduced until a solids or optical density based assay indicates good recovery (typically 95% or above for cell harvest with lower recoveries acceptable for difficult separations such as shear sensitive precipitates). However the work contained within

this thesis suggests that this is not always a sensible approach. Disruption of whole cells leads, in most cases, to yield loss. Because of the reduced degree of disruption occurring at high flow rates where the lock-nut of the centrifuge is covered by a liquid layer there may be cases where a reduced level of separation is acceptable because the reduced disruption and thus yield loss is more significant than the loss due to the reduced efficiency of the unit operation. A similar effect is obtained by reducing the rotational speed of the centrifuge; this will again reduce the efficiency of separation if the volumetric throughput is held constant but will also decrease disruption. It seems clear that for whole cell harvest steps at least, a more thorough investigation of the interaction between rotational speed, flow rate and disruption of the feed stream could yield a more efficient process and even extend the use of disk stack centrifuges to applications where they are currently considered too harsh. Of course, the best solution is to retrofit clarifiers with a hydro-hermetic feed zone. These however, are not currently available for machines larger than pilot scale.

Although operating in the manner suggested above reduces disruption to relatively strong whole cells, such measures did not prove sufficient to preserve the fragile PEG 8000 precipitate particles. The results contained in Chapter's 4 and 5 indicate that these are sufficiently weak that exposure to either of the shear based disruptive mechanisms proposed was enough to reduce the feed stream back to primary particles, thus making recovery much harder. The only exception to this was when the rotational speed of the centrifuge was severally reduced. In an industrial setting, however, this would necessitate a severe reduction in volumetric throughput which may not prove economic. Even this, however, serves to illustrate the point that centrifugation operations cannot be evaluated simply in terms of Sigma theory. This would suggest that if recovery is unacceptable one merely reduces the throughput until an acceptable recovery is obtained, and takes no account of the disruption to such particles which makes them harder to recover.

Finally although the laboratory scale mimics were not entirely successful in reproducing the disruption observed in the pilot scale machines, they did prove quite adequate in creating an "order of magnitude" estimate if operated in a sensible manner. Such estimates could be refined with the use of more sensitive computational methods

to calculate the shear forces present in the feed zone (see future work, Chapter 7). This has two very important applications. Firstly it would be useful to take a small amount of material and assess the likely disruption, and it's effect on process yield, at an early stage in the laboratory as an aid to deciding whether a disk stack centrifuge is really the appropriate unit operation for a task. Secondly, and potentially more importantly, as an aid to scale down. Much work has been conducted over the last decade working on the comparison of laboratory scale "bottle" centrifuges with an industrial separator. Sigma theory predicts that the appropriate calculations and scaling factors are used it is possible to predict to a high degree of confidence the performance of the industrial machine from a trial in the laboratory. This technique works well with shear insensitive materials (such as latex beads). However real feed stocks do not behave like latex particles. Any disruption to the feed suspension in the industrial separator will result in particles which are harder to recover than those used in the laboratory, and thus the laboratory scale results usually significantly overpredict the actual recovery. Use of a laboratory scale mimic to pre-shear a feed suspension before the bottle centrifuge is employed will correct this problem, and indeed, with precipitate suspensions should prove very successful as the particles tend to break to the same size distribution whenever a shear force of greater than a critical level is employed. Utilising this technique could therefore truly improve the application of scale-down to centrifugation and thus speed process development significantly.

7.0 FUTURE WORK

The further work which could usefully be pursued falls into two categories; that centred around the centrifuges themselves and work which could improve the accuracy of the lab-scale mimics.

- The shear rate estimates contained within this thesis are the best which can be made given the information currently available about the dynamic system that occurs within the feed zone of a high speed disk stack centrifuge. However, as was discussed in Chapter 5 the inaccuracy of these estimates, and particularly the volume over which the power is dissipated within the feed zone, is likely to be the greatest source of error in the work presented. Modern computational techniques such as Computational Fluid Dynamics (CFD) could allow these estimates to be greatly refined. CFD breaks a given geometry down to a grid of very small elements and solves the fundamental Navier Stokes equations iteratively until a cohesive solution for the entire system is obtained. Although commercially available codes cannot currently deal with a system as complex as a centrifuge feed zone, particularly with the particle tracking which would be essential to make use of such results, it cannot be long before this changes. The use of such a code would then allow estimates of shear rates and particle tracks to be made with a high degree of confidence.
- The study of the effect of the pilot scale centrifuges on a feed solution should be extended to include other centrifuge types and particularly the multichamber centrifuge. This is similar to a disk stack design in that again, under most operating conditions, first contact between the machine and the feed suspension will be at the lock-nut. A comparison of the degree of disruption should allow increased confidence in the theory of the lock-nut being key in damage observed.
- The study should be extended to include a third feed stock with a strength between that of *E.coli* and PEG 8000 precipitates. Preferably a suspension with a known yield stress should be used which will allow a more direct estimation of the forces experienced within feed zone to be made.

- The new technique of micromanipulation, developed at the University of Birmingham, promises the opportunity to measure the yield stress of whole cells. This information, in conjunction with the pilot scale experimentation and a CFD model should allow a precise estimate of the disruptive forces present in the centrifuge feed zones to be made and the mechanism of disruption to be confirmed.
- The "spinning disk" laboratory scale mimic has shown much promise in the area of yield loss prediction and as an aid to scale down. This system needs to be refined. The use of a variable speed motor to more precisely mimic the centrifuge lock-nut, together with a continuous mode of operation, will allow the mimic to more closely match the actual situation in the centrifuge.
- Scale down studies should be conducted comparing a laboratory scale bottle centrifuge to a process scale machine utilising the spinning disk mimic to "pre-shear" the feed to the lab centrifuge. This will confirm the utility of this approach as an aid to process design.

APPENDIX 1 CALCULATION OF SIGMA FACTOR

For a Disk Stack Centrifuge

$$\Sigma = \frac{2}{3g}\pi Z_s \omega^2 \cot\theta\left(R_0^3 - R_i^3\right)F_1$$

where ω = angular velocity (rad s^{-1} = 2π * revolutions per second)

Z_s = number of disks in stack (-)

θ = half the conical disk angle (degrees)

R_0 = outer disk radius (m)

R_i = inner disk radius (m)

g = acceleration due to gravity (m s^{-2})

and F_1 is given by;

$$F_1 = 1 - \frac{3Z_c b_c}{4\pi R_0} \cdot \frac{\left(1 - \left[\frac{R_i}{R_0}\right]^2\right)}{\left(1 - \left[\frac{R_i}{R_0}\right]^3\right)}$$

where F_1 = Σ correction factor for disk spacer caulks (-)

Z_c = number of caulks per disk (-)

b_c = caulk width (m)

The table overleaf shows sigma factors for the SAOOH, CSA-1 semi-hermetic and CSA-1 hydro-hermetic disk stack centrifuges. Note, in the case of the CSA-1 these are calculated at maximum rotational speed.

Parameter	SAOOH semi-hermetic DSC	CSA-1 hydro-hermetic DSC	CSA-1 semi-hermetic DSC
g ($m\ s^{-2}$)	9.81	9.81	9.81
Z_s (-)	37	47	43
RPM	10000	9810	9810
ω ($rad\ s^{-1}$)	1050	1030	1030
θ (deg)	38.5	38.5	38.5
R_0 (m)	0.0485	0.055	0.055
R_i (m)	0.0261	0.0261	0.0261
Z_c (-)	6	6	6
b_c (-)	0.005	0.006	0.006
F_1 (-)	0.875	0.864	0.864
Σ (m^2)	**919**	**1710**	**1565**

Table A1.1: The dimensions of the semi- and hydro-hermetic centrifuge bowls used in this study

NOTE: if comparing a disk stack centrifuge to another machine of a different type it is necessary to use an empirically-derived correction factor for non-ideal flow, benchmarked on a laboratory bottle centrifuge. These are 0.9 for a tubular bowl, 0.4 for a disk stack and approx. 0.85 for a multichamber.

APPENDIX 2 CALCULATION OF PRECIPITATE PARTICLE DENSITY

The equation governing the settling of particles in the Brookhaven BI-DCP 1000 photosedimentometer is given by;

$$\Delta\rho = \frac{18\mu \ln\left(R_d / R_s\right)}{\omega^2 d^2 t}$$

where $\Delta\rho$ = density difference between particle and spin fluid (Kg m^{-3})

μ = spin fluid dynamic viscosity (N s m^{-2})

R_d = radius of detector (m)

R_s = radius of injection of sample (m)

ω = angular velocity (rad s^{-1})

d = diameter of particle (m)

t = time to settle to detector radius (s)

The disc used with the instrument had radii R_d = 0.04822m & R_s = 0.04281m when using a spin fluid volume of 15 mL.

The spin fluid (8% PEG 8000, 5% NaCl, 0.1M KH_2PO_4, 5% Sucrose solution, pH 6.7) had a density of 1078 Kg m^{-3} (measured using a specific gravity bottle), and a viscosity of 0.0046 N s m^{-2}. The instrument was operated at rotational speeds in the range 1500-2500 rpm.

Cut/boost fluid was 1 mL as above without the addition of 5% sucrose.

1 mL of sample was loaded.

By using the cumulative fraction over particle size plot and the cumulative fraction under sedimentation time plot, both given in Chapter 4, to give the sedimentation time

and diameter of particle at each fraction, it is possible to calculate density for each fraction using the above equation, and thus obtain a particle size/density relationship for calculation of critical particle diameter, d_c.

APPENDIX 3 CONDITIONS OF PRECIPITATION

Bulk average density of precipitation suspension = 1084 Kg m^{-3} (specific gravity method)

Bulk viscosity of precipitate suspension at $G^* = 100\ s^{-1} = 12$ N s m^{-2} (measured using cup and bob viscometer)

Parameter	Pilot-scale reactor		Laboratory reactor	
	mixing in	ageing	mixing in	ageing
Volume (m^3)	0.042	0.042	0.00007	0.00007
Diameter impeller (m)	0.15	0.15	0.018	0.018
Diameter vessel (m)	0.5	0.5	0.045	0.045
Impeller speed (RPM)	220	93	880	380
time (min)	5	30	5	30
Torque (N m)	0.736	0.132	$2.93x10^{-4}$	$5.46x10^{-5}$
Shear rate (s^{-1})	183	50	179	50
Camp No.	$5.50x10^4$	$9.07x10^4$	$5.38x10^4$	$9.16x10^4$

Table A3.1: Dimensions of the reactors used during the precipitation experiments described in this thesis

The precipitation was carried out at an overall Camp number of $1.4x10^5$.

APPENDIX 4: DEFINED MEDIA RECIPE FOR α-AMYLASE FERMENTATION.

The recipe used for batch fermentation of *E.coli* JM 107 pQR 126 was that developed by Turner (1993) and modified by Fisher (1997) with the addition of yeast extract to some runs.

Component	Supplier	Grade	Concentration (gL^{-1})
$(NH_4)_2SO_4$	Sigma-Aldrich Company	>99%	10
NaCl	Sigma	>99.5%	2.5
Na_2HPO_4	Sigma	>99%	2.16
KH_2PO_4	Sigma	>99%	0.64
$FeSO_4.7H_2O$	Sigma	>99%	0.2
Citric acid	Sigma	-	0.2
trace element soln.*	-	-	1 mL^{-1}
thiamine	Sigma	-	0.05
Kanamycin a	Sigma	-	0.01
$MgSO_4.7H_2O$	Sigma	-	0.2
Polypropylene Glycol (PPG)	Merck Ltd.,		0.1 mL
glycerol	Merck Ltd.	-	30
Yeast Extract	Bovril	-	5-10

Trace Element Solution

Component	Supplier	Grade	Concentration (gL^{-1})
$CaCl_2$	Sigma	97%	10
H_3BO_3	Sigma	99%	4
$MnCl_4.4H_2O$	Sigma	-	2
$ZnSO_4.7H_2O$	Sigma	-	2
$CuSO_4.5H_2O$	Sigma	99%	0.4
$CoCl_2.6H_2O$	Sigma	-	0.4
$NaMoO_4.2H_2O$	Sigma	>99%	0.2

Table A4.1: Fermentation media used for the defined media fermentation of *E.coli* JM107 pQR126 presented in this work

Note: Yeast extract added only to some fermentation's at varying concentrations.

Media was made up as follows:

$(NH_4)_2SO_4$, NaCl, Na_2HPO_4, KH_2PO_4 and trace element solution were dissolved together in a small volume of the total media (approximately 5%). $FeSO_4.7H_20$ and Citric acid were dissolved together in a similar volume, and the two solutions added to the fermenter. The media volume was then adjusted to the final required volume minus both the glycerol solution volume and the inoculum volume, with R.O. quality water and sterilised in situ. Glycerol and $MgSO_4.7H_2O$ were made up together and sterilised in an autoclave. Kanamycin A and Thiamine were dissolved in 20 mL of R.O. quality water and filter sterilised into the glycerol solution, which was then added to the fermenter immediately prior to inoculation.

APPENDIX 5: SPHEROPLAST PRODUCTION AND STRENGTH TESTS

A5.1 Introduction

Although the centrifugation studies described in this thesis are limited to whole cell *E.coli* JM107 pQR126 and polyethylene glycol precipitates of yeast homogenate, some initial work was carried out to characterise the strength of spheroplasts formed from wild-type *E.coli* (strain JM107) in order to assess whether or not they would provide a suitable test system. These results are presented within this appendix.

As described in Chapter 1, a spheroplast is formed by chemical/biological treatment of the cell, and usually an osmotic shock step, causing the outer membrane to be stripped off and the periplasmic contents released into the surrounding liquid. The inner (cytoplasmic) membrane remains intact containing the majority of the protein in the cell and can be removed either by centrifugation or microfiltration. It is this unit that is known as a spheroplast. Thus the task of product purification is greatly simplified. It is such selective release that forms the basis of the advantages of periplasmic expression of product in a genetically modified organism.

As has previously been discussed (Chapter 1 and Chapter 6) it is believed that the structure within the *E.coli* cell wall responsible for it's strength and rigidity is the peptidoglycan layer, an elastic heteropolymer which exists as a gel-like layer within the periplasmic space. The chemical treatments involved in the formation of spheroplasts typically also need to break-up the peptidoglycan structure or the periplasmic contents may be trapped within it, and thus will not be released. The peptidoglycan layer is believed to be closely associated with the outer membrane. This means that after the selective disruption has been carried out the remaining spheroplasts are likely to be structurally very weak (compared to the original cells) and thus very susceptible to the shear forces developed during the separation process or processes necessary to remove them from the product (liquid) stream. Any disruption of spheroplasts caused during such a separation process will release their contents back into the product stream, thus

negating the whole expression strategy. Therefore it is desirable to quantify the damage that the shear forces developed in such a recovery process, particularly that of disk stack centrifugation, are likely to inflict. Furthermore, it was felt that as the spheroplasts were likely to be significantly weaker than the original whole cells a spheroplast suspension may form a better indicator of changing levels of disruption in a disk stack centrifuge than the cells themselves.

To this end it was decided to subject a spheroplast suspension to a range of different shear rates generated within the Instron capillary shear rheometer (see Chapter 5 for a full description of the apparatus) and observe the effects.

A5.2 Materials and Methods

A5.2.1 Shake Flask Culture (*E.coli* JM107)

40% w/v glycerol stocks containing *E.coli* JM107 were supplied by UCL's Department of Biochemistry and Molecular Biology and stored at -70^{0}C to be used as the cell line for this work. 2.0 L shake flasks were prepared with 500 mL of nutrient broth (Oxoid No.2, Oxoid Ltd., UK). These were inoculated direct from glycerol stocks with 1 mL of stock solution. This was then grown up in an orbital incubator (New Brunswick Scientific Ltd., UK) for 20 hours at 37^{0}C and an agitation rate of 200 rpm.

A5.2.2 Preparation of Spheroplasts

There are several different techniques for the selective removal of the outer membrane and release of the periplasmic contents. The system chosen for this work was that developed by French (1993) for use with *E.coli* JM107 pQR126 expressing α–amylase to the periplasmic space, which has been proved to work adequately both as a laboratory technique and at process scale (300L). This method involves the pre-

treatment of the cell wall with EDTA (to disrupt the outer membrane) and lysozyme (to attack the peptidoglycan backbone) in the presence of high concentrations of sucrose which places the cell under an osmotic pressure resulting in dewatering. After an incubation period cold water is added to the suspension resulting in a change in osmotic pressure which causes the cell to take up water extremely rapidly. It is this rapid expansion that the cell wall, weakened by the chemical and biological agents, is not able to withstand and the outer membrane and peptidoglycan layer "pop", releasing the contents of the periplasm into the lysis mixture. This process is explained in more detail in Chapter 1. The precise protocol adopted is given below.

The cells from the shake flasks were harvested in a Beckman J2-M1 laboratory scale centrifuge developing 6500 xG for 10 minutes. Throughout the spin cooling was used to maintain a constant temperature of 1^0C. The resulting pellets were re-suspended in a volume of lysis buffer equal to 20% of the original volume of cell broth. The lysis buffer is defined in Table A2.1 below, adjusted to pH 7.5 and at a temperature of below 5^0C.

Component	Supplier and grade	Concentration
Hen egg white lysozyme	Sigma-Aldrich Company, >98%	500 μg mL^{-1}
EDTA	BDH, Anal R	1 mM
sucrose	Sigma, >99%	40% w/v

Table A5.1 Components and concentration of cell lysis buffer used for the preparation of spheroplasts and release of the periplasmic contents (French, 1993).

The suspension was gently agitated using a magnetic stirrer for 15 minutes. After this time an equal volume of ice cold HPLC grade water (produced by a Maxima ion exchange unit, Elga Ltd., UK) was added batchwise to the suspension which was mixed and then left stationary for a further 15 minutes.

A5.2.3 Capillary Shear of Spheroplasts

Details of the Instron capillary shear rheometer and it's operation are given in Chapter 5. Each condition was repeated in triplicate to ensure the accuracy of the results.

A5.2.4 Biological Assays

The cytoplasmic enzyme glucose-6-phosphate dehydrogenase was used to measure disruption of spheroplasts in conjunction with the Bio-Rad^{TM} total protein assay. Full details of these assays can be found in Chapter 2.

A5.2.5 Homogenisation

To establish the levels of enzyme and protein equivalent to 100% disruption of spheroplasts a sample was homogenised at 600 bar pressure, 1 pass in an APV Lab 40 laboratory scale homogeniser (APV Manton-Gaulin, UK). This technique was identical to that employed with whole cells, and full details can be found in Chapter 2.

A5.3 Results

All shake flask cultures achieved a similar dry cell weight of approximately 4.4 gL^{-1}. All such cultures entered stationary phase due to oxygen depletion before harvesting and chemical lysis/osmotic shock to form spheroplasts. Therefore it was assumed that all spheroplast suspensions subjected to shear testing were of a similar strength.

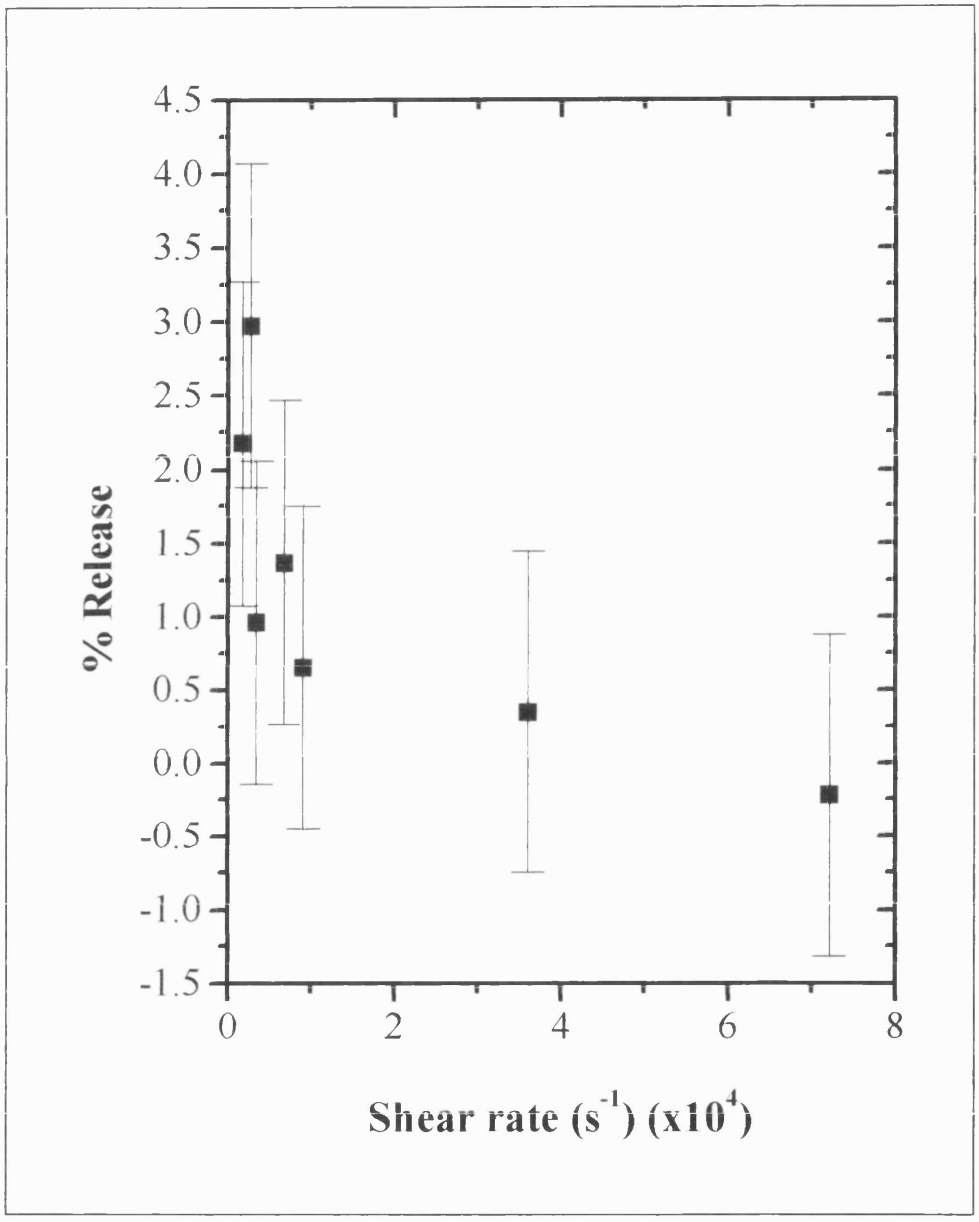

Figure A5.1: Release of protein from a spheroplast suspension in a capillary shear rheometer as a function of shear rate. Bio-Rad™ Total Protein assay used. 0% disruption defined as protein concentration (mg mL^{-1}) in un-sheared sample, 100% disruption defined as protein concentration (mg mL^{-1}) in homogenised sample (1 pass, 600 bar).

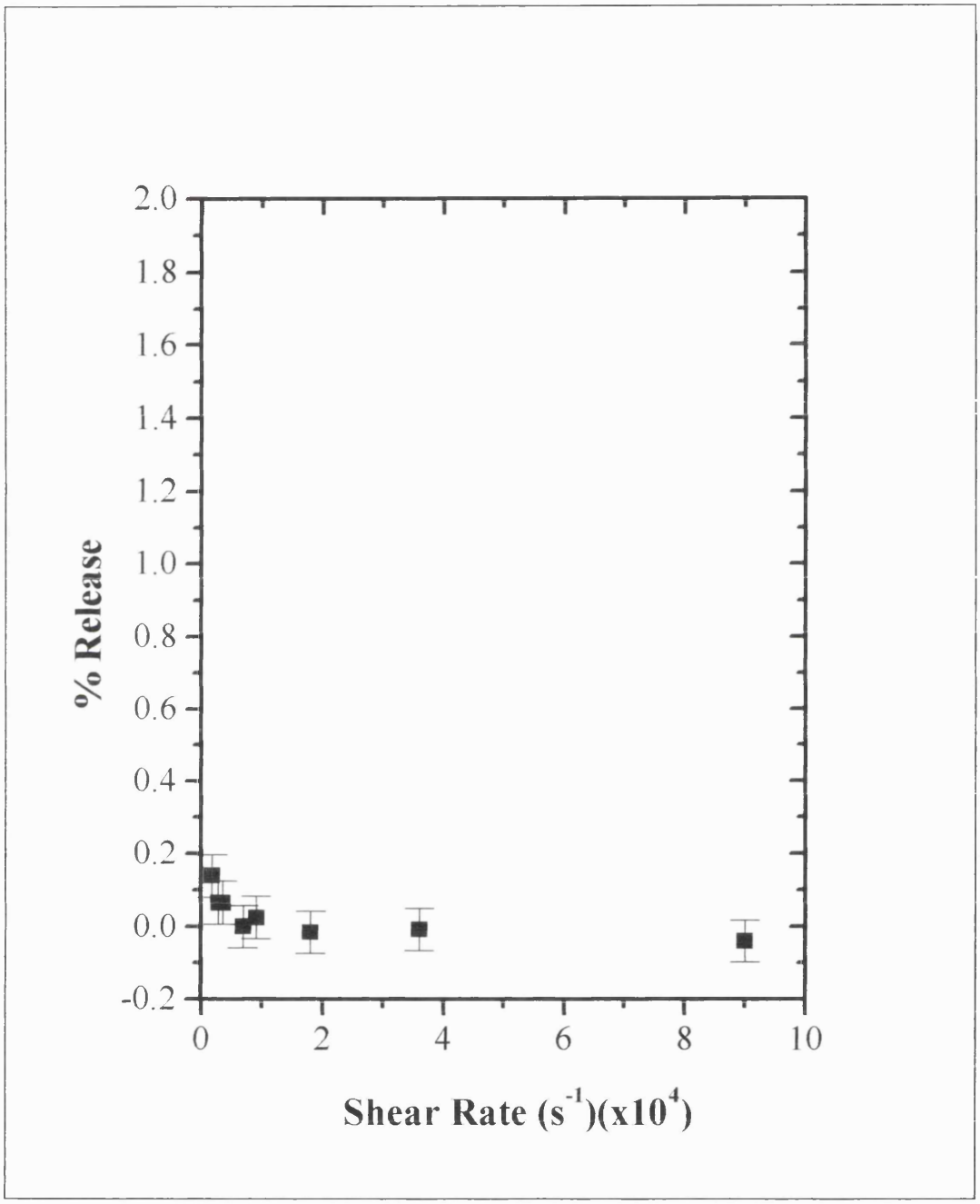

Figure A5.2: Release of G6-PDH from a spheroplast suspension in a capillary shear rheometer as a function of shear rate. 0% disruption defined as enzyme concentration (IU mL^{-1}) in un-sheared sample, 100% disruption defined as enzyme concentration (IU mL^{-1}) in homogenised sample (1 pass, 600 bar).

The proceeding figures show the release of both protein and the intracellular enzyme G-6-PDH obtained when exposing a spheroplast suspension to a uniform shear field in the range $1x10^3s^{-1}$ to $9x10^4s^{-1}$. Because of the design of the shear rheometer these shear rates correspond to variable residence times in the range 0.65s to 0.01s. All points are the mean of 3 observations. The graphs clearly show that no appreciable disruption occurred to the spheroplasts through exposure to the levels of shear tested. A trial at a constant shear rate of $9x10^4s^{-1}$ with residence times varied between 0.003 and 0.01 s was also conducted, and again no significant difference in release was observed.

The major difference between the two plots is the lower release levels observed utilising G-6-PDH as a marker than when measuring total protein levels. As a spheroplast is a single compartment system this was not expected. This finding corresponded with a higher standard error in the protein measurements than the G-6-PDH so was not statistically significant. However, as a substantial part of the work contained within this thesis relied on being able to measure cellular damage through biological rate assays, it was felt that it was important to confirm that enzyme activity was not significantly effected by exposure to shear in the rheometer. Therefore a standard solution of G-6-PDH (Sigma-Aldrich Company, UK) was exposed to a range of shear rates in the rheometer and the change in activity measured. The results are shown in Figure A5.3 overleaf.

The plot shows the assayed G-6-PDH activity after a stock solution of 0.06 IU mL^{-1} G-6-PDH was sheared in the Instron capillary shear rheometer at rates in the range $1x10^3s^{-1}$ to $9x10^4s^{-1}$. Again there was no appreciable difference indicating that the enzyme was in no way inactivated by exposure to these levels of shear.

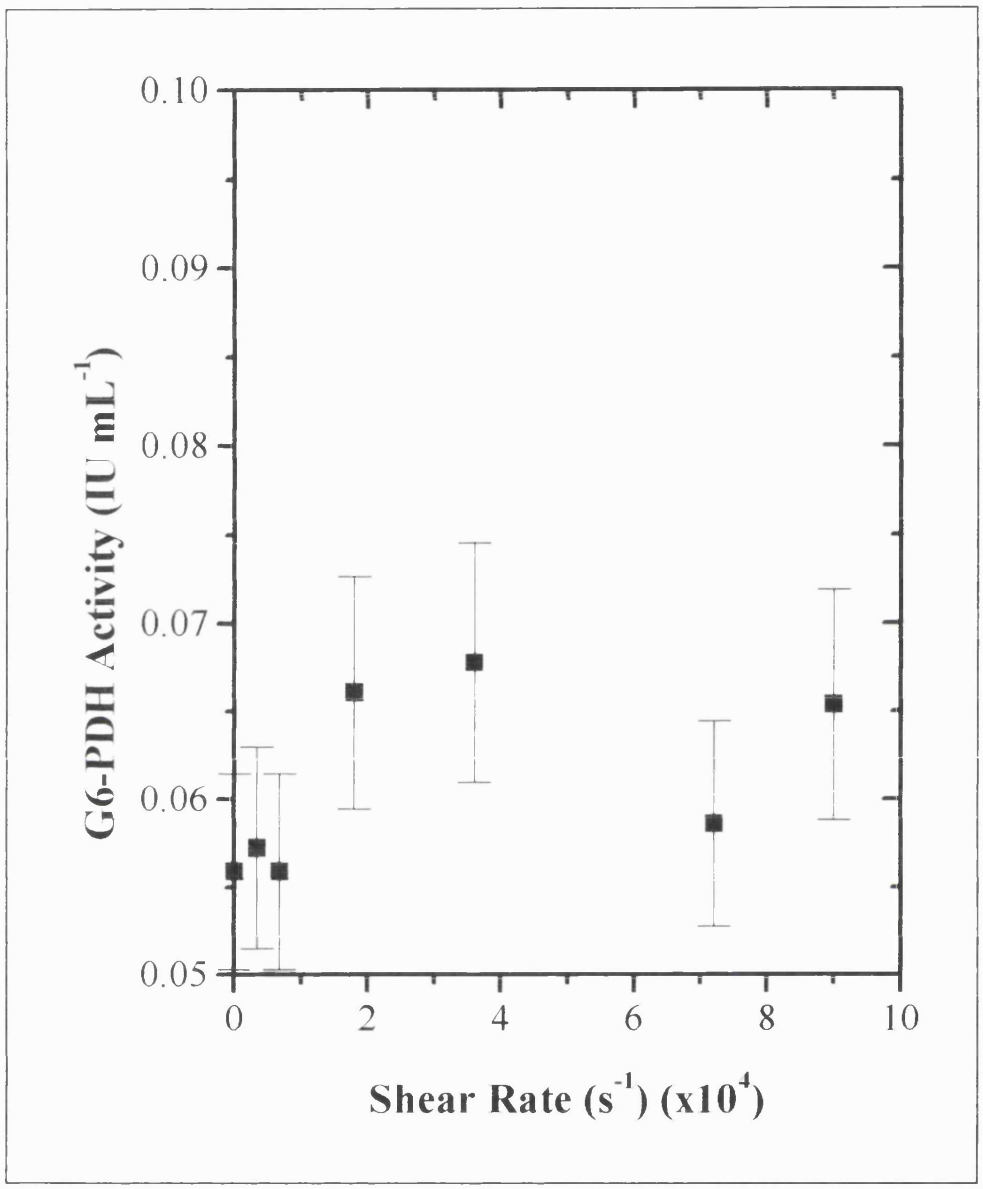

Figure A5.3: G-6-PDH activity after exposure to shear in the Instron capillary shear rheometer. Feed liquid 0.06 IU mL^{-1} G-6-PDH (Sigma-Aldrich Company, UK)

The final investigations undertaken were to assess both the stability of spheroplasts in a stirred tank and the efficiency of the spheroplasting process itself.

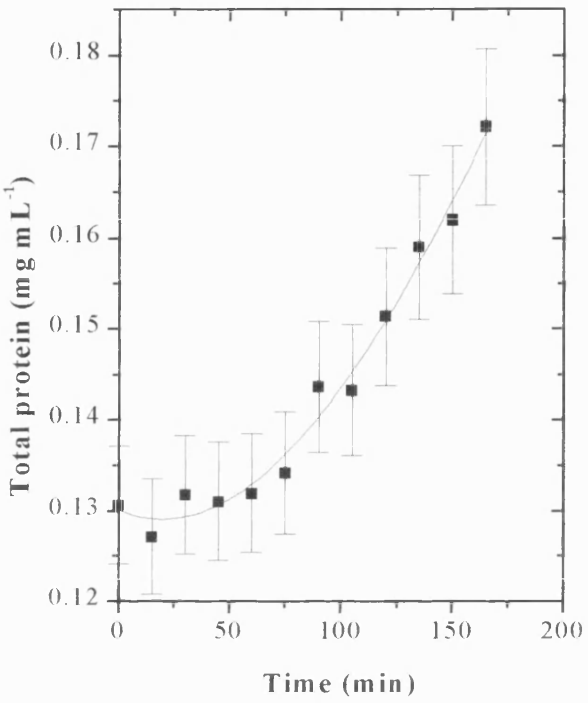

Figure A5.4: Increase in total protein levels with time when a spheroplast suspension is agitated in a stirred reactor. Bio-Rad™ Total Protein assay used. Total protein in suspension when fully disrupted (1 pass 600 bar through a high pressure homogeniser) was 0.65 mg mL⁻¹.

Figure A5.4 above shows the degradation of spheroplasts with time when stirred in a laboratory scale stirred reactor fitted with a Rushton Turbine at a shear rate of 50 s^{-1}. This was the minimum shear rate necessary to keep the suspension well mixed and thus corresponded to that which would be needed during any centrifugation trial. Although there clearly was some degradation over the time period tested it was not significant when compared to the total protein levels obtained after disrupting the spheroplasts totally in a high pressure homogeniser with the maximum release levels observed corresponding to 8% of the total.

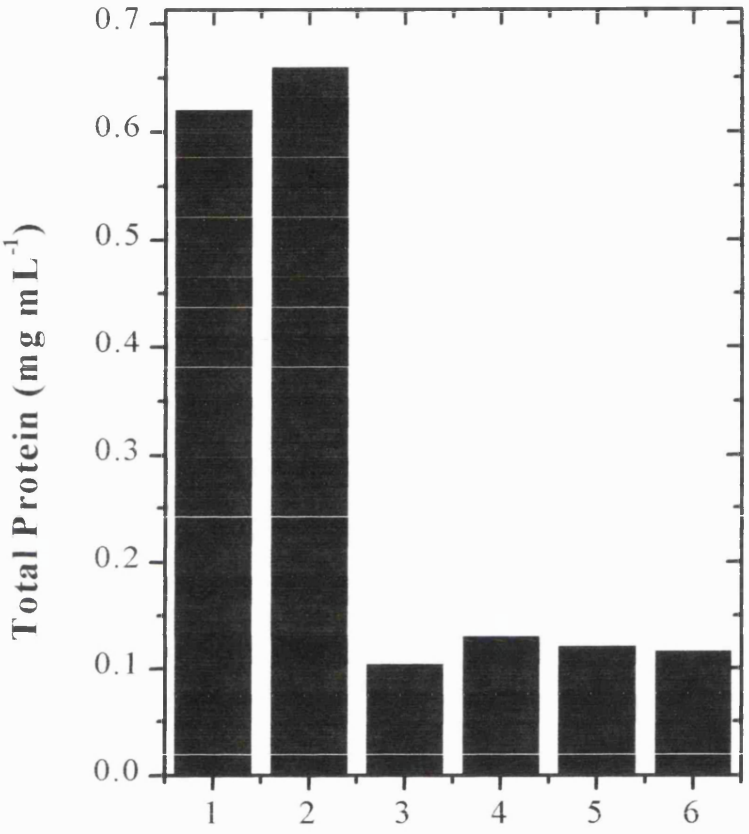

1=spheroplast homogenate (1 pass 600 bar)

2=spheroplast homogenate (2 pass 600 bar)

3=lysis buffer

4=osmotically shocked cells

5=original broth

6=centrifuge supernatant (6250g, 15min)

Figure A5.5: Total Protein levels throughout spheroplast process (measured using Bio-Rad™ Total Protein Assay)

Figure A5.5 shows the change in total protein levels observed throughout the spheroplasting process. It can be seen that the background protein present in the cell broth exited with the supernatant after the centrifugation step used to harvest the whole cells. The lysis buffer itself contained significant levels of protein which was as expected (it contained the enzyme lysozyme). There was very little increase in total protein levels observed after the spheroplasts were formed (this figure has been adjusted to take the change in volume during osmotic shock into account). This suggested either that the periplasm contained very little protein or that the spheroplasting process was relatively inefficient and significant numbers of cells remained intact.

The efficiency of spheroplast formation was investigated in a final experiment where a suspension of spheroplasts was Gram stained; intact Gram-negative *E.coli* cells appeared colourless/red when examined under a microscope, whereas spheroplasts behaved as Gram-positive organisms, and stained a violet colour. Upon counting cells on a slide it was discovered that approximately 76% of cells had formed spheroplasts, leaving 24% intact. Although this clearly indicates an un-optimised process step the percentage of un-effected cells is not sufficient to account for the small increase in protein levels observed during the spheroplasting process. This means that in the wild type *E.coli* here investigated relatively little protein was resident in the periplasm.

A5.4 Discussion

The results obtained when shearing the spheroplast *E.coli* cells in the shear rate range $1x10^3s^{-1}$ to $9x10^4s^{-1}$ clearly show that almost no damage is inflicted on the spheroplasts. Disruption was measured using both G-6-PDH and total protein and did show some variation, with protein analysis indicating between 0% and 3% release and G-6-PDH levels an order of magnitude lower. However, at the very low levels of both protein and enzyme being measured these differences were not statistically significant.

The lack of breakage contrasts strongly with the traditional view of the Gram-negative cell envelope obtaining all it's mechanical strength from the peptidoglycan layer, which is of course removed in the spheroplast preparation. However, mechanical rigidity should not be confused with resistance to disruption at mild shear levels. The cytoplasmic membrane offers little or no permeability barrier, and as such will allow the spheroplast to deform and lose liquid when subjected to a shearing force. In addition the spheroplast is still in an environment which is osmotically stronger than that in which it was grown. Although over time it will adjust to this, it is likely that it is still in a flaccid state when subjected to shear, and this will enhance the spheroplast's ability to resist disruption. A good analogy is to compare the spheroplast to a squash ball; it's at a relatively low internal pressure and thus deforms upon squeezing or impact. This is a similar finding to that published by Milburn and Dunnill (1994) who conducted high pressure homogenisation trials on yeast which had been frozen and then thawed. They showed that the cells became up to four times harder to disrupt with repeated freeze/thaw cycles. They attributed this to the semi-permeabilising of the cell membrane by the freeze/thaw process, which in turn left flaccid deformable cells which were resistant to disruption. A similar mechanism is probably occurring with the spheroplasts.

The spheroplast stability test showed the beginning of breakage after 75 minutes. The levels of protein released, however, were minimal compared to the protein levels contained in the suspension with an increase of only 0.05 mg mL^{-1} observed against approximately 0.65 mg mL^{-1} total protein contained within the spheroplasts.

When monitoring the release of total protein during the spheroplast process it was observed that nearly all free protein was removed during the original cell harvest. However, when the lysis mixture was assayed which should contains 0.5 mg mL^{-1} of lysozyme, only 0.1 mg mL^{-1} was detected. A subsequent study conducted filling plastic Eppendorf containers with lysis buffer to different volumes and then assaying for total protein showed a constant result, indicating that there were no grounds for believing that the lysozyme became associated with the container. Other work at UCL has,

however, indicated that the Bio-Rad™ total protein assay, particularly with a bovine albumin calibration curve, may not detect lysozyme accurately, and this is likely to account for the missing protein in the lysis buffer (Fisher, 1997).

Only a slight increase in total protein was observed when forming the spheroplasts indicating little protein was released. This was as expected as the majority of protein in a cell is generally cytoplasmic rather than periplasmic. Therefore, little protein is available for release when the outer membrane is removed, particularly in low cell density suspensions such as those used during this work.

The spheroplasting process was found to be adequately efficient, with approximately 76% of cells forming spheroplasts during the process.

A5.5 Conclusions

The spheroplasting process developed by French (1993) was found to perform adequately, with approximately 76% of cells releasing their periplasmic contents during the step. This corresponded to only a small increase in protein as the periplasmic space of *E.coli* contains little of the total protein associated with the cell.

The spheroplasts showed no significant breakage upon exposure to uniform shear fields approaching those estimated to be found in the feed zone of a disk stack centrifuge. This was contrary to expectations as a spheroplast has had it's peptidoglycan layer removed. The lack of breakage was attributed to the flaccid state of the spheroplasts after the osmotic shock process used to form them which allowed them to deform rather than rupture upon exposure to shear.

Because the spheroplasts were not found to be shear sensitive it was decided not to extend the study to centrifugation trials.

APPENDIX 6: THE INSTRON FOOD TESTER

Cross sectional area of capillary barrel $$a = \left(\frac{\pi . D_{ib}}{4}\right)^2 \quad \textbf{(A6.1)}$$

where D_{ib} = barrel internal diameter (9.54mm)

Suspension flow rate $$Q = X_i . a \quad \textbf{(A6.2)}$$

where X_i = drive speed ($m\ s^{-1}$)

Therefore Reynolds number in capillary Re_c is given by:

$$Re_c = \frac{\rho . Q . d_{ic}}{\mu . a} \quad \textbf{(A6.3)}$$

where ρ = density of suspension ($kg\ m^{-3}$)

d_{ic} = internal diameter of capillary (m)

μ = viscosity of solution ($N\ s\ m^{-2}$)

Mass average shear rate in capillary $$G_c^* = \left(\frac{8}{15}\right)\gamma_w \quad \textbf{(A6.4)}$$

where $$\gamma_w = \frac{4.Q}{\pi . R_c^3} \quad \textbf{(A6.5)}$$

γ_w = shear rate at capillary wall (s^{-1})

R_c = internal radius of capillary (m)

Residence time $$T_i = \frac{\pi . R_c{}^2 L_c}{Q} \quad \textbf{(A6.6)}$$

where L_c = length of capillary (m)

The above equations were used to obtain shear rates, Reynolds numbers and residence times available using the capillary shear rheometer. Equations used are those of Bell (1982).

Capillaries were available of internal diameter 0.1 mm, 0.15 mm, 0.2 mm, 0.33 mm and 0.575 mm. Capillary lengths of 30 mm, 50 mm, 75 mm, 100 mm, 150 mm and 200 mm were used. The Instron food tester was capable of drive speeds from 0.833 mm s^{-1} to 8.33 mm s^{-1}. This corresponded to defined shear rates of 1.7 x 10^3 s^{-1} to 1 x 10^6 s^{-1}. The capillary lengths available allowed a residence time range of 0.65 s to 0.02 s at the lowest shear rates, reducing to 0.0009 s to 0.006 s at the highest shear rate.

APPENDIX 7: CENTRIFUGE FEED ZONE DIMENSIONS

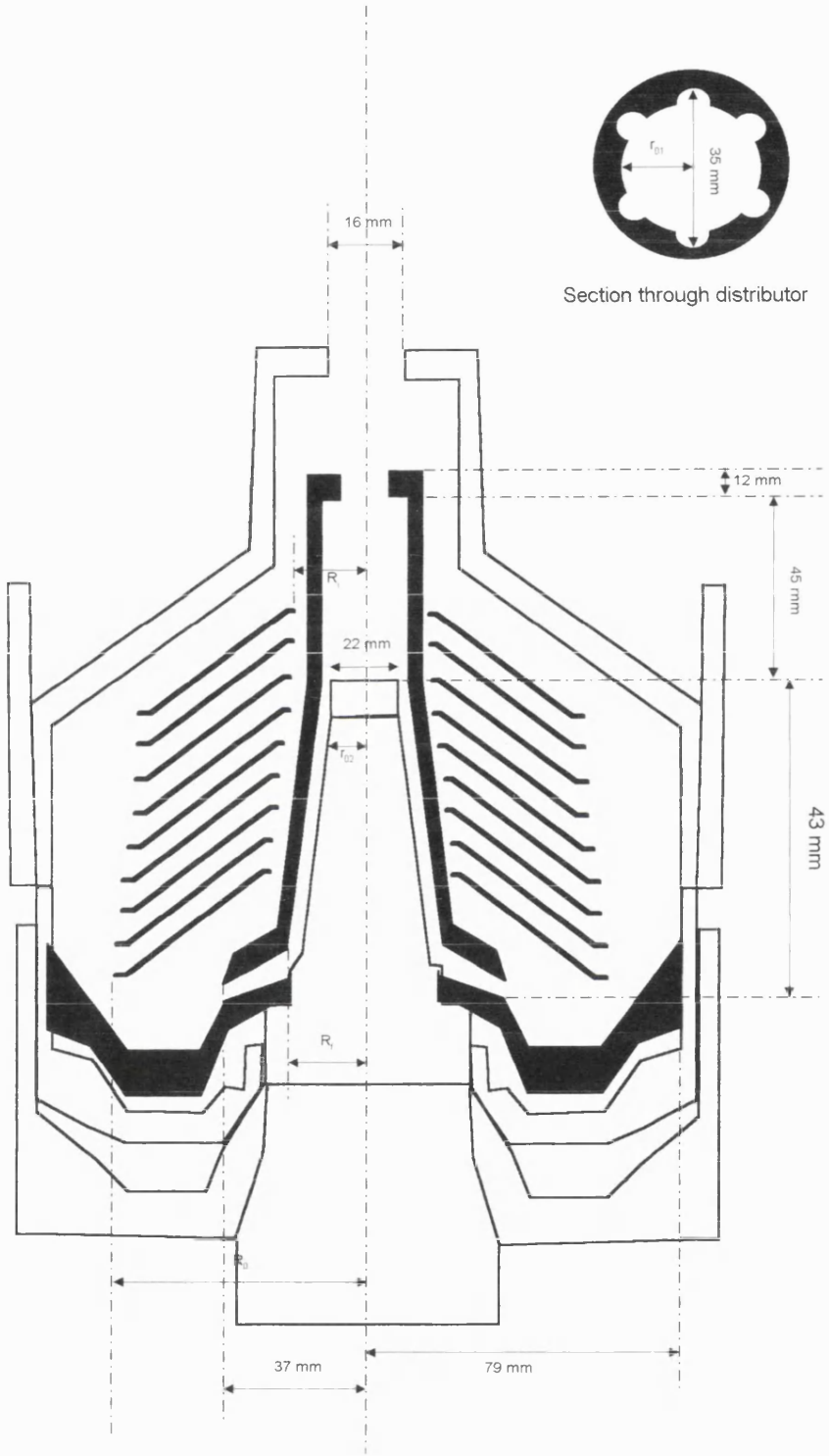

Figure A6.1: Section through the semi-hermetic feed disk stack centrifuge (Westfalia CSA-1, ***not to scale)***

Flow rate Q (Lh^{-1})	**R_i (m)**	**R_0 (m)**	**R_f (m)**	**r_0 (m)**	**feed zone volume (mL)**
all flow rates	0.0261	0.055	0.0175	-	-
50	"	"	"	r_{01} 0.015	2.5
150	"	"	"	r_{02} 0.0125	12
400	"	"	"	0	30

Table A6.1: Effect of flow rate on geometry values used in power dissipation calculations, semi-hermetic feed zone centrifuge

Flow rate Q (Lh^{-1})	**R_i (m)**	**R_0 (m)**	**R_f (m)**	**r_0 (m)**	**feed zone volume (mL)**
all flow rates	0.0261	0.055	0.0175	0	-
50	"	"	"	"	30
250	"	"	"	"	40

Table A6.2: Effect of flow rate on geometry values used in power dissipation calculations, hydro-hermetic feed zone centrifuge

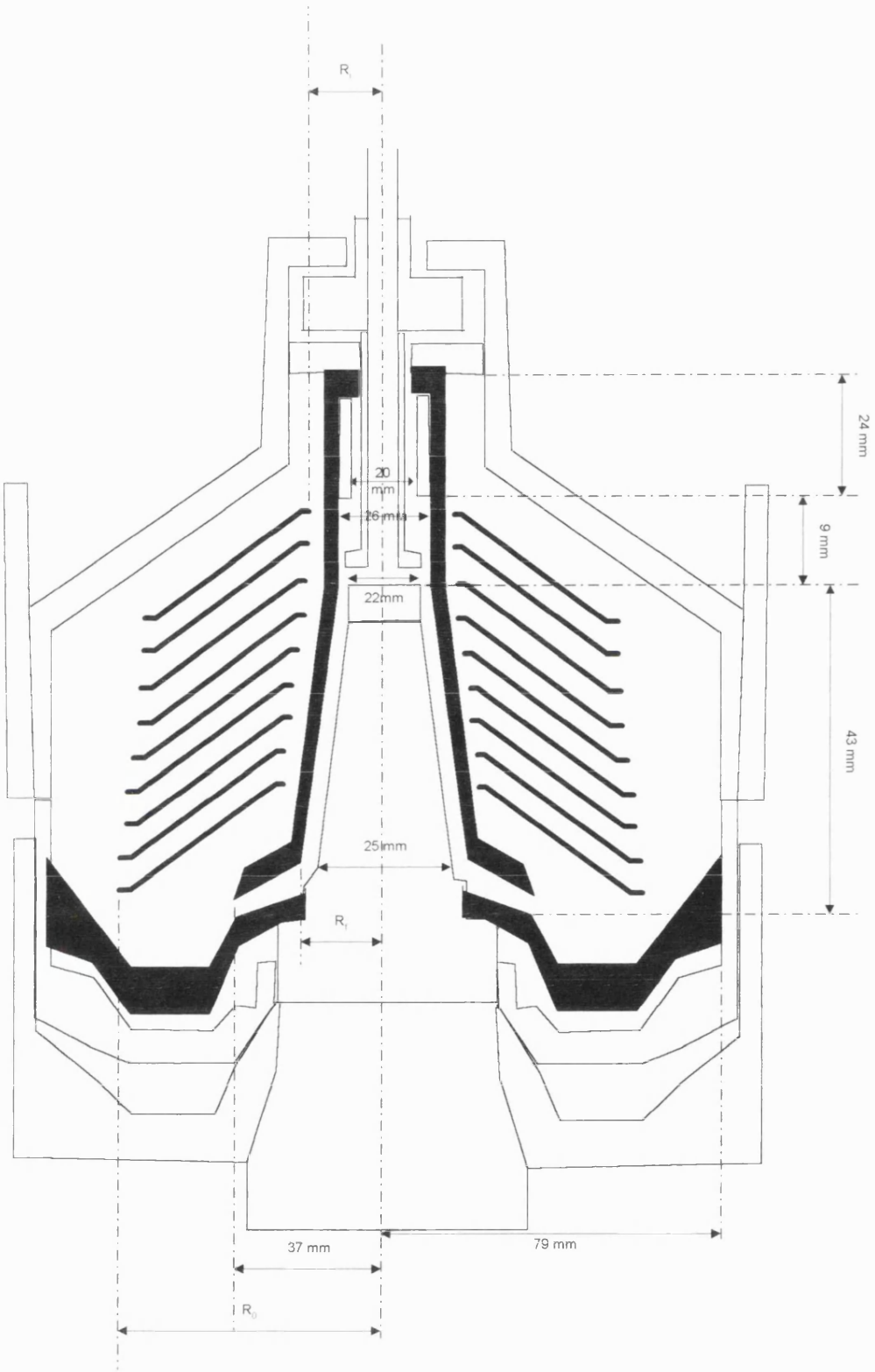

Figure A6.2: Section through the hydro-hermetic feed disk stack centrifuge (Westfalia CSA-1, ***not to scale)***

8.0 NOMENCLATURE

Symbols

a_a = α-amylase activity (I.U. min^{-1} mL^{-1})

a = polyethylene glycol interaction coefficient (-)

b_c = caulk width (m)

C_v = concentration of solids (volume basis)

C_p = polyethylene glycol concentration (Kg m^{-3})

C_{sup} = volume concentration of solids in supernatant (-)

C_f = volume concentration of solids in feed (-)

D_i = Impeller diameter (m)

D_{ib} = barrel internal diameter (m)

D_f = diffusivity (m^2 s^{-1})

D_{max} = maximum particle size (m)

E_T = centrifuge mass yield (-)

d = particle diameter (m)

d_1 = particle diameter (m)

d_2 = particle diameter (m)

d_{ic} = internal diameter of capillary (m)

d_l = diameter of lock-nut (m).

d_s = diameter of particle (m)

d_c = critical particle diameter (m)

E_R = Target enzyme concentration after passage through centrifuge (I.U. m L^{-1})

E_0 = Background level of target enzyme in feed suspension (I.U. m L^{-1})

E_{100} = 100 % release of target enzyme from feed suspension (I.U. m L^{-1})

F_1 = Σ correction factor to account for disk caulks

F_L = resistance of liquid phase to particle motion (N)

F_P = Effective force acting on particle in a centrifugal field (N)

f_p = protein self-interaction coefficient (-)

G_p = shear rate (s^{-1})

G^* = mass average shear rate (s^{-1})

g = acceleration due to gravity ($m\ s^{-2}$)

h = disk spacing (m)

h_p = particle separation distance (m)

k_1 = constant (equation 4.33) (-)

K_A = Rate constant, equation 4.3 ($m^3\ s^{-1}$)

K_B = Boltzmanns constant ($J\ K^{-1}$)

K_p = rate constant, equation 4.13 (-)

L_c = length of capillary (m)

m_s = mass of particle (Kg)

m_L = mass of liquid phase displaced by particle (Kg)

m_f = mass in centrifuge feed (Kg)

m_{sup} = mass in centrifuge supernatant (Kg)

m_{sed} = mass in centrifuge solids (Kg)

N = particle number concentration (No. μL^{-1})

N_i = agitator speed (RPS)

N_0 = Initial particle number concentration (No. μL^{-1})

n = constant, equation 4.33 (-)

Δp = change in pressure ($N\ m^{-2}$)

P_{pe} = Power leaving feed zone as potential energy in fluid (W)

P_{am} = Power supplied to increase angular momentum (W)

P_{ke} = Power leaving feed zone as kinetic energy in fluid (W)

P_d = power dissipation ($W\ m^{-3}$)

Q = volumetric flow rate through the centrifuge ($m^3\ s^{-1}$)

Q_{100} = volumetric throughput in centrifuge for 100% recovery of particle of size d_s ($m^3\ s^{-1}$)

q_s = specific throughput capacity ($m^3\ s^{-1}$)

R = universal gas constant ($J\ mol^{-1}\ K^{-1}$)

R_c = internal radius of capillary (m)

R_f = outer radius of feed zone (m)

R_o = outer disk radius (m)

R_i = inner disk radius (m)

R_d = radius of disc photosedimentometer detector (m)

R_s = radius of injected sample in disc photosedimentometer (m)

r = radial position of particle (m)

r_l = radius of lock-nut (m)

S = thickness of liquid layer in a tubular bowl centrifuge (m)

S_p = protein solubility (Kg m^{-3})

T = temperature (K)

T_M = motor torque (N m)

t = time (s)

V_g = settling velocity under gravity (m s^{-1})

V_g^* = hindered settling velocity under gravity (m s^{-1})

V_{gc} = critical settling velocity (m s^{-1})

V_{sa} = volume of sample equation 2.1 (mL)

V_v = volume of precipitation reactor (m^{-3})

V_Z = settling velocity in a centrifugal field (m s^{-1})

V_e = effective volume of centrifuge (m^3)

W = Stability ratio (-)

X = distance travelled by particle of diameter d_s in centrifugal field (m)

X_{50} = distance travelled by a particle of diameter d_s in a centrifugal field under flow rate such as 50% of particles are recovered (m)

X_i = drive speed (m s^{-1})

Z_s = number of disks in the disk stack

Z_c = number of caulks per disk

Greek Symbols

δ = thickness of boundary layer (m)

$\Delta\rho$ = particle-liquid density difference (Kg m^{-3})

ρ_S = density of the particles (Kg m^{-3})

ρ_L = density of the suspending fluid (Kg m^{-3})

ρ_p = density of precipitate particle of diameter d (Kg m^{-3})

μ = suspension dynamic viscosity (N s m^{-2})

ω = angular velocity of the centrifuge (rad s^{-1})

υ = kinematic viscosity of fluid (m^2 s^{-1})

τ = shear stress (N m^{-2})

Σ = equivalent separating area of a centrifuge (m^2).

λ = dimensionless number equation 3.16

θ = half the disk angle (degrees)

σ_p = particle geometric factor

μ_j = chemical potential of component j (J mol^{-1})

μ_j^0 = standard chemical potential of component j (J mol^{-1})

$\phi(h)$ = potential energy of interaction between two particles (J)

η = Kolmogorov scale of microturbulence (m)

ε = energy dissipation per unit mass of fluid (W Kg^{-1})

γ = constant, equation 4.12

λ_κ = Kolmogoroff scale of microturbulence (m)

ε = energy dissipation rate (J s^{-1})

9.0 SUPPLIERS

AS26 Tubular Bowl Centrifuge

Alfa Laval Separations Ltd.,
Sharples Division
Doman Road,
Camberley,
Surrey,
GU15 3DN.
UK.

APV Manton Gaulin Lab 40 High Pressure Homogeniser

APV Baker Ltd.,
14, Hansard Gate,
West Meadows Ind. Est.,
Derby,
DE21 6JN
UK

RT-DAS Fermentation Data Logger

Acquisistion Systems Ltd.,
Cedarmount House,
90A Owlsmoor Road,
Sandhurst,
Camberley,
Surrey.
GU15 4SS.
UK.

GS-15 benchtop Centrifuge

J2-M1 Laboratory Centrifuge

Beckman Instruments Ltd.,

Progress Road,

Sands Industrial Estate,

High Wycombe

Bucks.

HP12 4JL

UK

"Yeatex" Yeast Extract

Bovril Foods Limited,

Food Ingredients Division,

Claygate House,

Littleworth Road,

Esher,

Surrey.

KT10 9PN.

UK

BI-DCP 1000 Disc Photosedimentometer

Brookhaven Instruments Ltd.,

Chapel House,

Stock Wood,

Worcestershire,

B96 6ST.

UK

Rheomat 115 Viscometer

Contraves Industrial Products,

Times House,

Station Approach,

Ruislip,

Middlesex.

UK

Autoclaves

Denley Instruments Ltd.,

Natts Lane,

Billinghurst,

West Sussex.

RH14 9EY.

UK.

Maxima and Prima water units

Elga Products Ltd.,

Lane End,

High Wycombe,

Bucks.

HP14 3JH.

UK.

LH Fermenters

TCS Control Systems

Inceltech UK Ltd.,

22A Horseshoe Park,

Pangbourne,

Berkshire.

UK.

DOT and pH Probes

Ingold Division

Mettler-Toledo Ltd.,

64, Boston Road,

Beaument Leys,

Leicester.

LE4 1AW.

UK

Instron Food Tester

Instron Ltd.,

Coronation Road

High Wycombe

Bucks

HP12 3SY

UK

Uvikon 922 Spectrophotometer

Kontron Instruments Ltd.,

Blackmoor Lane,

Croxley Centre,

Watford,

Herts.

WD1 8XQ.

U.K.

Titretek Multiskan Plus MK2 Microtitre Plate Reader

Life Sciences International (Europe) Ltd.,

93-96 Chadwick Road,

Astmoor,

Runcorn,

Cheshire.

WA7 1PR.

UK.

Glycerol

Polypropylene glycol

Merck Ltd.,

Hunter Boulavard,
Magna Park,
Lutterworth,
Leicestershire.
LE17 4XN.
UK

Microbial Incubator
Orbital Shaker/Incubator
New Brunswick Scientific Ltd.,
Edison House,
163 Dixons Hill Road,
North Mimms,
Hatfield.
AL9 7JE.
UK

Agar Bacteriological (No.1)
Nutrient Agar No.2
Nutrient Broth No.2
Oxoid Ltd.,
Wade Road,
Basingstoke,
Hants.
RG24 0PW
UK.

Elzone 280 PC particle sizer
Particle Sizing Systems Ltd.,
Particle Data UK Ltd.,
Algers House,
Michaelchurch Escley,
Hereford,

HR2 0LR.

UK.

DCL High Activity Bakers Yeast

J.W. Pike Ltd.,

Unit 4,

Eley Estate,

Eley Road,

Edmonton,

London.

NW18 3BH.

UK.

Sundry Chemicals

Sigma-Aldrich Company Ltd.,

Fancy Road,

Poole,

Dorset.

BH12 4QH.

UK

MM8-80S Mass Spectrometer

VG Gas Analysis,

Nat Lane,

Winsford,

Cheshire.

CW7 3OH.

UK.

605 Di Peristaltic Pump

Watson Marlow Ltd.,

Falmouth

Cornwall

TR11 4RU

UK

SAOOH and CSA-1 Disk Stack Centrifuge

Westfalia Separator Ltd.,

Habig House,

Old Wolverton Road

Wolverton

Milton Keynes

MK12 5PY

UK

AS25 0.2μm syringe filter media

0.1 μm depth filter

Whatman Scientific Ltd.,

Whatman House,

St. Leonards Road,

20/20 Maidstone,

Kent.

ME16 0LS

UK.

10.O REFERENCES

P.A. Albertsson, *Adv. Prot. Chem.*, **24**, (1970), p.309

C.M. Ambler, *Chemical Engineering Progress*, **48 (3)**, pp 150-158

B.A. Andrews & J.A. Asenjo, *Tibtech*, **5**, 1987, pp. 273-277

P. Ayazi-Shamlou, S.F. Siddiqi & N.J. Titchener-Hooker, *Chem. Eng. Sci.*, **50**, 1994, pp. 1365-1385

S.M. Bahri & J.M. Ward, *J. Gen. Microbiol.*,**136**, 1990, pp.811-818.

J. Bailey & D. Ollis, *in Biochemical Engineering Fundamentals*, **2nd Ed.**, 1986, pp. 345

E. Barnea & J. Mizrahani, *The Chemical Engineering Journal*, **5**, 1973, pp 171-189

G. Barnickel, B. Leps & H. Labischinski, *Arch. Microbiol.*, **127**, 1980, pp. 195-201

G. Barnickel, D. Naumann, H. Bradaczek, H. Labischinski & P. Giesbrecht, *in The Target of Penicillin*, 1983, Walter de Gruyter, Berlin, pp. 61-66

G. Barnickel, D. Naumann, H. Bradaczek, H. Labischinski & P. Giesbrecht, *in The Target of Penicillin*, 1983b, Walter de Gruyter, Berlin, pp. 49-54

G.Baron & S. Wajc, *Chemical Engineering Technology*, **4**, 1979, p.333

M.E. Bayer, *J.Gen.Microbiol.*, **53**, 1968, pp. 395-404

M.E. Bayer, *J.Struct.Biol.*, **107**, 1991, pp. 268-280

E. Bech Jensen & S. Carlsen, *Biotech. Bioeng.*, **36**, 1990, pp.1-11

T. Becker, J.R. Ogez & S.E. Builder, *Biotechnol.Adv.*,**1**, 1983, pp.247-261

D.J. Bell, *Ph.D. Thesis*, University of London, 1982

D.J. Bell & P. Dunnill, *Biotechnol. & Bioengng.*, **24**, 1982, pp 1271-1285

D.J. Bell, M. Hoare & P. Dunnill, *Advance in Biochemical Engineering/Biotechnology*, **Vol. 26**, 1983, Ed. A. Feichter, Springer (New York), pp.1-72.

D.J. Bell & K.H. Brunner, *Filtration and Separation*, **20(4)**, 1983, pp. 274-301

P.Belter, "Recovery Processes: Past, Present, Future", *184th Amer.Chem.Soc.Mtg.*, September 1982.

H.U. Bergmeyer, *Methods of Enzymatic Analysis*, **Vols 1-10**, 3rd. Edition, 1983 (Verlag Chemie, Weinheim).

A. Bird, *Ph.D. Thesis*, University of London, 1997.

M.A. Blight, B. Kenny, C. Charvaux, A. Pimenta, C. Cecchi & I.B. Holland, *in Molecular Mechanisms of Transport*, 1992, Elsevier Science Publishers, pp. 207-216.

V. Braun, *Biochim. Biophys. Acta.*, **415**, 1975, pp. 335-377

S.W. Brown, H.P. Meyer & A. Fiechter, *Appl. Microbiol. Biotechnol.*, **23**,1985, pp.5-9.

K.H. Brunner & H. Hemfort, *Advances in Biotechnological Processes*, **8**, 1988, Ed. A. Mizrahi & R. Alan, Liss Inc., New York, pp 1-50

K.H. Brunner & O. Molerus, *German Chemical Engineering*, **2**,1979, pp 228-233

R.E. Burge, A.G. Fowler & D.A. Reaveley, *J. Mol. Biol.*, **117**, 1977, pp. 927-953

R.E. Burge, R. Adams, H.H.M. Balyuzi & D. Reaveley, *J.Mol.Biol.*, **117**, 1977, pp. 955-974

T.F. Busby & K.C. Ingham, *Vox. Sang.*, **39**, 1980, p.93

T.R. Camp & P.C. Stein, *J. Boston Soc. Civ. Engrs.*, **30**, 1943, pp. 219-238

R.S. Cherry & E.T. Papoutsakis, *Bioprocess Engng.*, **1**, 1986, pp. 29-41.

Y. Chisti & M. Moo-Young, *Enz.Microb.Technol.*, **8**, 1986, pp. 194-204

A.I. Clarkson, *Ph.D. Thesis*, 1994, University of London, UK.

L.N. Csonka, *Microbiol.Rev.*,**53**, 1989, pp.121-147

R.T. Coughlin *et al*, *Biochim.Biophys.Acta*, **821**, 1985, pp. 404-412

R.H. Cumming, J. Tuffnell & G. Street, *Biotechnol.Bioengng.*, **27**, 1985, pp. 887-889.

J.A. Currie, P. Dunnill & M.D. Lilly, *Biotechnol. Bioengng.*, **14**, 1972, pp. 725-736

S. Damodaran & J.E. Kinsella, *Biotechnol.Bioengng.*, **25**, 1983, pp. 761-770

I.W. Dawes & I. Sutherland, *Microbial Physiology*, **2nd Edition**, Blackwell Scientific Publications, 1992.

R.Datar & C.G. Rosen, *The Chemical Engineering Journal*, **34**, 1987, pp B49-B56

H.W. Doelle, K.N. Ewings & N.W. Hollywood, *Advs.Biochem.Eng.*, **23**, 1982, pp.1-35.

M.S. Doulah, *Biotechnol. Bioengng*, **19**, 1977, pp. 649-660

G. Emmerling, U. Henning & T. Gulik-Krzywicki, *Eur. J. Biochem.*, **78**, 1977, pp. 503-509

C.R. Engler, *in Comprehensive Biotechnology*, 1985, Ed. M. Moo-Young, Pergammon Press, Oxford, UK, **Vol 2, Ch. 20**, pp. 305-324.

C.R.Engler & C.W. Robinson, *Biotechnol. Bioengng.*, **23**, 1981, pp. 765-780

H. Felix, *Anal. Biochem.*, **120**, 1982, pp. 211-234

C. Filip, G. Fletcher, J.L. Wulff & C.F. Earhart, *J.Bact.*,**115**, 1978, pp. 717-722

E. Fisher, *Ph.D. Thesis*, University of London, 1997.

M. Follows, P.J. Hetherington, P. Dunnill & M.D. Lilly, *Biotechnol. Bioengng.*, **13**, 1971a, pp. 594-560

M. Follows, P.J. Hetherington, P. Dunnill & M.D. Lilly, *Trans.Inst.Chem.Engrs.*, **49**, 1971b, pp. 142-148

C. French, *Ph.D. Thesis*, University of London, 1993.

P.R. Foster, P. Dunnill & M.D. Lilly, *Biochim.Biophys.Acta.*, **317**, 1973, p. 505

J. Fu, D.B. Wilson & M.L. Shuler, *Biotech. Bioeng.*, **41**, 1993, pp. 937-946.

N.A. Fuchs, *The Mechanics of Aerosols*, 1964, Pergamon Press, London.

L.A. Glasgow & R.H. Luecke, *Indust. & Engng. Chem. Fund.*, **19**, 1980, pp. 148-156

R.E. Glass, *Gene Function*, Croom Helm, London, 1982

W. Gösele, *German Chemical Engineering*, **3**, 1983, pp. 353-359.

P. Greguss, *Int.Chem.Engng.*, **3(2)**, 1963, pp. 280-294

S.K. Gupta, *Chem.Eng.J.*, **22**, 1981, pp. 43-49

K. Han, H.C. Lim & J. Hong, *Biotech. Bioeng.*, **39**, 1992, pp.663-671.

S.T. Harrison, *Ph.D. Thesis*, 1990, University of Cambridge, UK.

S.T. Harrison, H.A. Chase & J.S. Dennis, *in Separations for Biotechnology*, **2**, 1990, Ed. D.L. Pyle, Elsevier Applied Science, London, UK. pp. 38-47

J.S. Harrison, K. Ukar & E. Keshavarz-Moore, *I.Chem.E.Annual Research Event*, 1994, UCL, UK. pp.244-246

J.S. Harrison, E. Keshavarz-Moore, P. Dunnill, M. Berry, A. Fellinger, L. Frenken, *Accepted for Biotech. Bioeng.*, 1996.

H. Harz *et al*, *Anal. Biochem.*, **190**, pp. 120-128

G. Hedenskog, H. Mogren & L. Enebo, *Biotechnol. Bioengng.*, **12**, 1970, pp. 947-959

A. Helenius & K. Simons, *Biochim.Biophys.Acta.*, **415**, 1975, pp. 29-79

D. Hettwer & H. Wang, *Biotechnol. Bioengng.*, **33**, 1989, pp. 886-895

R.S. Hill & D.L. Kime, *Chemical Engineering*, **83(16)**, 1976, pp. 89-94

M. Hoare, *Trans. Inst. Chem. Eng.*, **60**, 1982, pp. 157-163

M. Hoare, T.J. Narendranathan, T.J. Flint, D. Heywood-Waddington, D.J. Bell & P. Dunnill, *Indust. Engng. Chem.Fund.*, **21**, 1982, pp.402-406

Holtje & B. Glauner, *Res. Microbiol.*, **141**, 1990, pp. 75-89

W.H. Holms, *Current Topics in Cellular Regulation*, **28**, 1986, pp. 69-105.

H.W. Hsu, *Tachniques of Chemistry*, **16**, 1981, pp 767-784

D.E. Hughes, J.W.T. Wimpenny & D. Lloyd, *in Methods in Microbiology*, **Vol 5b**, 1971, Eds. J. Norris & D. Ribbon, Academic Press, New York, pp. 1-54

K.C. Ingham, *ibid.*, **186**, 1978, p. 106

K.J. Ives & A.G. Bhole, *Proc.A.S.C.E.Env.Eng.Div.*, **99 (EE1)**, 1973, p. 17

R.J. Kadner, *Mol. Microbiol.*, **4**, 1990, pp. 2027-2033

T. Kawabe, T. Ohshima, N. Uozumi, S. Iijima & T. Kobayashi, *Journal of Chem. Engng, of Japan*, **25(6)**, 1992, pp.702-707.

M.V. Keleman & J.E.E. Sharpe, *J. Cell.Sci.*, **35**, 1979, pp. 431-441

E.P. Kennedy, *Proc.Natl.Acad.Sci.USA*, **79**, 1982, pp. 1092-1095

J.Y. Kim & D.D.Y. Ryu, *Biotech. Bioeng.*, **38**, 1991, pp. 1271-1279.

E. Keshavarz-Moore, M. Hoare & P. Dunnill, *in Separations in Biotechnology*, 1987, Ed. M.S. Verall & M.J. Hudson, Ellis Horwood Ltd., UK.

Kirk-Othmer, *Encyclopaedia of Chemical Technology*, 2nd Ed., **Vol. 4**, 1992, p721

J.A. Kitchener & R.J. Gochin, *ibid.*, **15**, 1981, p. 585

B.T. Koh, U. Nakashimada, M. Pfieffer & M.G.S. Yap, *Biotech. Letts.*, **14(12)**, 1992, pp. 1115-1118.

M.R. Kula & K.H. Kroner, *Process Biochem.*, **13(4)**, 1978, p.7

M.R. Kula & H. Schutte, *Biotechnology Progress*, **3(1)**, 1987, pp. 131-142

H. Labischinski, *Eur.J.Biochem.*, **95**, 1979, pp. 147-155

H. Labischinski & L. Johannsen, *in Biological Properties of Peptidoglycan*, 1986, Walter de Gruyter, Berlin, pp. 37-42

H. Labschinski & H. Maidhof, *in Bacterial Cell Wall*, 1994, Elsevier, p.30

P. Landwall & T. Holme, *J. Gen. Microbiol.*, **103**, 1977 (a), pp. 345-352.

P. Landwall & T. Holme, *J. Gen. Microbiol.*, **103**, 1977 (b), pp. 353-358.

T.C. Laurent & P.H. Iverius, *Biochim. Biophys. Acta*, **133**, 1967, p 371

J.I. Lee, A. Kuhn & R.E. Dalbey, *J. Biol. Chem.*, **267**, 1992, pp. 938-943

M.D. Lilly & P. Dunnill, *in Fermentation Advances*, 1969, Ed. Perlman, Academic Press, London, UK.

S. Little, C. Campbell, I. Evans, E. Hayward, R. Lilley & M. Robinson, *Gene*, **83**, 1989, pp.321-329

S. Lory, *J.Bacteriol.*, **147**, 1992, pp. 3423-3428

G.W. Luli & W.R. Strohl, *Appl.Env.Microbiol.*, **56(4)**, 1990, pp. 1004-1011.

K.Mannweiler, *Ph.D. Thesis*, The Recovery of Biological Particles in High Speed Centrifuges with special reference to Feed-Zone Break-Up Effects, University of London, 1990

K. Mannweiler & M. Hoare, *Bioprocess Eng.*, **8**, 1992, pp. 19-25

T. Matsui, H. Sato, S. Sato, S. Mukataka & J. Takahashi, *Agric. Biol. Chem.*, **54(3)**, 1990, pp. 619-624.

J. Maybury, *personal communication*, UCLACBE , 1997

H.P. Meyer, C. Leist & A. Fiechter, *J. Biotechnol.*, **1**, 1984, pp. 355-358.

A.P.J. Middelberg & I.D.L. Bogle, *Biotechnol. Prog.*, **6**, 1990, pp. 225-261

S.I. Miekka & K.C. Ingham, *Arch. Biochem. Biophys.*, **191**, 1978, p. 525

P.T. Milburn & P. Dunnill, *Biotech. Bioeng.* ,**44**, 1994, pp. 736-744

T. Mizuno, *Biochemistry*, **86**, 1979, pp. 991-1000

D.C. Morrison, *in Handbook of Endotoxin*, **Vol 3**, 1985, Ed. L.J. Berry, Elsevier, Amsterdamn, pp.25-55.

A. Mukhopadhyay, *Biotech. Techniques*, **6(6)**, 1992, pp507-510

S.W. Nam, B.K. Kim, K.H. Son & J.H. Kim, *Biotech.letts.*, **9**, 1987, pp.489-494.

D. Naumann, G. Barnickel & H. Labischinski, *Eur.J.Biochem.*, **125**, 1982, pp. 505-515

H.L. Neu & L.A. Heppel, *J. Biol.Chem.*, **240**, 1965, pp. 3685-3692

H. Nikaido & M. Vaara, *Microbiol. Rev.*, **49**, 1985, pp.1-32

A.G. Ogston, *Biochem. J.* , **117**, 1970, p.85

D. Oliver & J. Beckwith, *Cell*, **25**, 1981, pp. 765-772

J.D. Pandya & L.A. Spielman, *Chem. Eng. Sci.*, **38(12)**, 1983-1992

T.J. Park, *J. Bacteriol*, **175**, 1993, pp. 7-11

J.Pierce, *Ph.D. Thesis*, University of London, 1997

H.J. Rehm & G. Reed (Ed.), *Biotechnology*, 2nd Edition, 1991 pp475-486

I. Reich & R.D. Vold, *Amer.Inst.Chem.Eng.J.*, **63**, 1959, pp. 1497-1501

J.F. Richardson & W.N. Zaki, *Transactions of the Institution of Chemical Engineers (Part I)*, **32**, 1954, pp.35-53

E.T. Rietschel, *in Bacterial Endotoxin: Chemical, Biological and Clinical Aspects*, 1984, Verlag Chemie, Weinheim, pp. 11-22

U. Rinas, H-A Kracke-Helm, & K. Schügerl, *Appl.Microbio.Biotechnol.*, **31**, 1989, pp.163-167.

A.D. Roberts, Z. Zang, T.W. Young & C.R. Thomas, *I.Chem.E. Annual Research Event*, 1994, UCL, UK. pp. 73-75

C.G. Rosen & R. Datar, *The Chemical Engineering Journal*, **34**, 1987, pp. B49-B56

S. Rottem & L.Leive, *J.Biol.Chem*, **252**, 1977, pp. 2077-2081

J. Rumpus, *Ph.D. Thesis*, University of London, 1997

C.H. Schein and M.H.M. Noteborn, *Biotechnology*, **(6)**, 1988, pp.291-294.

C.H. Schein *et al*, *Biochem.J.*, **283**, 1992, pp. 137-144

C.A. Schnaitmann, *J.Bact.*, **108**, 1971, pp. 545-552

H. Schutte, K.H. Kroner, H. Hustedt & M.R. Kula, *Enz. Microbiol Technol.*, **5**, 1983, pp. 143-148

H. Schlichting, *Boundary Layer Theory*, **7th Edition**, 1979, McGraw-Hill, pp.101-107.

S.K. Sharma, *Sep.Sci.Technol.*,**21**, 1986, pp. 701-726

N. Shimizu, S. Fukuzono, K. Fujimori, N. Nishimura and Y. Odawara, *J. Ferment. Technol.*, **66(2)**, 1988, pp.187-191.

Sikyta, *in Methods in Industrial Microbiology*, 1983, Ellis Horwwod Ltd., pp. 321-326

S.F. Siddiqi, *Ph.D. Thesis*, University of London, 1997, p.135

L.S. Skvortsov, *Theoretical Foundations of Chemical Engineering*, **18 (3)**, 1984, pp. 226-233

M. Smoluchowski, *Z. Phys.Chem.*, **92**, 1917, pp. 129-168

R.H. Snow, B.H. Kaye, C.E. Capes & G.C. Sresty, *in Perrys Handbook of Chemical Engineering*, 1988, 6th Edition, Eds. R.H. Perry & D. Green, McGraw-Hill, UK, pp. 8-34-36, 8-45-47

V.I. Sokolov, *Moderne Industriezentrifugen*, VEB Technik Verlag, Berlin Germany, 1971

P.F. Stanbury & A. Whitaker, *Principles of Fermentation Technology*, 1984, Pergammon Press, pp. 206-208

C.G. Stokes, *Trans. Cam. Phil. Soc.*, **9**, 1851, :8

D.K. Summers, *Trends in Biotechnology*, **9**, 1991, pp.273-278.

L. Svarovsky, Efficiency of Separation from Fluids, in *Solid Liquid Separation*, 1990, 2nd Edition, Butterworths, pp 33-63

N. Tambo & H. Hozumi, *Water Res.*, **13**, 1979, p.421

T. Tetsuaki, N. Katsui, A. Takeuchi, M. Takano & I. Shibasaki, *App.Env.Microbiol.*,**50**, 1985, pp. 298-303.

N.J. Titchener, *Ph.D. Thesis*, University of London, 1986.

B.G. Thompson, M. Kole & D.F. Gerson, *Biotech. Bioeng.*, **27**, 1985, pp. 818-824.

J.J. Thwaites & N.H. Mendelson, *Proc.Natl.Acad.Sci.USA*, **82**, 1985, pp. 2163-2167

D.T. Tomi & D.F. Bagster, *Trans.Inst.Chem.Eng.*, **56**, 1978a, pp. 1-8

D.T. Tomi & D.F. Bagster, *Trans.Inst.Chem.Eng.*, **56**, 1978b, pp. 9-18

M.E.O'K Trowbridge, *The Chemical Engineer*, 1962, pp A73-A87

J.J. Thwaites & N.H. Mendelson, *Proc.Natl.Acad.Sci.USA*, **82**, 1985, pp.2163-2167

C. Turner, *Ph.D. Thesis*, University of London, 1993.

J.P. Van der Linden, *Ph.D. Thesis*, University of Delft, Netherlands, 1987

E. Varga, *Ph.D. Thesis*, University of London, 1997

P.D. Virkar, M. Hoare, M.Y.Y. Chan & P. Dunnill, *Biotecnol. & Bioengng.*, **24**, 1982, pp. 871-887

L. Vrale & R.N. Jordan, *J.A.M. Water*, **63**, 1971, p. 52

H.E. Wade, *Patent No. 40344168*, London, 1968

D.I.C. Wang, C.L. Cooney, A.L. Demain, P. Dunnill, A.E. Humphrey & M.D. Lilly, *in Fermentation and Enzyme Technology*, 1978, John Wiley and Sons, London, pp.239-249.

A. Warnes, J.R. Stephenson, A.R. Fooks, J. Melling & M.R.W. Brown, *Biotech. Bioeng.*, **38**, 1991, pp. 1050-1058.

D.A.J. Wase & Y.R. Patel, *J. Chem.Tech.Biotechnol.*, **35B**, 1985, pp. 165-173

F.B. Wientjes, C.L. Woldringh & N. Nanninga, *J. Bacteriol.*, **173**, 1991, pp. 7684-7691

J. Wild, W. Walter, C. Gross & E. Altman, *J.Bacteriol.*, **175**, 1993, pp. 3992-3997.

C.A. Willus & B. Fitch, *Chemical Engineering Progress*, **69 (9)**, (1973), pp. 93-94

D.W. Zabriskie & E.J. Arcuri, *Enz. Microb. Technol.*, **8**, 1978, pp. 706-717.

J.Zastrow, *International Chemical Engineering*, **16(3)**, 1976, pp 515-518